Distributed Optimisation of LTE Systems

Middleton, Amy

Award date:
2019

Awarding institution:
University of Bath

Distributed Optimisation of LTE Systems

submitted by

Amy L. L. Middleton

for the degree of Doctor of Philosophy

of the

University of Bath

Department of Mathematical Sciences

August 2019

COPYRIGHT

Declaration of any previous Submission of the Work

The material presented here for examination for the award of a higher degree by research has not been incorporated into a submission for another degree.

.....

Amy Middleton

Declaration of Authorship

I am the author of this thesis, and the work described therein was carried out by myself personally.

.....

Amy Middleton

Acknowledgements

I would like to begin by thanking my supervisors, Antal, Jon and Keith. Not only for giving me the opportunity to work on this project with them but also for being so generous with their time and knowledge. It has been a privilege to benefit from their insights and guidance.

I have been fortunate to meet many wonderful people through the PhD and I am very grateful for all the help, advice and encouragement I have received. I won't list names but this includes my office mates and numerous others in the department. In particular, I would like to thank everyone in CNCB as it made such a positive difference to my time at Bath. Many of my happiest memories from the PhD involve Kevin and Miranda, I don't want to imagine what it would have been like with out the two of you. Also my former flatmate Marc, who made the first year of my PhD immeasurably better and has remained a wonderful friend throughout.

I am grateful to all friends met before the PhD who supported me before and throughout. The best compliment I have received is that I have the friends I deserve. I would like to thank Sophie and Charlotte who have always made an empathetic ear available and provided good advice and unwavering support. I love you both. Sophie for always offering a different perspective and helpful insights. Charlotte for the many uplifting conversations and visits.

I'd like to thank my family, in all forms, for everything they have done for me. Dad, you're always there when I need you. Thank you for always being so confident in my potential and for holding me to standards set by your belief in me, never accepting the limits placed on me by others. It made all the difference.

Lastly and most importantly, my partner Ruaridh:

Ruaridh, you have experienced every up and down of this journey with me and I couldn't have done it without you. Your love and support is behind every word, symbol, number, table and figure in this thesis.

Thank you, for everything.

Summary

This thesis concerns the mathematical modelling of self-organising wireless communication networks.

In particular the thesis considers small cell long term evolution (LTE) wireless communication networks, with femtocells as the devices in mind. Self-organisation consists of optimising various aspects of the network in a dynamic way. In this thesis we present a number of novel mathematical analyses, beginning by considering the network interactions and dynamics when three of the self-organisation objectives compete: coverage, quality and energy efficiency. The following chapters then select two of these objectives and develop policies that aid self-optimisation, and we benchmark the performance of these policies. A significant contribution is to show that reinforcement learning can be used to develop policies that require no direct knowledge of a node's neighbours and which outperform our benchmark. It is found that the ability of a node in this network to determine the distance to its nearest neighbours in a distributed way is important for the success of the policies that do not rely on reinforcement learning. Therefore the last part of the thesis develops heuristics that enable the estimation of these distances. In the last chapter the thesis proposes a new and particularly significant improvement (the 'Two-Part Pulse Method') to an existing patented method which BT hope to implement.

List of Publications

How close is the nearest transmitter in a wireless network?
Amy L.L. Middleton, Keith Briggs, Jonathan H.P. Dawes, Antal A. Jarai,
Submitted in January 2019.

This paper contributes to **Chapter 4** of this thesis.

Contents

List of Figures

List of Tables

List of Algorithms

Chapter 1

Introduction

Since ancient times communication systems have been used for sending information between parties. Early systems sent information over line-of-sight distances via smoke signals, by fire and by the use of mirrors with sunlight (heliographs). Simple messages could be conveyed using pre-determined signal combinations [69] and, with a network of line-of-sight distances, information could be sent a long way in a relatively short period of time. For example, built into the Great Wall of China, as well as many miles in front and behind the wall, were beacon towers. These towers allowed for the use of fire and smoke signals to send messages and were much faster and safer than a runner or rider [27]. It is believed that messages could be sent nearly 500 miles in mere hours [1].

In the 1800s, major advances began with wired communications. In 1844 Samuel Morse and Alfred Vail demonstrated a telegraphic message sent between Washington DC and Baltimore and a system for encoding messages which became known as Morse code was developed [64]. This meant that messages did not have to be pre-determined. On March 10th 1876 Alexander Graham Bell demonstrated a telephone call to his assistant Thomas Watson where the spoken word was transmitted [35]. Advances in radio communications then followed. In 1899 Guglielmo Marconi demonstrated long distance radio transmission between France and the UK, and then in 1901 he demonstrated the first transatlantic radio transmission between the UK and the USA [22].

This thesis concerns the distributed optimisation of cellular communication networks. It was AT&T Bell Labs that came up with the cellular concept. In December 1947, Douglas H. Ring and W. Rae Young, Bell Labs engineers, proposed hexagonal cells for mobile phones in vehicles [59]. Cellular systems exploit the fact that the power of a transmitted signal falls off over distance, allowing spatially separate locations to interfere minimally even using the same frequency.

Using this premise a cellular system divides a geographical area into adjacent non overlapping cells [52]. From 1G analogue networks in 1979 we have moved on through digital 2G, 3G, 4G networks and are now seeing the launch of 5G networks.

1.1 Research Context

Wireless communication is considered by many a necessity for modern life. It is uncommon to meet someone who does not own, or rely in some way upon, a mobile phone or similar device. When taking a journey on public transport one will observe many passengers not just having voice conversations on their phones but also interacting with devices such as tablets and laptops. These devices are not just used for professional purposes but are also important for how people entertain themselves and stay in contact with friends and family. The advances in the technology for mobile phones has meant that streaming content has become popular and in demand. The dramatic popularity and growth of Netflix gives an indication of the increasing demand on wireless networks. People wish to be able to stream content not just when they are at home but also whilst travelling or away from home. All of these activities place increasing demands upon wireless communications networks.

The importance of, and growing demand upon, wireless communications networks is recognised by governments. In its December 2017 Telecommunications Sector Report [77], the UK government reported that there is hardly a sector in the UK which will not rely in some shape or form on the connectivity provided by telecommunications, the services it enables, and the activities it supports. The failure of telecommunication systems, or the failure to invest in upgrading them to meet increasing demand, can have a direct and negative impact on people's ability to do business and to interact socially. As a result, telecommunications are considered to be part of the UK's critical national infrastructure.

We are in a time of rapid technological change and growing demand in the telecommunications industry and it is in this era that Self-Organising Networks (SONs) offer many benefits. The benefits of SONs include: energy and cost savings, improved network performance and customer experience. In 2019 we are seeing the launch of commercial 5G networks. Associated with this rollout is the emergence of small-cell densification [25]. Small-cells will no longer just fill gaps; they will be essential to enabling 5G, particularly in densely populated areas [25].

It is in dense small-cell networks that SON can have significant impact and

benefit. Global investments in SON technology are expected to grow at a compound annual growth rate of approximately 11% between 2019 and 2022; by the end of 2022, it has been estimated that SONs will account for a market worth $5.5 billion [67].

This research looks at the behaviour of the network as SON objectives compete, explores policies that aid self-optimisation and then develops heuristics to enable those policies.

1.1.1 Research Objectives

The heuristics proposed in this thesis aim to support SON technology for dense small-cell communication networks. We consider a set of transmitting devices distributed over two-dimensional space. Our main application area is cellular systems such as current 4G or future 5G networks. Each cell includes a fixed-location transceiver called a base station, capable of wireless connection to devices. Together these cells provide coverage over larger geographical areas than could be covered by a single large transmitter, a macrocell base station (MBS). There is a current trend for higher and higher densities of cells, and this necessitates research into fundamental aspects of network behaviour, such as those to be described here. The overall benefits of a higher density cellular network include increased capacity and reduced power consumption for user devices, assuming that the network can be efficiently managed and is sufficiently resilient and self-managing.

1.2 Thesis Layout

This thesis consists of six chapters. **Chapter 1** is the introduction and has two main parts. The first gives the context and objectives of this research. The second part gives a more detailed problem description in engineering terms and then summarises the mathematical methodology and modelling assumptions adopted. **Chapter 2** focuses on network interactions and behaviour when three self-organisation objectives compete. **Chapter 3** takes two of these three self-organisation objectives, SINR and Coverage, and develops power control policies that aid self-optimisation. **Chapter 4**, which has been submitted as a paper for publication, concerns distance estimation to nodes in a wireless communication network. The transmitters have uniform power settings. **Chapter 5** is organised into three main parts and concerns transmitters that have non-uniform power

settings. Methods of estimating the distance and power of neighbouring transmitters are explored. **Chapter 6** draws together the results from the previous chapters into a conclusion and discusses potential future work.

1.3 Engineering Background

In this subsection we give a description of the wireless communications engineering concepts and descriptions that we use. To build a mathematical model of a real-world scenario, in this case a small-cell wireless communications network, the first step is often to simplify it. We do this by making assumptions about the distribution of cells, the relationship between distance and signal, as well as causes of interference present in the network. This section details the assumptions made and describes the terms used.

We have discussed the importance of dense small-cell networks and the benefits that SON technologies offer. The small-cell base stations we consider are femtocells; we refer to them in this thesis as 'transmitters'.

Transmitters

In our research the base stations are femtocells; these are small devices, similar to the Wi-Fi hubs commonly found in residential homes, relatively inexpensive and can overlay an existing cellular network. Femtocells provide 4G, and will eventually provide 5G, coverage to user devices thus allowing for connectivity in areas where it is currently poor or absent. They can provide improved capacity and coverage to users [19] [79]. It is known that more than 50% of all voice calls and more than 70% of data traffic originates indoors. Femtocells send data through a broadband gateway over the internet and their deployment could efficiently relieve indoor traffic from expensive MBSs, allowing truly mobile users to experience higher capacity [19] [47].

Traditionally when a single large transmitter (MBS) was to be placed, a large amount of planning preceded its placement to ensure the location and configuration settings optimised the network's performance. However, as femtocells will be placed by end users [18], their locations will be unplanned and optimal configuration settings will not be known. As end-users cannot be expected to determine the optimal configuration settings for a femtocell, it is necessary that the network be capable of self-organisation.

Self-Organising Network

To be self-organising, the network should be self-optimising and self-diagnosing [72]. A self-optimising network is one where the transmitters in the network choose configuration settings which optimise the global network performance (see Subsection 1.3.3). The ability of a transmitter to initially self-configure is sometimes referred to as plug-and-play capability. To be self-diagnosing the network needs to have the ability to detect and adapt to change, such as the removal or addition of a transmitter, so that network performance is still maintained and optimised.

Receivers

These are the user devices that connect to the transmitters to receive signal, also referred to as user equipment (UE). A receiver can only be paired to one transmitter at a time, though a transmitter can have many paired receivers. Typically UE would be devices such as mobile phones, tablets and laptops.

Spatial distribution

The spatial distribution of transmitters and receivers is critical in determining the performance of the wireless network. Consider the use of femtocells in private homes, in semi-detached properties femtocells may be positioned very close together either side of the dividing property wall. Whereas in large detached properties or rural areas where properties are more sparsely distributed femtocells will be more isolated. As inter-node distances, which vary largely and are often not known a priori, significantly affect network performance a stochastic model for node locations (i.e. a planar Poisson point process, Definition 1.3) is needed. In situations where nodes are located, or move, randomly over a large area, the analytical tractability of the homogeneous Poisson point process has made it the most widely used model [5]. Further to this, it is the simplest random spatial process that does not assume any spatial structure.

Therefore to represent the distribution of femtocells, also called base stations or transmitters, we use a two-dimensional plane in which points are distributed according to a Poisson point process with intensity λ. A description of such a Poisson point process is given in Subsection 1.4.1.

Each femtocell in the network transmits a signal to be received by user devices. The amount of signal received will be determined by propagation effects and the distance and transmission strength.

1.3.1 Pathloss

Pathloss is the term used to describe the loss in signal strength (or power density) in an electromagnetic wave which results from its propagation along a specific path through space. The loss in power increases with the distance travelled; the exact relationship is determined by the medium travelled through and the length of the path.

Signal losses are commonly described as "near-field" or "far-field". When very close to a transmitter (near-field) there is very little pathloss, so that the signal received is considered to be constant. Outside the "near-field radius", pathloss is considered to be far-field and loss in power is assumed to be proportional to distance raised to some exponent. From [11] we understand that in real world scenarios pathloss is roughly as shown in Figure 1-1.

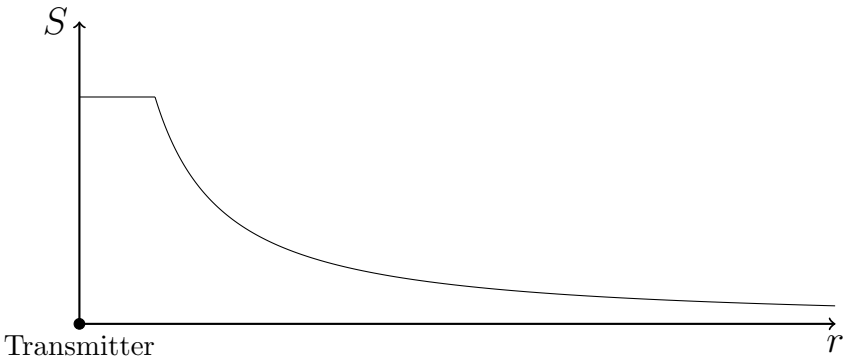

Figure 1-1: The real world reduction in received signal strength S, with $S \propto g(r)$, as the distance r from the transmitter increases.

Far-field pathloss

For analytical reasons, when modelling the problems considered in this thesis it has been necessary to assume all pathloss is far-field. This approach is common and is also used in [49], [68] and [87]; equations (7a) and (7b) in [68] give the conditions that must be satisfied.

When r represents the distance from the transmitter and the exponent $\gamma > 2$ the equation for far-field pathloss is given by

$$g(r) = r^{-\gamma}. \tag{1.3.1}$$

Using equation (1.3.1) causes received signal to tend to infinity when measured very close to a transmitter. This is shown in Figure 1-2.

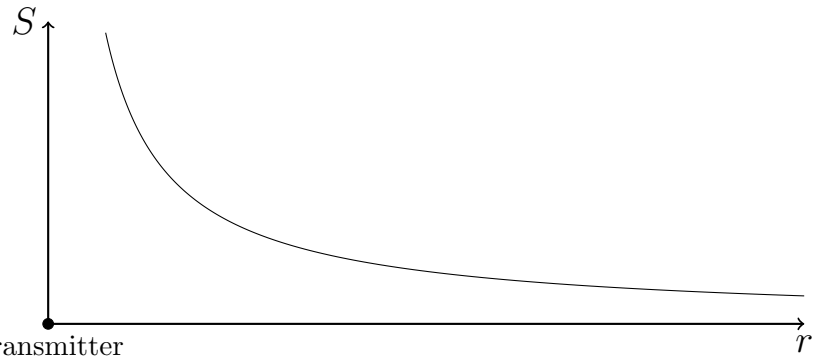

Figure 1-2: The far-field reduction in received signal strength S, with $S \propto g(r)$, as the distance r from the transmitter increases. It can be seen that $S \to \infty$ as $r \to 0$.

From [10] we understand that at BT it has been observed that reasonable agreement with field experimental data is achieved by taking $\gamma \approx 3.8$. For simplicity we use $\gamma = 4$ unless stated otherwise.

Near-field pathloss

When the unbounded nature of the received signal strength that results from (1.3.1) needs to be avoided, we use instead the modified "near-field pathloss" model

$$g(r) = (1 + r)^{-\gamma}. \tag{1.3.2}$$

This, in effect, shifts all measuring points away from the transmitter maintaining the far-field approximation at large r while avoiding singularities at small r. This is shown in Figure 1-3.

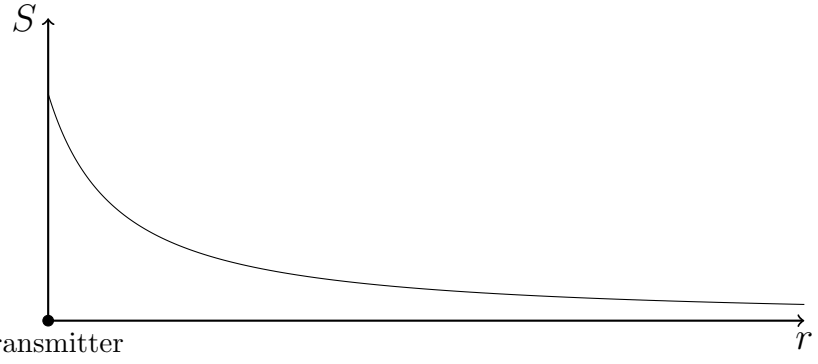

Figure 1-3: The near-field reduction in received signal strength S, with $S \propto g(r)$, as the distance r from the transmitter increases.

1.3.2 Fading

So far pathloss has been taken as the only cause of the reduction in the strength of signal as it travels over a distance. However, events such as obstacles being encountered, resulting in reflection or diffraction, can also cause a reduction in strength. We use the term *propagation effects* to describe the effects which, in addition to pathloss, cause a degradation in the signal reaching the receiver. We now consider the propagation effect known as fading. In Chapters 4 and 5 we show how it affects our ability to estimate the distance to the nearest transmitter.

A mobile channel has multi-path reception meaning that the signal broadcast to the receiver contains the direct "line of sight" wave as well as a large number of reflected waves. Fading refers to the reduction in signal strength that is caused when reflected waves interfere with the direct wave.

As an example we consider a moving mobile phone. The incoming radio signal is reflected off nearby objects (an effect referred to as shadowing) so that there are interference patterns and the intensity of the signal received by the phone varies with its location. The received signal strength can easily vary by 10 decibels (dB) as the phone's antenna moves through a distance similar to the wavelength of a radio signal (a few centimetres) [50].

The effect of fading is that the received signal S varies with time, the degree to which this occurs is dependent on the type of fading present. In this thesis we model fading as being Nakagami-m distributed, which we now discuss.

Nakagami-m Fading

Adapting the form given in [4] so that we do not condition received signal on the average local signal, we see that when the Nakagami-m distribution [56] is used to model the random variation of received signal due to small scale multipath fading then the probability density function (PDF) of the received signal takes the form of a Gamma distribution. Nakagami-m fading variables are $\mathsf{Gamma}(m, 1/m)$ distributed with $m \geq 1$. The larger the value of m the smaller the variance of the fading variables and the more the fluctuations in signal strength reduce. The special case when $m = 1$ is referred to as Rayleigh fading.

In a cellular system, such as the one being modelled, interference naturally comes from multiple sources. Nakagami-m fading is appropriate for modelling this as its distribution is that of the sum of independently and identically distributed Rayleigh fading factors.

Rayleigh Fading

Rayleigh fading assumes that a received multi-path signal consists of a large number of reflected waves which are identically independently distributed. It is therefore used to describe a wireless radio network and is appropriate for the model we consider.

As previously stated, Rayleigh fading is a special case of Nakagami-m fading recovered when $m = 1$. Nakagami-m fading variables are $\mathsf{Gamma}(m, 1/m)$ distributed and therefore Rayleigh fading variables are distributed $\mathsf{Exp}(1)$. As the fluctuations in signal strength, caused by fading variables, increase as m decreases, Rayleigh fading has the most extreme effect on observed signal. It is Rayleigh fading that we use in Chapter 4 when developing a heuristic for transmitter distance estimation in the presence of fading.

1.3.3 Network Performance

Network performance can be measured by the quality of the connections between transmitters and their paired user devices; these are devices which are designated to receive service from that one transmitter. A user device receives signal S_1 from its paired transmitter and interference I from non-paired transmitters.

Transmit Power

Regulations mean there is an upper limit for the power that a device can transmit on. Therefore any power setting P will be contained within the bounds

$$0 \leq P \leq P_{\max} < \infty.$$

Received Signal

Signal is the term we use to describe the signal strength received from a transmitter. It is determined by distance r, transmit power P_t, pathloss $g(r)$ and fading H. The equation for finding the signal strength S at distance r away from the transmitter is given by

$$S = P_t H g(r). \tag{1.3.3}$$

We assume that the signal S from a transmitter depends only on the distance r and not on the angle between transmitter and receiver: signals are broadcast in a radially symmetric fashion.

Interference

Interference refers to the received signal at a user device that does not come from the transmitter it is paired to. It can be thought of as unwanted signal. Let there be k transmitters a UE is not paired to and the unwanted signal from each be S_i, computed as in (1.3.3). The interference I at that UE is given by

$$I = \sum_{i=1}^{k} S_i. \tag{1.3.4}$$

Noise

Additive white Gaussian noise (AWGN) is the noise model widely used in telecommunications to mimic the effect of random processes that occur in the system that result in additional interference. In this thesis we represent noise with the symbol σ and take it to be constant throughout the system.

SINR

SINR stands for *signal to interference and noise ratio* and in the absence of noise it is simply referred to as SIR. It is an important and widely used Quality of Service (QoS) measure of a communication network's performance. In chapter 3 it is a measurement taken by receivers and communicated to their paired transmitter.

Equation (1.3.3) defined how the signal from a transmitter is calculated. We can use either equation (1.3.1) or (1.3.2) for the pathloss when calculating SINR.

The equation for SINR at a receiver i, where S_i is the signal from its paired transmitter, I_j is the unwanted signal received from transmitter T_j and σ is the noise, is

$$\text{SINR} = \frac{S_i}{\sum_{j \neq i} I_j + \sigma}, \tag{1.3.5}$$

and when $\sigma = 0$ this is called the SIR ratio. Additionally when the source of interference is mostly from other users, scaling the signal power also scales the interference by the same amount [68]. If for a receiver the SINR is too low then it would mean that a transmitter is unable to provide decodable signal to a receiver, resulting in a disruption of service. The likelihood of this happening is referred to as the outage probability.

Unless stated otherwise then the signal to interference ratio (SIR) or SINR when noise is considered is computed as in (1.3.5). If SINR is given in decibels

then this is computed as

$$\text{SINR } \mathbf{(dB)} = 10 \log_{10}(\text{SINR}). \tag{1.3.6}$$

Performance

In this thesis we use SINR to measure network performance. The higher the value of the SINR the better the connection quality. Optimal SINR network performance would be when each UE has the highest SINR possible for a given network configuration. Our aim in optimising SINR is to provide a good minimum standard of service rather than increase the maximum standard. Therefore improving and maintaining the minimum SINR in the network takes priority over achieving a high SIR for a minority.

In practice, achieving SINR optimisation is complicated by a lack of available information about the local network. The network should self-organise in a distributed way, i.e., without direct or indirect communication (e.g., relaying information via a central node). A transmitter will only have the SIR of its paired user devices; it will not know whether their minimum SIR is the network minimum and, by acting to increase their SIR, it could lower the SIR elsewhere in the network.

To increase SIR for paired user devices, a transmitter could provide more signal by increasing its transmit power. However this could result in increased interference and hence lower SIR elsewhere in the network. Figure 1-4 shows a non-optimal configuration of transmit powers. Consider the circumference of the discs to be where S falls below a set threshold.

Understanding the impact of changes, to configuration settings, on the local network will be critical for achieving optimal network performance. In Chapter 3 we show that a policy for setting transmit powers can be based solely on paired UE SINR observations. Additionally, in Chapter 4 we propose heuristics for estimating the distance to the nearest neighbour in the network, without requiring communication. This means the effects on SIR of configuration setting changes can be better understood, contributing to achieving desired network performance through distributed self-organisation.

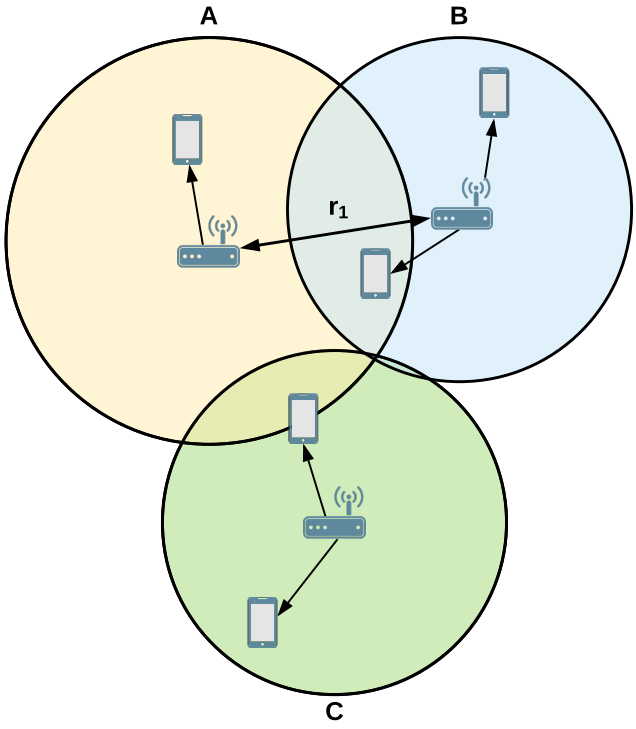

Figure 1-4: An example of a non-optimal configuration. The devices in the intersections A∩B and A∩C will have non-optimal SIRs due to interference from A. Reducing the signal strength, and hence coverage, of transmitter A would improve the SIR for those devices. The optimal signal strength for A could be informed by r_1, the distance to the nearest neighbour transmitter (B).

1.4 Mathematical Methodology

In this section we describe the mathematical methodology, as well as definitions and theorems, used in later chapters. Proofs of theorems, where included, are given in the appendices.

1.4.1 Efficient Generation of Transmitter Distances

In Chapters 3, 4 and 5 we simulate wireless communications networks. In Chapter 4 in particular, the ability to generate transmitter distances in an efficient, that is to say computationally fast, way is beneficial. This is due to the fact that it is necessary for us to generate a large number of sets of transmitters.

From [5] we understand that transmitter locations are assumed to be Poisson distributed for modelling purposes. Here we begin by defining a Spatial Poisson point process before describing the technique for efficiently generating transmitter distances from an origin.

We begin by defining a Poisson process which, as in [37], we define as follows.

Definition 1.1 (Poisson process)**.** *A Poisson process with intensity λ is a process $N = \{N(t) : t \geq 0\}$ taking values in the state space $S = \{0, 1, 2, \ldots\}$ such that:*

(a) $N(0) = 0$; *if* $s < t$ *then* $N(s) \leq N(t)$,

(b) $$\mathbf{P}\left[N(t+h) = n + m | N(t) = n\right] = \begin{cases} \lambda h + o(h) & \text{if } m = 1, \\ o(h) & \text{if } m > 1, \\ 1 - \lambda h + o(h) & \text{if } m = 0. \end{cases}$$

(c) if $s < t$, *the number* $N(t) - N(s)$ *of jumps in the interval* $(s, t]$ *is independent of the times of jumps during* $[0, s]$.

Since $N(t)$ is Poisson distributed with parameter λt, that is

$$\mathbf{P}[N(t) = j] = \frac{(\lambda t)^j}{j!} e^{-\lambda t}, \quad j \in \mathbb{Z}^+,$$

it follows that $\mathbf{E}[N(t)] = \lambda t$. Let the time of the nth arrival T_n be given by $T_n = \inf\{t : N(t) = n\}$. The *interarrival times* are given by $X_n = T_n - T_{n-1}$.

Theorem 1.1 (Interarrival times are exponentially distributed)**.** *The random variables $X_1, X_2, \ldots$ representing the interarrival times are independent and are exponentially distributed with parameter λ.*

Proof of this theorem is given in Section B.1 of Appendix B.

A Poisson point process is a random collection of points in which the number of points in an area Λ is distributed according to the $\mathsf{Poisson}(\lambda\Lambda)$ distribution with the number of points in disjoint sets independent. We define a Poisson point process as in [48].

Let $(X, \mathcal{X})$ be a measurable space. A measure ν on X is said to be s-finite if ν is a countable sum of finite measures.

Definition 1.2 (Poisson point process)**.** *Let λ be an s-finite measure on X. A Poisson process with intensity measure λ is a point process η on X with the two following properties:*

(i) For every $B \in \mathcal{X}$ the distribution of $\eta(B)$ is Poisson with parameter $\lambda(B)$, such that $\mathbf{P}[\eta(B) = k] = \mathsf{Poisson}(\lambda(B); k)$ $\forall k \in \mathbb{N}^+$.

(ii) For every $m \in \mathbb{N}$ and all pairwise disjoint sets $B_1, \ldots, B_m \in \mathcal{X}$ the random variables $\eta(B_1), \ldots, \eta(B_m)$ are independent.

We give a definition for a spatial Poisson point process below.

Definition 1.3 (Planar Poisson point process)**.** *A planar Poisson point process is a Poisson point process defined in the plane $\mathbf{R}^2$. For homogeneous Poisson point process with intensity λ and with $|\Lambda|$ the area of the region $\Lambda \subset \mathbf{R}^2$:*

(i) the probability of n points existing in Λ is given by

$$\mathbf{P}[N(\Lambda) = n] = \frac{(\lambda|\Lambda|)^n e^{-\lambda|\Lambda|}}{n!}$$

(ii) for finite integer $k \geq 1$, consider a collection of disjoint measurable sets $B_1, \ldots, B_k$ with the number of points in B_i written as $N(B_i)$. The finite-dimensional distribution is

$$\mathbf{P}[N(B_i) = n_i, i = 1, \ldots, k] = \prod_{i=1}^{k} \frac{(\lambda|B_i|)^{n_i}}{n_i!} e^{-\lambda|B_i|}.$$

From Theorem 5.1 in Chapter 5 of [48] we have the *mapping theorem* which we use to efficiently generate correctly distributed transmitter distances for the numerical simulations in this thesis. The theorem is as follows:

Theorem 1.2 (Mapping Theorem)**.** *Let ν be a point process on X with intensity measure λ and let $T : X \to Y$ be measurable. Then $T(\nu)$ is a point process with*

intensity measure $T(\lambda)$. If ν is a Poisson process, then $T(\nu)$ is a Poisson process too.

The proof, as given in [48], is in Section B.2 of Appendix B.

We note that when we map from the planar point process to the real line we go from a homogeneous Poisson point process to an inhomogeneous point process.

In practice, the Mapping theorem allows us to generate exponentially distributed random variables that we then "map" to variables that are Poisson distributed. We do this as follows: let λ be the intensity measure of the Poisson point process and then generate random variables x_i distributed $\sim \mathsf{Exp}(\frac{1}{\lambda\pi})$, exponentially with mean $\frac{1}{\lambda\pi}$. These exponential variables are then mapped to Poisson distributed variables by taking the square root of their cumulative sum. The distance to the kth point y_k is given by

$$y_k = \sqrt{\sum_{i=1}^{k} x_i}$$

where $x_i \in X \sim \mathsf{Exp}(\frac{1}{\lambda\pi})$.

Algorithm 1.1 Efficient Generation of Transmitter Distances

To generate the distances of N transmitters that are $\mathsf{Poisson}(\lambda|\Lambda|)$ distributed:
Generate N random variables x_i that are $\mathsf{Exponential}(\frac{1}{\lambda|\Lambda|})$ distributed.
Let y_k be the distance to the kth transmitter
while $k \leq N$ **do**
$y_k = \sqrt{\sum_{i=1}^{k} x_i}$

end while

This is more efficient than simulating a Poisson point process when only the distances (not the locations) are necessary. Where locations are required rather than just distances procedures such as those in [70] are used.

1.4.2 Reinforcement Learning

A Markov Decision Process (MDP) consists of a set of states S, a set of actions A, a set of transition probabilities P and a set of rewards R. A MDP has the Markov property in that it is memoryless, it is a decision process in that its purpose is to find a policy that determines which action to take (the decision) given the state.

Definition 1.4 (Markov Decision Process)**.** *A Markov decision process can be defined as a 4-tuple (S, A, P_a, R_a) where*

- *S is a set of states*
- *A is a set of actions*
- *$P_a[s, s'] \equiv \boldsymbol{P}[s_{t+1} = s' | s_t = s, a_t = a]$ is the probability that being in state s and taking action a at time t will result in being in state s' at time $t + 1$.*
- *$R_a(s, s')$ is the immediate reward received when action a causes a transition from state s to s'.*

In Chapter 3 we wish to find a policy for setting transmit powers so that an SINR based QoS metric is optimised. The problem to find a *policy* $\pi(s)$ that selects actions (transmit powers) relative to the state (observations of the network) so that the total received reward (a function of SINR) is maximised. In our problem the rewards, based on the change in SINR that results from taking an action of changing transmit power, will not be known. A MDP where the probabilities or rewards are unknown is a reinforcement learning problem.

In Figure 1-5 we show the structure of a reinforcement learning problem. From [71] we understand that the learner and decision maker, in our case the transmitters, is called the agent. What the agent interacts with is called the environment, which will be a wireless communications network. Reinforcement learning maps actions to situations so for any given situation an action is chosen that achieves a set goal. This mapping is referred to as a policy. When an action is chosen that moves the learner, also known as an *agent*, towards the goal this is reinforced by a numerical reward. A learner must discover what actions to take through a process of trial and error. The learner's aim is to maximise the total reward and manage the trade-off between exploitation (exploiting what has already been learned) and exploration (trying something new) [71].

Q-Learning

Figure 1-5 shows a reinforcement learning scheme and demonstrates that the actions chosen by the agent are determined by the policy $\pi(s)$ where s is the state. In Q-learning a look-up table, called the Q-table, is used to determine the policy $\pi(s)$. A Q-table gives the rewards associated with selecting an action a in state s. In a Q-table the states are the rows and the actions are the columns. The entry $Q(s, a)$ in the Q-table for selecting action a in state s is computed using the Q-function which we now describe.

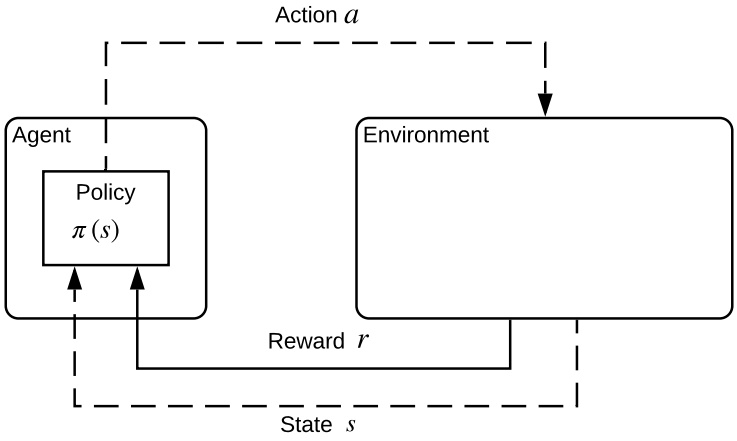

Figure 1-5: A reinforcement learning diagram showing that the policy determines an agent's action. This in turn can cause a change to the environment which determines the received reward and the resulting state of the agent.

At time t let s_t be the state, a_t be the action selected and r_t be the immediate reward received. The look-up table is updated using the Q-function.

$$Q^{new}(s_t, a_t) \leftarrow (1-\alpha) \cdot \underbrace{Q(s_t, a_t)}_{\text{old value}} + \underbrace{\alpha}_{\substack{\text{learning} \\ \text{rate}}} \overbrace{\left(\underbrace{r_t}_{\text{reward}} + \underbrace{\delta}_{\substack{\text{discount} \\ \text{factor}}} \cdot \underbrace{\max_a Q(s_{t+1}, a)}_{\substack{\text{estimate of optimal} \\ \text{future value}}} \right)}^{\text{learned value}} \tag{1.4.1}$$

The learning rate α determines to what extent new information overrides old. When $\alpha = 1$ then only the most recent information is considered and when $\alpha = 0$ only prior knowledge is used. Typically when a system is stochastic small α is used and when a system is deterministic $\alpha = 1$ is used. The discount factor δ determines the importance of future rewards. When $\delta = 0$ only immediate rewards are considered and when $\delta = 1$ long term rewards are given equal weighting as immediate rewards.

We work through a simple example to illustrate how this works in practice. Consider a system of two transmitters that have two transmit power options "high" H and "low" L and a set of receivers that pair to the highest signal and record SINR. We set our goal as having the average SINR be above a threshold value SINR_{Th}.

The agent is the pair of transmitters T_1 and T_2; the environment is the transmitters and the receivers. We wish to positively reinforce achieving an SINR

above the threshold and negatively reinforce having it be less than or equal to it. To do this we design the reward function as follows:

$$r_t = \begin{cases} +1 & \text{if SINR} > \text{SINR}_{Th}, \\ -1 & \text{if SINR} \leq \text{SINR}_{Th}. \end{cases} \tag{1.4.2}$$

Let the state of the system be the transmit powers of T_1 and T_2 and the SINR at the receivers. The set of states is

$$S = \{(H, L, \text{SINR}), (H, H, \text{SINR}), (L, H, \text{SINR}), (L, L, \text{SINR})\}.$$

There are four actions that the agent can take, these are to set the transmit powers P_1 and P_2 of T_1 and T_2 respectively. The set of actions is

$$A = \{P_1 \to H, P_1 \to L, P_2 \to H, P_2 \to L\}.$$

We initially set all values in the Q-table to be 0 and where an action is not possible from a given state we mark the square with —. Table 1.1 shows this initial Q-table.

States	Actions			
(P_1, P_2, SINR)	$P_1 \to H$	$P_1 \to L$	$P_2 \to H$	$P_2 \to L$
(H, L, SINR)	—	0	0	—
(H, H, SINR)	—	0	—	0
(L, H, SINR)	0	—	—	0
(L, L, SINR)	0	—	0	—

Table 1.1: The initial Q-table.

Before we can compute the entry for the Q-table using the Q-function we must set the learning rate α and the discount factor δ. As our system is deterministic we set that $\alpha = 1$. We set that $\delta = 1$ so that future rewards get the same weighting as immediate rewards. This is to allow for transitioning through a worse state to get to a better one. This gives the Q-function as

$$Q(s_t, a_t) = r_t + \max_a Q(s_{t+1}, a) \tag{1.4.3}$$

To begin the Q-learning we must select a state for the agent to begin in. We set that $P_1 = L, P_2 = L$ and pair the receivers according to highest received signal. We set that noise is a constant through the system and calculate the average SINR. We find that the value of the average SINR $= E$ and so the state

we begin in is (L, L, E). From this state there are two actions which can be taken: $P_1 \rightarrow H$ and $P_2 \rightarrow H$. We have equal probability of picking each and we select the action $P_1 \rightarrow H$.

When $P_1 = H$ and $P_2 = L$ the value of the average SINR $= B$ and $B <$ SINR_{Th}; therefore the immediate reward is $r = -1$. In state (H, L, B) all entries in the associated Q-table row are 0 and therefore

$$\begin{aligned} Q(s_0 = (L, L, E), a_0 = P_1 \rightarrow H) &= -1 + \max_a Q((H, L, B), a) \\ &= -1 + 0 \end{aligned} \tag{1.4.4}$$

We update our Q-table accordingly, which is Table 1.2. We are now in state

States	Actions			
(P_1, P_2, SINR)	$P_1 \rightarrow H$	$P_1 \rightarrow L$	$P_2 \rightarrow H$	$P_2 \rightarrow L$
(H, L, B)	—	0	0	—
(H, H, SINR)	—	0	—	0
(L, H, SINR)	0	—	—	0
(L, L, E)	-1	—	0	—

Table 1.2: The Q-table after the first update.

(H, L, B) and have two actions to choose from, $P_1 \rightarrow L$ and $P_2 \rightarrow H$. We are equally likely to select each action. We select the action $P_2 \rightarrow H$. As before we compute the average SINR in this state and determine the immediate reward. We find that SINR $= C$ and the value $C >$ SINR_{Th}, therefore the reward $r_1 = +1$. We compute the entry to update the Q-table.

$$\begin{aligned} Q(s_1 = (H, L, B), a_0 = P_2 \rightarrow H) &= +1 + \max_a Q((H, H, C), a) \\ &= +1 + 0 \end{aligned} \tag{1.4.5}$$

Updating the Q-table gives Table 1.3.

States	Actions			
(P_1, P_2, SINR)	$P_1 \rightarrow H$	$P_1 \rightarrow L$	$P_2 \rightarrow H$	$P_2 \rightarrow L$
(H, L, B)	—	0	+1	—
(H, H, C)	—	0	—	0
(L, H, SINR)	0	—	—	0
(L, L, E)	-1	—	0	—

Table 1.3: The Q-table after the second update.

We are now in state (H, H, C). We continue to interact with the system and

update the Q-table accordingly. In the course of interactions it is found that when $P_1 = L$ and $P_2 = H$ the value of the average SINR $= D$ and $D < \text{SINR}_{Th}$. After 17 iterations the Q-table is as shown in Table 1.4.

States	Actions			
(P_1, P_2, SINR)	$P_1 \to H$	$P_1 \to L$	$P_2 \to H$	$P_2 \to L$
(H, L, B)	—	-1	+1	—
(H, H, C)	—	0	—	0
(L, H, D)	+1	—	—	-1
(L, L, E)	0	—	0	—

Table 1.4: The Q-table after 17 updates.

The Q-table has converged to the action-values shown in Table 1.4 and further updates will not alter them. For example start in state (H, H, C), select action $P_1 \to L$, the immediate reward $r_{18} = -1$, the $\max_a Q((L, H, D), a) = +1$ and so $Q((H, H, C), P_1 \to L) = 0$ as before.

In our example the action-values are discrete and we repeatedly visit every state and try each action. Following the description of Q-learning in [80] it is proved in [81] that "Q-learning converges to the optimum action-values with probability 1 so long as all actions are repeatedly sampled in all states and the action-values are represented discretely". In our example these requirements are met and Q-learning converges to an optimal policy. The values in Table 1.4 are the optimum action-values and determine an optimal policy, showing which action to choose in each state.

Figure 1-6 shows the action-value of transitioning into a given state and the possible transitions between states. Each state is represented in the figure by the transmit powers P_1, P_2 of the two transmitters. The only state in which $\text{SINR} > \text{SINR}_{Th}$ is H, H. From any state the optimal action is the one with the highest value and should be selected. Actions with the same value are equally optimal.

A limitation of Q-learning is the requirement to store the look-up table. Therefore for large state spaces this becomes computationally intractable and deep Q-learning addresses this problem.

Deep Q-Learning

Deep Q-learning is an adaptation of Q-learning which uses function approximation so that it is not necessary to store and complete a look-up table using the Q-function. The advantage of this is that it allows for large state and action

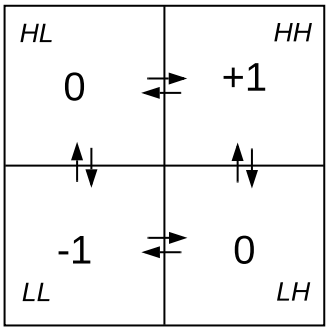

Figure 1-6: The values of the different system states learnt through Q-Learning. HH is the only state in which SINR $>$ SINR$_{Th}$.

spaces, that would have been too large for conventional Q-learning, to be used.

For the function approximation we use an Artificial Neural Network (ANN). ANNs are widely used for nonlinear function approximation. An ANN is so named as it is a network of interconnected nodes that have some of the properties of neurons, the main components of nervous systems [71].

The nodes compute a weighted sum of their input signals. To this they apply a nonlinear function, called the *activation function*, to produce the node's output which is referred to as its activation. For the activation function we use three different functions $g(x) = \tanh(x)$, the rectifier nonlinearity $g(x) = \max(0, x)$ and the sigmoid function $g(x) = (1 + e^{-x})^{-1}$. Figure 1-7 is a diagram of a node that shows the input function, activation function and output activation. The nodes in the input layer are different from the others in that their activations are the externally supplied values that are the inputs to the function the network is approximating [71].

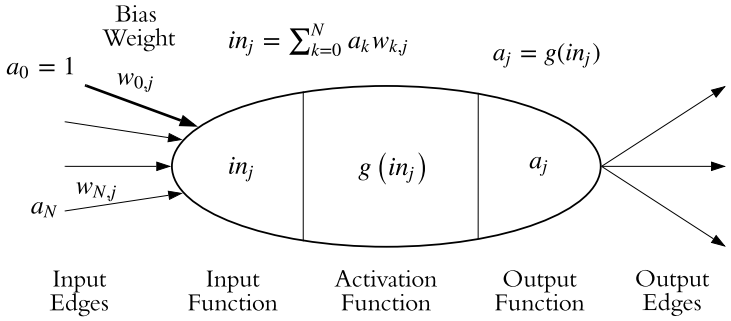

Figure 1-7: This diagram of a node in an ANN shows the input, activation function and activation.

An ANN is structured with multiple layers of these neuron-like nodes connected by edges, which can be directed. Every ANN will have an input and an output layer as well as at least one hidden layer. A hidden layer is simply a layer that is neither an input or output layer. The term "deep" in deep Q-learning indicates that an ANN with more than one hidden layer is used for the function approximation. If only one hidden layer is present in an ANN then it is referred to as shallow [34].

Figure 1-8 shows a generic feedforward ANN with one hidden layer. A feedforward ANN is one with no loops in the network so there are no paths by which a node's output can influence its input. If an ANN has even one loop then it is called a recurrent ANN. We use only the simpler feedforward networks.

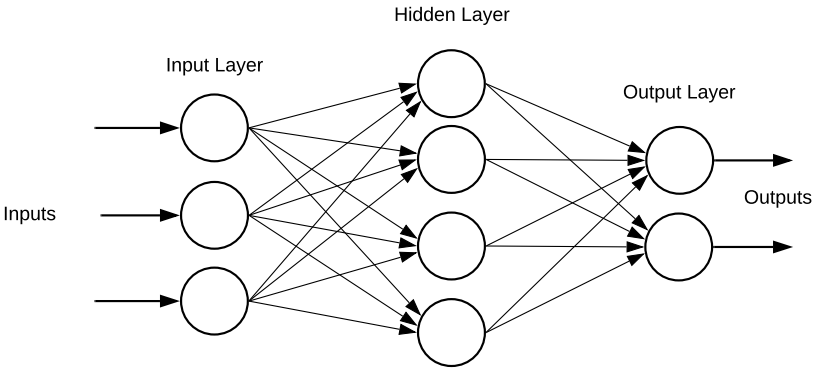

Figure 1-8: This is a generic feed-forward ANN with a single hidden layer. The circles represent the nodes.

The ANN we have described, given a current state, will approximate the Q-values of different actions. Let $Q(s, a; \theta)$ be the Q-function with parameters θ, with θ the set of weights in the neural network, that approximates these values. We aim to learn the parameters θ such that the optimal Q-function $Q^*(s, a) \approx Q(s, a; \theta)$. For the parameters θ_{i-1} the action value

$$Q(s_t, a_t; \theta_{i-1}) = \sum_{r_t, s_{t+1}} \mathbf{P}[r_t, s_{t+1} | s_t, a_t, \theta_{i-1}] \left(r_t + \gamma \max_a Q(s_{t+1}, a; \theta_{i-1}) \right). \quad (1.4.6)$$

The parameters are learnt by iteratively minimising a sequence of i functions of the parameters $L_i(\theta_i)$ defined as

$$L_i(\theta_i) = \sum_{s_t, a_t} \mathbf{P}[s_t, a_t] \left(Q(s_t, a_t; \theta_{i-1}) - Q(s_t, a_t; \theta_i) \right)^2. \quad (1.4.7)$$

The function (1.4.7) is called the loss function. It gives the mean squared error

of the action value following an update of the parameters (ANN weights).

Figure 1-9 shows a deep Q-learning scheme. We recognise that it is the same as the reinforcement learning scheme shown in Figure 1-5 except that an ANN determines the policy. We implement deep Q-learning in Chapter 3 to learn a

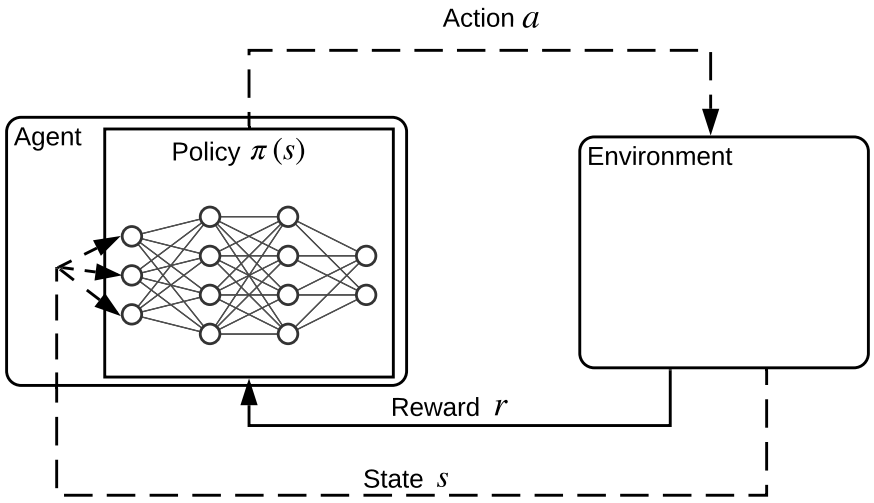

Figure 1-9: A deep Q-learning scheme where the policy is determined by a deep ANN.

policy for setting transmit powers so that a network QoS metric is improved. In that chapter we also apply a further reinforcement learning method known as Advantage Actor Critic which allows a continuous action space to be used.

1.4.3 Method of Moments

We use this method in Chapter 5 to improve the accuracy of transmitter distance estimations. The method of moments was introduced in 1887 by the Russian mathematician Pafnuty Chebyshev [17] [74]. It allows population parameters $\boldsymbol{\theta} = \{\theta_1, \ldots, \theta_k\}$ to be estimated by equating population sample values to population distribution moments given in terms of $\boldsymbol{\theta}$. This uses the Law of Large Numbers (LLN) which states that for a sequence of independent identically distributed random variables $X_1, X_2, \ldots, X_n$ with finite means μ then $\overline{X_n} = \frac{1}{n}\sum_{i=1}^{n} X_i \rightarrow \mu$ as $n \rightarrow \infty$. Therefore for a large sample size, a large n, the distributional mean $\mu = f(\boldsymbol{\theta})$ should be well approximated by the sample mean $\overline{X_n}$. The approximated population parameters, the method of moment estimators, are denoted by $\hat{\boldsymbol{\theta}} = \{\hat{\theta_1}, \ldots, \hat{\theta_k}\}$ and we write $\overline{X_n} = f(\hat{\boldsymbol{\theta}})$.

The number of such equations, such distribution moments, is the same as the number k of population parameters to be estimated. The steps, as presented in [82], to obtain k method of moment estimators are as follows:

Procedure 1.1 (Method of Moments)**.** *Estimate the parameters of a distribution by computing the sample moments.*

1. *For a model with k parameters compute functions for the first k moments*

$$\mu_1 = f_1(\theta_1, \ldots, \theta_k), \quad \ldots, \quad \mu_k = f_k(\theta_1, \ldots, \theta_k) \tag{1.4.8}$$

   such that we obtain equations for the first k moments in terms of k unknowns.

2. *Solve, if possible, these equations to obtain the k parameters in terms of the moments*

$$\theta_1 = g_1(\mu_1, \ldots, \mu_k), \quad \ldots, \quad \theta_k = g_k(\mu_1, \ldots, \mu_k) \tag{1.4.9}$$

3. *Take a sample $\boldsymbol{X} = \{X_1, \ldots, X_n\}$ of size n from the data and from this compute the first k sample moments,*

$$\overline{X} = \frac{1}{n}\sum_{i=1}^{n} X_i, \quad \ldots, \quad \overline{X^k} = \frac{1}{n}\sum_{i=1}^{n} X_i^k, \tag{1.4.10}$$

4. *Replace distribution moments μ_i with sample moments $\overline{X^i}$,*

$$\hat{\theta}_1(\boldsymbol{X}) = g_1(\overline{X}, \ldots, \overline{X^k}), \quad \ldots, \quad \hat{\theta}_k(\boldsymbol{X}) = g_k(\overline{X}, \ldots, \overline{X^k}) \tag{1.4.11}$$

   to obtain the ***method of moment estimators*** $\hat{\boldsymbol{\theta}} = \{\hat{\theta}_1, \ldots, \hat{\theta}_k\}$.

Step 3 uses the LLN for approximating the sample moments, therefore a larger sample should result in greater accuracy.

Reduced Sampling

High variability is likely to be encountered for higher sample moments (moments greater than the fourth), therefore their use is treated with suspicion [8]. Additionally, for a large number of parameters finding a solution to the system of equations (1.4.9) becomes less tractable and Step 2 of Procedure 1.1 may not be possible. Reducing the sample, in such a way that we reduce the number of

parameters to be estimated, allows for tractability and reliability to be recovered. It requires that a relationship between parameters and sample values can be assumed, so that a subsample can be taken where values relate only to chosen parameters. This is applied in Section 5.4 of Chapter 5.

1.4.4 The Master Equation

We now describe the methods and theory used in Chapter 2. We define a Wiener process and a stochastic differential equation (SDE) as follows.

Definition 1.5 (Wiener Process)**.** *A Wiener process* $\{W(t) : t \in \mathbb{R}^+\}$ *has the characteristic properties*

1. $W_0 = 0$ *a.s.*
2. W *has independent increments: for every* $t > 0$*, the future increments* $W_{t+u} - W_t$*,* $u \geq 0$*, are independent of the past values* W_s $s < t$*.*
3. W *has Gaussian increments:* $W_{t+u} - W_t$ *is normally distributed with mean* 0 *and variance* u*,* $W_{t+u} - W_t \sim \mathcal{N}(0, u)$*.*
4. W *has continuous paths: with probability* 1*,* W_t *is continuous in* t*.*

Definition 1.6 (Stochastic Differential Equation)**.** *The stochastic differential equation for the* n*-variable vector* $\boldsymbol{x}(t)$ *can be defined as*

$$d\boldsymbol{x}(t) = \boldsymbol{f}\left(\boldsymbol{x}(t), t\right) dt + \boldsymbol{M}\left(\boldsymbol{x}(t), t\right) d\boldsymbol{W}(t), \quad t \geq 0, \tag{1.4.12}$$

where $\boldsymbol{f} : \mathbb{R}^n \times \mathbb{R}^+ \to \mathbb{R}^n$*,* $\boldsymbol{M} : \mathbb{R}^n \times \mathbb{R}^+ \to \mathbb{R}^{n \times n}$ *and* $\boldsymbol{W}(t)$ *is a* n*-variable Wiener process.*

An SDE can describe the evolution of a Markov jump process, which is as defined below:

Definition 1.7 (Markov Jump Process)**.** *A Markov Jump Process is a continuous time, discrete space stochastic process. We consider a jump as being a system state change. Let* $\boldsymbol{n}$ *and* $\boldsymbol{n}'$ *be two distinct states the system can occupy. The time evolution of the probability* $\mathbf{P}[\boldsymbol{n}, t + \Delta t | \boldsymbol{n}', t]$ *is described by*

$$\lim_{\Delta t \to 0} \frac{\mathbf{P}[\boldsymbol{n}, t + \Delta t | \boldsymbol{n}', t]}{\Delta t} = T(\boldsymbol{n} | \boldsymbol{n}') \tag{1.4.13}$$

with $T(\boldsymbol{n}|\boldsymbol{n}')$ *the rate of transition from state* $\boldsymbol{n}'$ *to state* $\boldsymbol{n}$*.*

A master equation can describe a continuous time Markov process such as a Markov jump process.

Definition 1.8 (Master Equation)**.** *A master equation describes the time evolution of the probability that a system with discrete state space will be in a given state relative to the time variable t. A common representation is as follows*

$$\frac{d\vec{P}}{dt} = \boldsymbol{A}(t)\vec{P} \tag{1.4.14}$$

where $\vec{P}$ is the vector of the different system state probabilities and $\boldsymbol{A}(t)$ is the matrix of transition rates.

We now describe the Method of Kurtz which we use in Chapter 2 to represent a Markov jump process as an SDE.

1.4.5 Method of Kurtz

Originally developed to model chemical reactions, but we will use it in a different context, we present the method of Kurtz as in [88]. We begin by describing a Markov jump process in which each event causes the vector $\mathbf{n} \in \mathbb{N}^3$ to jump according to a jump vector $\mathbf{s} \in \mathbb{Z}^3$. The stochastic rate $\tilde{r}(\mathbf{n}, \mathbf{s})$ (or $r(\mathbf{x}, \mathbf{s})$ with $\mathbf{x} := \mathbf{n}/N$) at which the jumps $\mathbf{n} \to \mathbf{n} + \mathbf{s}$ take place are the jump rates. We note that $\tilde{r}(\mathbf{n}, \mathbf{s}) = r(\mathbf{x}, \mathbf{s})$. The sum of the components $\mathbf{n}$ is the overall size N of the system which is assumed to be constant. The finite collection of possible jumps $\mathbf{s}$ is denoted by the stoichiometric matrix $\mathbf{S}$ and the corresponding jump rates are summarised into a vector $\mathbf{r}(\mathbf{x})$. The kth column of $\mathbf{S}$, $\mathbf{s}_k$, corresponds to the kth element, r_k, of the vector $\mathbf{r}(\mathbf{x})$ and $\tilde{r}_k$ of the vector $\mathbf{r}(\mathbf{n})$.

The first step in the method of Kurtz [46] is to represent the Markov jump process as

$$\mathbf{n}(t) = \mathbf{n}(0) + \sum_{\mathbf{s}_k \in \mathbf{S}} \mathbf{s}_k \mathbb{P}^{(\mathbf{s}_k)} \left(\int_0^t N \tilde{r}_k d\tau \right). \tag{1.4.15}$$

where $\{\mathbb{P}^{(\mathbf{s})}(\xi) : \xi \geq 0\}$ is a collection of independent rate 1 Poisson processes [6] and r_k which is the kth element of $\mathbf{r}(\mathbf{x})$ describes the density dependent rate in the Markov system. Dividing by N gives:

$$\boldsymbol{x}(t) = \boldsymbol{x}(0) + \sum_{\boldsymbol{s}_k \in \boldsymbol{S}} \frac{1}{N} \boldsymbol{s}_k \mathbb{P}^{(\boldsymbol{s}_k)} \left(\int_0^t N r_k d\tau \right). \tag{1.4.16}$$

The Poisson process here can be approximately written in the form:

$$\mathbb{P}^{(s)}(t) \approx t + W(t), \tag{1.4.17}$$

where $W(t)$ is a Wiener process. Replacing each Poisson process $\mathbb{P}^{(\boldsymbol{s}_k)}(t)$ with $t + W^{(\boldsymbol{s}_k)}(t)$ in (1.4.16) gives the equation:

$$\boldsymbol{x}(t) = \boldsymbol{x}(0) + \int_0^t \left(\sum_{\boldsymbol{s}_k \in \boldsymbol{S}} \boldsymbol{s}_k r_k \right) d\tau + \sum_{\boldsymbol{s}_k \in \boldsymbol{S}} \boldsymbol{s}_k \frac{1}{N} W^{(\boldsymbol{s}_k)} \left(\int_0^t N r_k d\tau \right), \tag{1.4.18}$$

and so the $\boldsymbol{x}(t)$ satisfies a stochastic differential equation of the form:

$$d\boldsymbol{x}(t) = \left(\sum_{\boldsymbol{s}_k \in \boldsymbol{S}} \boldsymbol{s}_k r_k \right) dt + \frac{1}{\sqrt{N}} \sum_{\boldsymbol{s}_k \in \boldsymbol{S}} \boldsymbol{s}_k \sqrt{r_k} dW^{(\boldsymbol{s}_k)}(t). \tag{1.4.19}$$

1.4.6 Gillespie Stochastic Simulation Algorithm

The **Gillespie Algorithm** [33] is the classical stochastic simulation algorithm (SSA) for the stochastic modelling of chemical reactions. In contrast to ODEs, the Gillespie algorithm allows a discrete and stochastic simulation of a system with few reactants because reactions are explicitly simulated.

Procedure 1.2 (Gillespie Algorithm)**.** *The algorithm consists of the following steps:*

1. *Initialisation: Set* $t = 0$*, define reaction constants, and set initial population numbers.*
2. *Generate random numbers to determine the next reaction to occur and the time interval.*
3. *Update: increase the time by the randomly generated variable. Update population count based on the reaction that occured.*
4. *Iterate: return to step 2 unless simulation time is exceeded, number of reactions is exceeded or population is 0.*

1.4.7 Power Spectral Density

The Power Spectral Density (PSD) describes how the power of a signal (or time series) is distributed over frequency. Therefore computing the PSD will help to identify whether the signal has obvious periodic or quasi-periodic components.

This means that we can use it to investigate oscillations about equilibrium. We look at two methods of computing the PSD, the first method takes the discrete Fourier transform of a time series. The second method shows that for linear constant coefficient SDEs the PSD can be computed theoretically near a stable equilibrium point of the ODEs.

Computing the Discrete Fourier Transform

We compute the PSD of a signal by taking the discrete Fourier transform (DFT). We begin by defining the energy of a continuous-time signal.

Definition 1.9 (Energy)**.** *The energy E of a continuous-time signal $x(t)$ is*

$$E = \int_{-\infty}^{\infty} |x(t)|^2 dt. \tag{1.4.20}$$

When the total amount of energy is finite and the signal $x(t)$ is pulse-like (i.e. takes place in a fixed time window) we can use Parseval's theorem to express E in terms of frequency, rather than in terms of time as above. This relates the representation of energy in the time domain to that in the frequency domain.

Theorem 1.3 (Parseval's Theorem)**.** *We have that*

$$\int_{-\infty}^{\infty} |x(t)|^2 dt = \int_{-\infty}^{\infty} |\tilde{x}(f)|^2 df, \tag{1.4.21}$$

where $\tilde{x}(f) = \int_{-\infty}^{\infty} x(t) e^{-2\pi i f t} dt$ is the Fourier transform of the signal $x(t)$.

The angular frequency $\omega = 2\pi f$ and from (1.4.21) we find that, where we define the Fourier transform $\hat{x}(\omega)$ as

$$\hat{x}(\omega) = \tilde{x}\left(\frac{\omega}{2\pi}\right) = \int_{-\infty}^{\infty} x(t) e^{-i\omega t} dt \tag{1.4.22}$$

then

$$\int_{-\infty}^{\infty} |x(t)|^2 dt = \frac{1}{2\pi} \int_{-\infty}^{\infty} |\hat{x}(\omega)|^2 d\omega \tag{1.4.23}$$

and so we can also give the energy E from (1.4.20) in terms of angular frequency,

$$E = \frac{1}{2\pi} \int_{-\infty}^{\infty} |\hat{x}(\omega)|^2 d\omega. \tag{1.4.24}$$

Definition 1.10 (Energy Spectral Density)**.** *The Energy Spectral Density (ESD) describes how the energy E of a continuous-time signal $x(t)$ is distributed with*

frequency f or angular frequency ω. It is defined as

$$E(f) = |\tilde{x}(f)|^2 \quad or \quad E(\omega) = \frac{1}{2\pi}|\hat{x}(\omega)|^2. \tag{1.4.25}$$

When we consider continuous stochastic stationary signals over all time it is necessary for us to consider the power rather than the energy, which can be infinite. Power is the energy per unit time and therefore a stationary signal may have infinite energy but finite power. Using our definition of energy from (1.4.20) we define power as follows.

Definition 1.11 (Power)**.** *The average power P of a continuous-time signal $x(t)$ over all time is*

$$P = \lim_{T\to\infty} \frac{1}{T} \int_0^T |x(t)|^2 dt, \tag{1.4.26}$$

when the limit exists.

The ESD describes how the finite energy of a signal is distributed with frequency. The power spectral density (PSD) describes how the power of a signal that may have infinite energy is distributed with frequency. The PSD aims to represent a stochastic process not as a single realisation but averaged over multiple realisations, giving the expectation. As with ESD, to find the PSD of a continuous-time signal $x(t)$ we need to compute the Fourier transform $\hat{x}(\omega)$ of $x(t)$. As this may not exist for some signals (those with infinite energy) we work with the truncated Fourier transform [60], where signal is integrated over the finite interval $[0, T]$:

$$\hat{x}_T(\omega) = \int_0^T x(t)e^{-i\omega t} dt \tag{1.4.27}$$

which is the amplitude spectral density. We then adapt Parseval's Theorem as given in (1.4.23) to write the power P as given in (1.4.26) as

$$P = \lim_{T\to\infty} \frac{1}{2\pi T} \int_0^T |\hat{x}_T(\omega)|^2 d\omega. \tag{1.4.28}$$

We use this expression of power to define the PSD in terms of angular frequency.

Definition 1.12 (Power Spectral Density)**.** *The power spectral density (PSD), denoted by $\mathcal{P}(\omega)$, describes the distribution of power with angular frequency ω. It is defined as*

$$\mathcal{P}(\omega) = \lim_{T\to\infty} \frac{1}{2\pi T}|\hat{x}_T(\omega)|^2. \tag{1.4.29}$$

The time variable t and frequency variable ω are continuous in the above definition. When a time series is discrete and finite it is appropriate to use the

discrete Fourier transform (DFT) in place of the Fourier transform. When t, and therefore ω, are discrete such that we have N samples taken at Δt sampling intervals, this gives $T = N\Delta t$. Then there are N frequencies we can evaluate our time series at, these are given by

$$\omega_k = \frac{2\pi k}{N\Delta t} \quad \text{for} \quad k = 0, \ldots, N-1. \tag{1.4.30}$$

For the angular frequency ω_k, where x_m is the mth observation of the time series and $t = m\Delta t$, the truncated Fourier transform $\hat{x}_T(\omega_k)$ is replaced by

$$\begin{aligned} \hat{x}_T(\omega_k) \to y(\omega_k) &= \sum_{m=0}^{N-1} x_m e^{-i\omega_k m\Delta t}\Delta t. \\ &= \sum_{m=0}^{N-1} x_m e^{\frac{-i2\pi mk}{N}}\Delta t. \end{aligned} \tag{1.4.31}$$

Therefore the corresponding discretised expression for the PSD of a discrete and finite time series with N samples taken at Δt sampling intervals is given by

$$\mathcal{P}(\omega_k) = \lim_{T\to\infty} \frac{1}{2\pi T}|y(\omega_k)|^2, \tag{1.4.32}$$

where ω_k and $y(\omega_k)$ are as given in (1.4.30) and (1.4.31) respectively. It is common to write the DFT in the form

$$X_k = \sum_{m=0}^{N-1} x_m e^{-\frac{2\pi imk}{N}} \quad \text{for} \quad k = 0, \ldots, N-1 \tag{1.4.33}$$

in which case we would define

$$\mathcal{P}(\omega_k) = \lim_{T\to\infty} \frac{\Delta t^2}{2\pi T}|X_k|^2. \tag{1.4.34}$$

Computing the Spectrum Matrix

The second method of finding the PSD of a signal we give is to describe the system as a stochastic differential equation (SDE) and then compute the spectrum matrix $\boldsymbol{\mathcal{P}}(\omega)$. To compute the spectrum matrix we begin by defining a multivariate Ornstein-Uhlenbeck process in terms of an SDE as in [31]:

Definition 1.13 (Multivariate Ornstein-Uhlenbeck Process)**.** *We define this process by the linear stochastic differential equation*

$$d\boldsymbol{x}(t) = \boldsymbol{C}\boldsymbol{x}(t)dt + \boldsymbol{D}d\boldsymbol{W}(t), \tag{1.4.35}$$

where $\boldsymbol{C}$ *and* $\boldsymbol{D}$ *are constant matrices and the solution to* (1.4.35) *is*

$$\boldsymbol{x}(t) = e^{\boldsymbol{C}t}\boldsymbol{x}(0) + \int_0^t e^{\boldsymbol{C}(t-t')}\boldsymbol{D}d\boldsymbol{W}(t'). \tag{1.4.36}$$

We define the autocorrelation function as given in [73],

Definition 1.14 (Autocorrelation Function)**.** *Let* $x(t)$ *be a stationary stochastic process, then we define the autocorrelation* $G(\tau)$ *of the process as:*

$$G(\tau) = \lim_{T\to\infty} \frac{1}{T}\int_0^T x(t)x(t+\tau)dt. \tag{1.4.37}$$

As an Ornstein-Uhlenbeck process has a stationary solution [31] its autocorrelation function can be given in terms of its stationary covariance matrix $\boldsymbol{\sigma}$ and constant matrix $\boldsymbol{C}$ as follows:

$$\boldsymbol{G}(\tau) = \begin{cases} \exp(\tau\boldsymbol{C})\boldsymbol{\sigma} & \text{if } \tau \geq 0; \\ \boldsymbol{\sigma}\exp(-\tau\boldsymbol{C}^{\boldsymbol{T}}) & \text{if } \tau < 0. \end{cases} \tag{1.4.38}$$

Where $\boldsymbol{C}$ is the same as in (1.4.35) and $\boldsymbol{C\sigma} + \boldsymbol{\sigma C} = \boldsymbol{D}\boldsymbol{D}^{\mathrm{T}}$ with $\boldsymbol{D}$ from (1.4.35).

The Wiener-Khinchin theorem relates the autocorrelation function to the power spectral density by use of the Fourier transform. From [84] and [43] we get

Theorem 1.4 (Wiener-Khinchin Theorem)**.** *The Power Spectral Density of the stochastic process* $x(t)$ *is the Fourier Transform of its autocorrelation function*

$$\mathcal{P}(\omega) = \frac{1}{2\pi}\int_{-\infty}^{\infty} \mathrm{e}^{-i\omega\tau}G(\tau)d\tau \tag{1.4.39}$$

where the autocorrelation function $G(\tau)$ *of* $x(t)$ *is as defined in* (1.4.38)*.*

Proof of this theorem is in Section A.1 of Appendix A.

We use the formula for the autocorrelation function of an Ornstein-Uhlenbeck process given in (1.4.38) in the Wiener-Khinchin Theorem. This gives that the spectrum matrix of an Ornstein-Uhlenbeck process can be computed directly :

Theorem 1.5 (Spectrum Matrix in Stationary State)**.** *The spectrum matrix* $\mathcal{P}(\omega)$ *of a multivariate Ornstein-Uhlenbeck process as defined above is given by*

$$\boldsymbol{\mathcal{P}}(\omega) = \frac{1}{2\pi}(\mathbf{C} - i\omega\mathbf{I})^{-1}\mathbf{D}\mathbf{D}^{\mathbf{T}}(\mathbf{C} - i\omega\mathbf{I})^{-\dagger} \tag{1.4.40}$$

with $-\dagger$ *denoting the inverse conjugate transpose.*

Proof of this theorem, as given in [31] and [88], is in Section A.2 of Appendix A.

Chapter 2

Three Competing Self-Organisation Objectives

In this chapter we consider the dynamics of a wireless network that is aiming to satisfy three potentially competing aims through self-organisation. These three aims are: to raise the minimum SINR, to increase signal coverage and to improve energy efficiency. We explore the system dynamics that arise whilst these three potentially competing aims are worked on. Our major simplification is that spatial effects are not incorporated: all transmitters interfere with all others but can vary their transmit power levels.

To justify our mean field approach to this problem we note that SINR and coverage will be measured by user devices that pair to the transmitter providing the strongest signal. We make two assumptions: firstly that the transmitters are dense and secondly that the user devices are mobile and move randomly through the dense network of transmitters. Therefore the spatial effects can be disregarded and the transmitters considered interchangeable. Energy efficiency is counted across all transmitters and so all transmitters are interchangeable when optimising this.

To do this we use methods more commonly associated with modelling species interactions and predator-prey models.

2.1 Problem Formulation

We consider a wireless communication network consisting of N transmitters, where we take N to be large. The dynamics are assumed independent from the spatial configuration or distribution of transmitter locations. Each transmitter has a choice of three available power settings, high **H**, low **L** and off **O**. Our

competing policy aims are: (i) reduce total power consumption by the network, (ii) provide complete coverage to the underlying region, and (iii) increase SINR as far as possible. A higher power setting consumes more energy yet increases coverage. From the introduction we understand that the impact on SINR of changing transmit power is dependent on the spatial configuration and transmit powers of the other transmitters in the network. For simplicity, we do not consider spatial configuration but assume that SINR will be improved if a pair of transmitters change from having the same to different transmit powers. This assumption is explored in Chapter 3 which looks at optimising transmit powers.

We select at random a pair of transmitters from our network and examine their settings. It follows from the above that for any pair of transmitters there are six states they could be in regarding their power settings: **OO**, **OL**, **OH**, **HH**, **LH** and **LL**. Three of these states **OO**, **OL** and **LL** are not considered to contribute to the three optimisation aims. From [14] we understand that the significant investment incurred to provide additional transmitter capability means that available resources would not go unused. Therefore **HH** would always be chosen in place of **LL**, **LH** in place of **OL** and **OH** in place of **OO**. As a result once the states **LL**, **OL** and **OO** are transitioned out of they are not returned to; therefore, we do not consider them part of our dynamical system.

We wish to derive the ODEs that comprise the mean-field description of the system dynamics. Our derivation begins with the stochastic process underlying the dynamics and our notation follows [6], [23] and [53]. As previously stated, we have a collection of N transmitters, where each transmitter is in one of three states H, L or O. The system evolves stochastically, through a set of processes which involve pairs of sites. Pairs of sites evolve stochastically and independently of other pairs of sites according to the following rules:

$$OH \xrightarrow{\alpha} HH \tag{2.1.1}$$

$$LH \xrightarrow{\beta} OH \tag{2.1.2}$$

$$HH \xrightarrow{\gamma} LH \tag{2.1.3}$$

In each transmitter pairing one transmitter has power setting H. Equation (2.1.1) shows that the second transmitter transitions from state O to H at rate α, it would do this aiming to improve coverage. Equation (2.1.2) shows that to reduce energy consumption it transitions from state L to O at rate β and (2.1.3) shows that to improve SINR it changes from H to L at rate γ. Figure 2-1 illustrates the interaction of these three optimisation objectives on the state of a transmitter

power pairing. It also illustrates that once the states **LL**, **OL** and **OO** are transitioned out of they are not returned to and further to this they lead to the three states we do consider.

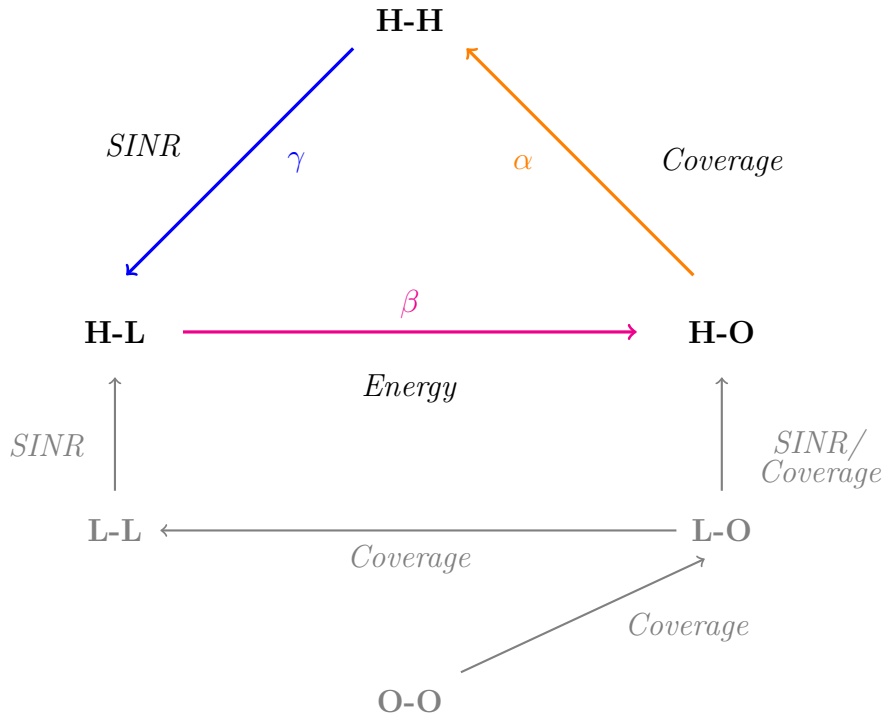

Figure 2-1: A possible interaction of the three objectives: SINR, Energy and Coverage. One of the transmitters is set to H and the second transmitter reacts accordingly to achieve each of the three objectives selfishly (competitive rather than cooperative). The respective rates of change for each of the objectives are given by α, γ, β. It also shows in grey the interaction of the three transient states that lead to the three recurrent states.

The rate parameters α, β, γ can be thought of as per capita transition rates such that if α stands for any one of these parameters then $N \triangle t \alpha$ is a probability. In particular, if time is rescaled by $1/N$, then α^{-1} can be thought of as a characteristic time for the transition to occur.

2.1.1 Markov Jump Process

We now consider the formulation of this problem as a stochastic process. We base the formulation on [23] which follows the notation in [53] and [6]. We fix the number of transmitters in the system as N and denote by n_j the number of transmitters with power j.

$$N = n_H + n_L + n_O \quad \text{where } n_j \in \mathbb{Z}^+, n_j \geq 0.$$

The state of the system is fully described by $(n_H, n_L, n_O) := \mathbf{n}$ and the stochastic dynamics are that of a discrete space, continuous time Markov chain.

The transition rates $T(\mathbf{n}'|\mathbf{n})$ from state $\mathbf{n}$ to state $\mathbf{n}'$ are given by expressions similar to equation (1) of [53]:

$$\begin{aligned} T_1\big((n_H+1, n_L, n_O-1)|\mathbf{n}\big) &= \alpha N \frac{2n_O n_H}{N(N-1)}, \\ T_2\big((n_H, n_L-1, n_O+1,)|\mathbf{n}\big) &= \beta N \frac{2n_L n_H}{N(N-1)}, \\ T_3\big((n_H-1, n_L+1, n_O)|\mathbf{n}\big) &= \gamma N \frac{n_H(n_H-1)}{N(N-1)}. \end{aligned} \tag{2.1.4}$$

We assume that these transitions are independent and take place at the above constant rates.

The probability of the system being in state $\mathbf{n}$ at time t is defined as $\mathbf{P}[\mathbf{n}, t]$. As in Section 3 of [23] we let $\mathbf{P}[\mathbf{n}, t|\mathbf{n}_0, t_0]$ denote the probability that the system is in state $\mathbf{n}$ at time t given that it was in state $\mathbf{n}_0$ at time t_0, where $t_0 < t$. The Markov property implies the Chapman-Kolmogorov equation

$$\mathbf{P}[\mathbf{n}, t+s|\mathbf{n}_0, 0] = \sum_{\mathbf{n}'} \mathbf{P}[n, t+s|\mathbf{n}', t]\mathbf{P}[\mathbf{n}', t|\mathbf{n}_0, 0], \tag{2.1.5}$$

and as the Markov process is time-homogeneous this can be simplified to

$$\mathbf{P}[\mathbf{n}, t+s|\mathbf{n}_0, 0] = \sum_{\mathbf{n}'} \mathbf{P}[\mathbf{n}, s|\mathbf{n}', 0]\mathbf{P}[\mathbf{n}', t|\mathbf{n}_0, 0]. \tag{2.1.6}$$

Suppressing the conditional dependence on the initial condition $\mathbf{n} = \mathbf{n}_0$ at $t = 0$ and taking $s = \triangle t$ to be a small time increment we can write that

$$\mathbf{P}\left[\mathbf{n}, t+\Delta t\right] = \sum_{\mathbf{n}'} \mathbf{P}[\mathbf{n}, \triangle t|\mathbf{n}', 0]\mathbf{P}[\mathbf{n}', t], \tag{2.1.7}$$

where, with $n' \neq n$,

$$\mathbf{P}[\mathbf{n}, \triangle t|\mathbf{n}', 0] = \Delta t T(\mathbf{n}|\mathbf{n}') + O(\triangle t^2). \tag{2.1.8}$$

Equation (2.1.7) is the evolution operator that generates $\mathbf{P}[\mathbf{n}, t+\triangle t]$ from $\mathbf{P}[\mathbf{n}, t]$. Let $\triangle t$ be very small such that with high probability no more than one reaction occurs. Equation (2.1.8) gives the conditional probability of being in state $\mathbf{n}$ at time $\triangle t$ given that the system was in state $\mathbf{n}'$ at time 0. It is expressed in terms of transition rate to the leading order of $\triangle t$.

From equations (2.1.7) and (2.1.8) we can write that

$$\mathbf{P}\left[\mathbf{n}, t+\Delta t\right] - \mathbf{P}[\mathbf{n}, t] = \sum_{\mathbf{n}'} \Delta t T(\mathbf{n}|\mathbf{n}')\mathbf{P}[\mathbf{n}', t]. \tag{2.1.9}$$

As in [78] and [23], in order to write write these transitions using more compact notation, we introduce three step operators $\mathbb{E}_O$, $\mathbb{E}_L$ and $\mathbb{E}_H$ that act to increment the variables indicated by the respective subscripts:

$$\mathbb{E}_O[f(\mathbf{n})] := f(n_O + 1, n_L, n_H) \tag{2.1.10}$$

$$\mathbb{E}_L[f(\mathbf{n})] := f(n_O, n_L + 1, n_H) \tag{2.1.11}$$

$$\mathbb{E}_H[f(\mathbf{n})] := f(n_O, n_L, n_H + 1) \tag{2.1.12}$$

Naturally these step operators have inverses that decrement the respective arguments by 1. Using these step operators it is straightforward to compute $\mathbf{P}[\mathbf{n}, t+\Delta t]$ in terms of $\mathbf{P}[\mathbf{n}, t]$:

$$\begin{aligned}\mathbf{P}[\mathbf{n}, t+\Delta t] = \mathbf{P}[\mathbf{n}, t] &+ (\mathbb{E}_O\mathbb{E}_H^{-1} - 1)\left[T(n_O - 1, n_L, n_H + 1|\mathbf{n})\Delta t\mathbf{P}[\mathbf{n}, t]\right] \\ &+ (\mathbb{E}_O^{-1}\mathbb{E}_L - 1)[T(n_O + 1, n_L - 1, n_H|\mathbf{n})\Delta t\mathbf{P}[\mathbf{n}, t]] \\ &+ (\mathbb{E}_L^{-1}\mathbb{E}_H - 1)[T(n_O, n_L + 1, n_H - 1|\mathbf{n})\Delta t\mathbf{P}[\mathbf{n}, t]] \\ &+ O(\Delta t^2)\end{aligned} \tag{2.1.13}$$

Continuous formulation

We scale the variables such that, where j is the power setting, $x_j = n_j/N$ and we can define $\mathbf{x} = \frac{1}{N}(n_H, n_L, n_O) := (x_H, x_L, x_O)$. Then we define a probability density in terms of these variables:

$$\mathbf{P}[\mathbf{x}, t, N] := \mathbf{P}[\mathbf{n}, t]. \tag{2.1.14}$$

The step operators (2.1.10)-(2.1.12) can be redefined as

$$\mathbb{E}_H[g(\mathbf{x})] := g(x_O, x_L, x_H + 1/N) \tag{2.1.15}$$

$$\mathbb{E}_L[g(\mathbf{x})] := g(x_O, x_L + 1/N, x_H) \tag{2.1.16}$$

$$\mathbb{E}_O[g(\mathbf{x})] := g(x_O + 1/N, x_L, x_H) \tag{2.1.17}$$

By introducing (2.1.14) and equations (2.1.4) into (2.1.13), and tidying it up

we can write the evolution of the discrete probability density (2.1.13) in the form:

$$\begin{aligned}\frac{\mathbf{P}[\mathbf{x}, t+\Delta t, N] - \mathbf{P}[\mathbf{x}, t, N]}{\Delta t} =& (\mathbb{E}_O \mathbb{E}_H^{-1} - 1)\left[\alpha \frac{2x_O x_H N^2}{N-1}\mathbf{P}[\mathbf{x}, t, N]\right] \\ &+ (\mathbb{E}_O^{-1}\mathbb{E}_L - 1)\left[\beta \frac{2x_L x_H N^2}{N-1}\mathbf{P}[\mathbf{x}, t, N]\right] \\ &+ (\mathbb{E}_L^{-1}\mathbb{E}_H - 1)\left[\gamma \frac{x_H(x_H - 1/N)N^2}{N-1}\mathbf{P}[\mathbf{x}, t, N]\right] \\ &+ O(N\Delta t).\end{aligned} \tag{2.1.18}$$

Equation (2.1.18) is the master equation.

2.1.2 Representation as a Stochastic Differential Equation

Detailed in [6] are two roughly equivalent paths that take us, for large N, from a Markov jump process to a diffusion process (SDE). One way is to follow Van Kampen [78] who focuses on the Fokker-Planck (or"master") equation which describes how the probability distribution of the Markov process evolves. The other way is to follow Kurtz [46] who focuses on the Markov process itself.

We begin with following Van Kampen, showing that the Kramers-Moyal expansion of the master equation is a Fokker-Planck equation and then representing the Fokker-Planck equation as an SDE.

Kramers-Moyal Expansion and Fokker-Planck Equation

We expand the step operators (2.1.15) to (2.1.17) with a Taylor series expansion of sufficiently high order (only the first two terms are needed for what follows to $O(1/N^2)$). The step operators have the obvious inverses and composition properties. We use the notation $\exp(\cdot)$ to denote a Taylor series expansion, using this notation we can write, for example

$$\mathbb{E}_O^{-1}[g(\mathbf{x})] := g\left(x_O - \frac{1}{N}, x_L, x_H\right) \equiv \exp\left(-\frac{1}{N}\frac{\partial}{\partial x_O}\right) g(\mathbf{x})$$

and

$$\mathbb{E}_L^{-1}\mathbb{E}_H[g(\mathbf{x})] := g\left(x_O, x_L - \frac{1}{N}, x_H + \frac{1}{N}\right) \equiv \exp\left(\frac{1}{N}\left(\frac{\partial}{\partial x_H} - \frac{\partial}{\partial x_L}\right)\right) g(\mathbf{x}).$$

Inserting the Taylor series expansions of the step operators (2.1.17)-(2.1.15) into the master equation (2.1.18) is referred to as the Kramers-Moyal expansion.

An example of the Taylor series expansion of one of the terms is

$$(\mathbb{E}_O\mathbb{E}_H^{-1}-1)\left[\alpha\frac{2x_Ox_H}{N-1}\mathbf{P}[\mathbf{x},t,N]\right]=\left(\frac{\partial}{\partial x_O}-\frac{\partial}{\partial x_H}\right)[2\alpha x_Ox_H\mathbf{P}] + \frac{1}{2N}\left(\frac{\partial}{\partial x_O}-\frac{\partial}{\partial x_H}\right)^2[2\alpha x_Ox_H\mathbf{P}] + O\left(\Delta t,\frac{1}{N^2}\right). \quad (2.1.19)$$

From [60] we know that the Kramers-Moyal expansion of (2.1.18) takes the form

$$\frac{\partial\mathbf{P}}{\partial t}=\sum_{v=1}^{\infty}\left(-\frac{\partial}{\partial\mathbf{x}}\right)^v D^{(v)}(\mathbf{x})\mathbf{P}. \quad (2.1.20)$$

Additonally, as an approximation, we truncate this expansion such that coefficients $D^{(v)}$ with $v\geq 3$, which are of higher order, are disregarded. This reduces (2.1.20) to

$$\frac{\partial\mathbf{P}}{\partial t}=-\frac{\partial}{\partial\mathbf{x}}[D^{(1)}(\mathbf{x})\mathbf{P}]+\frac{\partial^2}{\partial\mathbf{x}^2}[D^{(2)}(\mathbf{x})\mathbf{P}]$$

which is recognisable as the Fokker-Planck equation that takes the general form:

$$\frac{\partial}{\partial t}p[\mathbf{x},t]=-\frac{\partial}{\partial\mathbf{x}}[\mu(\mathbf{x})p[\mathbf{x},t]]+\frac{\partial^2}{\partial\mathbf{x}^2}[D(\mathbf{x},t)p[\mathbf{x},t]]. \quad (2.1.21)$$

We assume that $\mathbf{P}[\mathbf{x},t,N]$ has a well-defined limit function $p[\mathbf{x},t]$

$$p[\mathbf{x},t]=\lim_{N\to\infty}\mathbf{P}[\mathbf{x},t,N]. \quad (2.1.22)$$

Therefore, if we define the vector field $\boldsymbol{u}(\boldsymbol{x})$ as:

$$\boldsymbol{u}(\boldsymbol{x}):=\begin{bmatrix}x_H(2\alpha x_O-\gamma x_H)\\ x_H(\gamma x_H-2\beta x_L)\\ 2x_H(\beta x_L-\alpha x_O)\end{bmatrix} \quad (2.1.23)$$

and a matrix $\boldsymbol{B}(\boldsymbol{x})$ as:

$$\boldsymbol{B}(\boldsymbol{x}):=\frac{1}{N}\begin{bmatrix}x_H(2\alpha x_O+\gamma x_H) & -\gamma x_Hx_H & -2\alpha x_Ox_H\\ -\gamma x_Hx_H & x_H(\gamma x_H+2\beta x_L) & -2\beta x_Lx_H\\ -2\alpha x_Ox_H & -2\beta x_Lx_H & 2x_H(\alpha x_O+\beta x_L)\end{bmatrix} \quad (2.1.24)$$

the Kramer-Moyal expansion means that the master equation (2.1.18) can be

represented by the Fokker-Planck equation

$$\frac{\partial p}{\partial t} = -\frac{\partial}{\partial \boldsymbol{x}}(\mathbf{u}p) + \frac{1}{2}\frac{\partial}{\partial \boldsymbol{x}}\left(\frac{\partial}{\partial \boldsymbol{x}}\right)^T(\boldsymbol{B}p). \tag{2.1.25}$$

It is clear that when $N \to \infty$ the diffusion terms go to zero. Therefore passing to the limit $N \to \infty$ we find that the Kramers-Moyal expansion of equation (2.1.18) gives

$$\begin{aligned}\frac{\mathbf{P}[\mathbf{x}, t+\Delta t] - \mathbf{P}[\mathbf{x}, t]}{\Delta t} &= \left(\frac{\partial}{\partial x_O} - \frac{\partial}{\partial x_H}\right)[2\alpha x_O x_H p] \\ &+ \left(\frac{\partial}{\partial x_L} - \frac{\partial}{\partial x_O}\right)[2\beta x_L x_H p] \\ &+ \left(\frac{\partial}{\partial x_H} - \frac{\partial}{\partial x_L}\right)\left[\gamma x_H^2 p\right] + O(\Delta t).\end{aligned} \tag{2.1.26}$$

At leading order $1/N$ and in the limit $\Delta t \to 0$ equation (2.1.26) can be simplified to

$$\frac{\partial p}{\partial t} + \nabla \cdot (\boldsymbol{u}(\boldsymbol{x})p) = 0 \tag{2.1.27}$$

where $\boldsymbol{u}(\boldsymbol{x})$ is the vector field defined in (2.1.23). Note that $\nabla = \begin{pmatrix} \frac{\partial}{\partial x_H} \\ \frac{\partial}{\partial x_L} \\ \frac{\partial}{\partial x_O} \end{pmatrix}$.

From [31], [78] and [60] we know that there is a connection between the Fokker-Planck equation and stochastic differential equations (SDEs).

Theorem 2.1 (Connection between Fokker-Planck and Stochastic Differential Equations)**.** *The Fokker-Planck equation describes the evolution of the transition probability of an n variable Markov process $\boldsymbol{x}(t)$. Given that the Fokker-Planck equation for the conditional probability density $p(\boldsymbol{x}, t|\boldsymbol{x}_0, t_0) \equiv p$ is*

$$\frac{\partial p}{\partial t} = -\frac{\partial}{\partial \boldsymbol{x}}(\boldsymbol{u}(\boldsymbol{x})p) + \frac{1}{2}\frac{\partial}{\partial \boldsymbol{x}}\left(\frac{\partial}{\partial \boldsymbol{x}}\right)^T(\boldsymbol{B}(\boldsymbol{x})p) \tag{2.1.28}$$

then $\boldsymbol{x}(t)$ can be modelled by a multivariable system of SDEs defined for n variables as

$$d\boldsymbol{x}(t) = \boldsymbol{u}(\boldsymbol{x}, t)dt + \boldsymbol{M}(\boldsymbol{x}, t)d\boldsymbol{W}_t, \tag{2.1.29}$$

where $d\boldsymbol{W}_t$ is an n-variable Wiener process and $\boldsymbol{M}(\boldsymbol{x})\boldsymbol{M}(\boldsymbol{x})^T = \boldsymbol{B}(\boldsymbol{x})$.

Therefore the master equation for our system (2.1.18) can be respresented as the SDE (2.1.29), where $\boldsymbol{u}$ and $\boldsymbol{B}$ are as defined in (2.1.23) and (2.1.24) respectively.

Method of Kurtz

We remind ourselves of the description given in Chapter 1. Each event causes the vector $\mathbf{n} \in \mathbb{N}^3$ to jump according to a jump vector $\boldsymbol{s} \in \mathbb{Z}^3$. The stochastic rate $\tilde{r}(\mathbf{n}, \boldsymbol{s})$ (or $r(\boldsymbol{x}, \boldsymbol{s})$ with $\boldsymbol{x} := \mathbf{n}/N$) at which the jumps $\mathbf{n} \to \mathbf{n} + \boldsymbol{s}$ take place are the transition rates given in (2.1.4). As before N is the overall size of the system as well as the sum of the components of $\mathbf{n}$. The finite collection of possible jumps $\boldsymbol{s}$ is denoted by the stoichiometric matrix $\boldsymbol{S}$ and the corresponding jump rates are summarized into a vector $\boldsymbol{r}(\boldsymbol{x})$. For our system the stoichiometric matrix $\boldsymbol{S}$ is

$$\boldsymbol{S} = \begin{bmatrix} 1 & 0 & -1 \\ 0 & -1 & 1 \\ -1 & 1 & 0 \end{bmatrix}. \tag{2.1.30}$$

and the corresponding rate vector $\boldsymbol{r}(\boldsymbol{x})$ is

$$\boldsymbol{r}(\boldsymbol{x}) = \begin{bmatrix} 2\alpha x_H x_O \\ 2\beta x_H x_L \\ \gamma x_H x_H \end{bmatrix}. \tag{2.1.31}$$

The kth column of $\boldsymbol{S}$, $\boldsymbol{s}_k$, corresponds to the kth element of the vector $\boldsymbol{r}(\boldsymbol{x})$, r_k, and $\boldsymbol{x}(t)$ satisfies an SDE of the form:

$$d\boldsymbol{x}(t) = \left(\sum_{\boldsymbol{s}_k \in \boldsymbol{S}} \boldsymbol{s}_k r_k \right) dt + \frac{1}{\sqrt{N}} \sum_{\boldsymbol{s}_k \in \boldsymbol{S}} \boldsymbol{s}_k \sqrt{r_k} dW^{(\boldsymbol{s}_k)}(t). \tag{2.1.32}$$

Where $\boldsymbol{s}_{ki}$ is the ith element of the vector $\boldsymbol{s}_k$, an alternative expression of (2.1.32) can be achieved by defining:

$$\boldsymbol{u}(\boldsymbol{x}) := \boldsymbol{S}\boldsymbol{r}(\boldsymbol{x}), \quad \text{and} \quad \boldsymbol{B}_{i,j}(\boldsymbol{x}) := \frac{1}{N} \sum_{\boldsymbol{s}_k \in \boldsymbol{S}} r_k \boldsymbol{s}_{ki} \boldsymbol{s}_{kj}, \tag{2.1.33}$$

such that,

$$\boldsymbol{u}(\boldsymbol{x}) = \begin{bmatrix} 2\alpha x_H x_O - \gamma x_H x_H \\ \gamma x_H x_H - 2\beta x_H x_L \\ 2\beta x_H x_L - 2\alpha x_H x_O \end{bmatrix} \tag{2.1.34}$$

and for $\boldsymbol{B}(\boldsymbol{x}) = \{\boldsymbol{B}_{i,j}(\boldsymbol{x})\}$,

$$\boldsymbol{B}(\boldsymbol{x}) = \frac{1}{N}\begin{bmatrix} 2\alpha x_H x_O + \gamma x_H x_H & -\gamma x_H x_H & -2\alpha x_H x_O \\ -\gamma x_H x_H & \gamma x_H x_H + 2\beta x_H x_L & -2\beta x_H x_L \\ -2\alpha x_H x_O & -2\beta x_H x_L & 2\alpha x_H x_O + 2\beta x_H x_L \end{bmatrix} \tag{2.1.35}$$

as in (2.1.23) and (2.1.24) respectively.

This gives that $\boldsymbol{u}(\boldsymbol{x})$ is the vector field of means of the first term of the right hand side of (2.1.32) and $\boldsymbol{B}(\boldsymbol{x})$ is the covariance function of the second term. Therefore where $\boldsymbol{B}(\boldsymbol{x}) = \boldsymbol{M}(\boldsymbol{x})\boldsymbol{M}^{\boldsymbol{T}}(\boldsymbol{x})$ we can write the SDE given in (2.1.32) as

$$d\boldsymbol{x}(t) = \boldsymbol{u}(\boldsymbol{x})dt + \boldsymbol{M}(\boldsymbol{x})d\boldsymbol{W}_t, \tag{2.1.36}$$

where $\boldsymbol{W}_t$ is a three-dimensional Wiener process.

In both (2.1.32) and (2.1.36) we see that as $N \to \infty$ only the deterministic term remains giving $d\boldsymbol{x}(t) = \boldsymbol{u}(\boldsymbol{x})dt$.

2.2 Existence and Stability of Equilibria

From $\boldsymbol{u}(\boldsymbol{x})$, the vector field defined in (2.1.23) and (2.1.33), we have the nonlinear ODEs (2.2.1) that comprise the usual mean-field description of the dynamics.

$$\begin{aligned} \dot{x}_H &= x_H(2\alpha x_O - \gamma x_H), \\ \dot{x}_L &= x_H(\gamma x_H - 2\beta x_L), \\ \dot{x}_O &= 2x_H(\beta x_L - \alpha x_O). \end{aligned} \tag{2.2.1}$$

Equations (2.2.1) show that equilibrium occurs when $2c = 2\alpha x_O = \gamma x_H = 2\beta x_L$. As $x_H + x_L + x_O = 1$ and $x_O = \frac{c}{\alpha}, x_L = \frac{c}{\beta}, x_H = \frac{2c}{\gamma}$ we find that

$$c = \frac{1}{\alpha^{-1} + \beta^{-1} + 2\gamma^{-1}}. \tag{2.2.2}$$

To study the stability of the equilbrium point $(x_H^*, x_L^*, x_O^*) = (\frac{2c}{\gamma}, \frac{c}{\beta}, \frac{c}{\alpha})$ we start by finding the Jacobian matrix

$$J_{(x_H^*, x_L^*, x_O^*)} = \begin{bmatrix} 2\alpha x_O - 2\gamma x_H & 0 & 2\alpha x_H \\ 2\gamma x_H - 2\beta x_L & -2\beta x_H & 0 \\ 2\beta x_L - 2\alpha x_O & 2\beta x_H & -2\alpha x_H \end{bmatrix}. \tag{2.2.3}$$

We find the value of the Jacobian matrix at the equilbrium point

$$J_{(\frac{2c}{\gamma},\frac{c}{\beta},\frac{c}{\alpha})} = \begin{bmatrix} -2c & 0 & \frac{4\alpha c}{\gamma} \\ 2c & -\frac{4\beta c}{\gamma} & 0 \\ 0 & \frac{4\beta c}{\gamma} & -\frac{4\alpha c}{\gamma} \end{bmatrix}. \tag{2.2.4}$$

The stability of the equilibrium can be analysed using the eigenvalues where $\det(J_{(\frac{2c}{\gamma},\frac{c}{\beta},\frac{c}{\alpha})} - \lambda I) = 0$.

$$\det(J_{(\frac{2c}{\gamma},\frac{c}{\beta},\frac{c}{\alpha})} - \lambda I) = -\lambda\left(\lambda^2 + \frac{2c}{\gamma}(\lambda\,(2\alpha + 2\beta + \gamma) + 4\alpha\beta)\right) = 0 \tag{2.2.5}$$

The eigenvalues are

$$\begin{aligned} \lambda_1 &= 0 \\ \lambda_2 &= -\frac{c}{\gamma}\left(2\alpha + 2\beta + \gamma + \sqrt{\gamma^2 + 4\left(\alpha^2 + \beta^2 - \frac{\alpha\beta\gamma}{c}\right)}\right) \\ \lambda_3 &= -\frac{c}{\gamma}\left(2\alpha + 2\beta + \gamma - \sqrt{\gamma^2 + 4\left(\alpha^2 + \beta^2 - \frac{\alpha\beta\gamma}{c}\right)}\right). \end{aligned} \tag{2.2.6}$$

We have that $c, \alpha, \beta, \gamma > 0$. As $\mathbf{Tr}\left(J_{(\frac{2c}{\gamma},\frac{c}{\beta},\frac{c}{\alpha})}\right) < 0$ and $\mathbf{Det}\left(J_{(\frac{2c}{\gamma},\frac{c}{\beta},\frac{c}{\alpha})}\right) = 0$ we know that we have stable fixed points.

Existence and Stability of Equilibria

For c as defined in equation (2.2.2) the system of ODEs in (2.2.1) has a unique interior equilibrium point. We note that when $x_H = 0$ then the system will be unable to move from this state. Therefore for a small N the system could be unstable to small disturbances that result in any state where $x_H = 0$ being reached.

Reduction to Two Dimensions

From the continuous formulation of the problem we have that $\mathbf{x} = \frac{1}{N}(n_O, n_L, n_H)$ such that $x_j = \frac{n_j}{N}$ where j is the power setting. Therefore $x_O + x_L + x_H = 1$ and $x_O = 1 - x_H - x_L$. Using this we can reduce equation (2.2.1) to

$$\begin{aligned} \dot{x}_H &= x_H(2\alpha(1 - x_H - x_L) - \gamma x_H), \\ \dot{x}_L &= x_H(\gamma x_H - 2\beta x_L). \end{aligned} \tag{2.2.7}$$

From which we see that at equilibrium $2\alpha(1-x_L) = x_H(\gamma+2\alpha)$ and $\gamma x_H = 2\beta x_L$. Therefore $\alpha(1 - x_H) = x_L(\beta + \alpha)$. As before, to study the stability of the equilibrium point $(x_H, x_L) = (\frac{2c}{\gamma}, \frac{c}{\beta})$ we find the Jacobian matrix.

$$J_{(x_H,x_L)} = \begin{bmatrix} 2\alpha(1 - x_L) - 2x_H(2\alpha + \gamma) & -2\alpha x_H \\ 2\gamma x_H - 2\beta x_L & -2\beta x_H \end{bmatrix}.$$

The value of the Jacobian matrix at this equilibrium point is

$$J_{(\frac{2c}{\gamma},\frac{c}{\beta})} = \begin{bmatrix} -\frac{2c(\gamma+2\alpha)}{\gamma} & -\frac{4\alpha c}{\gamma} \\ 2c & -\frac{4\beta c}{\gamma} \end{bmatrix}.$$

From this we find the trace and determinant. The determinant $\mathbf{Det}(J_{(\frac{2c}{\gamma},\frac{c}{\beta})}) = \frac{8\alpha\beta c}{\gamma}$ and the trace $\mathbf{Tr}(J_{(\frac{2c}{\gamma},\frac{c}{\beta})}) = \frac{-2c}{\gamma}(2(\beta + \alpha) + \gamma)$. As before, we have that α, β, $\gamma > 0$ and $c > 0$. Therefore the trace $\mathbf{Tr} < 0$ and the determinant $\mathbf{Det} > 0$ and we have either a stable focus or stable node. When $\mathbf{Tr}^2 - 4\mathbf{Det} > 0$ we will have a stable node, and when $\mathbf{Tr}^2 - 4\mathbf{Det} < 0$ a stable focus. We find that

$$\mathbf{Tr}^2 - 4\mathbf{Det} = \frac{4c^2}{\gamma^2}\left((\gamma - 2(\beta + \alpha))^2 - 16\alpha\beta\right). \tag{2.2.8}$$

We set that $\alpha = \mu\gamma$ and $\beta = \nu\gamma$, where $\mu, \nu > 0$ and from this we get that

$$\begin{aligned} \mathbf{Tr}^2 - 4\mathbf{Det} &= 4c^2\left(1 + 4\nu^2 + 4\mu^2 - 8\mu\nu - 4\mu - 4\nu\right) \\ &= 16c^2\left((\nu - \mu)^2 - (\nu + \mu) + \frac{1}{4}\right) \end{aligned} \tag{2.2.9}$$

We note that $c = \gamma\mu\nu(2\mu\nu + \nu + \mu)^{-1}$. Let $u = \nu + \mu$ and $v = \nu - \mu$, then

$$\mathbf{Tr}^2 - 4\mathbf{Det} = 16c^2\left(v^2 - u + \frac{1}{4}\right). \tag{2.2.10}$$

As $16c^2 > 0$ whether we have a node or focus depends on the sign of $v^2 - u + \frac{1}{4}$, which we recognise as a parabola $u = v^2 + \frac{1}{4}$. This is shown in Figure 2-2.

Reparametrisation

In order to further study the dynamical properties of (2.2.7) we rescale time by a factor of $dt \to \frac{1}{x_H}d\tau$. Then (2.2.7) becomes

$$\dot{\tilde{x}}_H = 2\alpha(1 - \tilde{x}_L) - \tilde{x}_H(2\alpha + \gamma) \tag{2.2.11}$$

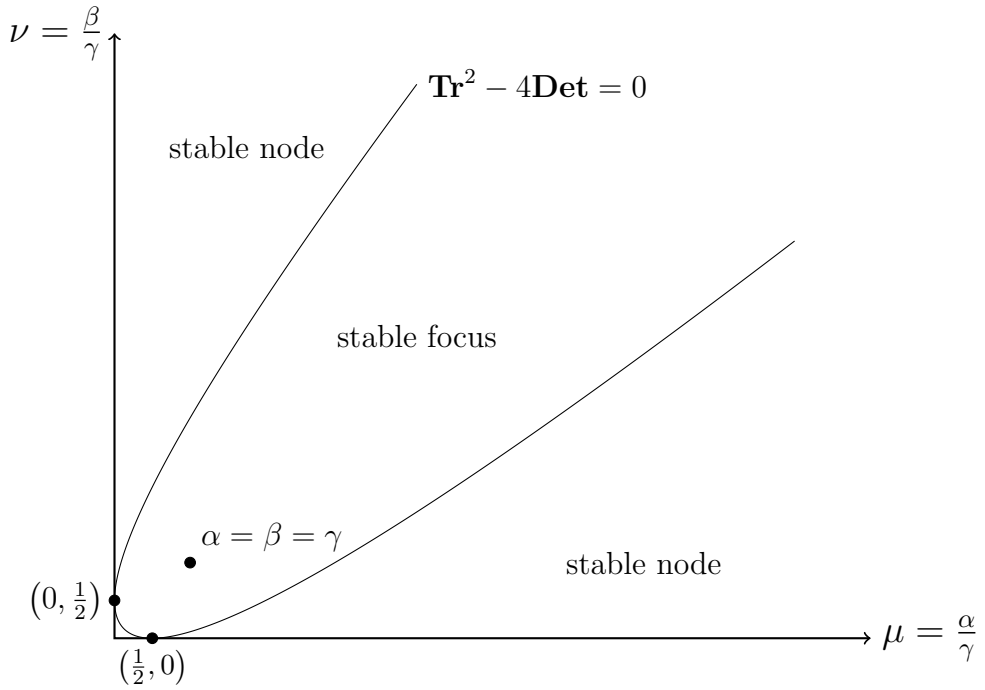

Figure 2-2: This shows the three regions where we have will have a stable node and the region where we will have a stable focus.

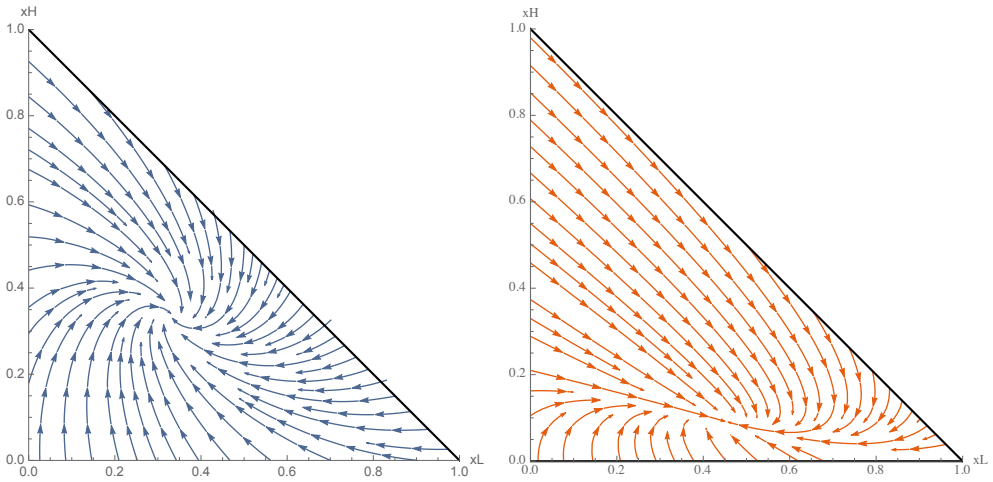

(a) $(\alpha, \beta, \gamma) = (1, 1, 2)$, the equilibrium point $(x_L^*, x_H^*) = (\frac{1}{3}, \frac{1}{3})$

(b) $(\alpha, \beta, \gamma) = (1, 1, 10)$ the equilibrium point $(x_L^*, x_H^*) = (0.45, 0.098)$

Figure 2-3: Phase portraits of the two-dimensional system in the (x_L, x_H) plane.

$$\dot{\tilde{x}}_L = \gamma\tilde{x}_H - 2\beta\tilde{x}_L \tag{2.2.12}$$

We find the Jacobian matrix at equilibrium

$$J_{(\tilde{x}_H^*, \tilde{x}_L^*)} = \begin{bmatrix} -2\alpha - \gamma & -2\alpha \\ \gamma & -2\beta \end{bmatrix}.$$

At equilibrium $\dot{\tilde{x}}_H = \dot{\tilde{x}}_L = 0$; this tells us that $\gamma\tilde{x}_H = 2\beta\tilde{x}_L$. The value of the Jacobian matrix at equilibrium point is

$$J_{(\frac{2c}{\gamma}, \frac{c}{\beta})} = \begin{bmatrix} -2\alpha - \gamma & -2\alpha \\ \gamma & -2\beta \end{bmatrix}.$$

The eigenvalues of $\mathrm{Det}(J - \lambda I)$ are

$$\begin{aligned} \lambda &= \frac{1}{2}\left(-2\alpha - 2\beta - \gamma + \sqrt{(2\alpha + 2\beta + \gamma)^2 - 8(2\alpha\beta + \beta\gamma - \alpha\gamma)}\right) \\ \lambda &= \frac{1}{2}\left(-2\alpha - 2\beta - \gamma - \sqrt{(2\alpha + 2\beta + \gamma)^2 - 8(2\alpha\beta + \beta\gamma - \alpha\gamma)}\right) \end{aligned} \tag{2.2.13}$$

and $\mathbf{Tr}(J) = -2\alpha - 2\beta - \gamma$ and $\mathbf{Det}(J) = -2\frac{\alpha\beta\gamma}{c}$. Therefore we have either a stable focus or a stable node. Setting $\mathbf{Tr}^2 - 4\mathbf{Det} = 0$ gives that $(\gamma + 2\beta - 2\alpha)^2 - 8\beta\gamma = 0$. As shown in Figure 2-2.

2.3 Analysis

We use numerical simulations to analyse the behaviour of the system both approaching and at equilibrium. We use two methods of simulation, firstly we plot the solution to the ODEs that describe the system which represents an infinite and continuous realisation of the dynamics. Secondly, we simulate a discrete and finite realisation of the system.

2.3.1 Simulations

ODEs

The trajectories of x_H, x_L, x_O are described by the system ODEs we gave in (2.2.1). In Figure 2-4a we show the system approaching and maintaining equilibrium when $x_H(0) = 0.05$, $x_L(0) = 0.9$, $x_O(0) = 0.05$ and $\alpha = 1$, $\beta = 1$, $\gamma = 4$. From Figure 2-2 we know that for these rate parameter values equilibrium will be a stable focus. We do not observe oscillations in the trajectories as they approach equilibrium. This is due to the imaginary part of the eigenvalues being small. In

fact, for these parameter values it is when we see the PSD peak. For the parameter values used (2.2.6) gives that $\lambda = 0, \lambda = -0.8 - 0.4i$ and $\lambda = -0.8 + 0.4i$. In Figure 2-4b we plot the absolute value of the ODE minus the equilibrium value, for example for x_H we plot $|\dot{x}_H - x_H^*|$. Subtracting the drift terms and taking the absolute value mean that it is possible to see the oscillations. For both plots in Figure 2-4 all parameter values are the same.

Stochastic simulation

We wish to be able to simulate a realisation of our system with jumps. We use the Gillespie stochastic simulation algorithm, described in Subsection 1.4.6, to do this. In contrast to ODEs, the Gillespie algorithm allows a discrete and stochastic simulation of a system with few reactants because every reaction is explicitly simulated.

In Algorithm 2.1 we give the specific algorithm used for our simulations. An implementation of Algorithm 2.1 is shown in Figure 2-5 in which the ODEs are also plotted. We see that the GSSA closely fits the trajectories of the ODEs, with some oscillations.

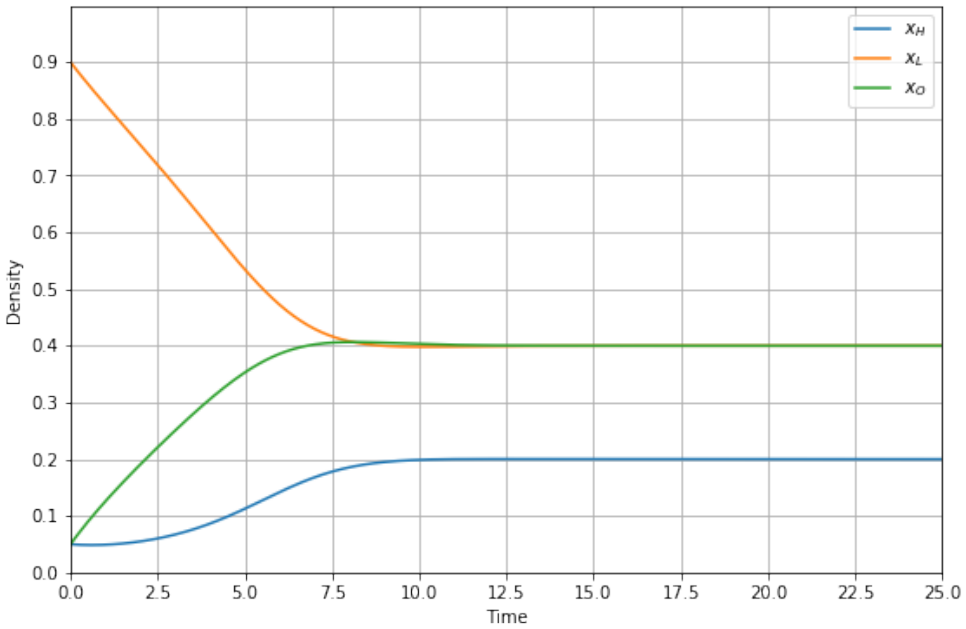

(a) Trajectories of ODES

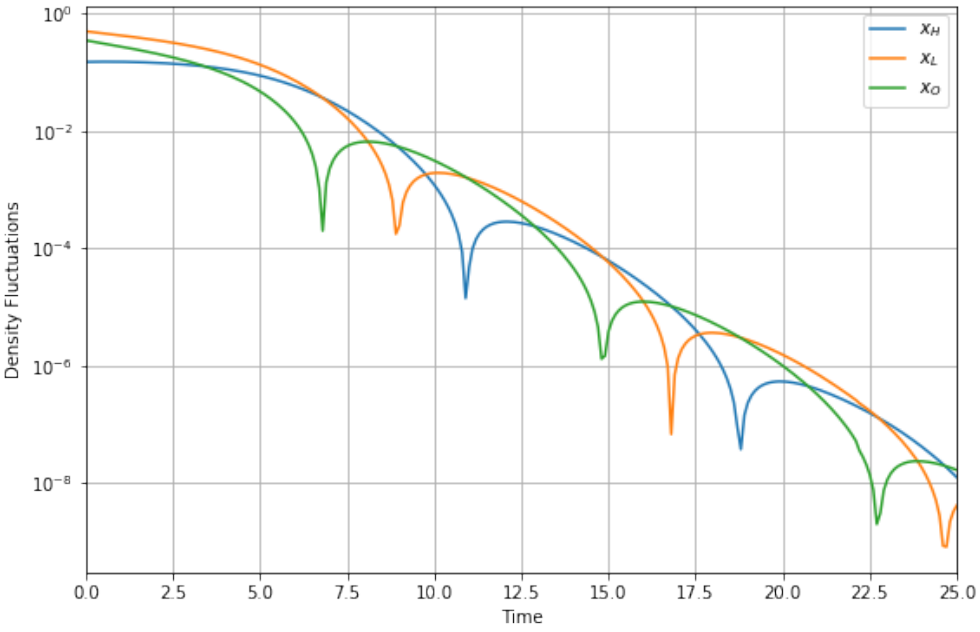

(b) Oscillations in ODEs

Figure 2-4: For $\alpha = 1$, $\beta = 1$, $\gamma = 4$ and $x_H(0) = 0.05$, $x_L(0) = 0.9$, $x_O(0) = 0.05$. Subfigure 2-4a shows the trajectories of the ODEs for these parameter values. In Subfigure 2-4b we plot the absolute difference from equilibrium $|\dot{\boldsymbol{x}} - \boldsymbol{x}^*|$ for the ODEs.

Algorithm 2.1 Gillespie Stochastic Simulation Algorithms

Assign integer values to n_O, n_L, n_H and N such that $N = n_O + n_L + n_H$.
Set a time limit and/or an iteration limit.
Set values for the rates α, β, γ.
time $= 0$ ▷ Initialise time
while time $<$ time limit **do**
    $x = X \sim \text{Unif}(0, 1)$
    $P_1 = \frac{N(2\alpha n_O n_H)}{N(N-1)}$
    $P_2 = \frac{N(2\beta n_L n_H)}{N(N-1)}$
    $P_3 = \frac{N(\gamma(n_H-1)n_H)}{N(N-1)}$
    $P_0 = P_1 + P_2 + P_3$
    if $x \leq P_1/P_0$ **then**
        $n_O = n_O - 1$
        $n_H = n_H + 1$
    else if $x \leq (P_1 + P_2)/P_0$ **then**
        $n_L = n_L - 1$
        $n_O = n_O + 1$
    else
        $n_H = n_H - 1$
        $n_L = n_L + 1$
    end if
    $k = K \sim \text{Exp}(1/P_0)$ ▷ time interval after which the reaction occured
    time $=$ time $+ k$ ▷ Update time
end while

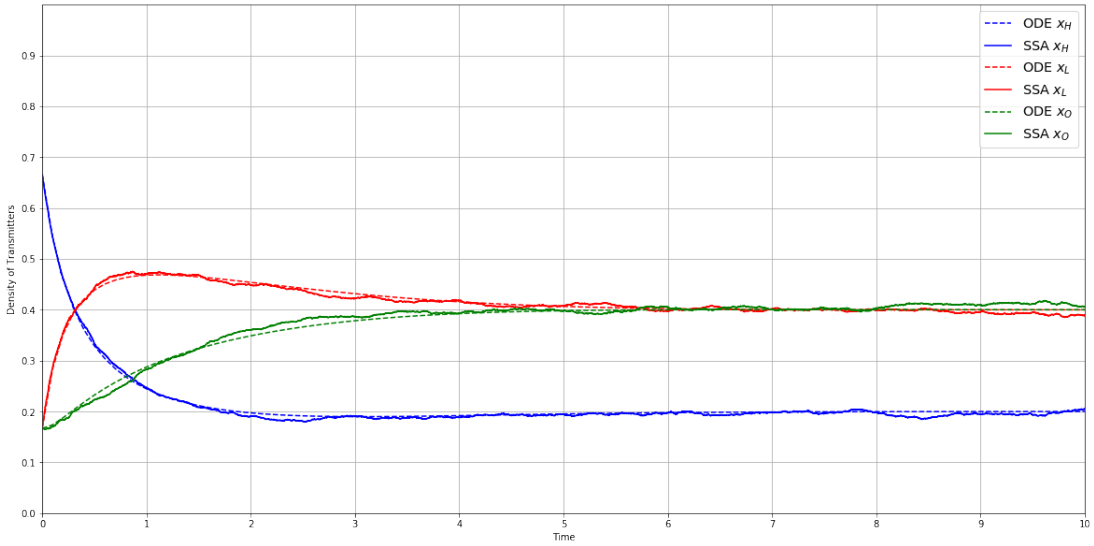

(a) For $0 \leq t \leq 10$ we observe how the system reaches equilbrium in more detail.

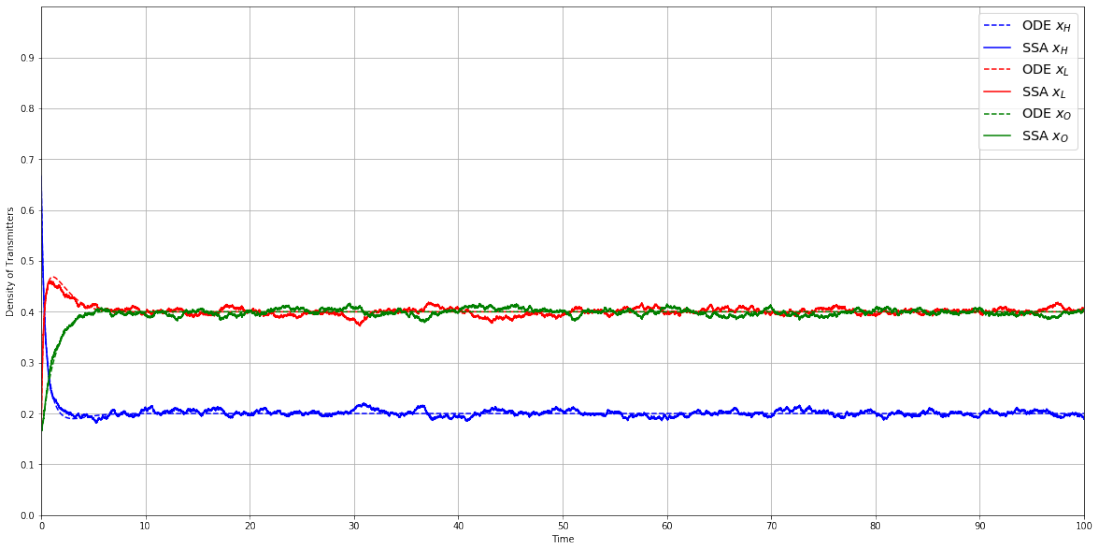

(b) For $0 \leq t \leq 100$ we see how the system reaches and then oscillates around equilibrium.

Figure 2-5: For Figures 2-5b and 2-5a the reaction rates are: $\alpha = 1$, $\beta = 1$, $\gamma = 4$. The total number of transmitters $N = 6000$, and initially $n_H = 4000$, $n_L = 1000$, $n_O = 1000$. Therefore $\mathbf{x}(0) = (0.66, 0.17, 0.17)$. We observe that the ODEs reach equilibrium such that, as $t \to \infty$, $\mathbf{x}(t) = (0.2, 0.4, 0.4)$. However the SSA oscillates around the equilibrium.

To better understand the behaviour of the finite system, which we simulate using the Gillespie SSA, and its oscillations around equilbirium we consider the power spectral density.

2.3.2 Power Spectral Density

In Subsection 2.1.2 we used the method of Kurtz to define our system as the SDE

$$d\boldsymbol{x}(t) = \boldsymbol{u}(\boldsymbol{x}, t)dt + \boldsymbol{M}(\boldsymbol{x})d\boldsymbol{W}(t), \tag{2.3.1}$$

where $\boldsymbol{u}(\boldsymbol{x}, t)$ and $\boldsymbol{M}(\boldsymbol{x})$ are defined in terms of the stoichiometric matrix $\boldsymbol{S}$ (2.1.30) and rate vector $\boldsymbol{r}(\boldsymbol{x}, t)$ (2.1.31) such that

$$\boldsymbol{u}(\boldsymbol{x}, t) = \begin{bmatrix} 2\alpha x_H x_O - \gamma x_H x_H \\ \gamma x_H x_H - 2\beta x_H x_L \\ 2\beta x_H x_L - 2\alpha x_H x_O \end{bmatrix} \tag{2.3.2}$$

and $\boldsymbol{M}(\boldsymbol{x})\boldsymbol{M}^T(\boldsymbol{x}) = \boldsymbol{B}(\boldsymbol{x})$ with

$$\boldsymbol{B}(\boldsymbol{x}) = \frac{1}{N}\begin{bmatrix} 2\alpha x_H x_O + \gamma x_H x_H & -\gamma x_H x_H & -2\alpha x_H x_O \\ -\gamma x_H x_H & \gamma x_H x_H + 2\beta x_H x_L & -2\beta x_H x_L \\ -2\alpha x_H x_O & -2\beta x_H x_L & 2\alpha x_H x_O + 2\beta x_H x_L \end{bmatrix}. \tag{2.3.3}$$

In equation (2.2.3) we gave the Jacobian matrix of our system $\boldsymbol{J}_{(\boldsymbol{x},t)}$. Let $\boldsymbol{x}(t) = \boldsymbol{x}^* + \boldsymbol{y}(t)$ with $\boldsymbol{y}(t) = (y_H, y_L, y_O)$, then it follows that

$$\begin{aligned} \frac{d(\boldsymbol{x}^* + \boldsymbol{y}(t))}{dt} &= \boldsymbol{u}(\boldsymbol{x}^* + \boldsymbol{y}(t), t) + O(\boldsymbol{y}^2) \\ &= \boldsymbol{u}(\boldsymbol{x}^*) + \boldsymbol{J}_{(\boldsymbol{x}^*)}\boldsymbol{y}(t) + O(\boldsymbol{y}^2) \\ &= \boldsymbol{J}_{(\boldsymbol{x}^*)}\boldsymbol{y}(t) + O(\boldsymbol{y}^2) \end{aligned} \tag{2.3.4}$$

as $\boldsymbol{u}(\boldsymbol{x}^*) = 0$. We define a matrix $\boldsymbol{A}(\boldsymbol{x}^*) := \boldsymbol{J}_{(\boldsymbol{x}^*)}$. When the system is at equilibrium, $\boldsymbol{x}^* = (\frac{2c}{\gamma}, \frac{c}{\beta}, \frac{c}{\alpha})$, the matrices $\boldsymbol{A}(\boldsymbol{x}^*)$ and $\boldsymbol{M}(\boldsymbol{x}^*)$ are constant and we define

$$\boldsymbol{A} := \boldsymbol{A}(\boldsymbol{x}^*) = \frac{2c}{\gamma}\begin{bmatrix} -\gamma & 0 & 2\alpha \\ \gamma & -2\beta & 0 \\ 0 & 2\beta & -2\alpha \end{bmatrix}, \tag{2.3.5}$$

and $\boldsymbol{M} := \boldsymbol{M}(\boldsymbol{x}^*, t)$ with $\boldsymbol{M}\boldsymbol{M}^T = \boldsymbol{B}$ and

$$\boldsymbol{B} := \boldsymbol{B}(\boldsymbol{x}^*, t) = \frac{4c^2}{N\gamma}\begin{bmatrix} 2 & -1 & -1 \\ -1 & 2 & -1 \\ -1 & -1 & 2 \end{bmatrix}. \tag{2.3.6}$$

Therefore when the system is at equilibrium we can write (2.3.1) as

$$d\boldsymbol{y}(t) = \boldsymbol{A}\boldsymbol{y}(t)dt + \boldsymbol{M}d\boldsymbol{W}(t). \tag{2.3.7}$$

From Definition 1.13 we recognise (2.3.7) as describing a multivariate Ornstein-Uhlenbeck process and Theorem 1.5 gives that the spectrum matrix $\boldsymbol{\mathcal{P}}(\omega)$ of this process is given by

$$\boldsymbol{\mathcal{P}}(\omega) = \frac{1}{2\pi}(\boldsymbol{A} - i\omega\mathbf{I})^{-1}\boldsymbol{B}(\boldsymbol{A} - i\omega\mathbf{I})^{-\dagger}. \tag{2.3.8}$$

To compute the spectrum matrix $\boldsymbol{\mathcal{P}}(\omega)$, we find $(\mathbf{A} - i\omega\mathbf{I})^{-1}$ and $(\mathbf{A} - i\omega\mathbf{I})^{-\dagger}$,

$$(\mathbf{A} - i\omega\mathbf{I})^{-1} = y\begin{bmatrix} (4\alpha c + i\gamma\omega)(-4i\beta c + \gamma\omega) & -16i\alpha\beta c^2 & 4\alpha c(-4i\beta c + \gamma\omega) \\ 2c\gamma(-4i\alpha c + \gamma\omega) & \gamma(-2ic + \omega)(4\alpha c + i\gamma\omega) & -8i\alpha c^2\gamma \\ -8i\beta c^2\gamma & 4\beta c\gamma(-2ic + \omega) & \gamma(-2ic + \omega)(4\beta c + i\gamma\omega) \end{bmatrix} \tag{2.3.9}$$

where $y = \left(\omega\left(-4\alpha c\left(4\beta c + 2\gamma c + i\gamma\omega\right) + \gamma\left(-2ic + \omega\right)\left(-4i\beta c + \gamma\omega\right)\right)\right)^{-1}$, and

$$(\mathbf{A} - i\omega\mathbf{I})^{-\dagger} = y^*\begin{bmatrix} (4\alpha c - i\gamma\omega)(4i\beta c + \gamma\omega) & 2c\gamma(4i\alpha c + \gamma\omega) & 8i\beta c^2\gamma \\ 16i\alpha\beta c^2 & \gamma(2ic + \omega)(4\alpha c - i\gamma\omega) & 4\beta c\gamma(2ic + \omega) \\ 4\alpha c(4i\beta c + \gamma\omega) & 8i\alpha c^2\gamma & \gamma(2ic + \omega)(4\beta c - i\gamma\omega) \end{bmatrix} \tag{2.3.10}$$

where $y^* = \left(\omega\left(-4\alpha c\left(4\beta c + 2\gamma c - i\gamma\omega\right) + \gamma\left(2ic + \omega\right)\left(4i\beta c + \gamma\omega\right)\right)\right)^{-1}$.

The diagonal elements of $\boldsymbol{\mathcal{P}}(\omega)$ correspond to the frequency spectrum of the elements of $\boldsymbol{x}$. The element $\mathcal{P}_{1,1}(\omega)$ describes the frequency spectrum of $x_H(t)$ and we find that

$$\mathcal{P}_{1,1}(\omega) = \frac{4c^2\gamma\left(16\alpha^2c^2 + 16\alpha\beta c^2 + 16\beta^2c^2 + \gamma^2\omega^2\right)}{\pi N\left((8\alpha\beta\gamma c)^2 + \gamma^2\omega^2\left(4c^2(4\alpha^2 + 4\beta^2 + \gamma^2) + \gamma^2\omega^2\right)\right)}. \tag{2.3.11}$$

The element $\mathcal{P}_{2,2}(\omega)$ describes the frequency spectrum of $x_L(t)$ and

$$\mathcal{P}_{2,2}(\omega) = \frac{4c^2\gamma\left(16\alpha^2c^2 + 8\alpha c^2\gamma + \gamma^2\left(4c^2 + \omega^2\right)\right)}{\pi N\left((8\alpha\beta\gamma c)^2 + \gamma^2\omega^2\left(4c^2(4\alpha^2 + 4\beta^2 + \gamma^2) + \gamma^2\omega^2\right)\right)}. \tag{2.3.12}$$

Lastly, the element $\mathcal{P}_{3,3}(\omega)$ describes the frequency spectrum of $x_O(t)$ and

$$\mathcal{P}_{3,3}(\omega) = \frac{4c^2\gamma\left(16\beta^2c^2 + 8\beta c^2\gamma + \gamma^2\left(4c^2 + \omega^2\right)\right)}{\pi N\left((8\alpha\beta\gamma c)^2 + \gamma^2\omega^2\left(4c^2(4\alpha^2 + 4\beta^2 + \gamma^2) + \gamma^2\omega^2\right)\right)}. \tag{2.3.13}$$

The Trace of $\boldsymbol{\mathcal{P}}(\omega)$, which describes the frequency spectrum of the sum of all three elements of $\mathbf{x}(t)$, is therefore given by

$$\mathbf{Tr}(\boldsymbol{\mathcal{P}}(\omega)) = \frac{4c^2\gamma\left(32\alpha^2c^2 + 32\beta^2c^2 + 8\alpha\beta\gamma c + 8\gamma^2c^2 + 3\gamma^2\omega^2\right)}{\pi N\left((8\alpha\beta\gamma c)^2 + \gamma^2\omega^2\left(4c^2(4\alpha^2 + 4\beta^2 + \gamma^2) + \gamma^2\omega^2\right)\right)}. \tag{2.3.14}$$

Peak PSD

To find the angular frequency ω_0 at which the PSD of x_H, x_L and x_O peaks, we differentiate the corresponding diagonal entry of $\boldsymbol{\mathcal{P}}(\omega)$ with respect to ω. In each case we find that $\mathcal{P}'(\omega_0) = 0$ has five solutions but only two where it is possible that $\omega_0 \in \mathbb{R}^+$ as we require. The first of these two solutions is $\omega_0 = 0$, the second solution for each case is given below:

For x_H, where we differentiate $\mathcal{P}_{1,1}(\omega)$,

$$\omega_0 = \frac{2c\sqrt{2}}{\gamma}\sqrt{-2\alpha^2 - 2\beta^2 - 2\alpha\beta + (2\alpha + 2\beta + \gamma)\sqrt{\alpha\beta}} \tag{2.3.15}$$

we find when $\alpha = 1$, $\beta = 1$ and $\gamma = 4$ then $\omega_0 = 0.4$.

For x_L, where we differentiate $\mathcal{P}_{2,2}(\omega)$,

$$\omega_0 = \frac{2c}{\gamma}\sqrt{-\gamma^2 - 4\alpha^2 - 2\alpha\gamma + (2\alpha + 2\beta + \gamma)\sqrt{2\alpha\gamma}} \tag{2.3.16}$$

we find when $\alpha = 1$, $\beta = 1$ and $\gamma = 1.5$ then $\omega_0 = 0.210249$.

For x_O, where we differentiate $\mathcal{P}_{3,3}(\omega)$,

$$\omega_0 = \frac{2c}{\gamma}\sqrt{-\gamma^2 - 4\beta^2 - 2\beta\gamma + (2\alpha + 2\beta + \gamma)\sqrt{2\beta\gamma}} \tag{2.3.17}$$

we find when $\alpha = 1$, $\beta = 1$ and $\gamma = 1.5$ then $\omega_0 = 0.210249$.

There is no set of positive real values $\{\alpha,\ \beta,\ \gamma\}$ such that there exists an $\omega_0 > 0$ with $\omega_0 \in \mathbb{R}$ for each of x_H, x_L and x_O; however for the set $\{1, 1, 2\}$ then $\omega_0 = 0$ for all three elements. This is the case for the trace of $\boldsymbol{\mathcal{P}}(\omega)$ where $\omega_0 = 0$ for the set of values $\{1, 1, 2\}$ but there is no set $\{\alpha, \beta, \gamma\} \in \mathbb{R}^+$ such that $\omega_0 > 0$ and $\omega_0 \in \mathbb{R}$.

For each of x_H, x_L and x_O we have presented a set of values $\{\alpha, \beta, \gamma\}$ and the resulting angular frequency ω_0 at which the peak PSD occurs. We show in

Figures 2-6 and 2-7 that these peaks in PSD are small and, unless only ω local to ω_0 is considered, can be difficult to detect.

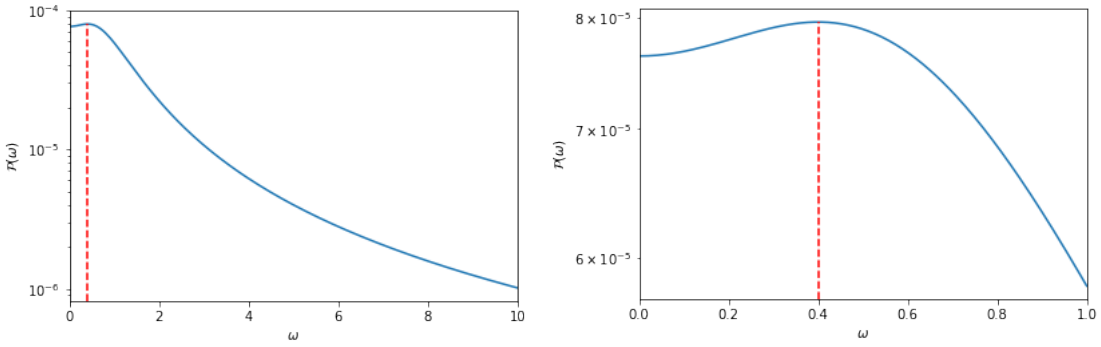

(a) PSD of x_H for $0 \leq \omega \leq 10$.

(b) PSD of x_H for $0 \leq \omega \leq 0.6$.

Figure 2-6: Both 2-6a and 2-6b show the PSD of x_H when $\alpha = 1$, $\beta = 1$, $\gamma = 4$ and $N = 500$. The peak in PSD occurs at $\omega_0 = 0.4$ which is marked by a dashed red line in both 2-6a and 2-6b. In 2-6b a smaller range of ω values are used so that the peak is more distinct, and in both subfigures a log scale y-axis is used to make the peak in PSD more easily observable.

When $\alpha = \beta$ then $\mathcal{P}_{2,2}(\omega) = \mathcal{P}_{3,3}(\omega)$ and x_L and x_O will have the same PSD. Therefore, we will represent the peak in PSD for both x_H and x_O in Figure 2-7, where we show the peak in PSD.

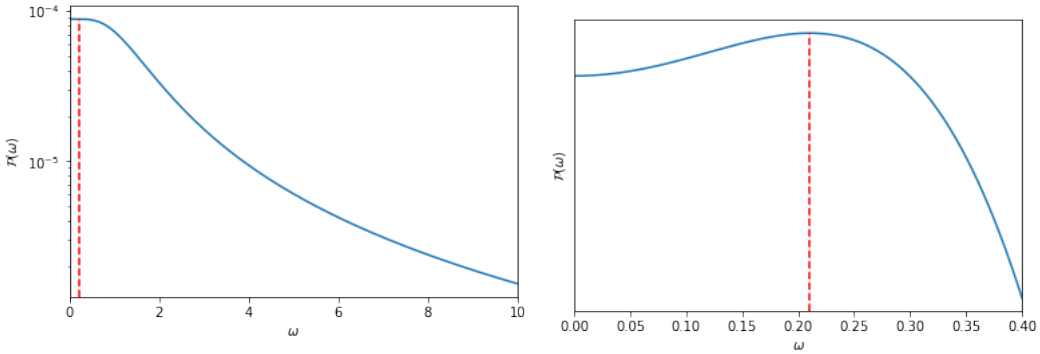

(a) PSD of x_L and x_O for $0 \leq \omega \leq 10$.

xs

(b) PSD of x_L and x_O for $0 \leq \omega \leq 0.2$.

Figure 2-7: Both 2-7a and 2-7b show the PSD of x_L when $\alpha = 1$, $\beta = 1$, $\gamma = 1.5$ and $N = 500$. The peak in PSD occurs at $\omega_0 = 0.210249$ which is marked by a dashed red line in both 2-7a and 2-7b. In 2-7b a smaller range of ω values are used so that the peak is more distinct, and in both subfigures a log scale y-axis is used to make the peak in PSD more easily observable.

We wish to analyse the sustained oscillations about equilibrium seen in Figures 2-5. We have computed $\mathcal{P}(\omega)$. This gives the result for an infinite system. We wish to compare this to a result for the finite system we simulate using the GSSA.

We compare this result to what we observe from our stochastic simulation of the system using the fast Fourier transform.

Comparing the PSD from the two methods

Two methods for computing the PSD have been described. These are taking the DFT of the timeseries we generate through the Gillespie SSA and computing the spectrum matrix $\boldsymbol{\mathcal{P}}(\omega)$.

Computational limits prevent the comparison of the two methods at the peak ω values. As already stated, the peak in the PSD is very small and for it to be noticeable the variance in the Gillespie SSA would have to be even smaller. This requires the system size N to be suitably large. As given in equation (1.4.30)

$$\omega_k = \frac{2\pi k}{N\Delta t} \quad \text{for} \quad k = 0, \ldots, N-1.$$

For large N the value of ω ranges from 0 to approximately $\frac{2\pi}{\Delta t}$, and so it is Δt that determines the size of the range. It is necessary to scale the reaction rates α, β, γ inversely with N to prevent the times between reactions becoming very small. If they are not then the overall rate of reactions increases. For a plot of the peak PSD to be informative we would require k to be reasonably large ($K > 100$) and, for a large N where α, β, γ are small, this would require a large time step which would miss the majority of interactions.

We found in Subsection 2.3.2 that when $(\alpha, \beta, \gamma) = (1, 1, 4)$ a peak in the PSD of x_H occurs at $\omega = 0.4$. We also found that when $(\alpha, \beta, \gamma) = (1, 1, 1.5)$ a peak in the PSD of x_L and x_O occurs when $\omega = 0.210249$. For these two sets of values of α, β, γ we compare the PSD of x_H, x_L and x_O obtained through the two different methods in Figures 2-8 to 2-10. The system size $N = 500$, the time step $\Delta t = 0.05$, the total time $T = 500$ and we average over 1000 repeats.

We note that for both sets of values of (α, β, γ) we observe an exact match of the numerically computed PSD to the theoretically computed PSD. For example, in Figure 2-8a we observe the peak in the PSD of x_H at $\omega = 0.04$ in the GSSA results. We show a comparison for small values of ω as for larger values there is a discrepancy between the theoretical and numerical results is introduced. This is a result of the numerical results not representing a continuous infinite system but rather a finite one of size $N = 500$ for discrete time steps. Increasing the system size N and observation time T whilst also decreasing the time step Δt reduces the discrepancy between the two methods but is computationally expensive.

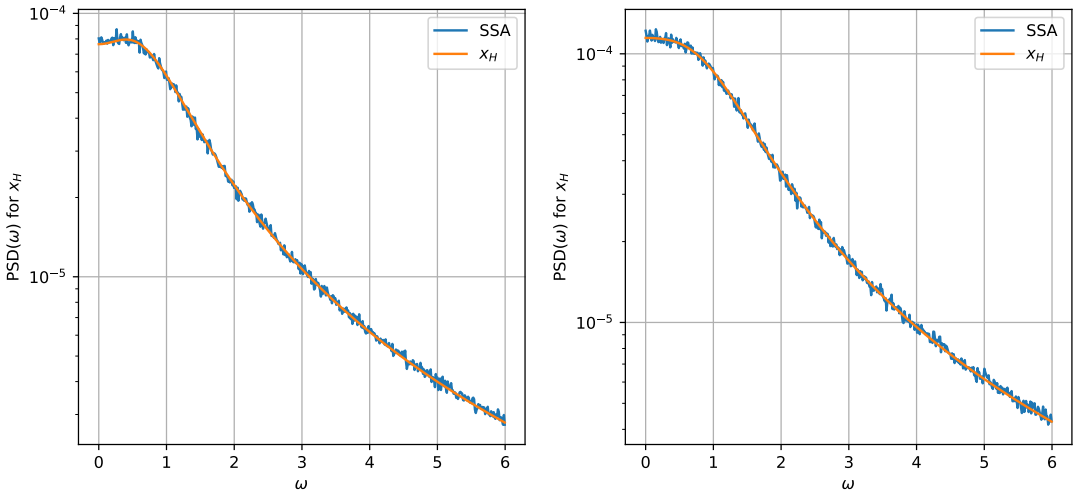

(a) $(\alpha, \beta, \gamma) = (1, 1, 4)$ (b) $(\alpha, \beta, \gamma) = (1, 1, 1.5)$

Figure 2-8: The PSD of x_H shown for $0 \leq \omega \leq 6$ for the two sets of values of (α, β, γ).

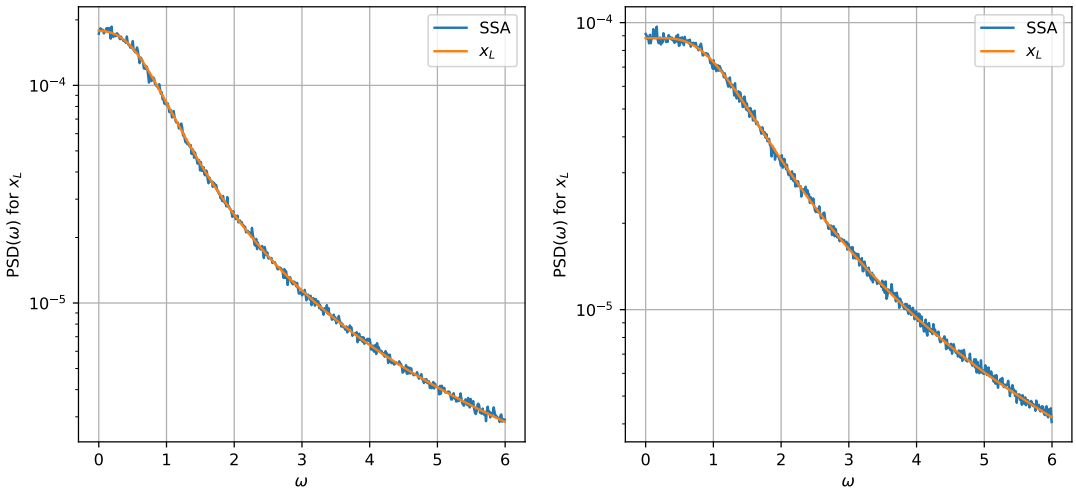

(a) $(\alpha, \beta, \gamma) = (1, 1, 4)$ (b) $(\alpha, \beta, \gamma) = (1, 1, 1.5)$

Figure 2-9: The PSD of x_L shown for $0 \leq \omega \leq 6$ for the two sets of values of (α, β, γ).

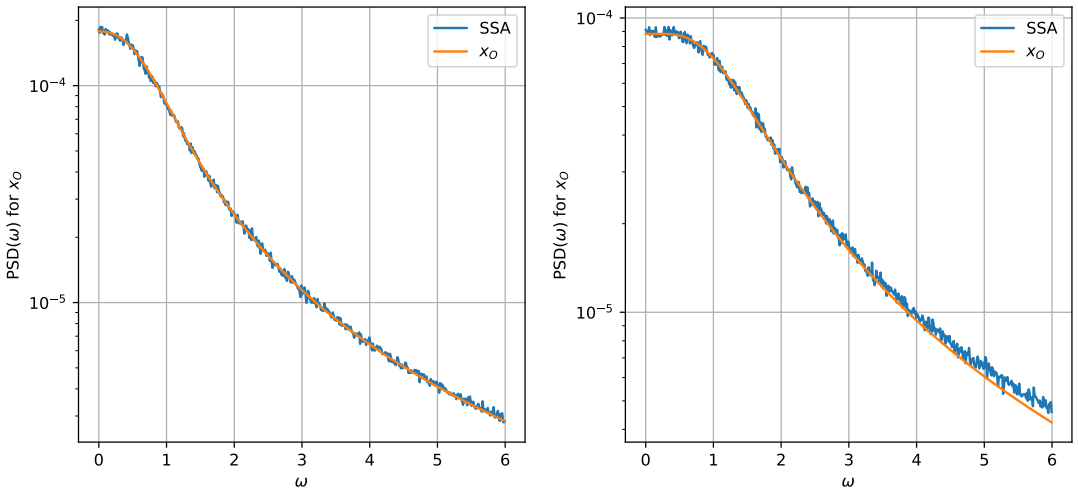

(a) $(\alpha, \beta, \gamma) = (1, 1, 4)$ (b) $(\alpha, \beta, \gamma) = (1, 1, 1.5)$

Figure 2-10: The PSD of x_O shown for $0 \leq \omega \leq 6$ for the two sets of values of (α, β, γ)

Short Summary

In this chapter we considered a simple model of the interaction between three competing system-level objectives: increase the minimum SINR, increase signal coverage and reduce energy use. The model ignored the spatial distribution of transmitters and formulated the problem stochastically, as a Markov jump process, with the overall state of the system described by the total number of transmitters in each of the three states: High (H), Low (L) and Off (O).

In the limit of a large number of transmitters, the Markov jump process could be closely approximated by either a multivariate SDE (Subsection 2.1.2) or by the ODEs describing the mean-field limit of the system dynamics (Section 2.2). Analysis of the ODEs showed that a unique interior equilibrium point exists for all combinations of the rate parameters, and that it is always stable. There do not appear to be any deterministic periodic orbits for the mean-field ODEs, but the stable equilibrium can be either a stable focus or a stable node, see Figure 2-2.

For a finite system size there are stochastic fluctuations around the equilibrium point, with frequencies of the same order as the rate parameters. Comparisons between the predicted power spectral density (PSD) and numerical simulations using the Gillespie stochastic simulation algorithm show excellent agreement, see Figures 2-8 to 2-10. In cases where the PSD has a peak at a positive value

of the frequency ω, the peak is not very high, suggesting that detection of a characteristic frequency in the stochastic dynamics would be difficult in practice.

Chapter 3

Self-Optimising Transmit Powers

In Chapter 2 we explored the system dynamics as three self-optimisation policies competed. Two of the three objectives were for quality of service (QoS) improvement. One of these two QoS objectives was the system-wide optimisation (i.e. increase) of SINR, the other was the system-wide optimisation (i.e. increase) of coverage. To achieve the SINR optimisation the policy for any pair of transmitters sharing the transmit power H was for one transmitter to change to the lesser power L. In this chapter we consider spatially distributed transmitters and show that this policy of changing from uniform transmit powers can optimise SINR.

3.1 Transmit Power Optimisation

It is shown in [36] that optimizing transmit powers allows for improved SINR and SIR (referred to as Carrier to interference ratio (CIR) in that paper). Optimising transmit powers is an area that has been widely studied for many decades and various schemes for power control, centralized or distributed, based on different transmission models and application needs have been proposed. As our interest is in self-organisation we consider distributed algorithms.

In [61] two of the three optimisation objectives from Chapter 2 are considered. These are to increase energy efficiency (minimise power consumption) whilst maximising the percentage of devices that achieve some minimum SINR (improve QoS). It proposes an algorithm that is distributed and stable at equilibrium. The algorithm is a trial and error learning algorithm. Further examples of distributed algorithms for cellular wireless networks include those given in [20], [28] and [89] that we briefly describe.

The distributed algorithm in [28] either succeeds or fails at having all users' QoS reach a target value. Similarly, the distributed algorithm in [89] aims to

meet an SINR target rather than find the best SINR achievable. The distributed algorithm in [20] aims for the best SINR achievable but requires communication between devices (femtocells) when SINR is low. None of these algorithms achieves our aim whilst meeting our requirements. We wish to achieve the best SINR possible for each transmitter rather than a target value and to do so without communication between transmitters.

Minimum SINR

We consider the problem of maximising the minimum SINR. In a given system let the set of M receivers be $R = \{R_i : i = 1, ..., M\}$ and the set of N transmitters be $T = \{T_j : j = 1, ..k, ..., N\}$. Let P_j be the power-setting of transmitter T_j, σ_i the noise at receiver R_i and $r_{j,i}$ the distance between T_j and R_i with $g(r_{j,i})$ the pathloss function. Then, where $P_{\min}$ and $P_{\max}$ are the minimum and maximum transmit powers, the problem of maximising the miniumum SINR subject to transmit powers can be written as

$$\begin{aligned} \text{maximise} \quad & \min_{i,j} \frac{P_j g(r_{j,i})}{\sum_{k \neq j} P_k g(r_{k,i}) + \sigma_i} \\ \text{subject to} \quad & 0 \leq P_{\min} \leq P_j \leq P_{\max}. \end{aligned} \tag{3.1.1}$$

We recognise equation (3.1.1) as being a generalised linear-fractional program and a quasiconvex optimisation problem as described in [9]. In [9] the bisection method is proposed as being a way of solving such quasiconvex optimisation problems. Lieven Vandenberghe has written modules to do this in Julia, Python and R. In [66] the author explains that they attempted solving it using these modules but the solvers failed. They tried approaches other than the Python tools but were unable to find a complete package designed to cope with this type of problem. The difficulty arose from the fact that the objective function is not smooth and the solvers (modules) use gradient methods and therefore produce irrelevant results.

In [20] it is stated that because many QoS metrics are nonlinear functions of SIR, which is in turn a nonlinear (and neither convex nor concave) function of transmit powers, in general power control optimisation or feasibility problems are difficult non-linear optimisation problems that may appear to be NP-hard problems. It is found in [20] that when SIR is much larger than 0dB, a class of nonlinear optimisation called Geometric Programming (GP) can be used to efficiently compute the globally optimal power control in many of these problems and efficiently determine the feasibility of user requirements by returning either

a feasible (and indeed optimal) set of powers or a certificate of infeasibility.

As our priority when optimising the SINR is to increase the lowest values of SINR, we expect to encounter values close to or less than 0dB. In addition to this, a requirement of any distributed heuristic we propose is that it not place computational demands on the transmitters. The distributed heuristics we have so far discussed do not meet these requirements. Therefore rather than use one of these described distributed heuristics as a benchmark, by which to measure the performance of the power control policies we propose in Section 3.2, we instead benchmark policy performance against a policy named 'Smart' that we received from Keith Briggs at BT. The 'Smart' policy only uses the distance of the nearest transmitter to determine power level and so does use transmitter resources.

3.1.1 Uniform Power Settings

Before proposing policies for power control in Section 3.2 we first show that, with the exception of two transmitters and no noise, uniform powers are not optimal for SINR. When there are two transmitters and noise is present we show this by perturbing away from the case where powers are uniform and showing this leads to improvement. For three transmitters with no noise we show numerically that uniform powers are not optimal. Further cases are shown by numerical simulation in Section 3.2.

We show that in one dimension, where transmitters are distributed randomly along the real line, uniform power settings for the transmitters results in larger areas of 'low SINR' than otherwise. First let us begin by defining 'low SINR'. Recall that SINR is the ratio of signal to interference plus noise, and so

$$\text{Low SINR} \ := \frac{\text{Signal}}{\text{Noise} + \text{Interference}} \leq c, \quad \text{for } c > 0.$$

We now want to answer the following question, what is the expected 'thickness' of an area of low SINR between any two transmitters along the real line? To answer this we define the signal received from a transmitter T_i as

$$S_i = P_i g(r_i)$$

where γ is the pathloss exponent, r_i is the distance from T_i, $g(r_i)$ is a function of this distance and P_i is the power setting of T_i. Let σ be noise; it can be considered constant. Previously we have defined interference $I_i = \sum_{j \neq i} S_j$. However, in one dimension the interference in the SINR between two transmitters, T_i and T_j, only

comes from the neighbour transmitter so $I_i = S_j$ and the noise σ represents signal received from other transmitters on the line.

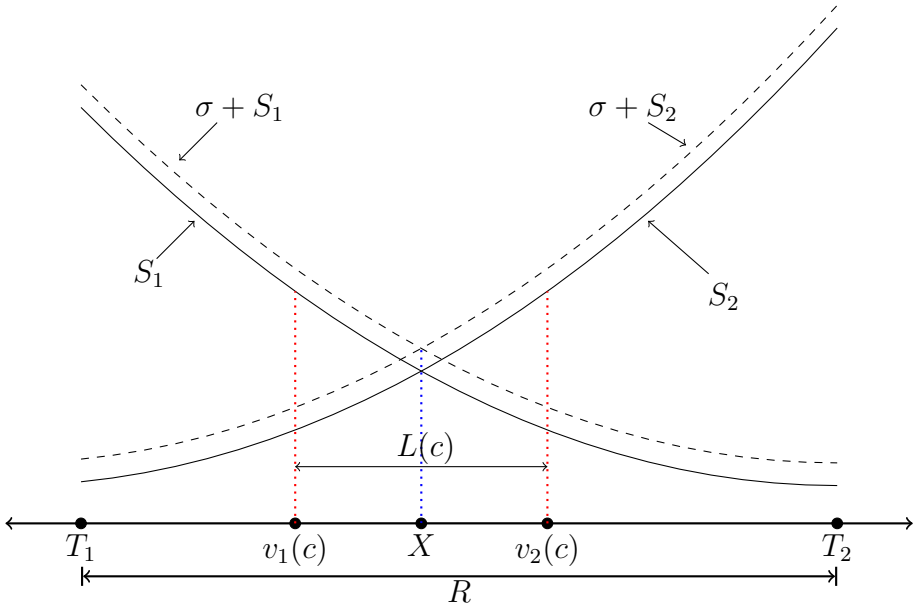

Figure 3-1: The signal, interference and noise between two transmitters T_1 and T_2. They have different strengths of signal, shown by S_1 and S_2, and the distance between them is denoted by R. The dashed lines represent the 'interference plus noise' contributed from one transmitter to the other. We have marked on the figure significant points relating to the SINR between them. Definitions of these points are given in the text.

On Figure 3-1, T_1 and T_2 mark the positions on the real line of two transmitters. We wish to find the length of the interval between them where SINR is low. We have marked with X the point where the maximum SINR is lowest, at this point

$$X : \quad \frac{S_1}{\sigma + S_2} = \frac{S_2}{\sigma + S_1}. \tag{3.1.2}$$

That is, a user cannot improve their SINR by switching to pair with the other transmitter. For a transmitter T_1 we define the region of 'low SINR' to be the subset of the line where

$$\frac{S_1}{\sigma + S_2} \leq c, \quad \text{for } c > 0. \tag{3.1.3}$$

The points at which 'low SINR' begins for transmitters T_1 and T_2 are marked on our diagram by $v_1(c)$ and $v_2(c)$ respectively. At $v_1(c)$

$$\frac{S_1}{\sigma + S_2} = c \tag{3.1.4}$$

and at $v_2(c)$

$$\frac{S_2}{\sigma + S_1} = c. \tag{3.1.5}$$

We wish to find the length $L(c)$ of the 'low SINR' interval and from (3.1.4) and (3.1.5) we see that

$$L(c) = |v_1(c) - v_2(c)|. \tag{3.1.6}$$

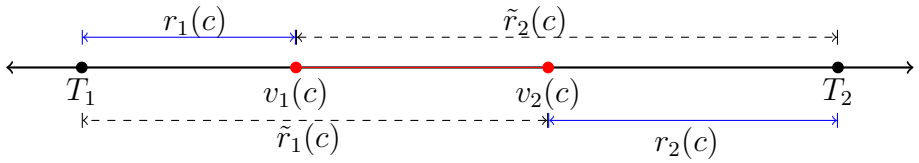

Figure 3-2: Illustration of the definitions of $\tilde{r}_2$, $\tilde{r}_1$, r_1 and r_2.

We will now compute $L(c)$. We begin by defining R as the distance between T_1 and T_2, so that at any point between them $r_1 + r_2 = R$. We then define $r_1(c)$ as the distance from $v_1(c)$ to T_1, $\tilde{r}_2(c)$ as the distance from $v_1(c)$ to T_2, $\tilde{r}_1(c)$ as the distance from $v_2(c)$ to T_1 and $r_2(c)$ as the distance from $v_2(c)$ to T_2. The definitions of these distances are illustrated in Figure 3-2. From our definitions of $v_1(c)$ and $v_2(c)$, given in equations (3.1.4) and (3.1.5) respectively, it follows that

$$c = \frac{P_1 g(r_1(c))}{P_2 g(\tilde{r}_2(c)) + \sigma} = \frac{P_2 g(r_2(c))}{P_1 g(\tilde{r}_1(c)) + \sigma}. \tag{3.1.7}$$

For clarity we write that $r_1(c) = r_1$, $r_2(c) = r_2$, $\tilde{r}_1(c) = \tilde{r}_1$ and $\tilde{r}_2(c) = \tilde{r}_2$. Additionally we know that $r_1 + \tilde{r}_2 = R$ and $\tilde{r}_1 + r_2 = R$, therefore (3.1.7) can be written as

$$c = \frac{P_1 g(r_1)}{P_2 g(R - r_1) + \sigma} = \frac{P_2 g(r_2)}{P_1 g(R - r_2) + \sigma}. \tag{3.1.8}$$

We can also note that $L(c) = |R - r_1 - r_2|$. Our aim is to minimise $L(c)$, where the two independent variables are P_1 and P_2. For ease of computation we will define $g(r) = r^{-\gamma}$, so that we using a far-field pathloss model given by equation (1.3.1) in Subsection 1.3.1. We will begin with the simplest case, setting $\sigma = 0$.

Two transmitters without noise, $\sigma = 0$

To remove noise effects we set $\sigma = 0$. To minimise the length of the interval within which we have 'low SINR' we must minimise the distance $L(c)$ between $v_1(c)$ and $v_2(c)$. This is equivalent to maximising $r_1 + r_2$ over allowed power settings. We will show that $r_1 + r_2$ is maximised when $P_1 = P_2$ and therefore show that uniform powers are optimal for two transmitters with no noise in one

dimension.

At $v_1(c)$

$$c = \frac{P_1 r_1^{-\gamma}}{P_2 \tilde{r}_2^{-\gamma}} \tag{3.1.9}$$

and at $v_2(c)$

$$c = \frac{P_2 r_2^{-\gamma}}{P_1 \tilde{r}_1^{-\gamma}}. \tag{3.1.10}$$

We define the ratio ω of the power P_1 of transmitter T_1 to the power P_2 of transmitter T_2, and write

$$\omega = \frac{P_1}{P_2}. \tag{3.1.11}$$

We wish to isolate r_1 and r_2 from equations (3.1.9) and (3.1.10) respectively. Using that $r_1 = R - \tilde{r}_2$ and $r_2 = R - \tilde{r}_1$, together with the substitution (3.1.11), we find that at $v_1(c)$

$$r_1 = R\left(\frac{(\omega^{-1}c)^{-1/\gamma}}{1 + (\omega^{-1}c)^{-1/\gamma}}\right) \tag{3.1.12}$$

and at $v_2(c)$

$$r_2 = R\left(\frac{(\omega c)^{-1/\gamma}}{1 + (\omega c)^{-1/\gamma}}\right). \tag{3.1.13}$$

Simplifying we see that

$$r_1 = R\left(\frac{1}{c\omega^{-1/\gamma} + 1}\right) \tag{3.1.14}$$

and

$$r_2 = R\left(\frac{1}{c\omega^{1/\gamma} + 1}\right). \tag{3.1.15}$$

Our aim is to find ω, the relationship between P_1 and P_2, such that $r_1 + r_2$ is maximised. From equations (3.1.14) and (3.1.15) we know that

$$r_1 + r_2 = R\left(\frac{1}{1 + c\omega^{-1/\gamma}} + \frac{1}{1 + c\omega^{1/\gamma}}\right). \tag{3.1.16}$$

When the power settings are equal $\omega = 1$ and

$$r_1 + r_2 = \frac{2R}{1 + c}. \tag{3.1.17}$$

When power settings are not equal $\omega \neq 1$. Equal powers are not optimal if

$$R\left(\frac{1}{1 + \omega^{1/\gamma}c} + \frac{1}{1 + \omega^{-1/\gamma}c}\right) > R\left(\frac{2}{1 + c}\right), \tag{3.1.18}$$

with $\omega \in \mathbb{R}^+$, and $\omega \neq 1$.

We rearrange and simplify (3.1.18) as follows: first cancel the factor of R and then expand the fractions on left hand side so that they share a common denominator before adding them, this achieves

$$\frac{2 + c\left(\omega^{-1/\gamma} + \omega^{1/\gamma}\right)}{1 + c^2 + c\left(\omega^{-1/\gamma} + \omega^{1/\gamma}\right)} > \frac{2}{1+c} \tag{3.1.19}$$

We then multiply both sides of (3.1.19) by the denominator of its left hand side before subtracting $c\left(\omega^{-1/\gamma} + \omega^{1/\gamma}\right)$ from both sides. This yields

$$2 > \frac{2(1+c^2)}{1+c} + \frac{2c\left(\omega^{-1/\gamma} + \omega^{1/\gamma}\right)}{1+c} - c\left(\omega^{-1/\gamma} + \omega^{1/\gamma}\right) \tag{3.1.20}$$

From which we obtain

$$\frac{2\left(1 - \frac{(1+c^2)}{1+c}\right)}{c\left(\frac{2}{1+c} - 1\right)} > \omega^{1/\gamma} + \omega^{-1/\gamma}. \tag{3.1.21}$$

The left hand side of (3.1.21) can be simplified. Its denominator is given by

$$c\left(\frac{2}{1+c} - 1\right) = \frac{c(1-c)}{1+c}$$

and its numerator can similarly be simplified:

$$2\left(1 - \frac{(1+c^2)}{1+c}\right) = \frac{2c(1-c)}{1+c}.$$

Therefore the left hand side of (3.1.21) can be simplified to give

$$\frac{\frac{2c(1-c)}{1+c}}{\frac{c(1-c)}{1+c}} = 2$$

and so (3.1.21) leads to the condition

$$2 > \omega^{-1/\gamma} + \omega^{1/\gamma}. \tag{3.1.22}$$

Multiplying both sides of (3.1.22) by $\omega^{1/\gamma}$ and then simplifying we find that we require

$$\left(\omega^{1/\gamma} - 1\right)^2 < 0. \tag{3.1.23}$$

There exists no ω, where $\omega \in \mathbb{R}^+$, that satisfies (3.1.23). Therefore for two

transmitters in one dimension equal power settings minimise the length of the region of low SIR between them. Uniform power settings are optimal in this case.

If this is true in one dimension then it is intuitive that it would also be true in two dimensions as the area of low SINR would be minimised by equal power settings.

Two transmitters with noise, $\sigma > 0$

Where noise is given by σ then at $v_i(c)$ and $v_j(c)$ then

$$c = \frac{P_1 r_1^{-\gamma}}{P_2 \tilde{r}_2^{-\gamma} + \sigma} = \frac{P_2 r_2^{-\gamma}}{P_1 \tilde{r}_1^{-\gamma} + \sigma}$$

We find that when $\sigma > 0$ uniform transmit powers does not minimise the length of low SINR. As before we set that $P_1 = \omega P_2$ and note that $\tilde{r_2} = R - r_1$ and $\tilde{r_1} = R - r_2$. We also set that $y = \frac{\sigma}{P_2}$, this gives that

$$c = \frac{\omega r_1^{-\gamma}}{(R - r_1)^{-\gamma} + y} = \frac{r_2^{-\gamma}}{\omega(R - r_2)^{-\gamma} + y}. \tag{3.1.24}$$

In the case without noise we showed that the length of low SINR was minimised when $\omega = 1$. We differentiate with respect to ω to understand how perturbances in ω has on the length of low SINR from the case when $\omega = 1$ with noise present. We find that

$$\frac{dr_1}{d\omega} = \frac{r_1^{-\gamma}}{\gamma\left(c(R - r_1)^{-\gamma-1} + \omega r_1^{-\gamma-1}\right)} \tag{3.1.25}$$

and

$$\frac{dr_2}{d\omega} = \frac{-c(R - r_2)^{-\gamma}}{\gamma\left(c\omega(R - r_2)^{-\gamma-1} + r_2^{-\gamma-1}\right)}. \tag{3.1.26}$$

We observe that when $\omega = 1$ the denominators are equal and note that $R - r_2 > r_1$. As $r_1 < R - r_2$ then $r_1^{-\gamma} > (R - r_2)^{-\gamma}$. Therefore from the case where transmit powers are uniform and $\omega = 1$ we see that

$$\frac{d(r_1 + r_2)}{d\omega} = \frac{r_1^{-\gamma} - c(R - r_2)^{-\gamma}}{\gamma\left(c(R - r_2)^{-\gamma-1} + r_2^{-\gamma-1}\right)}, \quad \text{with } r_1 = r_2. \tag{3.1.27}$$

Therefore when the fixed constant $c \geq 1$, and there exists a solution to (3.1.24), then

$$\frac{d(r_1 + r_2)}{d\omega} > 0. \tag{3.1.28}$$

This shows that changes in ω, that is moving away from uniform transmit powers, further reduces the length of low SINR. We conclude that uniform transmit powers are not optimal for two transmitters when noise is present.

Three transmitters without noise

In contrast to the two transmitter case (without noise), equal power settings are not optimal when three transmitters are present. Here we show that when there are three transmitters present, the total length of the intervals where SINR is unacceptably low is minimised by taking unequal power settings for the three.

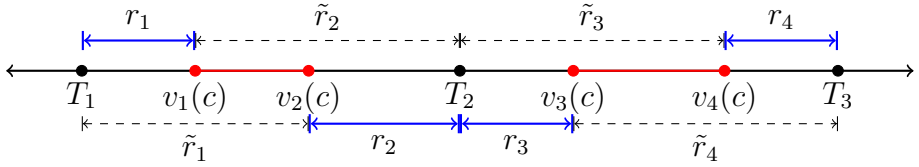

Figure 3-3: Illustration of the definitions of $\tilde{r}_1$, $\tilde{r}_2$, $\tilde{r}_3$, $\tilde{r}_4$, r_1, r_2, r_3 and r_4. We wish to minimise the sum of red lengths (the regions of low SIR), which is the same as maximising the sum of the blue distances (regions of acceptable SIR).

We define R to be the distance from T_1 to T_3, such that $R = |T_1 - T_3|$. Let α where $0 < \alpha < 1$. Then we define the distance from transmitter T_1 to T_2 to be αR such that $\alpha R = |T_1 - T_2|$, and the distance from T_2 to T_3 to be $(1-\alpha)R$ such that $(1-\alpha)R = |T_2 - T_3|$.

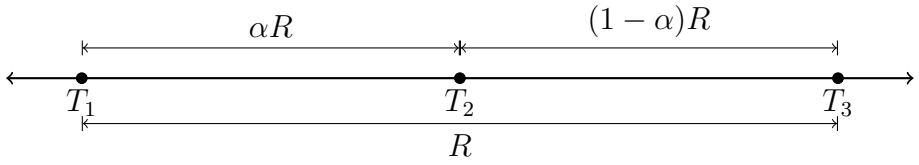

Figure 3-4: Illustration of the definitions of the distances between T_1, T_2 and T_3.

We define the power settings of the transmitters relative to each other so that $P_1 = \omega P_2$ and $P_3 = \mu P_2$.

To minimise the region of low SIR, we wish to maximise $r_1 + r_2 + r_3 + r_4$. For a fixed constant $c > 0$, we find using our definitions that:

at $v_1(c)$

$$1 + c = \frac{\omega r_1^{-\gamma}}{(\alpha R - r_1)^{-\gamma} + \mu(R - r_1)^{-\gamma}} \tag{3.1.29}$$

at $v_2(c)$

$$c = \frac{r_2^{-\gamma}}{\omega(\alpha R - r_2)^{-\gamma} + \mu(R - (\alpha R - r_2))^{-\gamma}} \tag{3.1.30}$$

at $v_3(c)$

$$c = \frac{r_3^{-\gamma}}{\omega(\alpha R + r_3)^{-\gamma} + \mu(R - (\alpha R + r_3))^{-\gamma}} \tag{3.1.31}$$

at $v_4(c)$

$$c = \frac{\mu r_4^{-\gamma}}{(R - r_4 - \alpha R)^{-\gamma} + \omega(R - r_4)^{-\gamma}} \tag{3.1.32}$$

We will show a contradiction to the statement that uniform transmit powers are optimal for three transmitters. For a fixed SIR threshold (and therefore c) we denote the constant $(c)^{-1}$ by c. Let α, γ and R also be fixed. Rewriting the above expressions we see that for our variables r_1, r_2, r_3, r_4 and μ, ω:

at $v_1(c)$

$$\omega c = \left(\frac{\alpha R}{r_1} - 1\right)^{-\gamma} + \mu \left(\frac{R}{r_1} - 1\right)^{-\gamma} \tag{3.1.33}$$

at $v_2(c)$

$$c = \omega \left(\frac{\alpha R}{r_2} - 1\right)^{-\gamma} + \mu \left(\frac{(1-\alpha)R}{r_2} + 1\right)^{-\gamma} \tag{3.1.34}$$

at $v_3(c)$

$$c = \omega \left(\frac{\alpha R}{r_3} + 1\right)^{-\gamma} + \mu \left(\frac{(1-\alpha)R}{r_3} - 1\right)^{-\gamma} \tag{3.1.35}$$

at $v_4(c)$

$$\mu c = \left(\frac{(1-\alpha)R}{r_4} - 1\right)^{-\gamma} + \omega \left(\frac{R}{r_4} - 1\right)^{-\gamma} \tag{3.1.36}$$

We show with numerical simulation that uniform powers are not optimal by showing an example where moving away from uniform powers improves SIR. We set that $P_1 = P_3 = P_{\max}$ and $\alpha = 0.5$. This gives that $r_1 = r_4$ and $r_2 = r_3$. We set that $v = \omega = \mu$ and note that $v \geq 1$. Therefore we can write equations (3.1.34) and (3.1.35) as

$$c = v \left(\left(\frac{0.5R}{r_2} - 1\right)^{-\gamma} + \left(\frac{0.5R}{r_2} + 1\right)^{-\gamma} \right), \tag{3.1.37}$$

and equations (3.1.33) and (3.1.36) as

$$c - \left(\frac{R}{r_1} - 1\right)^{-\gamma} = \frac{1}{v} \left(\frac{0.5R}{r_1} - 1\right)^{-\gamma}. \tag{3.1.38}$$

From equation (3.1.37) we see that r_2 and r_3 will descrease as P_2 decreases and v increases. However, we observe in (3.1.38) that increasing v so that powers are not uniform allows for an increase in r_1 and r_4. In Figure 3-5 we show that

uniform powers actually maximise the percentage of low SIR. In this figure we relax the requirement that a solution must always exist for equations (3.1.33) to (3.1.36).

Let us fix a maximum power $P_{\max}$ and set that $P_1 = P_{\max}$. As we defined $P_1 = \omega P_2$ and $P_3 = \mu P_2$ then $\omega \geq 1$ and $\mu \geq 1$. We also set a minimum power $P_{\min} > 0$ so that we do not reduce this to a two transmitter problem and no longer satisfy equations (3.1.33) to (3.1.36).

Let $\alpha = 0.5$, $R = 8$, $P_{\max} = 4$, $\gamma = 4$ and $c = 1.5$. In Figure 3-5 we show that the lowest percentage of SIR is not achieved when all three transmitters have the same transmit power. The percentage of receivers observing low SIR is lowest on the plot when transmitter T_3 has power $p_3 = 0.25$ and transmitter T_2 has power p_2 between 3.5 and 4. As low SINR is not minimised when all three transmitters have power $P = 4$ this shows that uniform transmit powers are not optimal.

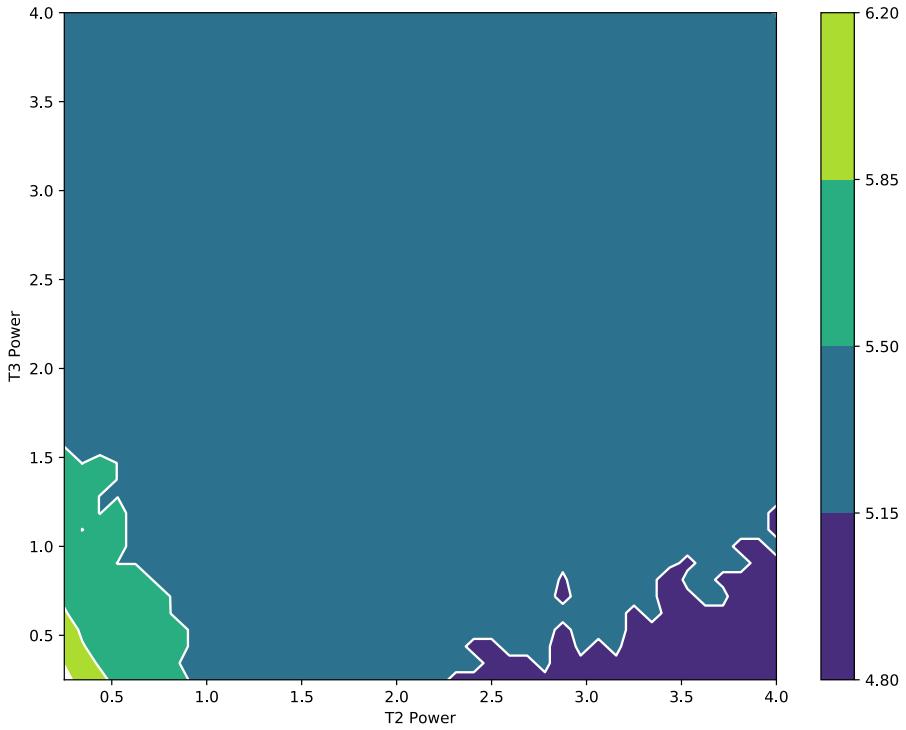

Figure 3-5: Percentage of receivers observing low SIR as a function of transmitter powers for T_2 and T_3. The top right corner is where the three transmitters have uniform transmit powers $P_1 = P_2 = P_3 = 4$. The colour bar represents the percentage of 'low SIR' area. The SIR is measured by 1601 transmitters uniformly spaced along the line the transmitters were placed along. The Transmitters were at locations $(0,0), (4,0), (8,0)$. Transmitter T_1 has power $P_1 = 4$, this is fixed as the powers of the other transmitters are varied.

We have shown that uniform powers are optimal in the trivial case of two

transmitters with no noise present. We have shown that when there are three transmitters, or noise is present for two transmitters, then uniform powers are not optimal. We will show in the next section that this holds for larger numbers of transmitters by implementing the policy 'Constant' which sets transmit powers to be uniform. We will also show that non-uniform powers that were set without using network considerations do not perform better than uniform powers by implementing a policy named 'Random'.

3.2 Self Optimising Power Control Algorithms

Power control algorithms are in effect policies that control the transmit powers of transmitters. In this section we identify and develop policies that improve some low quantile of the SINR and also provide good coverage. The strategies need to work in a distributed way.

3.2.1 Transmit Power Policies

We placed Poisson distributed points in a plane and these points are considered to be the locations of transmitters in a model cellular network. Each transmitter is assigned an initial power setting P, and that power setting will be updated according to a *policy*. To measure how a policy has performed, points on the plane are chosen at random and the SINR at that point is recorded, in effect taking a sample of the SINR. We set that the noise $\sigma = 0.001$. Samples are taken until a specified accuracy criterion is met. For the results shown below, samples were taken until every 5th quantile had a confidence interval of 95%. To do this we adapted the sampling module in [16] so that the performance of the policies could be compared directly to each other. The seven different power control policies are described below.

Smart policy

For each transmitter the distance to its nearest neighbour d_1 is found. Its power setting P is set as $P = \min(d_1^\gamma, P_{\max})$ where γ is the pathloss exponent. The result of this is that the interference I its nearest neighbour receives from it I_1 is limited to $I_1 \leq 1$.

This policy, that we received from Keith Briggs at BT [12] , is used to benchmark the performance of all other policies.

Constant policy

All transmitters have the same power setting P, where we set $P = P_{\max}$. This policy builds on the work of the previous section in showing the system-wide SINR when transmit powers are uniform.

This policy shows that uniform transmit powers are not optimal.

Random policy

Each transmitter has a power setting that is a random number between 0 and the maximum power P_{max}.

This policy shows that non-uniform transmit powers that are set without using network considerations do not improve performance.

Switch-off policy

This is similar to the *smart* strategy but differs in that it imposes a condition.

Let P and P_1 be the power setting of the transmitter and its nearest neighbour transmitter. Let d_1 and d_2 be the distance to the nearest and second nearest transmitter respectively.

A minimum distance d_{min} is specified, if $d_1 \geq d_{min}$ then the smart strategy is used as above. However, if $d_1 < d_{min}$ and $P_1 > 0$ then switch off. If $d_1 < d_{min}$ and $P_1 = 0$ then the distance to the second nearest neighbour d_2 is found and $P = \min(d_2^\gamma, P_{max})$.

Algorithm 3.1 Switch-off policy

Set d_{min} and compute d_1 and d_2
if $d_1 \geq d_{min}$ **then**
    $P = d_1^\gamma$
else if $P_1 > 0$ **then**
    $P = 0$
else
    $P = \min(d_2^\gamma, P_{max})$.
end if

Switch-off Cluster (SOC) policy

Let P and P_1 be the power setting of the transmitter and its nearest neighbour transmitter. Let d_1 be the distance to the nearest transmitter. Let d_{min} be a distance from the transmitter and denote the distance and power of all transmitters

within the minimum distance by d_i and P_i respectively. Let d_k be the smallest transmitter distance greater than d_{min}.

This strategy was devised to address the circumstance where a number of transmitters are clustered together. It uses a defined minimum distance d_{min} and the distance to the nearest neighbour d_1. If $d_1 \geq d_{min}$ then $P = \min(d_1^\gamma, P_{max})$. Otherwise, when $d_1 < d_{min}$ find all transmitters within d_{min}. If any transmitters within d_{min} have $P > 0$ then set the current transmitter to have $P = 0$. If all neighbouring transmitters within d_{min} have $P = 0$ then, find the distance d_k of the nearest neighbour transmitter outside of d_{min} and set for the current transmitter $P = \min(d_k^\gamma, P_{max})$.

This can be thought of as placing an exclusion zone around each transmitter, so that there is no more than one transmitter switched on within an area specified by d_{min}. However, this policy requires a transmitter to determine the distance and power of every transmitter with distance d_{min}.

Algorithm 3.2 Switch-off Cluster policy

```
Set d_min and compute d_1
if d_1 ≥ d_min then
    P = min(d_1^γ, P_max)
else
    Identify all transmitters within d_min, and return d_i and P_i
    if ∃ P_i > 0 then
        P = 0
    else
        P = min(d_k^γ, P_max)
    end if
end if
```

3.2.2 Policy Performance

We evaluate the performance of the policies we have described by applying them to a set of transmitters and then measuring SINR. The SINR CDF curve that results from use of the 'Constant policy' demonstrates that uniform powers are not optimal for SINR. Similarly, the SINR CDF curve that results from use of the 'Random policy' demonstrates that non-uniform powers set without consideration of the network do not perform better than uniform powers.

We chose to have 500 transmitters. To generate their locations, as coordinates, pairs of random numbers were generated between 0 and 1, these were then scaled by $\sqrt{\pi 500}$. For a given set of locations the different policies were applied and,

once all transmitters had updated, the sampler in [16] was used to estimate the quantiles of the SINR. The performance of the different policies is shown in Figure 3-6.

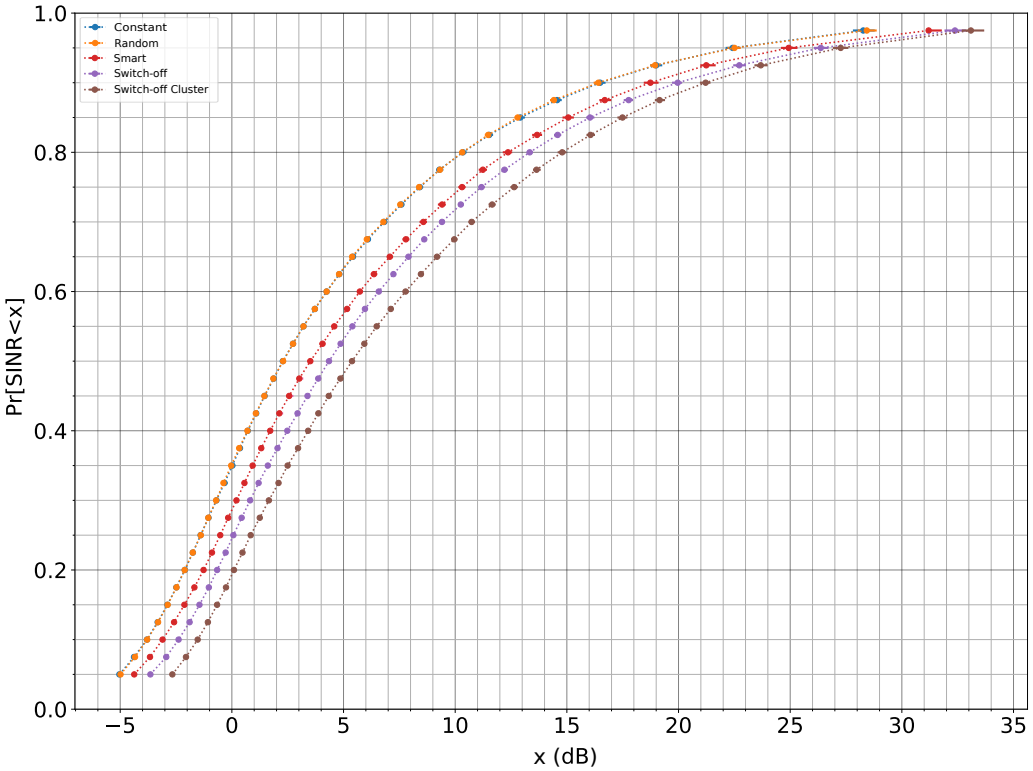

Figure 3-6: Probability that a randomly sampled SINR is less than a given value x (in dB), for each of the seven policies, applied to a set of 500 fixed transmitter locations. We set $d_{min} = 2$. The confidence interval was 95%. The policies *Constant* and *Random* perform very similarly, they are plotted on top of one another and are the worst performing. The policy *Switch-off Cluster* outperforms all other policies.

It can be seen that 'Switch-off Cluster' is the best performing policy. Though it is important to note that how well it performs is dependent on d_{min} being set appropriately. In Figure 3-10 we show the results with varying values of d_{min}.

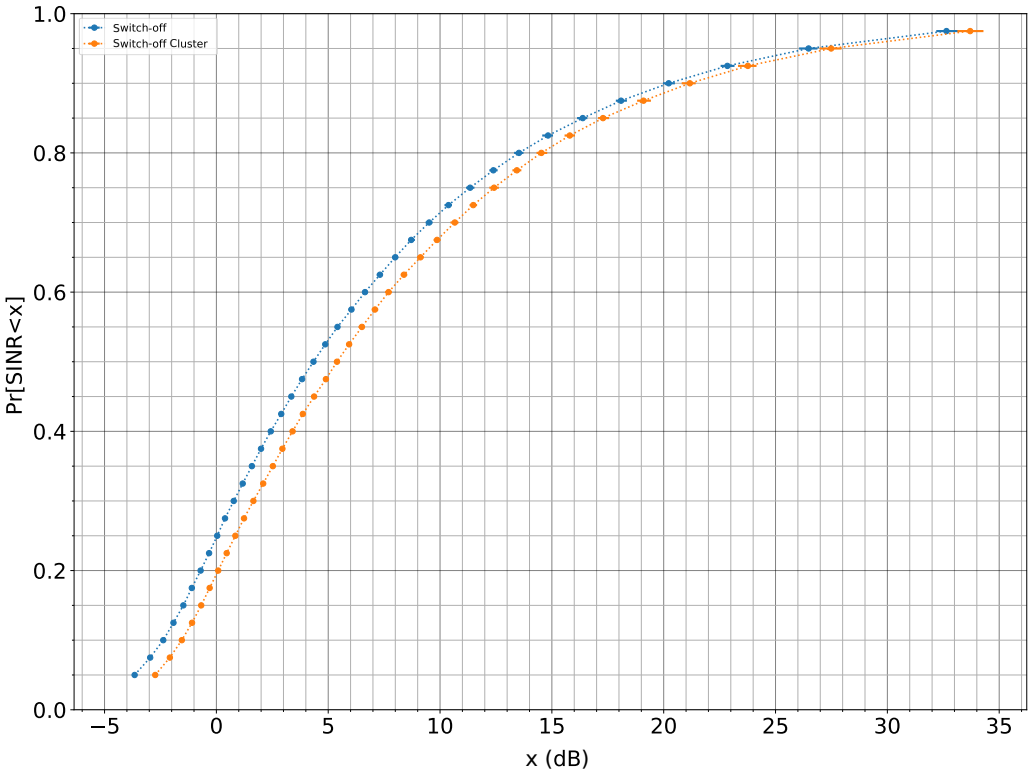

Figure 3-7: Probability that a randomly sampled SINR is less than a given value x (in dB) for each of the two *switch-off* policies: switch-off and switch-off cluster. There were 500 trasmitters placed with an average density of $\frac{\sqrt{500}}{\sqrt{\pi}}$ and we set $d_{min} = 2$. The locations of the transmitters are fixed and each strategy was run through once. The confidence interval was 95%. Switch-off cluster is the best performing policy and in 3-8 we show how it performs as d_{min} is varied.

In Figure 3-7 we compare the performance of the two switch-off policies, given in Algorithms 3.1 and 3.2. The performance of these policies is determined by the choice of d_{min}. We see that Switch-off Cluster is the best performing of the two policies. In Figure 3-8 the effect of varying the d_{min} on the performance of the SOC policy is shown. It shows that as d_{min} is increased from 0.5 to 2.0 the policy performance noticeably improves, however from 2.0 to 3.0 these improvements tail off.

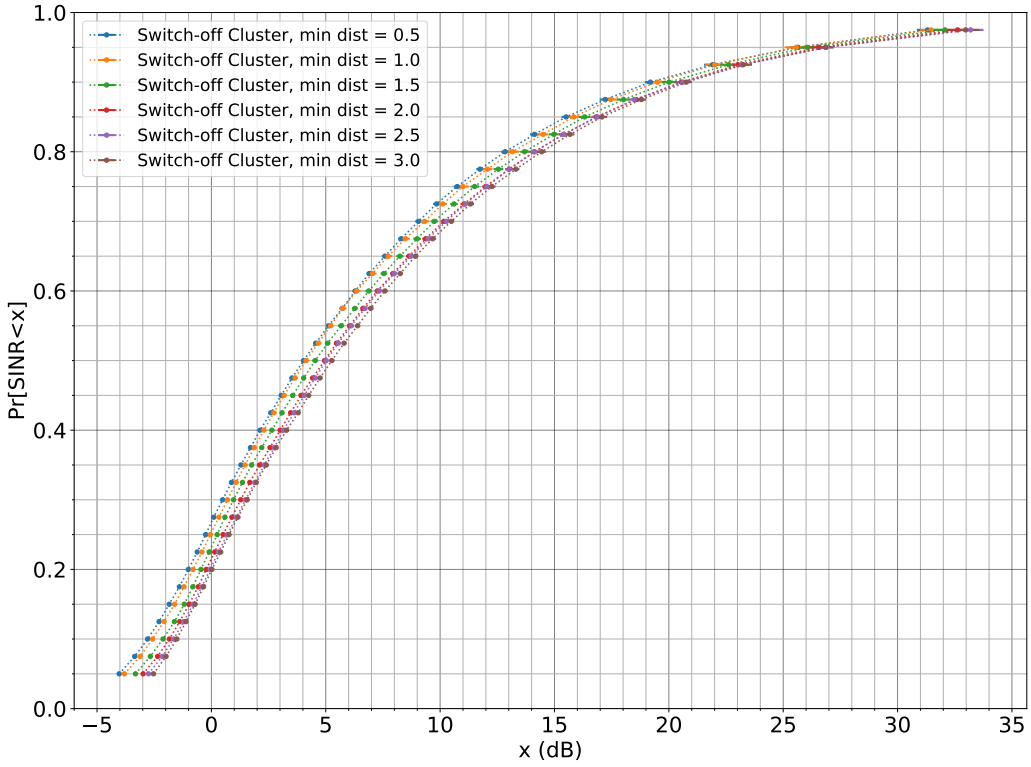

Figure 3-8: Probability that a randomly sampled SINR is less than a given value x (in dB), for the SOC policy applied to a set of 500 fixed transmitter locations. The value of d_{min} increased from 0.5 to 3.0 in step sizes of 0.5. The locations of the transmitters were kept the same as in the previous figures and the confidence interval was kept at 95%.

In the following section, the distribution of the SINR is shown in heatmaps, for the examples illustrated here.

SINR spatial distribution

How is the SINR distributed over the transmitter locations? Answering this question may provide further insight into the performances of the power control algorithms we are exploring. We would like to visualise the SINR along with the transmitter locations and whether a transmitter was on or off.

To create our visualisation we begin by creating a plane with periodic x and y axes that range from 0 to 40. The periodic axes prevents the effect of transmitters close to an axis receiving less interference. We randomly generate 500 transmitter locations which we fix and keep constant as we vary d_{min}. For comparison we

have used the same transmitter locations in Figures 3-10 and 3-8. After two complete iterations of the SOC algorithm transmitter powers do not change and so there is no further improvement in SINR. This is shown in Figure 3-9 where, in addition to observing that a second complete iteration only achieves a slight improvement in SINR, subsequent iterations do not result in improvement. The slight variance between the CDF curves at higher values of SINR is a result of the random sampler used and far-field pathloss. Higher values of SINR occur when measurements are taken at small distances to the paired transmitter and small changes in this distance have relatively large effects on SINR.

Transmitters which are off are shown in white and those that are on are shown in red. The colourbar which relates the plotted heatmap to values of SINR in dB is standardised across all six plots so that the plots can be directly compared. SOC is the best performing power control algorithm. In Figure 3-8 it is shown how its performance varies with d_{min}. We will now look at how the distribution of SINR varies for those same transmitter locations and values of d_{min}. In Figures 3-10a to 3-10f we show the SINR after two complete iterations of the SOC algorithm.

In Section 3.3 we use reinforcement learning methods to learn policies that do not require knowledge of distances or power settings of other transmitters in the network. We will show that they only require the SINR of user devices paired to a transmitter to establish an effective power control policy.

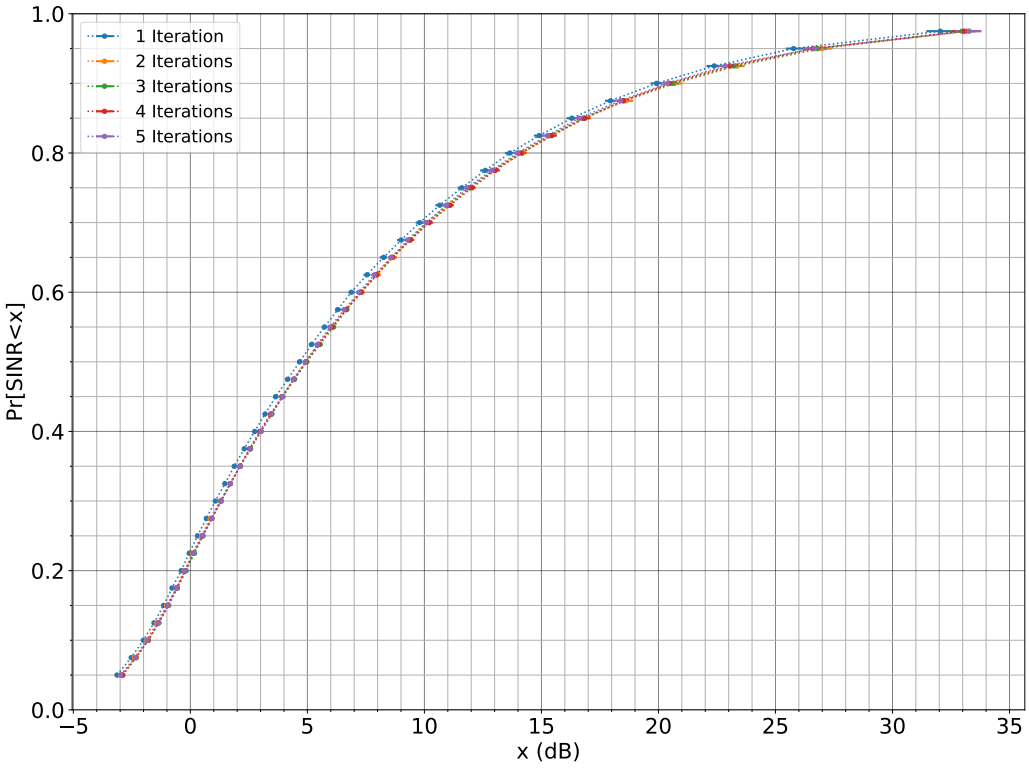

Figure 3-9: Probability that a randomly sampled SINR is less than a given value x (in dB), for the SOC policy after a given number of complete iterations.

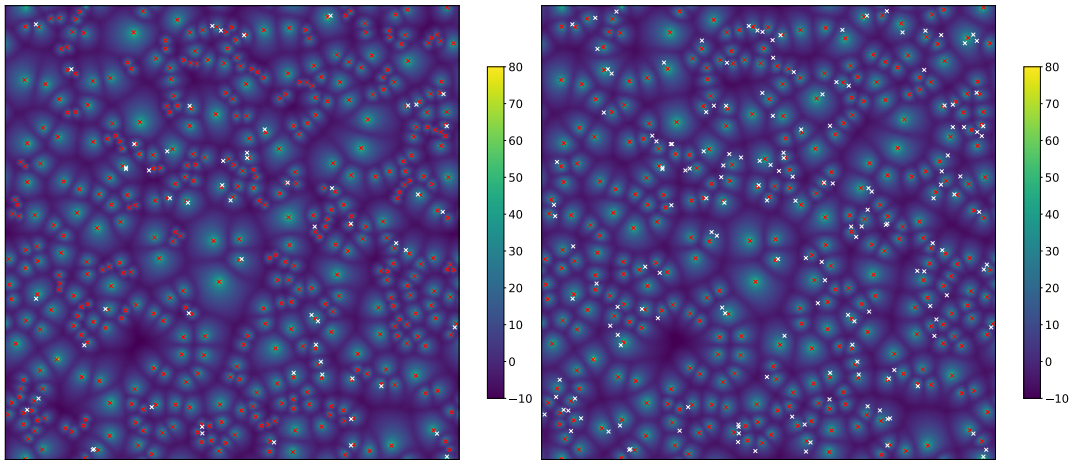

(a) $d_{min} = 0.5$ (b) $d_{min} = 1.0$

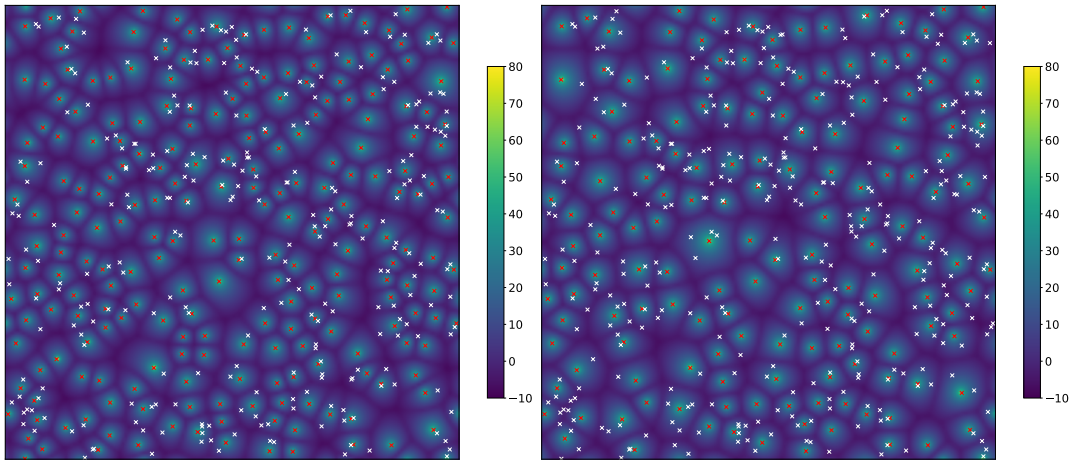

(c) $d_{min} = 1.5$ (d) $d_{min} = 2.0$

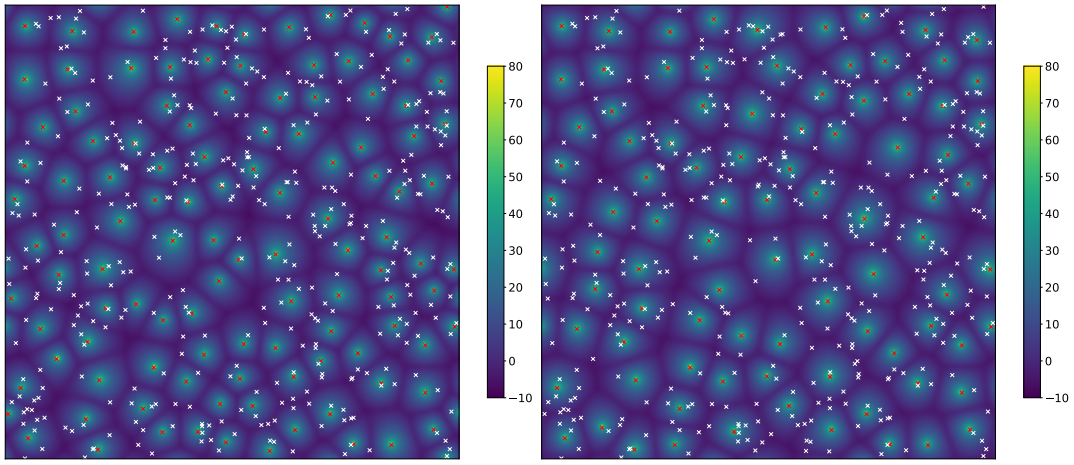

(e) $d_{min} = 2.5$ (f) $d_{min} = 3.0$

Figure 3-10: Heatmaps showing the distribution of SINR in a periodic domain $0 \leq x, y \leq 40$ with periodic boundary conditions. The colourbar is the same for all figures so they can be easily compared. There are 500 transmitters. Switched-off transmitters are shown in white and those that are on are marked in red. The transmitter locations are the same as those used to generate Figures 3-6 to 3-8.

3.3 Power Control Policies via Reinforcement Learning

In Subsection 3.2.1 we proposed and compared different policies for power control. A part of the process for developing the policies was to observe the results (the heatmaps) and identify scenarios which caused low SINR. For example, when implementing the policy 'Switch-off' and observing the SINR heatmaps we noticed that there were low SINR areas where multiple transmitters were clustered together. We devised a policy to perform better in this scenario which we named SOC. In Figure 3-7 it can be seen that the SOC policy outperforms the 'Switch-off' policy, in fact it outperforms all other policies. We learnt from interacting with the system and devised an effective policy.

From Subsection 1.4.2, where we introduced reinforcement learning, we know that learning a policy through interacting with a system can be made a reinforcement learning problem. To formulate a reinforcement learning problem there must be a defined agent, reward, environment, set of states and set of actions. Various scheme designs have been used when applying reinforcement learning to communication network optimisation problems.

It was found in [32] that Q-learning, when used for learning a power control policy, quickly becomes unusable as the state-action set grows due to the required usage of tables to store transitional data. Additionally the required number of data samples becomes prohibitively large. When we implemented Q-learning we found that, even using buckets to reduce the state set as in [65], after a large number of iterations the Q-table remained sparse. This resulted in an optimal policy not being found. As in [32] we moved to deep Q-learning where an ANN is chosen to represent the Q-function as described in Section 1.4.2 of Chapter 1.

3.3.1 Deep Q-learning

We wish to devise a policy that achieves the highest SINR possible for each receiver given the network's spatial configuration. We formulate the problem as a multi-agent cooperative learning scheme. This means that each transmitter is an agent and agents learn a shared policy. It is found in [62] that cooperative learning leads to more robust reactions to network dynamics compared to independent learning (when each agent learns a separate policy).

The use of an ANN to approximate the Q-function means that convergence to an optimal policy is no longer guaranteed. In [30] it is shown using empirical

evidence that the deep Q-learnt multi-agent policy for interference control in a radio network was suboptimal. Additionally, the convergence proof used for the single-agent case [54] cannot be extended to multi-agent settings. Proof of convergence for the general multi-agent setting is an open problem [62].

Although the policies we propose may be suboptimal they offer significant improvement over the benchmark policy 'Smart' and require minimum network knowledge. Additionally, we propose offline policies. After sufficient initial training the policy will be fixed. The learnt policy will then be implemented, reducing the computational demands placed on transmitters. We train our policies on a small network of transmitters to learn a policy and then implement this learnt policy on independent larger networks.

We now describe the design of our learning scheme before presenting the results. We fix the pathloss exponent $\gamma = 4$, we also fix noise $\sigma = 0.001$, the density of transmitters is π^{-1}. For computing received signal strength S we use the far-field pathloss model and do not include fading variables. We set the maximum power $P_{\max} = 25$, on which the area of the disc around the transmitter where $S \geq 1$ is expected to contain 4 other transmitters.

Actions

The actions and reward function are consistent throughout the implementation of our deep Q-learning schemes. For any transmitter let d_1, d_2, d_3 be the distances to its first, second and third nearest neighbour transmitters respectively. Let P_{d_1}, P_{d_2}, P_{d_3} be transmit powers such that the received signal at the first, second and third nearest neighbour transmitters respectively is 1. When a transmitter is switched off its transmit power is written as P_{d_0}. The set of actions an agent chooses from are setting the transmit power to one of four values:

$$\boldsymbol{A} = \{P_{d_0}, P_{d_1}, P_{d_2}, P_{d_3}\}. \tag{3.3.1}$$

Reward Function

The reward function r_t is based on the SINR observed by receivers paired to the agent. We record the SINR of all receivers within radius l of the acting transmitter (our agent). We set that $l = 2$ as the density of transmitters $\lambda = \pi^{-1}$, we expect a disc of radius $l = 2$ to contain the nearest three neighbours. From recorded SINRs we compute the value of the 20^{th}, 50^{th} and 75^{th} percentiles, we write these as SINR_{20}, SINR_{50}, SINR_{75}. The reward function is computed as follows. Let SINR_l be the SINR observed in a disk of radius l around the agent before it acts.

We denote the ith percentile of the SINR recorded by receivers in this disc as $\text{SINR}_{l,i}$. Then,

$$r_t = \begin{cases} +25 & \text{if } \text{SINR}_{20} > \text{SINR}_{l,20}, \\ -25 & \text{if } \text{SINR}_{20} < \text{SINR}_{l,20}, \\ 0 & \text{if } \text{SINR}_i = \text{SINR}_{l,i} \text{ for } i = 20, 50, 75, \\ +5 & \text{if } \text{SINR}_{20} = \text{SINR}_{l,20} \text{ and} \\ & \quad \text{SINR}_i > \text{SINR}_{l,i} \text{ for } i = 50 \text{ or } i = 75, \\ -5 & \text{if } \text{SINR}_{20} = \text{SINR}_{l,20} \text{ and} \\ & \quad \text{SINR}_i < \text{SINR}_{l,i} \text{ for } i = 50 \text{ and } i = 75. \end{cases} \tag{3.3.2}$$

States

We use three different sets of observations to determine an agent's state: $\boldsymbol{S_1}$, $\boldsymbol{S_2}$ and $\boldsymbol{S_3}$. The first set of observations we use is

$$\boldsymbol{S_1} = \{P, \text{SINR}_{20}, \text{SINR}_{50}, \text{SINR}_{70}\}. \tag{3.3.3}$$

To show that the addition of transmitter distances does not improve on the policy achieved with $\boldsymbol{S_1}$ we also use the set of observations

$$\boldsymbol{S_2} = \{P, d_1, d_2, d_3, \text{SINR}_{20}, \text{SINR}_{50}, \text{SINR}_{70}\}, \tag{3.3.4}$$

and, to show that the addition of further SINR measurements does not improve on the policy achieved with $\boldsymbol{S_1}$, we use the observation set

$$\begin{aligned} \boldsymbol{S_3} = \{P, \text{SINR}_0, \text{SINR}_{10}, \text{SINR}_{20}, \text{SINR}_{30}, \text{SINR}_{40}, \text{SINR}_{50}, \\ \text{SINR}_{60}, \text{SINR}_{70}, \text{SINR}_{80}, \text{SINR}_{90}, \text{SINR}_{100}\}. \end{aligned} \tag{3.3.5}$$

We show in the results subsubsection that neither of the larger observation sets $\boldsymbol{S_2}$ or $\boldsymbol{S_3}$ improve the policy performance achieved with $\boldsymbol{S_1}$. Supporting that knowledge of its own transmit power and SINR observations of paired receivers is enough for effective policy development.

Training

We trained our offline policy by placing 50 transmitters randomly onto a plane with periodic boundary conditions and area 50π. We placed 625 receivers (measurement points) spaced uniformly in a lattice configuration over the plane. After every action receivers re-pair to pair to the transmitter they received the highest

signal from.

We configured an ANN with two hidden layers, with each hidden layer consisting of 64 nodes. For the activation function, as stated in the introduction, we used three different functions $g(x) = \tanh(x)$, the rectifier non-linearity $g(x) = \max(0, x)$ and the sigmoid function $g(x) = (1 + e^{-x})^{-1}$. We used the TensorFlow library [2] for the implementation and training of the ANNs.

We trained the agent on 200 sets of 50 randomly placed transmitters with density $\lambda = \pi^{-1}$ on a periodic plane, for 200 steps per set. We initiliaised the ANN parameters θ, the set of all weights, using the He uniform variance scaling initialiser (HUVSI) from the Keras library [21] which cites [40]. Let n be the number of inputs into a node, HUVSI sets the weights for that node to be random variables that are distributed $\mathsf{Unif}\left(-\sqrt{\frac{6}{n}}, \sqrt{\frac{6}{n}}\right)$. We update the parameters using Adam, an optimisation algorithm introduced in [44], for first-order gradient-based optimisation of the objective function (1.4.7) based on adaptive estimates of lower-order moments. We used Adam for its computational efficiency as this was one of our main constraints.

Results

We found that the rectifier non-linearity resulted in a policy that was outperformed by policies that used the other two activation functions, which produced polices that performed similarly to each other. We present the results where we used the activation function $f(x) = \tanh(x)$ in the nodes of the neural network.

Figure 3-11 shows the CDF of the SINR for the four policies from subsection 3.2.1: 'Smart', 'Switch-off' and 'Switch-off Cluster', as well as the policy from deep Q-learning "DQL S1", in which uses $\boldsymbol{S_1}$. All policies were implemented on the same set of 500 randomly placed transmitters on a periodic plane. We see that SOC performs best followed by the deep Q-learning policy. We used an adaptation of the sampler in [16] to measure SINR and generate the CDF curves.

Figure 3-12 is a heatmap of the SINR when the deep Q-learning policy is implemented, the white crosses indicate where a transmitter has been switched off. From looking at the heatmap it is clear that improvements to coverage could be achieved by switching some transmitters back on. This could be further work in improving the reward function to achieve this objective alongside the objective of SINR.

Figure 3-13 shows how the proportion of transmitters on each of the four available power settings changed as the policy was iteratively applied to the

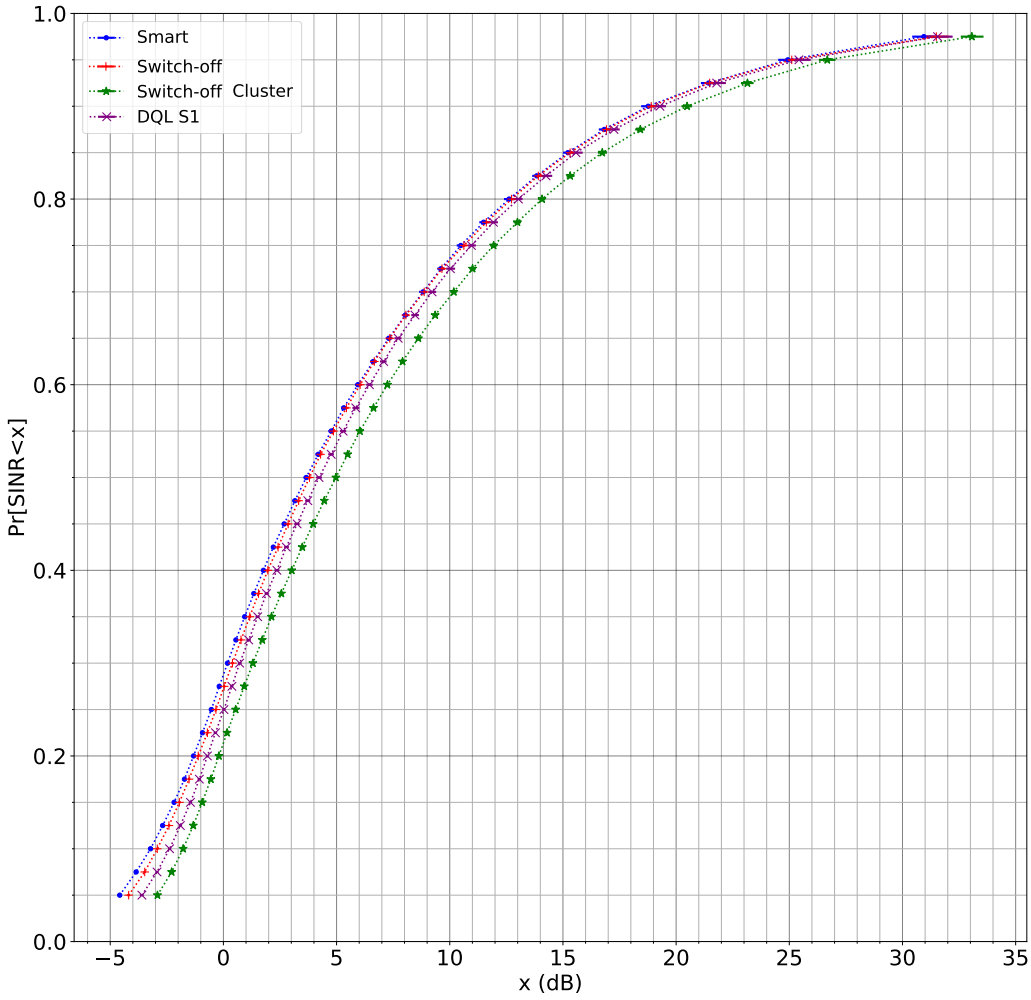

Figure 3-11: Probability that a randomly sampled SINR is less than a given value x (in dB). We show, for 500 transmitters on a periodic plane, the performance of the deep Q-learning policy, with $\boldsymbol{S_1}$ for states, against the policy 'Smart' and the two policies that outperform it.

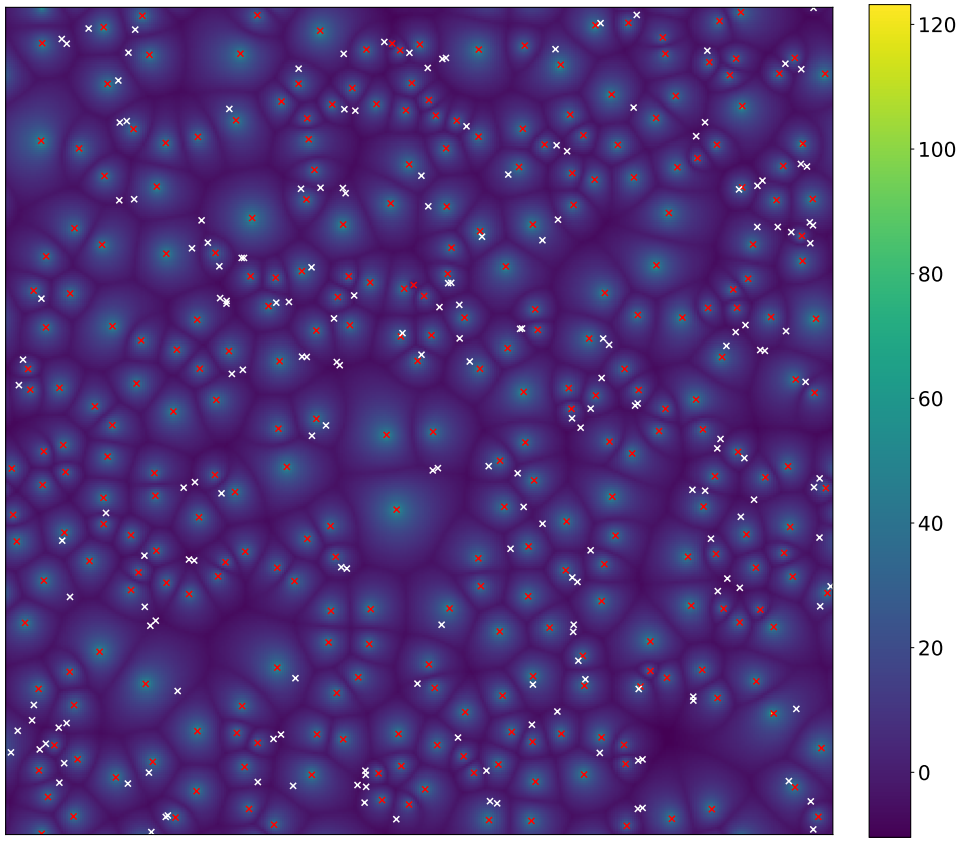

Figure 3-12: A heatmap showing the distribution of SINR (dB) on a plane with periodic boundary conditions after 2500 iterations of the deep Q-learning policy on 500 transmitters.

transmitters. We see that after 2500 iterations transmitters were either switched off or on the maximum available power.

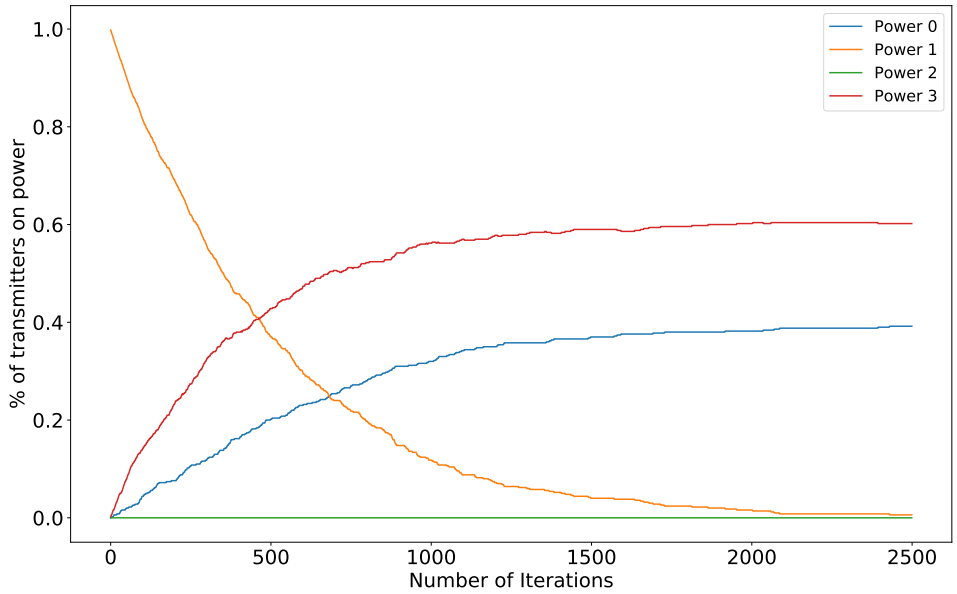

Figure 3-13: The proportion of transmitters on a given power setting changing as the learnt policy is iterated through. There were 500 transmitters and Powers $0, 1, 2, 3$ correspond to $P_{d_0}, P_{d_1}, P_{d_2}, P_{d_3}$ as in (3.3.1). We see that ultimately transmitters are either on maximum power or switched off.

3.3.2 Advantage Actor Critic

Q-learning and deep Q-learning are value-based reinforcement learning methods as the policy $\pi(a|s)$ is determined by the action values. Deep Q-learning is a value-based *model-free* reinforcement learning method as the Q function is replaced by a function approximator, a deep ANN. Value-based reinforcement learning methods require that the set of actions be finite and discrete. In our work so far, this requirement limited the actions possible for an agent to switching off or setting its transmit power relative to one of its three nearest neighbours.

In this subsection we show that, when a continuous action set is used, a policy can be learnt that performs similarly to the SOC algorithm, even with only observations of SINR from paired receivers. To enable use of a continuous set of actions we combine a policy-based reinforcement learning method together with deep Q-learning in what is known as an actor critic architecture. In particular we use a variant of the asynchronous advantage actor critic (A3C) method introduced

in [55]. We don't apply it asynchronously meaning it is termed advantage actor critic (A2C). We use the TensorFlow library [2] for implementation and training of the ANNs and for the A2C implementation we used [41] which is based on [26].

n-step Q-learning

Q-learning can be slow to learn optimal action-values as it takes many updates before reward propagates to the relevant states and actions. This is shown in the example in Subsection 1.4.2 of Chapter 1, where convergence to optimal action-values takes 17 updates. The Q-learning we exampled is called one-step Q-learning in [55], as the Q-table is updated after one action or "step". A method of propagating rewards in the Q-table faster is by using n-step returns [58] [80]. In n-step Q-learning the Q-table entry $Q(s, a)$ is updated with the n-step return which we define.

Definition 3.1 (n-step return)**.** *Let $\gamma \in (0, 1]$ be the discount factor, r_t be the reward at step t, and n the number of steps taken, then the n-step return*

$$R_t = \sum_{k=0}^{n-1} \gamma^k r_{t+k}. \tag{3.3.6}$$

This results in a single reward directly affecting the values of n preceding state action pairs,

$$Q(s_{t:t+n-1}, a) \leftarrow r_t + \gamma r_{t+1} + \ldots + \gamma^{n-1} r_{t+n-1} + \max_a \gamma^n Q(s_{t+n}, a). \tag{3.3.7}$$

This makes the process of propagating rewards to relevant state-action pairs potentially much more efficient [55]. Implementing n-step Q-learning in the example of Q-learning given in Chapter 1 with $n = 2$ we find that only 10 updates, rather than 17, are required in order to converge to optimal action-values.

Policy-based methods

Policy-based methods learn a parametrised policy that can select actions without a value function. This independence from a value function is what enables the use of a continuous action set. Let $\boldsymbol{\theta} \in \mathbb{R}^d$ be the policy's parameter vector. The parametrised policy $\pi(a|s, \boldsymbol{\theta}) = \mathbf{P}[A_t = a|S_t = s, \boldsymbol{\theta}_t = \boldsymbol{\theta}]$, the probability that at time t action a is taken in state s with parameter $\boldsymbol{\theta}$.

The parameters θ are updated by performing, typically approximate, gradient ascent on $\mathbf{E}[R_t]$ where R_t is as defined in (3.3.6). In [85] the REINFORCE algorithm is introduced. This updates the parameters with the gradient $\nabla_\theta \ln \pi(a_t|s_t;\theta)R_t$, which is an unbiased estimate of $\nabla_\theta \mathbb{E}[R_t]$ [55]. Subtracting a learned function of the state $b_t(s_t)$, known as a baseline [85], from the return R_t it is possible to reduce the variance of this estimate while keeping it unbiased. This gives the gradient as $\nabla_\theta \ln \pi(a_t|s_t;\theta)(R_t - b_t(s_t))$.

We note that we use the identity $\nabla \ln x = \frac{\nabla x}{x}$ in the expression of the gradients.

Advantage Actor Critic

Let us define the value of a state s under policy π as $V^\pi(s) = \mathbf{E}[R_t|s_t = s]$. We set the baseline in the policy-based method REINFORCE with baseline to be an estimate of the value such that $b_t(s_t) \approx V^\pi(s_t)$. We note that the action value under a policy π is $Q^\pi(s,a) = \mathbf{E}[R_t|s_t = s, a]$, the expected return of selecting action a in state s. Therefore the quantity $R_t - b_t$ can be thought of as an estimate of the *advantage* $A(a_t, s_t)$ of selecting action a_t in state s_t,

$$A(a_t, s_t) = Q(a_t, s_t) - V(s_t). \tag{3.3.8}$$

The approach of combining this policy-based method with n-step deep Q-learning is known as an actor-critic architecture where the policy π is the actor and the baseline b_t is the critic [71] [24]. Advantage actor critic (A2C) is when the policy-based method uses the advantage (3.3.8) as the baseline. Figure 3-14 illustrates the way the methods are combined.

A2C maintains a policy $\pi(a_t|s_t;\theta)$ and an estimate of the value function $V(s_t;\theta_v)$. A2C uses the n-step return defined in Definition 3.1 to update both the policy and the value-function. The advantage actor critic algorithm is given in Algorithm 3.3.

In Algorithm 3.3 the term $(R - V(s_t;\theta_v))$ gives the estimated advantage function $A(s_t, a_t; \theta, \theta_v) = \sum_{i=0}^{n-1} \gamma^i r_{t+i} + \gamma^n V(s_{t+n};\theta_v) - V(s_t;\theta_v)$. The parameters θ, θ_v of the policy and value function are shown as being separate, however in practice some of the parameters may be shared. Indeed, it is unlikely to be crucial whether the parameters are shared and in fact a single ANN can be used rather than two separate ANNs [55]. We found that policies performed similarly regardless of whether parameters were shared, and that a single ANN with shared parameters offered improved computational efficiency. Therefore we use a single

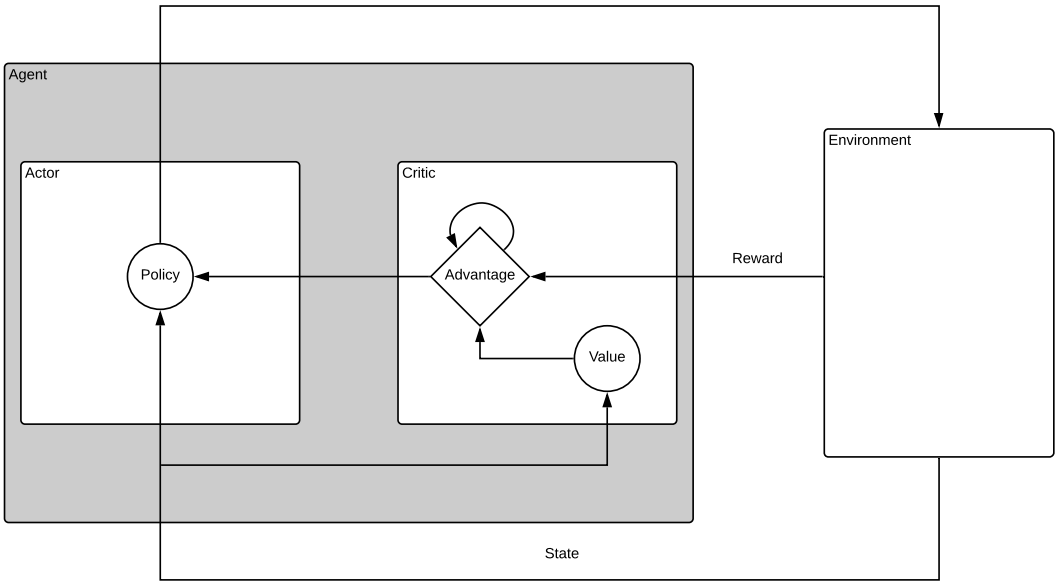

Figure 3-14: The architecture of advantage actor critic.

Algorithm 3.3 Advantage Actor Critic

The policy and value parameter vectors are θ and θ_v respectively
$T_{\max}$ is the total number of iterations to be performed.
n is the number of iterations (steps) in an update.
while $T \leq T_{\max}$ **do**
  Reset gradients $d\theta \leftarrow 0$ and $d\theta_v \leftarrow 0$
  $t = 0$
  Get state s_t
  while $t < n$ **do**
    Perform a_t according to policy $\pi(a_t|s_t;\theta)$
    Receive reward r_t and new state s_{t+1}
    $t \leftarrow t + 1$
    $T \leftarrow T + 1$
  end while
  $R = V(s_t;\theta_v)$
  for $i \in \{t-1, \ldots, 0\}$ **do**
    $R \leftarrow r_i + \gamma R$
    Accumulate policy gradients: $d\theta \leftarrow d\theta + \nabla_\theta \ln \pi(a_i|s_i;\theta)(R - V(s_i;\theta_v))$
    Accumulate value gradients: $d\theta_v \leftarrow d\theta_v + \partial(R - V(s_i;\theta_v))^2/\partial\theta_v$
  end for
  Update θ and θ_v using $d\theta$ and $d\theta_v$ respectively
end while

ANN that shares parameters.

In our implementation we use a single feed-forward ANN with one softmax output for the policy $\pi(a_t|s_t;\theta)$ and one linear output for the value function $V(s_t;\theta_v)$, all non-output layers are shared. Additionally, it was found in [55], as originally proposed in [86], that adding the entropy H of the policy π to the objective function improved exploration by discouraging premature convergence to suboptimal deterministic policies. Therefore in practice we update the ANN parameters with the gradient $d\theta'$ of the loss $L(\theta')$ that is a combination of the policy entropy, value gradient and policy gradient as follows:

$$L(\theta') = d\theta + \beta H(\pi(a|s;\theta)) + Cd\theta_v, \tag{3.3.9}$$

where hyperparameter β controls the strength of the entropy regularisation term, θ' is all the ANN parameters and hyperparameter C is the value coefficient. The update of the parameters θ' by the gradient $d\theta'$ is performed using RMSProp, an optimisation method for ANNs introduced in [75].

Reward Function

We use the reward function (3.3.2) given in Section 3.3.1 for A2C. The reward function determines the objective of the policy to be learnt and therefore it is important that it is constant across methods that are being compared as otherwise the policies will differ in terms of priority and objective.

Actions

Our motivation for implementing the advantage actor critic method is the continuous action set it allows. We allow an agent to set its transmit power to any positive real value upto the maximum allowed power $P_{\max}$. Therefore the action set

$$\boldsymbol{A} = \{a \in \mathbb{R} | 0 \leq a \leq P_{\max}\}, \tag{3.3.10}$$

where we set that $P_{\max} = 25$ to be consistent with previous work.

States

To determine an agent's state we use the set of observations $\boldsymbol{S_1}$, $\boldsymbol{S_2}$ or $\boldsymbol{S_3}$ as defined in (3.3.3), (3.3.4) and (3.3.5) respectively. We note that when the set of actions is continuous then the states will also be continuous. Inclusion of the states $\boldsymbol{S_2}$ and $\boldsymbol{S_3}$ shows that, with a continuous set of actions, additional

observations of distance and SINR do improve policy performance. This can be seen in Figure 3-16.

Training

We train on 200 sets of 50 randomly placed transmitters with density $\lambda = \pi^{-1}$ on a periodic plane. As with deep Q-learning we train for 200 steps per set. We configure the ANN with two hidden layers, each with 64 nodes, and the hyperbolic tangent activation function. We initialise the ANN parameters θ, the set of all node input weights, using the orthogonal initialiser introduced in [63] which sets the weights as follows. For each layer of the ANN, let n be the number of inputs into each node and m be the number of nodes. An $n \times m$ matrix of random numbers, that are distributed $\mathcal{N}(0, 1)$, is generated. From the thin singular value decomposition of this matrix we obtain an orthogonal $n \times m$ matrix, the elements of which are the initial weights for each node in that layer. For updating the parameters we accumulate updates with a step size of $n = 5$. We set the hyperparameter values $\gamma = 0.99$, $\beta = 0.01$ and $C = 0.25$. Figure 3-15 shows the total reward received in each episode for the three different state sets.

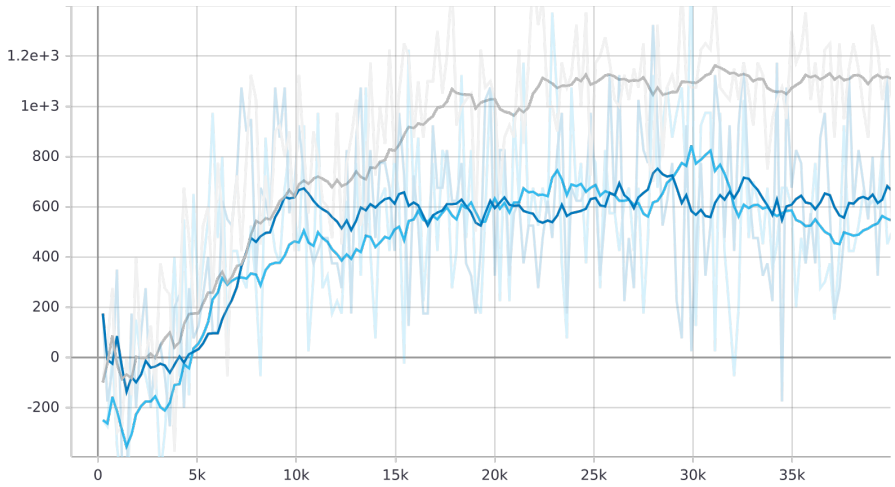

Figure 3-15: The reward received in each of the 40000 steps during training. The x-axis gives the step and the y-axis gives the reward. We smooth the reward for each scenario to make it clearer. The plot is generated in TensorFlow using TensorBoard. The grey line depicts the use of $\boldsymbol{S_3}$, the dark blue line $\boldsymbol{S_1}$ and the light blue line $\boldsymbol{S_2}$.

We observe in Figure 3-15 that the use of $\boldsymbol{S_3}$ allows much higher rewards to be received then either $\boldsymbol{S_1}$ or $\boldsymbol{S_2}$. This indicates that, with a continuous set of actions, additional input regarding SINR results in an improved policy but input

regarding distances does not. This is shown in the results.

Results

We compare the performance of the policies when the three different state sets are used. We find that additional input regarding SINR results in an improved policy when the action set is continuous. This is shown in Figure 3-16 where the line "A2C S3", which shows the results on the SINR of using advantage actor critic with $\boldsymbol{S_3}$, is further right than the lines showing the results when $\boldsymbol{S_1}$ or $\boldsymbol{S_2}$ are used.

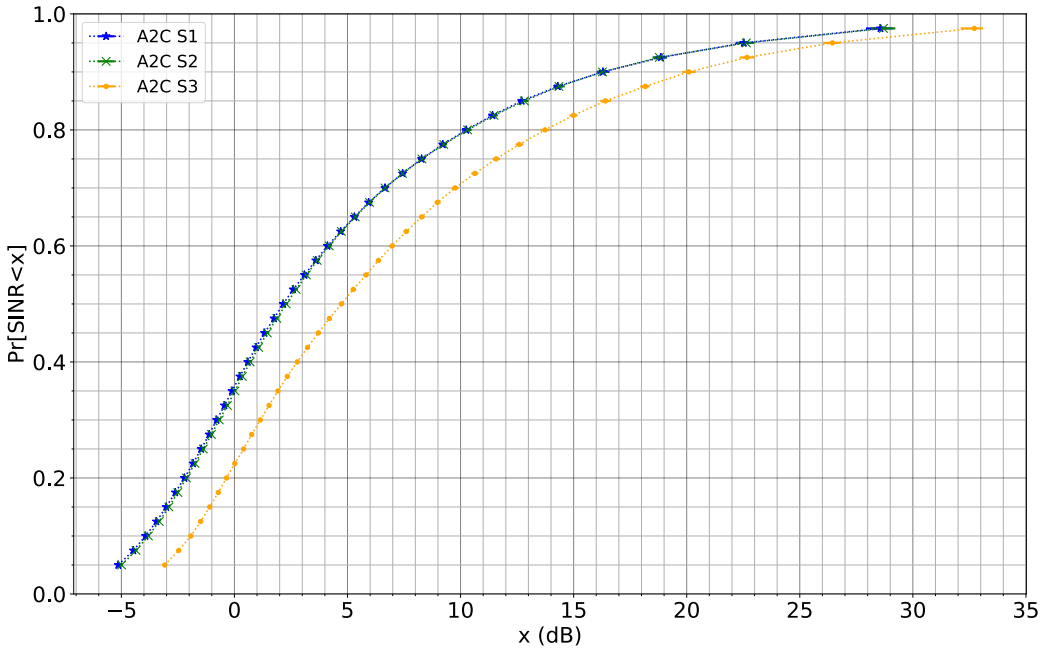

Figure 3-16: Probability that a randomly sampled SINR is less than a given value x (in dB). We show, for 500 transmitters on a periodic plane, the performance of the advantage actor critic policies with $\boldsymbol{S_1}$, $\boldsymbol{S_2}$ and $\boldsymbol{S_3}$. These are depicted by the lines labelled 'A2C S1', 'A2C S2' and 'A2C S3' respectively. It shows that the use of $\boldsymbol{S_3}$ results in an improved policy.

In Figure 3-17 we show that when using A2C with a continuous action set and set of observations $\boldsymbol{S_3}$, the learnt policy's performance comes close to that of Switch-off Cluster. We also show that it outperforms deep Q-learning with $\boldsymbol{S_3}$ and the benchmark policy 'Smart'.

Figure 3-18 is a heatmap of the SINR at the receiver locations across the periodic plane. We can identify transmitters in this figure that could have better transmit power settings and therefore believe that further training, adjustments

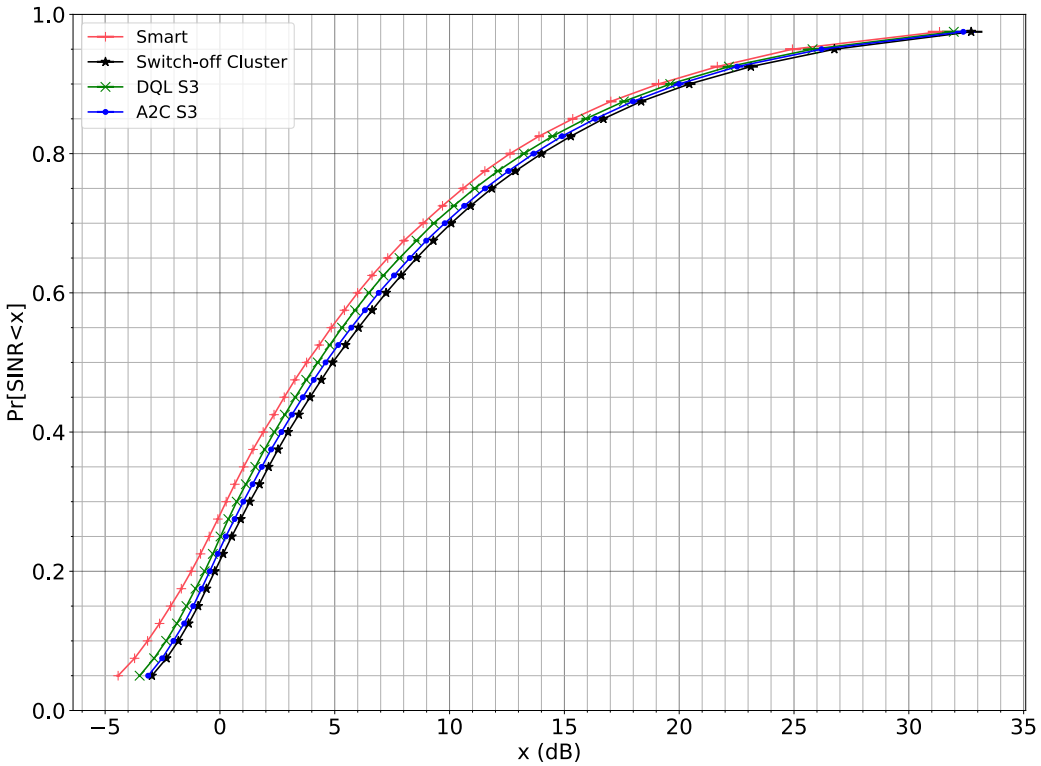

Figure 3-17: Probability that a randomly sampled SINR is less than a given value x (in dB). We show, for 500 transmitters on a plane with periodic boundary conditions, the performance of the advantage actor critic policy using $\boldsymbol{S_3}$ against the policy 'Smart', the deep Q-learning policy using $\boldsymbol{S_3}$ and SOC.

to the reward function or even allowing the policy to be updated during implementation should be explored.

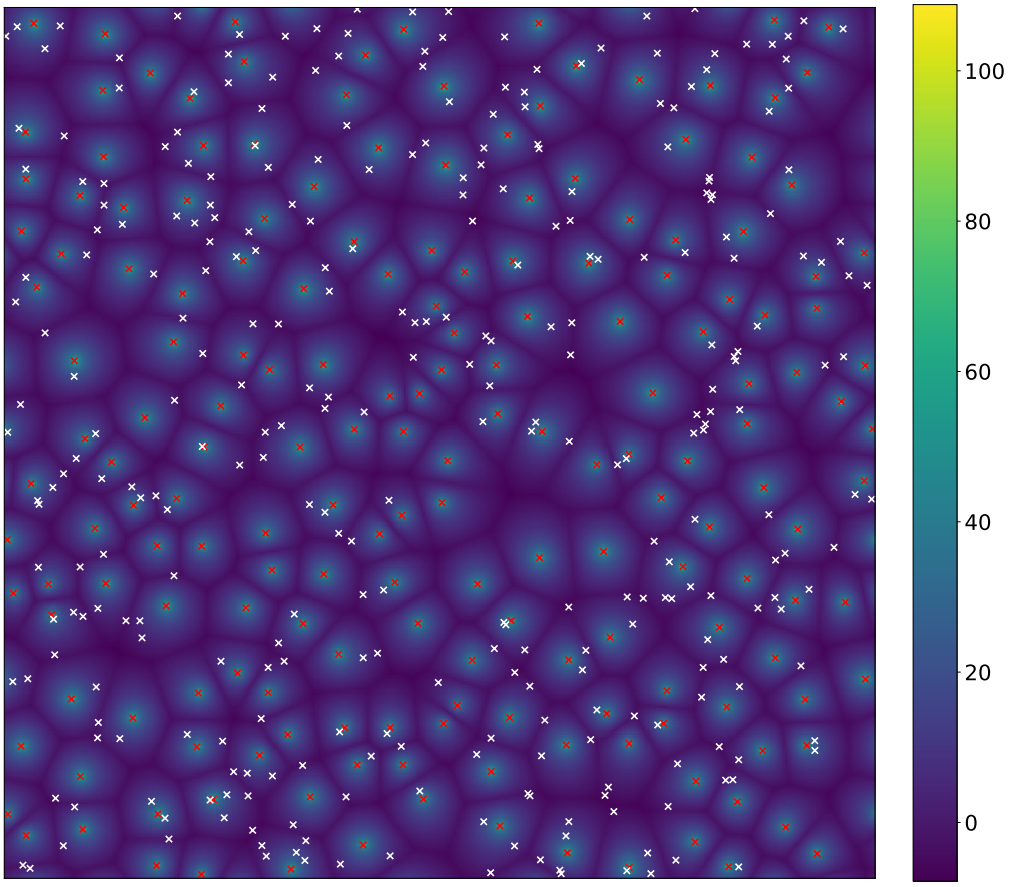

Figure 3-18: Heatmap showing SINR for 500 transmitters on a plane with periodic boundary conditions. Transmit powers were set by the A2C policy that used $\boldsymbol{S_3}$ to determine states. The CDF of this policy performance is shown in Figure 3-17.

3.4 Short Summary

We began this chapter by showing that, with the exception of the case where there are only two transmitters and no noise, uniform transmit powers are not always optimal for SINR. We went on to show that non-uniform powers set without consideration of the network do not perform better than uniform powers.

We have developed a new power control algorithm, Switch-Off Cluster (SOC), that outperforms BT's benchmark policy 'Smart'. The SOC algorithm does, however, require knowledge of the distances and powers of the transmitters within a minimum distance d_{min}; in Chapters 4 and 5 we propose heuristics for estimating

these distances and powers. SOC is the 'Smart' algorithm when $d_{\min} = 0$ and as we increase $d_{\min}$ it takes into account clusters of transmitters which leads to improved performance. The SOC algorithm only requires a few complete iterations (every transmitter in the network updating once) to have reached its optimal configuration.

It has been shown that reinforcement learning methods, of deep Q-learning and methods of actor-critic, can be used to develop effective transmit power policies. In this chapter, we have shown that using Advantage Actor Critic (A2C) and training on a network a tenth of the size of the large one that the policy is deployed on and using only partial information (a transmitter's power and the SINR at paired devices) it performs similarly to SOC. A2C allows for SINR to be optimised in a truly distributed way as each transmitter need only know its own power and the SINR of its paired devices. With minimal training both methods can produce a power control policy that does not require neighbour transmitter distances to be known and matches the performance of SOC. Further work, such as improving the reward structure and training for these methods is discussed in Section 6.2 of Chapter 6.

Chapter 4

Uniform Power Distance Estimation

We showed in Chapter 3 that it is not optimal for all transmitters to be on the same power setting. As described in Subsection 1.3.3, the network should self-organise without requiring transmitters to communicate with each other. Given that transmitters are on a uniform power setting, the policies we proposed in Chapter 3 showed that knowledge of the distance to their nearest neighbour would be a significant help in making power level adjustments that improve performance. In this chapter and the next, we consider this challenge: given only the total signal received from all other transmitters, and their distribution in the plane, estimate the distance to the nearest transmitter. In this chapter we assume transmit powers are uniform. In Chapter 5 we remove this assumption.

This chapter is organised in two main parts. In the first part we find an asymptotic heuristic to estimate the distance to the nearest transmitter in a wireless network in the absence of fading. In the second part we find the probability density function of the distance to the nearest transmitter in a wireless network with Rayleigh fading in effect. In both instances we use numerical simulations to evaluate the performance of the proposed heuristics.

4.1 Asymptotic Heuristic

The total signal is S and if there is only a single transmitter, the relation when transmit power $P = 1$ and pathloss is far-field, $S = R^{-\gamma}$ implies that the distance R to that transmitter can be computed directly: $R = S^{-1/\gamma}$ with γ the pathloss exponent. This heuristic should also be reasonable in the case of more than one transmitter, if one transmitter is much closer to the origin than the others. In

the case of multiple transmitters contributing to the total received signal S, our aim is to improve on the natural heuristic $R_1 = S^{-1/\gamma}$ where R_1 is defined to be the distance to the nearest transmitter. It is assumed that the only interference present in the network is from other transmitters. After establishing the preliminaries and stating the main result, we begin by presenting a specific case in Subsection 4.1.1 before deriving a form for general $\gamma > 2$ and any number $k \geq 2$ of transmitters in Subsection 4.1.2.

Preliminaries

In this chapter we use $\sim$ to indicate asymptotic equivalence and $\approx$ to indicate approximate equivalence. Let $0 < R_1 < R_2 < \dots$ denote the distances of the Poisson points from the origin taken in increasing order. Then $S = \sum_{i \geq 1} R_i^{-\gamma}$ (this sum converges with probability 1, if $\gamma > 2$). We condition on a measured signal $S = s$. Then $R_1 \geq s^{-1/\gamma}$ always, and heuristically, $s^{-1/\gamma}$ should be a good approximation of R_1, at least if s is not small [83]. We are interested in the expected error of this heuristic $\mathbf{E}\big[R_1 - s^{-1/\gamma} \,\big|\, S = s\big]$, as $s \to \infty$.

It will make computations easier to split S into a sum of two terms as follows. Fix a constant radius $0 < \rho < \infty$, and let N be the number of transmitters (Poisson points) inside the disk of radius ρ centred at the origin. Note that N is distributed $\mathsf{Poisson}(\lambda\pi\rho^2)$. We write $S = S' + \bar{S}$, where $S' = \sum_{i=1}^{N} R_i^{-\gamma}$ is the contribution of transmitters within radius ρ, and $\bar{S}$ is the contribution of all other transmitters. We first argue that $\bar{S}$ can be neglected. This is because $\bar{S} = O(1)$, with an exponentially fast decaying probability tail, which can be seen from the fact that its Laplace transform is finite in a neighbourhood of 0. Therefore, for large s, it is asymptotically equivalent to consider S' instead of $\bar{S}$. This argument is further supported by the fact that we find Theorem 4.1 is independent of the chosen value of ρ (that is, only the error of the asymptotics depends on ρ).

Theorem 4.1 (Asymptotic Heuristic)**.** *Where R_1 is the distance to the nearest transmitter, λ is the density of the transmitters, γ is the pathloss exponent and s is the observed signal then for $\gamma > 2$*

$$\mathbf{E}\Big[R_1 - s^{-1/\gamma} \,\Big|\, S' = s\Big] \sim \frac{2\lambda\pi}{\gamma}\, a(\gamma)\, s^{-3/\gamma}, \quad \text{as } s \to \infty, \tag{4.1.1}$$

with

$$a(\gamma) = \gamma\, 2^{(2-\gamma)/\gamma} \left[{}_2F_1\left(\frac{\gamma+2}{\gamma}, -\frac{2}{\gamma}; \frac{\gamma-2}{\gamma}; \frac{1}{2}\right) - {}_2F_1\left(\frac{\gamma+3}{\gamma}, -\frac{2}{\gamma}; \frac{\gamma-2}{\gamma}; \frac{1}{2}\right)\right]. \tag{4.1.2}$$

We recall that the hypergeometric series is given by

$$ {}_2F_1(a,b;c;z) = \sum_{n=0}^{\infty} \frac{(a)_n (b)_n}{(c)_n} \frac{z^n}{n!} \tag{4.1.3} $$

with $(q)_n = q(q+1)...(q+n-1)$.

To explain this in more detail, for a fixed ρ we obtain the result:

$$ \mathbf{E}\Big[R_1 - s^{-1/\gamma} \,\Big|\, S' = s,\, N = k \Big] \sim \frac{2\,(k-1)\,\rho^{-2}}{\gamma}\, a(\gamma)\, s^{-3/\gamma} \tag{4.1.4} $$

as $s \to \infty$, for $k \geq 1$, $0 < \rho < \infty$.

Then, following the derivation of the general result in section 4.1, we argue that the conditional distribution of N given $S' = s$ satisfies

$$ \mathbf{P}[N = k \,|\, S' = s] \sim e^{-\lambda\pi\rho^2} \frac{(\lambda\pi\rho^2)^{k-1}}{(k-1)!}, \quad \text{as } s \to \infty, \text{ for } k \geq 1,\ 0 < \rho < \infty. \tag{4.1.5} $$

So removing the conditioning on k by multiplying (4.1.4) by (4.1.5) and summing over $k = 1, 2, \ldots$ yields the expression in the right hand side of (4.1.1). The details of this part of the calculation are shown in Subection 4.1.2.

4.1.1 Example: Computations when $N = k = 3$, $\gamma = 4$

Here, as an example, we give the computations when there are exactly three transmitters in the disk of radius 1 around the origin, and the pathloss exponent is $\gamma = 4$. We choose the case $k = 3$ for our example as it demonstrates all the methods used for cases where k is higher, which $k = 2$ does not, and is the shortest computation to do so. Observe that when $N = k = 1$ and $S' = s$, then $R_1 = s^{-1/\gamma}$, so (4.1.4) holds trivially. Also observe that $N = k = 0$ is impossible when $S' = s > 0$.

Given that the points are Poisson distributed, the probability density of having three points in a disk of radius $\rho = 1$ at radii r_1, r_2, r_3 is

$$ f_{R_1,R_2,R_3,N=3}(r_1,r_2,r_3) = (2\lambda\pi)^3 e^{-\lambda\pi} r_1 r_2 r_3 \quad 0 < r_1 < r_2 < r_3 < 1. $$

As we have assumed that $\gamma = 4$ and there are no propagation effects, it follows that $r_i = s_i^{-1/4}$ and so $|dr_i/ds_i| = (1/4)s_i^{-5/4}$. Substituting these expressions gives the probability function in terms of signal rather than distance:

$$ f_{S_1,S_2,S_3,N=3}(s_1,s_2,s_3) = e^{-\lambda\pi}(2\lambda\pi)^3 (1/4)^3 s_1^{-3/2} s_2^{-3/2} s_3^{-3/2} \quad 1 < s_3 < s_2 < s_1 < \infty. $$

Conditioning on $N = 3$ and $S' = S_1 + S_2 + S_3 = s$, and expressing $S_1 = s - S_2 - S_3$ gives

$$f_{S_2,S_3 \mid N=3,S'=s}(s_2, s_3 \mid s) = \frac{1}{Z_{3,s}}(s - s_2 - s_3)^{-3/2} s_2^{-3/2} s_3^{-3/2},$$

with $s_1 := s - s_2 - s_3 > s_2 > s_3 > 1$, and where the normalizing constant is

$$Z_{3,s} = \int_1^{s/3} ds_3 \int_{s_3}^{(s-s_3)/2} ds_2 \, (s - s_2 - s_3)^{-3/2} s_2^{-3/2} s_3^{-3/2}.$$

The limits on the integrands come from the restriction that $s_1 > s_2 > s_3 > 1$ and $s_1 + s_2 + s_3 = s$.

The expected error of the heuristic, in the case where $k = 3$, can be written as

$$\mathbf{E}\Big[R_1 - s^{-1/4} \,\Big|\, N = 3,\ S_1 + S_2 + S_3 = s\Big] = \frac{1}{Z_{3,s}} \int_1^{s/3} \int_{s_3}^{(s-s_3)/2} \frac{(s - s_2 - s_3)^{-1/4} - s^{-1/4}}{(s - s_2 - s_3)^{3/2} s_2^{3/2} s_3^{3/2}} ds_2 ds_3. \quad (4.1.6)$$

By two further substitutions this integral becomes simpler to approximate. Firstly, we scale out the dependence on s by setting $s_i = s x_i$. This gives the expression

$$\frac{1}{Z_{3,s}} s^{-11/4} \int_{1/s}^{1/3} \int_{x_3}^{(1-x_3)/2} \frac{(1 - x_2 - x_3)^{-1/4} - 1}{(1 - x_2 - x_3)^{3/2} x_2^{3/2} x_3^{3/2}} dx_2 dx_3. \quad (4.1.7)$$

We write

$$(1 - x_3 - x_2)^{-1/4} - 1 = \left[(1 - x_3 - x_2)^{-1/4} - (1 - x_2)^{-1/4}\right] + \left[(1 - x_2)^{-1/4} - 1\right],$$

and we make a further substitution which changes the upper limit of the inner integral to a constant, and 'factorises' the integrand into parts that depend on the variables separately. Namely, set $x_2 = (1 - x_3) y_2$ and $x_3 = y_3$, so $dx_2 = (1 - x_3) dy_2$, $dx_3 = dy_3$. This results in $(1 - x_2 - x_3) = (1 - y_3)(1 - y_2)$. Therefore we can

write the double integral in (4.1.7) as

$$\underbrace{\int_{\frac{1}{s}}^{\frac{1}{3}} \frac{1}{(1-y_3)^{\frac{9}{4}} y_3^{\frac{3}{2}}} \int_{\frac{y_3}{(1-y_3)}}^{\frac{1}{2}} \frac{(1-y_2)^{-\frac{1}{4}}-1}{(1-y_2)^{\frac{3}{2}} y_2^{\frac{3}{2}}} dy_2 dy_3}_{I_1} + \underbrace{\int_{\frac{1}{s}}^{\frac{1}{3}} \frac{(1-y_3)^{\frac{-1}{4}}-1}{(1-y_3)^2 y_3^{\frac{3}{2}}} \int_{\frac{y_3}{(1-y_3)}}^{\frac{1}{2}} \frac{1}{(1-y_2)^{\frac{3}{2}} y_2^{\frac{3}{2}}} dy_2 dy_3}_{I_2} \quad (4.1.8)$$

We start by analysing the leading order term I_1, noticing that the main contribution comes from small y_3, y_2. The inner integral $\int_{\frac{y_3}{(1-y_3)}}^{\frac{1}{2}} \frac{(1-y_2)^{\frac{-1}{4}}-1}{(1-y_2)^{\frac{3}{2}} y_2^{\frac{3}{2}}} dy_2$ approaches a finite value as $y_3 \to 0$, and can therefore be treated as a constant. The exact value of the limit is given by

$$\begin{aligned} a(\gamma = 4) &:= \int_0^{\frac{1}{2}} \frac{(1-y_2)^{\frac{-1}{4}}-1}{(1-y_2)^{\frac{3}{2}} y_2^{\frac{3}{2}}} dy_2 \\ &= 2\sqrt{2} \left[{}_2F_1\left(\frac{3}{2}, -\frac{1}{2}; \frac{1}{2}; \frac{1}{2}\right) - {}_2F_1\left(\frac{7}{4}, -\frac{1}{2}; \frac{1}{2}; \frac{1}{2}\right) \right] \\ &\approx 0.59202228363... \end{aligned}$$

The error of replacing $\frac{y_3}{1-y_3}$ by 0 is

$$-\int_0^{\frac{y_3}{1-y_3}} \frac{(1-y_2)^{-1/4}-1}{(1-y_2)^{\frac{3}{2}} y_2^{\frac{3}{2}}} dy_2 = -\int_0^{y_3} \frac{1}{4} \frac{1}{y_2^{\frac{1}{2}}} dy_2 + O(y_3^{3/2}) = -\frac{1}{2} y_3^{1/2} + O(y_3^{3/2})$$

for small y_3.

Now we evaluate the outer integral of I_1,

$$\int_{\frac{1}{s}}^{\frac{1}{3}} \frac{a - \frac{1}{2} y_3^{1/2} + O(y_3^{3/2})}{(1-y_3)^{\frac{9}{4}} y_3^{\frac{3}{2}}} dy_3 = a\, 2\sqrt{s} - \frac{1}{2} \log s + O(1).$$

Therefore, $I_1 = 2a\sqrt{s} - \frac{1}{2}\log(s) + O(1)$, as $s \to \infty$.

Now we evaluate I_2 from equation (4.1.8). We begin by finding that $\int_{\frac{y_3}{(1-y_3)}}^{\frac{1}{2}} \frac{1}{(1-y_2)^{\frac{3}{2}} y_2^{\frac{3}{2}}} dy_2$ diverges as $2y_3^{-1/2} + O(1)$ as $y_3 \to 0$. We substitute this

into the outer integral and find that as $y_3 \to 0$

$$I_2 = \int_{\frac{1}{s}}^{\frac{1}{3}} \frac{(1-y_3)^{\frac{-1}{4}} - 1}{(1-y_3)^2 y_3^{\frac{3}{2}}} \left[\frac{2}{y_3^{1/2}} + O(1) \right] dy_3 = 2 \int_{\frac{1}{s}}^{\frac{1}{3}} \frac{(1-y_3)^{\frac{-1}{4}} - 1}{(1-y_3)^2 y_3^{\frac{4}{2}}} dy_3 + O(1)$$
$$= \int_{\frac{1}{s}}^{\frac{1}{3}} \frac{\frac{1}{4}y_3 + O(y_3^2)}{(1-y_3)^2 y_3^2} dy_3 + O(1)$$
$$= \frac{1}{2} \log s + O(1).$$

Combining I_1 and I_2, it is seen that equation (4.1.8) is

$$\int_{1/s}^{1/3} \int_{x_3}^{(1-x_3)/2} \frac{(1-x_2-x_3)^{-1/4} - 1}{(1-x_2-x_3)^{3/2} x_2^{3/2} x_3^{3/2}} dx_2 dx_3 = 2a\sqrt{s} - \frac{1}{2} \log s + \frac{1}{2} \log s + O(1)$$
$$= 2a\sqrt{s} + O(1). \tag{4.1.9}$$

Referring to equation (4.1.7), it is necessary to factor in $\frac{s^{-\frac{11}{4}}}{Z_{3,s}}$. The normalising constant $Z_{3,s}$ is found, using similar subsitutions as before, to be

$$Z_{3,s} = \int_1^{\frac{s}{3}} \int_{s_3}^{\frac{(s-s_3)}{2}} \frac{1}{(s-s_2-s_3)^{\frac{3}{2}} s_2^{\frac{3}{2}} s_3^{\frac{3}{2}}} ds_2 ds_3 = 2s^{-\frac{3}{2}} + O(s^{-2}).$$

Therefore $\frac{s^{-\frac{11}{4}}}{Z_{3,s}} = 2s^{-\frac{5}{4}} + O(s^{-\frac{7}{4}})$ and

$$\mathbf{E}\Big[R_1 - s^{-1/4} \Big| N = 3,\, S_1 + S_2 + S_3 = s \Big] = a\, s^{-\frac{3}{4}} + O(s^{-\frac{5}{4}}), \quad \text{as } s \to \infty.$$

The expected error of the asymptotic heuristic in the case $k = 3$, $\gamma = 4$ has been found.

4.1.2 Computations for $k \geq 2$ and $\gamma > 2$

In a disk of radius ρ, where $0 < \rho < \infty$ and with points distributed $\mathsf{Poisson}(\lambda\pi\rho^2)$ the probability of there being k points in the disk is given by

$$f_{R_1,\ldots,R_k}(r_1 \ldots r_k) = (2\lambda\pi)^k r_1 \ldots r_k e^{-\lambda\pi\rho^2} = (2\lambda\pi)^k e^{-\lambda\pi\rho^2} \prod_{i=1}^{k} r_i \tag{4.1.10}$$

We can write (4.1.10) in terms of signal contributions, we define $s_1 > s_2 > s_3 > \ldots$ to be the received signal strengths from the ordered transmitters. We know

that $r_i = s_i^{-\frac{1}{\gamma}}$ and therefore

$$f_{S_1,\ldots,S_k}(s_1 \ldots s_k) = (2\lambda\pi)^k e^{-\lambda\pi\rho^2} \prod_{i=1}^{k} \frac{1}{\gamma} s_i^{-\frac{\gamma+2}{\gamma}}. \tag{4.1.11}$$

The variable s_1 can be expressed as $s_1 = s - s_2 - s_3 - \ldots - s_k$, so that (4.1.11) can be written as

$$f_{S_2,\ldots,S_k}(s_2 \ldots s_k) = \left(\frac{2\lambda\pi}{\gamma}\right)^k e^{-\lambda\pi\rho^2} (s - s_2 - .. - s_k)^{-\frac{\gamma+2}{\gamma}} \prod_{i=2}^{k} s_i^{-\frac{\gamma+2}{\gamma}} \tag{4.1.12}$$

Therefore the expected error of $R_1 = S^{-1/\gamma}$, when all observed signal is attributed R_1, can be written as

$$\mathbf{E}\left[R_1 - S^{-\frac{1}{\gamma}} | \sum_{i=1}^{k} S_i = s, N = k\right] = \frac{W_{k,s}}{Z_{k,s}} = \frac{1}{Z_{k,s}} \int_{\rho^{-\gamma}}^{\frac{s}{k}} \ldots \int_{s_3}^{\frac{s-s_3}{s}} \frac{(s - s_2 - \ldots - s_k)^{-\frac{1}{\gamma}} - s^{-\frac{1}{\gamma}}}{(s - s_2 - \ldots - s_k)^{\frac{\gamma+2}{\gamma}} s_2^{\frac{\gamma+2}{\gamma}} \ldots s_k^{\frac{\gamma+2}{\gamma}}} ds_2 \ldots ds_k \tag{4.1.13}$$

where

$$W_{k,s} = \int_{\rho^{-\gamma}}^{\frac{s}{k}} \ldots \int_{s_3}^{\frac{s-s_3}{s}} \frac{(s - s_2 - \ldots - s_k)^{-\frac{1}{\gamma}} - s^{-\frac{1}{\gamma}}}{(s - s_2 - \ldots - s_k)^{\frac{\gamma+2}{\gamma}} s_2^{\frac{\gamma+2}{\gamma}} \ldots s_k^{\frac{\gamma+2}{\gamma}}} ds_2 \ldots ds_k \tag{4.1.14}$$

and

$$Z_{k,s} = \int_{\rho^{-\gamma}}^{\frac{s}{k}} \ldots \int_{s_3}^{\frac{s-s_3}{2}} (s - s_2 - \ldots - s_k)^{-\frac{\gamma+2}{\gamma}} s_2^{-\frac{\gamma+2}{\gamma}} \ldots s_k^{-\frac{\gamma+2}{\gamma}} ds_2 \ldots ds_k. \tag{4.1.15}$$

Our aim is to find an expression for $\mathbf{E}\left[R_1 - s^{-1/\gamma} \middle| N = k, S' = s\right]$ in terms of γ and k. To do this we must evaluate equations (4.1.14) and (4.1.15).

Equation (4.1.15)**: evaluating** $Z_{k,s}$

To evaluate (4.1.15) we use methods which are illustrated in Subsection 4.1.1. Firstly, as initially used for equation (4.1.7), we scale out the dependence on s by setting $s_i = sx_i$. This gives that

$$1 = \sum_{i=1}^{k} x_i, \quad \text{and} \quad x_1 > \ldots x_{i-1} > x_i \ldots > x_k.$$

We then make a further change of variables, defined as follows.

Definition 4.1. *We define the variable y_i. For $1 \leq i \leq k$,*

$$y_i := x_i \left(\sum_{m=1}^{i} x_m \right)^{-1}. \tag{4.1.16}$$

From the above definition we find the following lemma.

Lemma 4.1. *For x_i and y_i, where $1 \leq i \leq k-1$,*

$$\left(1 - \sum_{m=i+1}^{k} x_m \right) = \prod_{m=i+1}^{k} (1 - y_m). \tag{4.1.17}$$

To derive Lemma 4.1 we begin by using Definition 4.1 to write

$$x_i = y_i \left(1 - \sum_{m=i+1}^{k} x_m \right). \tag{4.1.18}$$

From this, where $m \leq k$ we see that

$$\begin{aligned} \left(1 - \sum_{m=i+1}^{k} x_m \right) &= \left(1 - y_{i+1} \left(1 - \sum_{m=i+2}^{k} x_m \right) - \sum_{m=i+2}^{k} x_m \right) \\ &= (1 - y_{i+1}) \left(1 - \sum_{m=i+2}^{k} x_m \right) \\ &= (1 - y_{i+1}) (1 - y_{i+2}) \left(1 - \sum_{m=i+3}^{k} x_m \right) \\ &= \prod_{m=i+1}^{k} (1 - y_m). \end{aligned} \tag{4.1.19}$$

In terms of the y variables we find that the multiple integrals simplify: the integrands are functions of a single y_i variable and the integration limits are expressed in terms of y_{i+1}. Therefore equation (4.1.15) can be written as

$$\begin{aligned} &Z_{k,S} = \\ &S^{-\frac{(2k+\gamma)}{\gamma}} \int_{\frac{1}{S\rho^\gamma}}^{\frac{1}{k}} y_k^{-\frac{(\gamma+2)}{\gamma}} (1 - y_k)^{\frac{(2-2k-\gamma)}{\gamma}} dy_k \int_{\frac{y_k}{1-y_k}}^{\frac{1}{k-1}} y_{k-1}^{-\frac{(\gamma+2)}{\gamma}} (1 - y_{k-1})^{\frac{(2-2(k-1)-\gamma)}{\gamma}} dy_{k-1} \\ &\quad \ldots \int_{\frac{y_4}{1-y_4}}^{\frac{1}{3}} y_3^{-\frac{(\gamma+2)}{\gamma}} (1 - y_3)^{\frac{(-4-\gamma)}{\gamma}} dy_3 \int_{\frac{y_3}{1-y_3}}^{\frac{1}{2}} y_2^{-\frac{(\gamma+2)}{\gamma}} (1 - y_2)^{\frac{(-2-\gamma)}{\gamma}} dy_2. \end{aligned} \tag{4.1.20}$$

By defining an iterative sequence J_k we can express (4.1.20) more concisely. We define J_k as follows.

Definition 4.2 (Iterative sequence J_k)**.** *For all* $3 \leq l \leq k$*:*

$$\begin{aligned} J_2 &:= 1 \\ J_l &:= \int_{\frac{y_l}{1-y_l}}^{\frac{1}{l-1}} y_{l-1}^{-\frac{(\gamma+2)}{\gamma}} (1 - y_{l-1})^{\frac{(2-2(l-1)-\gamma)}{\gamma}} dy_{l-1} J_{l-1}. \end{aligned} \tag{4.1.21}$$

Note that J_l is a function of y_l. Therefore,

$$Z_{k,S} = S^{-\frac{(2k+\gamma)}{\gamma}} \int_{\frac{1}{S\rho^\gamma}}^{\frac{1}{k}} y_k^{-\frac{(\gamma+2)}{\gamma}} (1 - y_k)^{\frac{(2-2k-\gamma)}{\gamma}} dy_k J_k \tag{4.1.22}$$

By evaluating (4.1.20) we find that the leading order terms give

$$\begin{aligned} Z_{k,S} \approx \left(\frac{\gamma}{2}\right)^{(k-1)} \Bigg(&\frac{1}{(k-1)!} \rho^{2(k-1)} S^{-\frac{(\gamma+2)}{\gamma}} - 2^{\frac{2}{\gamma}} \frac{1}{(k-2)!} \rho^{2(k-2)} S^{-\frac{(\gamma+4)}{\gamma}} \\ &+ O\left(S^{-\frac{(\gamma+6)}{\gamma}}\right)\Bigg) \end{aligned} \tag{4.1.23}$$

and therefore we find for $k \geq 3$, $\gamma > 2$ and $0 < \rho < \infty$ that

$$Z_{k,s} = Z_{k,s}^{\gamma,\rho} \sim \left(\frac{\gamma}{2}\right)^{k-1} \frac{1}{(k-1)!} \rho^{2(k-1)} s^{-\frac{(\gamma+2)}{\gamma}}, \quad \text{as } s \to \infty. \tag{4.1.24}$$

Equation (4.1.14)**: evaluating the integral**

Our aim is to evaluate equation (4.1.13). As we have evaluated (4.1.15) and found the result stated in (4.1.24), what remains is for us to evaluate

$$W_{k,S} = \int_{\rho^{-\gamma}}^{\frac{s}{k}} \dots \int_{s_3}^{\frac{s-s_3}{s}} \frac{(s - s_2 - \dots - s_k)^{-\frac{1}{\gamma}} - s^{-\frac{1}{\gamma}}}{(s - s_2 - \dots - s_k)^{\frac{\gamma+2}{\gamma}} s_2^{\frac{\gamma+2}{\gamma}} \dots s_k^{\frac{\gamma+2}{\gamma}}} ds_2 \dots ds_k. \tag{4.1.25}$$

To do this we begin as previously by using the substitution $s_i = sx_i$ and the change of variabled defined in Definition 4.1. This allows us to then use the substitution given in (4.1.17). From this we find that the numerator of the integrand in (4.1.25) is given by

$$(s - s_2 - \dots - s_k)^{-\frac{1}{\gamma}} - s^{-\frac{1}{\gamma}} = s^{-\frac{1}{\gamma}} \sum_{j=2}^{k} \left(\left[(1 - y_j)^{-\frac{1}{\gamma}} - 1\right] \prod_{i=j+1}^{k} (1 - y_i)^{-\frac{1}{\gamma}} \right). \tag{4.1.26}$$

By noting that the denominator of the integrand in (4.1.25) is the same as in the normalising constant defined by (4.1.15) we know that, following the above substitutions, it can be expressed in the same form as before, i.e. equation (4.1.20).

We now define an iterative sequence $Q_k^{(j)}$, where j is the variable summed over in (4.1.26).

Definition 4.3 (The iterative sequence $Q_k^{(j)}$)**.** *Fix $k \geq 3$, then define the quantities $Q_l^{(j)}$, for $1 \leq l \leq k$ and $2 \leq j \leq k$, as follows:*

1. *For all $2 \leq j \leq k$:*
$$Q_1^{(j)} := 1$$

2. *For $2 \leq l \leq j-1$, we define*
$$Q_l^{(j)} := \int_{\frac{y_{l+1}}{1-y_{l+1}}}^{\frac{1}{l}} y_l^{-\frac{(\gamma+2)}{\gamma}} (1-y_l)^{\frac{2-2l-\gamma}{\gamma}} Q_{l-1}^{(j)} dy_l$$

3. *For $2 \leq l = j \leq k$, we define*
$$Q_l^{(j)} := \int_{\frac{y_{l+1}}{1-y_{l+1}}}^{\frac{1}{l}} y_l^{-\frac{(\gamma+2)}{\gamma}} (1-y_l)^{\frac{2-2l-\gamma}{\gamma}} \left[(1-y_l)^{-\frac{1}{\gamma}} - 1\right] Q_{l-1}^{(j)} dy_l$$

4. *For $j+1 \leq l \leq k$, we define*
$$Q_l^{(j)} := \int_{\frac{y_{l+1}}{1-y_{l+1}}}^{\frac{1}{l}} y_l^{-\frac{(\gamma+2)}{\gamma}} (1-y_l)^{\frac{1-2l-\gamma}{\gamma}} Q_{l-1}^{(j)} dy_l.$$

Note that we define the lower limit of the outermost integral in $Q_k^{(j)}$ separately, setting $\frac{y_{k+1}}{1-y_{k+1}} := \frac{1}{S\rho^{-\gamma}}$.

Using the iterative sequence $Q_k^{(j)}$, we can express expression (4.1.25) concisely as
$$W_{k,s} = s^{-\frac{(2k+\gamma+1)}{\gamma}} \sum_{j=2}^{k} Q_k^{(j)} \tag{4.1.27}$$
and therefore equation (4.1.13) can be expressed as
$$\mathbf{E}\left[R_1 - s^{-1/\gamma} \,\middle|\, \sum_{i=1}^{k} S_i = s, N = k\right] = \frac{1}{Z_{k,s}} \left(s^{-\frac{(2k+\gamma+1)}{\gamma}} \sum_{j=2}^{k} Q_k^{(j)}\right). \tag{4.1.28}$$

What remains is for us to find the evaluated form of $\sum_{j=2}^{k} Q_k^{(j)}$, in terms of γ and k. The details of this are given in Subsection 4.1.3, in which we show the following theorem.

Theorem 4.2 (Summation of $Q_k^{(j)}$)**.** *For $Q_k^{(j)}$ as in Definition 4.3 then $\forall \gamma > 2$*

$$\sum_{j=2}^{k} Q_k^{(j)} = a(\gamma) \frac{\gamma^{(k-2)}}{2^{(k-2)}(k-2)!} y_{k+1}^{\frac{-2(k-2)}{\gamma}} + O\left(y_{k+1}^{\frac{\gamma-2(k-1)}{\gamma}}\right). \tag{4.1.29}$$

By combining this with (4.1.28) and substituting $y_{k+1} = \frac{1}{S\rho^{\gamma}}$ we find that

$$\mathbf{E}\left[R_1 - S^{-\frac{1}{\gamma}} | \sum_{i=1}^{k} s_i = S, N = k\right] = \frac{1}{Z_{k,S}} \left(a(\gamma) S^{-\frac{(\gamma+5)}{\gamma}} \left(\frac{\gamma}{2}\right)^{(k-2)} \frac{1}{(k-2)!} \rho^{2(k-2)} + O\left(S^{\frac{-2\gamma-3}{\gamma}} \rho^{2k-2-\gamma}\right)\right). \tag{4.1.30}$$

Therefore when considering highest order terms,

$$\begin{aligned} \mathbf{E}\left[R_1 - s^{-1/\gamma} \,\middle|\, N = k,\, S' = s\right] &\sim \frac{1}{Z_{k,s}^{\gamma,\rho}} a(\gamma) \left(\frac{\gamma}{2}\right)^{k-2} \frac{1}{(k-2)!} \rho^{2(k-2)} s^{-1-5/\gamma} \\ &\sim \frac{a(\gamma)\, 2\,(k-1)}{\gamma} \rho^{-2} s^{-3/\gamma}, \quad \text{as } s \to \infty. \end{aligned}$$

If we wished to consider the order of the error of this expectation we can consider some of the lower order terms.

Summing over values of $k \geq 1$

Finally, we want to sum these estimates over $k \geq 1$. To do this rigorously, we would need to take into account the k-dependence in the constants in our error terms. However, we are going to neglect the k-dependence in our error terms, and check the result of our computation against numerical simulation. Intuitively, we anticipate that these constants contribute decreasing amounts to the error terms as k increases and should decay sufficiently rapidly to produce a convergent error term which could be bounded uniformly if required.

We first need

$$\begin{aligned} f_{S'}(s) &= \sum_{k=1}^{\infty} e^{-\lambda\,\pi\,\rho^2}\,\left(\frac{2\,\lambda\,\pi}{\gamma}\right)^k\,Z_{k,s}^{\gamma,\rho} \\ &\sim e^{-\lambda\,\pi\,\rho^2}\sum_{k=1}^{\infty}\left[\left(\frac{2\,\lambda\,\pi}{\gamma}\right)^k\,\left(\frac{\gamma}{2}\right)^{k-1}\,\frac{1}{(k-1)!}\,\rho^{2(k-1)}\,s^{-1-2/\gamma}\right] \\ &= \frac{2\,\lambda\,\pi}{\gamma}\,s^{-1-2/\gamma}\,e^{-\lambda\,\pi\,\rho^2}\sum_{k=1}^{\infty}\frac{(\lambda\,\pi\,\rho^2)^{k-1}}{(k-1)!} \\ &= \frac{2\,\lambda\,\pi}{\gamma}\,s^{-1-2/\gamma},\quad \text{as } s\to\infty. \end{aligned}$$

With this estimate at hand, we can compute

$$\begin{aligned} \mathbf{P}[N=k\,|\,S'=s] &= \frac{1}{f_{S'}(s)}\,e^{-\lambda\,\pi\,\rho^2}\left(\frac{2\,\lambda\,\pi}{\gamma}\right)^k\,Z_{k,s}^{\gamma,\rho} \\ &\sim \frac{\gamma}{2\,\lambda\,\pi\,s^{-1-2/\gamma}}\left(\frac{2\,\lambda\,\pi}{\gamma}\,e^{-\lambda\,\pi\,\rho^2}\frac{(\lambda\,\pi\,\rho^2)^{k-1}}{(k-1)!}\,s^{-1-2/\gamma}\right) \\ &= e^{-\lambda\,\pi\,\rho^2}\,\frac{(\lambda\,\pi\,\rho^2)^{k-1}}{(k-1)!},\quad \text{as } s\to\infty,\text{ for } k=1,2,\ldots. \end{aligned}$$

That is, conditionally on a large signal, the number of *extra transmitters* (in addition to the nearest one), is asymptotically $\mathsf{Poisson}(\lambda\,\pi\,\rho^2)$. This yields

$$\begin{aligned} \mathbf{E}\Big[R_1 - s^{-1/\gamma}\,\Big|\,S'=s\Big] &\sim \sum_{k=1}^{\infty} e^{-\lambda\,\pi\,\rho^2}\,\frac{(\lambda\,\pi\,\rho^2)^{k-1}}{(k-1)!}\,\frac{2(k-1)\,a(\gamma)\,\rho^{-2}}{\gamma}\,s^{-3/\gamma} \\ &\sim \frac{2\,\lambda\,\pi}{\gamma}\,a(\gamma)\,s^{-3/\gamma}, \end{aligned} \tag{4.1.31}$$

as $s\to\infty$, independent of the value of ρ. Therefore we find that

$$\mathbf{E}\Big[R_1\Big|S'=s\Big] \sim s^{-1/\gamma} + \frac{2\lambda\pi}{\gamma}a(\gamma)s^{-3/\gamma}. \tag{4.1.32}$$

4.1.3 Evaluating $\sum_{j=2}^{k} Q_k^{(j)}$ (Proof of Theorem 4.2)

We give the details of the computations for the general case of the asymptotic heuristic (4.1.32). We wish to evaluate

$$W_{k,s} = \int_{\rho^{-\gamma}}^{\frac{s}{k}} \ldots \int_{s_3}^{\frac{s-s_3}{s}} \frac{(s-s_2-\ldots-s_k)^{-\frac{1}{\gamma}} - s^{-\frac{1}{\gamma}}}{(s-s_2-\ldots-s_k)^{\frac{\gamma+2}{\gamma}}\,s_2^{\frac{\gamma+2}{\gamma}}\ldots s_k^{\frac{\gamma+2}{\gamma}}}\,ds_2\ldots ds_k. \tag{4.1.33}$$

In Subection 4.1.2 we found that expression (4.1.33) can be expressed concisely as

$$W_{k,s} = s^{-\frac{(2k+\gamma+1)}{\gamma}} \sum_{j=2}^{k} Q_k^{(j)}. \tag{4.1.34}$$

By recalling from Subsection 4.1.2 the definition of the iterative sequence $Q_k^{(j)}$, Definition 4.3, we find the evaluated form of $\sum_{j=2}^{k} Q_k^{(j)}$ in terms of γ and k. This is done in three steps:

(1). We find $Q_k^{(2)}$

  (a) in the case when $2 < \gamma < 4$

  (b) in the case when $\gamma = 4$

  (c) in the case when $\gamma > 4$

(2). We find $Q_{j+m}^{(j)}$ where $j > 2$ and $0 \leq m \leq k - j$

  (a) in the case when γ is not an even integer.

  (b) in the case when γ is an even integer.

(3). Finally we show that the evaluated form of $\sum_{j=2}^{k} Q_k^{(j)}$ is unchanged for all $\gamma > 2$.

Step 1:

We will begin by evaluating $Q_k^{(j)}$ in the special case where $j = 2$. Due to $Q_k^{(2)}$ beginning from part 3 of Definition 4.3, rather than part 2, $Q_k^{(2)}$ always produces the leading order term. For this reason we start with $Q_2^{(2)}$.

$$\begin{aligned} Q_2^{(2)} &= \int_{\frac{y_3}{1-y_3}}^{\frac{1}{2}} y_2^{-\frac{(\gamma+2)}{\gamma}} (1-y_2)^{\frac{-2-\gamma}{\gamma}} \left[(1-y_2)^{-\frac{1}{\gamma}} - 1\right] Q_1^{(2)} dy_2 \\ &= \int_0^{\frac{1}{2}} \frac{(1-y_2)^{-\frac{1}{\gamma}} - 1}{y_2^{\frac{\gamma+2}{\gamma}} (1-y_2)^{\frac{2+\gamma}{\gamma}}} dy_2 - \int_0^{\frac{y_3}{1-y_3}} \frac{(1-y_2)^{-\frac{1}{\gamma}} - 1}{y_2^{\frac{\gamma+2}{\gamma}} (1-y_2)^{\frac{2+\gamma}{\gamma}}} dy_2 \\ &= a(\gamma) - \int_0^{\frac{y_3}{1-y_3}} \frac{(1-y_2)^{-\frac{1}{\gamma}} - 1}{y_2^{\frac{\gamma+2}{\gamma}} (1-y_2)^{\frac{2+\gamma}{\gamma}}} dy_2 \\ &= a(\gamma) - \frac{1}{\gamma-2} y_3^{\frac{\gamma-2}{\gamma}} + O\left(y_3^{\frac{2\gamma-2}{\gamma}}\right) \end{aligned} \tag{4.1.35}$$

Therefore, from part 4 of Definition 4.3, we find that

$$Q_3^{(2)} = \int_{\frac{y_4}{1-y_4}}^{\frac{1}{3}} \left[a(\gamma) y_3^{\frac{-\gamma-2}{\gamma}} - \frac{1}{(\gamma-2)} y_3^{\frac{-4}{\gamma}} + O\left(y_3^{\frac{\gamma-4}{\gamma}}\right) \right] dy_3. \tag{4.1.36}$$

From (4.1.36) we can see that there are three cases, relating to the value of γ, in which $Q_3^{(2)}$ will evaluate differently. These are: $2 < \gamma < 4$, $\gamma = 4$ and $\gamma > 4$. Using the iterative sequence defined in Definition 4.3, we find the evaluated form of $Q_k^{(2)}$ in each of these three cases.

1(a):

For $2 < \gamma < 4$.

$$Q_3^{(2)} = a(\gamma)\frac{\gamma}{2}y_4^{-\frac{2}{\gamma}} + O\left(y_4^{\frac{\gamma-4}{\gamma}}\right)$$

and from integrating this iteratively, using part 2 of Definition 4.3, we find that

$$Q_k^{(2)} = a(\gamma)\left(\frac{\gamma}{2}\right)^{(k-2)}\frac{1}{(k-2)!}y_{k+1}^{-\frac{2(k-2)}{\gamma}} + O\left(y_4^{\frac{\gamma-2(k-1)}{\gamma}}\right), \tag{4.1.37}$$

1(b):

For $\gamma = 4$,

$$Q_3^{(2)} = a(4)2y_4^{-\frac{1}{2}} + \frac{1}{2}\log(y_4) + O(1)$$

and from integrating this iteratively, using part 2 of Definition 4.3, we find that

$$Q_k^{(2)} = a(4)\frac{2^{(k-2)}}{(k-2)!}y_{k+1}^{\frac{2-k}{2}} - \frac{2^{(k-4)}}{(k-3)!}\log(y_{k+1})y_{k+1}^{\frac{3-k}{2}} + O\left(y_{k+1}^{\frac{3-k}{2}}\right), \tag{4.1.38}$$

1(c):

For $\gamma > 4$

$$Q_3^{(2)} = a(\gamma)\frac{\gamma}{2}y_4^{-\frac{2}{\gamma}} + O(1)$$

and from integrating this iteratively, using part 2 of Definition 4.3, we find that

$$Q_k^{(2)} = a(\gamma)\left(\frac{\gamma}{2}\right)^{(k-2)}\frac{1}{(k-2)!}y_{k+1}^{-\frac{2(k-2)}{\gamma}} + O\left(y_{k+1}^{\frac{6-2k}{\gamma}}\right). \tag{4.1.39}$$

In (4.1.38) we see that when $\gamma = 4$ a log term is introduced. However, in (4.1.9) we saw this term cancels with the leading order term from $Q_k^{(3)}$. We will now find the evaluated form of $Q_k^{(j)}$ for $j \geq 3$ and show that log terms either cancel or are of a lower order than existing terms and so can be disregarded.

Step 2:

For $2 \leq l < j$ we evaluate part 2 of Definition 4.3. As y_l is small we use that $(1 - y_l) \approx 1$ and $\frac{y_{l+1}}{(1-y_{l+1})} \approx y_{l+1}$ to find that

$$Q_l^{(j)} = \frac{\gamma^{l-1}}{2^{(l-1)}(l-1)!}y_{l+1}^{2(1-l)/\gamma} - \left(\frac{\gamma}{2}\right)^{(l-1)}\frac{1}{(l-2)!}\left(\frac{1}{2}\right)^{-\frac{2}{\gamma}}y_{l+1}^{-\frac{2(l-2)}{\gamma}} + O\left(y_{l+1}^{2(3-l)/\gamma}\right), \tag{4.1.40}$$

where the third order term will only exist for $l \geq 3$.

To evaluate $Q_j^{(j)}$, part 3 of Definition 4.3, we use the Taylor approximation to find that $\left[(1-y_l)^{-\frac{1}{\gamma}} - 1\right] = \frac{1}{\gamma} y_l + O\left(y_l^2\right)$ and so

$$Q_j^{(j)} = \int_{\frac{y_{j+1}}{1-y_{j+1}}}^{\frac{1}{j}} \left(\frac{1}{\gamma} y_j^{-\frac{2}{\gamma}} + O\left(y_j^{\frac{\gamma-2}{\gamma}} \right) \right) Q_{j-1}^{(j)} dy_j. \tag{4.1.41}$$

By setting $l = (j-1)$ in (4.1.40) and using this result in (4.1.41) we find that

$$Q_j^{(j)} = \int_{\frac{y_{j+1}}{1-y_{j+1}}}^{\frac{1}{j}} \frac{\gamma^{j-3}}{2^{(j-2)}(j-2)!} y_j^{\frac{-2(j-1)}{\gamma}} - \frac{\gamma^{j-3}}{2^{(j-2-\frac{2}{\gamma})}(j-3)!} y_j^{\frac{-2(j-2)}{\gamma}} + O\left(y_j^{-\frac{2(j-3)}{\gamma}} \right) dy_j \tag{4.1.42}$$

If we now define an integer m such that $0 \leq m \leq k-j$, then we can write

$$\begin{aligned} Q_{j+m}^{(j)} = \int_{\frac{y_{j+m+1}}{1-y_{j+m+1}}}^{\frac{1}{j+m}} & \frac{\gamma^{j+m-3}}{2^{(j-2)}(j-2)!} (2(j-2)-\gamma) \left(\prod_{n=j-2}^{j+m-2} \frac{1}{2n-\gamma} \right) y_{j+m}^{\frac{2-2(j+m)}{\gamma}} \\ - \frac{\gamma^{j+m-3}}{2^{(j-2-\frac{2}{\gamma})}(j-3)!} & (2(j-3)-\gamma) \left(\prod_{n=j-3}^{j+m-3} \frac{1}{2n-\gamma} \right) y_{j+m}^{\frac{4-2(j+m)}{\gamma}} + O\left(y_{j+m}^{\frac{6-2(j+m)}{\gamma}} \right) dy_{j+m} \end{aligned} \tag{4.1.43}$$

It can be seen from (4.1.43) that a log term will occur if $\gamma = 2(j+m) - 2x$ and $x \in \{1,2,3\}$. Therefore there are two cases, relating to the value of γ, in which $Q_{j+m}^{(j)}$ will evaluate differently.

2(a):

The first is the case where γ is not an even integer, in this case we find that

$$\begin{aligned} Q_{j+m}^{(j)} = & \frac{\gamma^{j+m-2}}{2^{(j-2)}(j-2)!} \left(\prod_{n=j-1}^{j+m-1} \frac{1}{2n-\gamma} \right) y_{j+m+1}^{\frac{-2(j+m-1)+\gamma}{\gamma}} \\ & - \frac{\gamma^{j+m-2}}{2^{(j-2-\frac{2}{\gamma})}(j-3)!} \left(\prod_{n=j-2}^{j+m-2} \frac{1}{2n-\gamma} \right) y_{j+m+1}^{\frac{-2(j+m-2)+\gamma}{\gamma}} + O\left(y_{j+m+1}^{\frac{-2(j+m-3)+\gamma}{\gamma}} \right) \end{aligned} \tag{4.1.44}$$

and can retrieve $Q_k^{(j)}$ by substituting $j+m=k$.

$$Q_k^{(j)} = \frac{\gamma^{k-2}}{2^{(j-2)}(j-2)!} \left(\prod_{n=j-1}^{k-1} \frac{1}{2n-\gamma} \right) y_{k+1}^{\frac{-2(k-1)+\gamma}{\gamma}} + O\left(y_{k+1}^{\frac{-2(k-2)+\gamma}{\gamma}} \right) \tag{4.1.45}$$

2(b):

We start with the second case being where, in (4.1.43), γ is an even integer satisfying $\gamma = 2(j+m) - 2x$ for $x \in \{1,2,3\}$. However, as $\forall \epsilon > 0,\ \log(y) \ll y^{-\epsilon}$ as $y \downarrow 0$, we observe that for $\epsilon < \frac{2}{\gamma}$

$$O\left(\log(y) y^{\frac{\gamma+2(x+1)-2k}{\gamma}}\right) < O\left(y^{-\epsilon} y^{\frac{\gamma+2(x+1)-2k}{\gamma}}\right) = O\left(y^{\frac{2}{\gamma}} y^{-\epsilon} y^{\frac{\gamma+2x-2k}{\gamma}}\right) < O\left(y^{\frac{\gamma+2x-2k}{\gamma}}\right).$$

Therefore we only need to consider $x = 1$ as log terms from larger values of x would not be leading order. So the second case is $\gamma = 2(j+m) - 2$ and we find that,

$$Q_k^{(j)} = \frac{\gamma^{k-3}}{2^{(k+j-\frac{\gamma}{2}-3)}(j-2)!} \frac{(2j-4-\gamma)}{(k-\frac{\gamma}{2}-1)!} \left(\prod_{n=j-2}^{\frac{\gamma-2}{2}} \frac{1}{2n-\gamma}\right) \log(y_{k+1}) y_{k+1}^{\frac{\gamma-2(k-1)}{\gamma}} + O\left(y_{k+1}^{\frac{\gamma-2(k-1)}{\gamma}}\right). \quad (4.1.46)$$

Otherwise, the form of $Q_k^{(j)}$ is as given in (4.1.45).

Step 3:

We will now show that $\forall \gamma > 2$

$$\sum_{j=2}^{k} Q_k^{(j)} = a(\gamma) \frac{\gamma^{(k-2)}}{2^{(k-2)}(k-2)!} y_{k+1}^{\frac{-2(k-2)}{\gamma}} + O\left(y_{k+1}^{\frac{\gamma-2(k-1)}{\gamma}}\right). \quad (4.1.47)$$

We will show that any log terms introduced by (4.1.46) either cancel or are of a lower order than existing terms.

For $2 < \gamma < 4$, in step 1(a), we showed that $Q_k^{(2)}$ is given by (4.1.37). As in this case γ is not an even integer, we know from step 2(a) that $Q_k^{(j)}$ is given by (4.1.45). Therefore for $2 < \gamma < 4$ we have found $Q_k^{(j)}$ for $2 \le j \le k$. Summing over j gives (4.1.47).

For $\gamma = 4$, in step 1(b), we showed that $Q_k^{(2)}$ is given by (4.1.38). As in this case γ is an even integer, we look to step 2(b) to find the form of $Q_k^{(j)}$. In step 2(b) it was found that a leading order log term would only occur when $\gamma = 2(j+m) - 2$, when $\gamma = 4$ this is when $j = 3$. When $\gamma = 4$ and $j = 3$ we use (4.1.46) and recover that

$$Q_k^{(3)} = \frac{2^{(k-4)}}{(k-3)!} \log(y_{k+1}) y_{k+1}^{\frac{3-k}{2}} + O\left(y_{k+1}^{\frac{3-k}{2}}\right) \quad (4.1.48)$$

which cancels the log term in (4.1.38). For $3 < j \le k$, $Q_k^{(j)}$ is given by (4.1.45). Therefore for $\gamma = 4$ we have found $Q_k^{(j)}$ for $2 \le j \le k$. Summing over j gives

(4.1.47).

For $\gamma > 4$, in step 1(c), we showed that $Q_k^{(2)}$ is given by (4.1.39). As for $j > 2$, γ may satisfy $\gamma = 2(j+m) - 2$ we consider 2(b). We find that $\forall \epsilon < \frac{\gamma-4}{4}$,

$$O\left(\log(y) y^{\frac{\gamma-2(k-1)}{\gamma}}\right) < O\left(y^{-\epsilon} y^{\frac{\gamma-2(k-1)}{\gamma}}\right) < O\left(y^{\frac{6-2k}{\gamma}}\right) \tag{4.1.49}$$

and therefore any log terms are of lower order and can be disregarded.

Therefore, we find that $\forall \gamma > 2$

$$\sum_{j=2}^{k} Q_k^{(j)} = a(\gamma) \frac{\gamma^{(k-2)}}{2^{(k-2)}(k-2)!} y_{k+1}^{\frac{-2(k-2)}{\gamma}} + O\left(y_{k+1}^{\frac{\gamma-2(k-1)}{\gamma}}\right). \tag{4.1.50}$$

4.1.4 Comparison with Numerical Simulations

We use numerical simulations to assess and compare the performance of the asymptotic approximation (4.1.32) with the heuristic $R_1 = s^{-1/\gamma}$. To do this we begin by simulating the distribution of R_1 for a given value of S. As R_1 is conditioned on s, it is important that there is small variance in the values of s accepted for a simulation. For a simulation with a chosen value $S = s^*$ we accepted all samples where $s \in [0.98s^*, 1.02s^*]$. For the simulations with $\gamma = 4$ and $\gamma = 6$, we collected 2×10^6 samples. For the simulation with $\gamma = 3$, we collected 5×10^6 samples. The choices regarding accuracy and sample size provide an acceptable trade-off between simplicity of simulation and accuracy. The simulations produce values close to our theoretical values. The distribution of R_1 where $\gamma = 4$ for $S = 50$ and $S = 1000$ can be seen in Figures 4-1 and 4-2 respectively.

As previously stated, transmitter locations are taken to be distributed according to a Poisson point process. We consider them Poisson points distributed in a disk, with the origin at the centre. As we are only interested in the distances of these transmitters to the origin, not their location, the Mapping theorem can be used to efficiently generate correctly distributed distances. To ensure independence a new set of transmitter distances were generated for each sample. Efficiency is required as, due to randomness, achieving an acceptable value of S can require a large number of samples to be generated. We gave the method for efficiently generating transmitter distances in Subsection 1.4.1.

Figure 4-3 compares the accuracy of the two heuristics for different values of pathloss, $\gamma = 3, 4, 6$, over a range of values of S. The values for pathloss were chosen to be close to observed real world values and demonstrate the differences

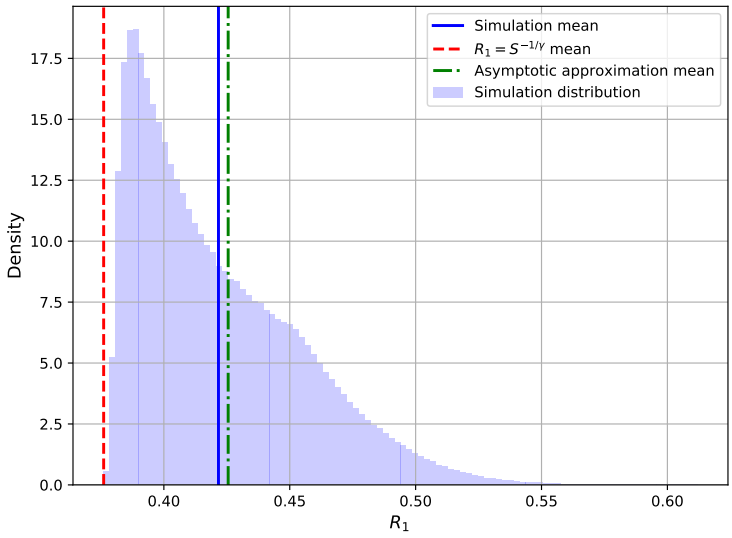

Figure 4-1: Observed signal $S = 50$ and pathloss $\gamma = 4$. R_1 is the distance to the nearest transmitter. This value for S is considered small. Observe the interesting shape of the simulation distribution; this is described in [42]. The mean of the asymptotic approximations, applied to each of the 2×10^6 sample values of S, is close to the simulation mean of R_1. This supports that (4.1.32) offers an accurate estimation of R_1. Further to that it offers a significant improvement over the heuristic $R_1 = s^{-1/4}$.

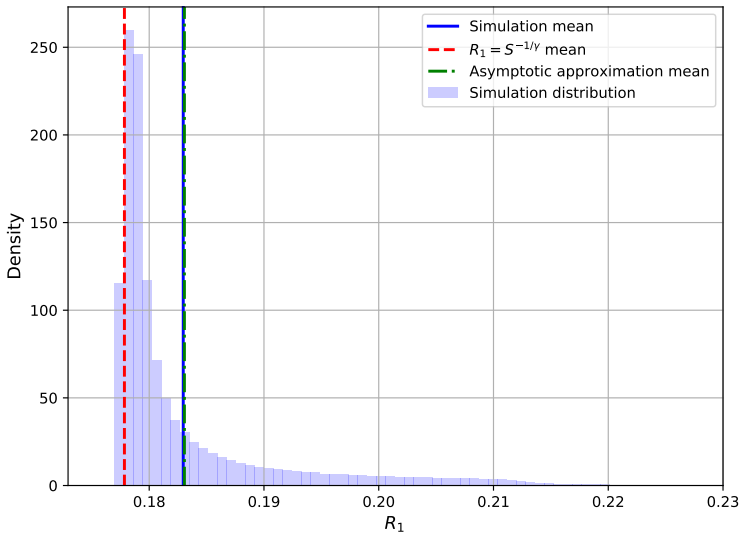

Figure 4-2: Observed signal $S = 1000$ and pathloss $\gamma = 4$. R_1 is the distance to the nearest transmitter. The mean value of R_1 from the simulation aligns with the mean asymptotic approximation, verifying that it is highly accurate. Although the heuristic $R_1 = S^{-1/4}$ has improved in accuracy compared to Figure 4-1 it remains significantly less accurate. Figure 4-3 shows how the accuracy of asymptotic heuristic and $R_1 = S^{-1/\gamma}$ increases with signal.

for values of γ higher and lower than $\gamma = 4$.

The accuracy of the asymptotic heuristic for low values of S can be seen in Figure 4-3 to increase as γ decreases. This is due to the order of the error being $O(S^{\frac{\gamma+1}{\gamma}})$ as shown in Section 4.1. However, the heuristic $R_1 = S^{-\frac{1}{\gamma}}$ has error of order $O(S^{-\frac{3}{\gamma}})$ and therefore accuracy increases with γ. This behaviour can also be seen in Figure 4-3.

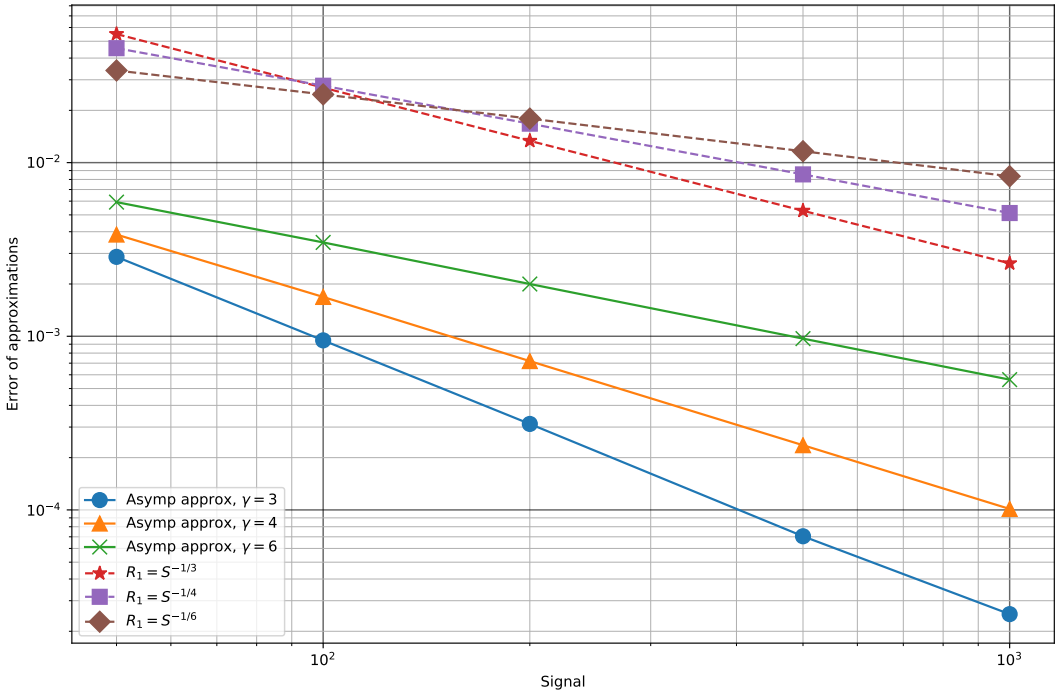

Figure 4-3: This graph shows on log-log axes the error of the approximations decreasing as signal increases, for different values of γ. The gradients of the lines support the heuristics. This is shown in figure 4.1. The absolute error of approximations is the absolute value of the difference between the estimate and the actual value, given a percentage of the actual value, (e.g., error $= \frac{100(\text{estimate-actual})}{\text{actual}}$). It is shown that the asymptotic approximation is more accurate than the heuristic $R_1 = S^{1/\gamma}$, even for low values of S.

The numerical simulations show that even for moderate values of S our asymptotic heuristic appears to give a good estimate of the expected error.

Heuristic	**Expected Slope**	**Observed Slope**
Asymptotic Approximation, $\gamma = 3$	-5/3 (-1.67)	-1.581
Asymptotic Approximation, $\gamma = 4$	-5/4 (-1.25)	-1.214
Asymptotic Approximation, $\gamma = 6$	-5/6 (-0.83)	-0.786
$R_1 = S^{-1/3}$	-3/3 (-1.00)	-1.015
$R_1 = S^{-1/4}$	-3/4 (-0.75)	-0.730
$R_1 = S^{-1/6}$	-3/6 (-0.50)	-0.468

Table 4.1: The numerically estimated slopes of the lines plotted in Figure 4-3, given under the heading Observed Slope, can be compared with the expected slope derived from the theory. It is found that the expected slopes closely match. Showing that the the simulations support the theoretical results.

4.2 Rayleigh Fading

In a cellular system, such as the one being modelled, interference comes from multiple sources. We wish to be able to estimate the distance to the nearest transmitter in a wireless network. In Section 4.1 we considered the signal without fading.

We now ask the question of whether the distance to the nearest transmitter can also be accurately estimated when the effect of fading is applied to the observed signal. To answer this we begin in Subection 4.2.1 by finding a scaling factor that can be used to scale the faded signal to the values it would have taken been had fading not been in effect. The recovered signal can then be used in conjunction with a distance heuristic to estimate the distance to the nearest transmitter. The scaling factor can be used for different values of m in Nakagami-m fading, though we use the Rayleigh fading case where $m = 1$ as an example. In Subection 4.2.2 we develop a heuristic for finding the expected distance to the nearest transmitter based on observed faded signal at the origin. Both methods are then checked and compared against numerical simulations in Subection 4.2.3.

4.2.1 Scaling Factors

We recollect some scaling properties of the total signal, with and without fading, from [39, Section 5.1]. First recall that the total signal without fading is

$$S(\lambda) = \sum_{i=1}^{\infty} R_i(\lambda)^{-\gamma},$$

where we write the argument λ to emphasize that the distribution of S depends on λ. When fading is present, we have instead a total signal

$$T(\lambda) = \sum_{i=1}^{\infty} H_i R_i(\lambda)^{-\gamma},$$

where $H_1, H_2, \ldots$ are independent random variables. (Note that in [39] observed total signal is referred to as interference and denoted by $I(\lambda)$, where λ is the density of the Poisson distributed transmitters.) By calculating Laplace tranforms, it is shown in [39, Section 5.1.7] that $T(\lambda)$ has the same distribution as $S(\mathbf{E}[H^{2/\gamma}]\lambda)$. It is also shown in [39, Corollary 5.4] that for any $a > 0$ $S(a\lambda)$ has the same distribution as $a^{\gamma/2}S(\lambda)$. It follows from these two facts that

$$T(\lambda) \stackrel{\mathrm{d}}{=} \mathbf{E}[H^{2/\gamma}]^{\gamma/2} S(\lambda),$$

where $\stackrel{\mathrm{d}}{=}$ means equal in distribution. We now compute the scaling factor in front of $S(\lambda)$, for Nakagami-m fading.

As stated before, Nakagami-m fading is distributed $\mathsf{Gamma}(m, 1/m)$. The probability density function of the $\mathsf{Gamma}(\alpha, \theta)$ distribution with shape $\alpha > 0$ and scale $\theta > 0$ is

$$f(x; \alpha, \theta) = \frac{1}{\Gamma(\alpha)\theta^{\alpha}} x^{\alpha-1} e^{-\frac{x}{\theta}} \quad \text{for } 0 < x < \infty,$$

and therefore

$$\mathbf{E}[H^{2/\gamma}] = \frac{1}{\Gamma(m)(1/m)^m} \int_0^{\infty} h^{\frac{2}{\gamma}+m-1} e^{-mh}\, dh.$$

As $\int_0^{\infty} h^{\frac{2}{\gamma}+m-1} e^{-mh}\, dh = (1/m)^{\frac{2}{\gamma}+m}\Gamma(\frac{2}{\gamma}+m)$, it is found that

$$\mathbf{E}[H^{2/\gamma}] = \frac{\Gamma(\frac{2}{\gamma}+m)(1/m)^{\frac{2}{\gamma}}}{\Gamma(m)},$$

and hence we define

$$c(\gamma, m) := \mathbf{E}\left[H^{2/\gamma}\right]^{\gamma/2} = \left(\frac{\Gamma(\frac{2}{\gamma}+m)}{\Gamma(m)}\right)^{\gamma/2} \frac{1}{m}. \tag{4.2.1}$$

Based on this scaling, a simple heuristic is:

$$R_1(\lambda) \approx S(\lambda)^{-1/\gamma} \stackrel{\mathrm{d}}{=} c(\gamma, m)^{1/\gamma}\, T(\lambda)^{-1/\gamma}. \tag{4.2.2}$$

We refer to this heuristic as '$R_1 = T^{-1/\gamma}$ with scaling'. The asymptotic heuristic (4.1.32) combined with the scaling factor gives

$$\mathbf{E}\Big[R_1\Big|T=t\Big] \approx t^{-1/\gamma}c(\gamma,m)^{1/\gamma} + \frac{2\lambda\pi}{\gamma}a(\gamma)t^{-3/\gamma}c(\gamma,m)^{3/\gamma}. \tag{4.2.3}$$

We refer to this heuristic as 'Asymptotic heuristic with scaling'. We improve on these in the next section, in the case of Rayleigh fading, where the effect is the strongest.

4.2.2 Distance Estimation with Rayleigh Fading

The effect of Rayleigh fading is described by the random variable $H_1 \sim \text{Exp}(1)$, with probability density function

$$f_{H_1}(h_1) = e^{-h_1} \quad \text{where } h_1 > 0.$$

In order to simplify computations, we are going to assume that there is a single transmitter in the disc of radius $\rho = 1/\sqrt{\lambda\pi}$ (this choice of the radius makes the average number of transmitters in this disc equal to 1). Let $\tilde{S}_1$ be the signal contributed by this sole transmitter, so that by setting $k = 1$ in (4.1.11) we get

$$f_{\tilde{S}_1}(s_1) = 2\lambda\pi e^{-\lambda\pi\rho^2}\frac{1}{\gamma}s_1^{-\frac{\gamma+2}{\gamma}} = \frac{2}{\gamma\,\rho^2}\,e^{-1}\,s_1^{-\frac{\gamma+2}{\gamma}}, \quad \rho^{-\gamma} < s_1 < \infty. \tag{4.2.4}$$

As an approximation, we replace T by the random variable

$$\tilde{T}_1 = H_1\,\tilde{S}_1.$$

The joint probability density function of $\tilde{S}_1$ and H_1, as they are assumed independent, is given by

$$f_{\tilde{S}_1,H_1}(s_1,h_1) = \frac{2}{\gamma\rho^2}s_1^{-\frac{\gamma+2}{\gamma}}e^{-h_1}e^{-1}.$$

Then the joint probability density function of $\tilde{T}_1$ and H_1 is found to be

$$f_{\tilde{T}_1,H_1}(t_1,h_1) = \frac{2}{\gamma\rho^2}h_1^{\frac{2}{\gamma}}t_1^{-\frac{(\gamma+2)}{\gamma}}e^{-h_1}e^{-1}, \quad 0 < t_1 < \infty,\, 0 < h_1 < \rho^\gamma t_1.$$

Since

$$\int_0^{\rho^\gamma t_1} h_1^{2/\gamma}e^{-h_1}dh_1 = G\left(\frac{\gamma+2}{\gamma}, \rho^\gamma t_1\right),$$

where G denotes the lower incomplete Gamma-function. Therefore, the marginal density of $\tilde{T}_1$ is given by

$$f_{\tilde{T}_1}(t_1) = \frac{2}{\gamma\rho^2} t_1^{-\frac{(\gamma+2)}{\gamma}} e^{-1} G\left(\frac{\gamma+2}{\gamma}, \rho^\gamma t_1\right), \quad 0 < t_1 < \infty.$$

We can use this to find

$$f_{H_1|\tilde{T}_1=t_1}(h_1) = \frac{f_{\tilde{T}_1,H_1}(t_1,h_1)}{f_{\tilde{T}_1}(t_1)} \frac{1}{G\left(\frac{\gamma+2}{\gamma}, \rho^\gamma t_1\right)} h_1^{\frac{2}{\gamma}} e^{-h_1}, \quad 0 < h_1 < \rho^\gamma t_1.$$

Since we made the approximation that T is attributed entirely to the nearest transmitter, we have $t_1 = \tilde{S}_1 H_1 = R_1^{-\gamma} H_1$ and therefore $H_1 = t_1 R_1^\gamma$. From this we find

$$f_{R_1|\tilde{T}_1=t_1}(r_1|t_1) = f_{H_1|\tilde{T}_1=t_1}(h_1|t_1)\frac{dh_1}{dr_1} = f_{H_1|\tilde{T}_1=t_1}(h_1|t_1) t_1 \gamma r_1^{\gamma-1}$$

and therefore we find the following theorem.

Theorem 4.3 (Fading Approximation)**.** *When Rayleigh fading is in effect, t_1 is the observed signal and γ is the pathloss exponent then the distribution of the distance R_1 to the nearest transmitter, conditional on t_1, is given by*

$$f_{R_1|\tilde{T}_1=t_1}(r_1) = \left[\frac{\gamma t_1^{\frac{\gamma+2}{\gamma}}}{G\left(\frac{\gamma+2}{\gamma}, \rho^\gamma t_1\right)}\right] r_1^{\gamma+1} e^{-t_1 r_1^\gamma}, \quad 0 < r_1 < \rho. \tag{4.2.5}$$

This shows the effect that the radius of the disk has on the probability density function. We note that when t_1 is large the value of G does not depend as strongly on ρ as it does when t_1 is small. This can be attributed to the asymptotic behaviour of the lower incomplete gamma function $G(s,x) \to \Gamma(s)$ as $x \to \infty$.

From this we are able to find that the expected distance to the nearest transmitter, conditional on observed faded signal at the origin, is given by

$$\mathbf{E}[R_1|\tilde{T}_1 = t_1] = \frac{\Gamma\left(\frac{\gamma+3}{\gamma}\right)}{t_1^{\frac{1}{\gamma}} G\left(\frac{\gamma+2}{\gamma}, \rho^\gamma t_1\right)} \tag{4.2.6}$$

To summarise, we have shown that when Rayleigh fading is in effect if the observed total signal T takes the value t then a very simple heuristic would be to use $(cT)^{-1/\gamma}$ where c is a scaling factor which makes cT have the same expected value as S (the total signal in the absence of fading). We propose an improvement

on this which is an approximate probability distribution of R_1 depending on the measured value of $T = t$. We show that this is a considerable improvement and, being a distribution, provides additional information. The approximate probability density of R_1 conditioned on the measured total signal T taking the value t is given by

$$f_{R_1\,|\,T}(r_1\,|\,t) \approx \frac{1}{Z(t,\gamma,\lambda)} r_1^{\gamma+1}\, e^{-t\, r_1^{\gamma}}, \quad 0 < r_1 < (\lambda\pi)^{-1/2},$$

where the normalization $Z(t,\gamma,\lambda)$ can be expressed in terms of the lower incomplete Gamma function.

The performance of (4.2.5) and (4.2.6) against numerical simulations is shown in Figures 4-4 and 4-5.

4.2.3 Numerical Simulations

To check the accuracy of the Rayleigh fading distance estimate, derived in Section 4.2.2, we simulate Poisson distributed points contributing Rayleigh faded signal to an origin, at which the total signal T is recorded. As the expected distance to the nearest transmitter R_1 depends on T, simulation results were stored depending on the value of T observed. Five values of T were chosen that ranged from low to high: 50, 100, 200, 500 and 1000. Any simulation where T was within 2% of one of the five values was stored. We generated 1×10^6 samples for each of the five values of T.

The stored numerical simulations for the five values of T allow the accuracy of the Rayleigh fading distance estimate to be evaluated. The approximated distribution and expected mean of R_1, given in equations (4.2.5) and (4.2.6) respectively, are compared to the numerical results obtained through the simulations. Figures 4-4 and 4-5 show the distribution of the distance to the nearest neighbour for a low and a high value of T respectively. They confirm that the theoretical results perform well across a range of values for T. The agreement is better for the large value of T in accordance with the observation made above that G is sensitive to ρ.

We also wish to assess the accuracy of the fading approximation (4.2.6) against the heuristics (4.1.32) and $R = S^{-1/\gamma}$ when they are combined with the scaling factor (4.2.1). We note that in the scaling factor $\rho = 1$ as the density of the points simulated was $\lambda = 1/\pi$. The scaling factor used together with the simple heuristic $R = S^{-1/\gamma}$ gives (4.2.2) and is referred to as '$R_1 = T^{-1/\gamma}$ with scaling'. The scaling factor used together with the asymptotic heuristic (4.1.32) gives (4.2.3)

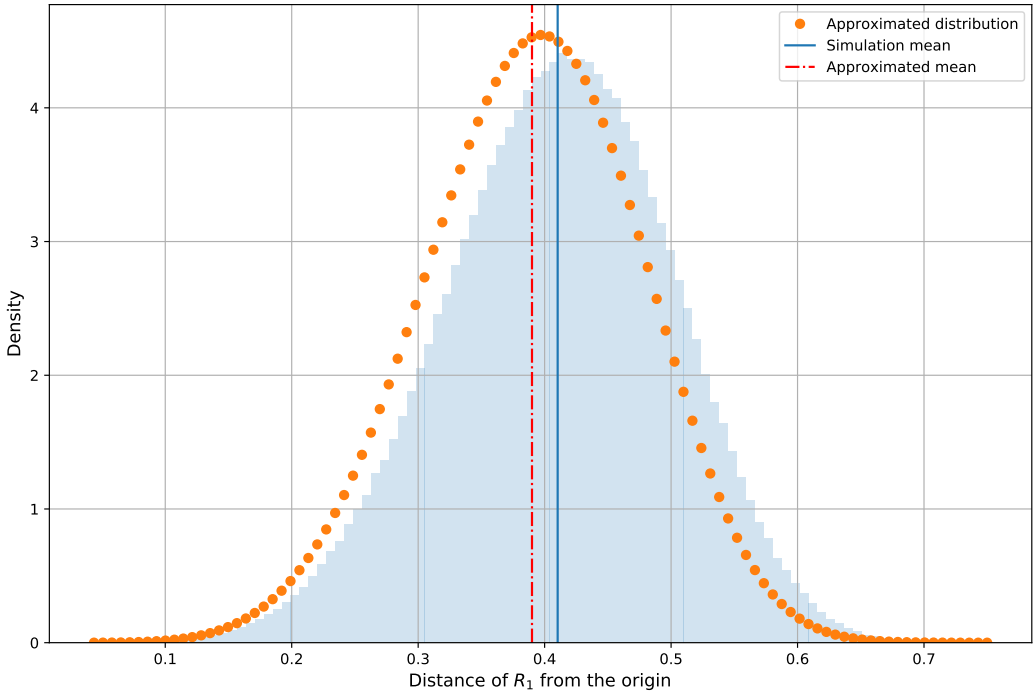

Figure 4-4: The distribution of R_1 for the low value $T = 50$ when $\gamma = 4$. The histogram shows the distribution of R_1 obtained through numerical simulations. Equation (4.2.5), referred to as 'Approximated distribution', has the correct shape but has a slight shift to the left. The expected mean R_1 from equation (4.2.6) is close to the mean obtained through numerical simulations but, as with the distribution, has a shift to the left.

which is referred to as 'Asymptotic heuristic with scaling'. The performance of (4.2.3) and (4.2.2), compared to the fading approximation (4.2.6), when $\gamma = 4$, is shown in Figure 4-6. In Figure 4-6 we note that the 'Asymptotic heuristic with scaling' (4.2.3) outperforms '$R_1 = T^{-1/4}$ with scaling' (4.2.2). As a result, in Figure 4-7 we then compare the 'Asymptotic heuristic with scaling' against the 'Fading approximation' for $\gamma = 3, 4, 6$. In Figure 4-7 we observe that, of the three heuristics tried, the fading approximation is the most accurate method of estimating the distance R_1 in the case with Rayleigh fading. We then wish to know, when it is known whether Rayleigh fading is in effect and so the appropriate heuristic can be used, how does the accuracy of the fading approximation compare to the accuracy of the asymptotic heuristic? Figure 4-8 compares the accuracy of these two heuristics, when used appropriately, for a range of values of observed signal.

In Figure 4-6, where $\gamma = 4$ and observed signal ranges from 50 to 1000, it can be seen that '$R_1 = T^{-1/4}$ with scaling' does not perform as well as the 'Fading approximation' or the 'Asymptotic heuristic with scaling'. The curve

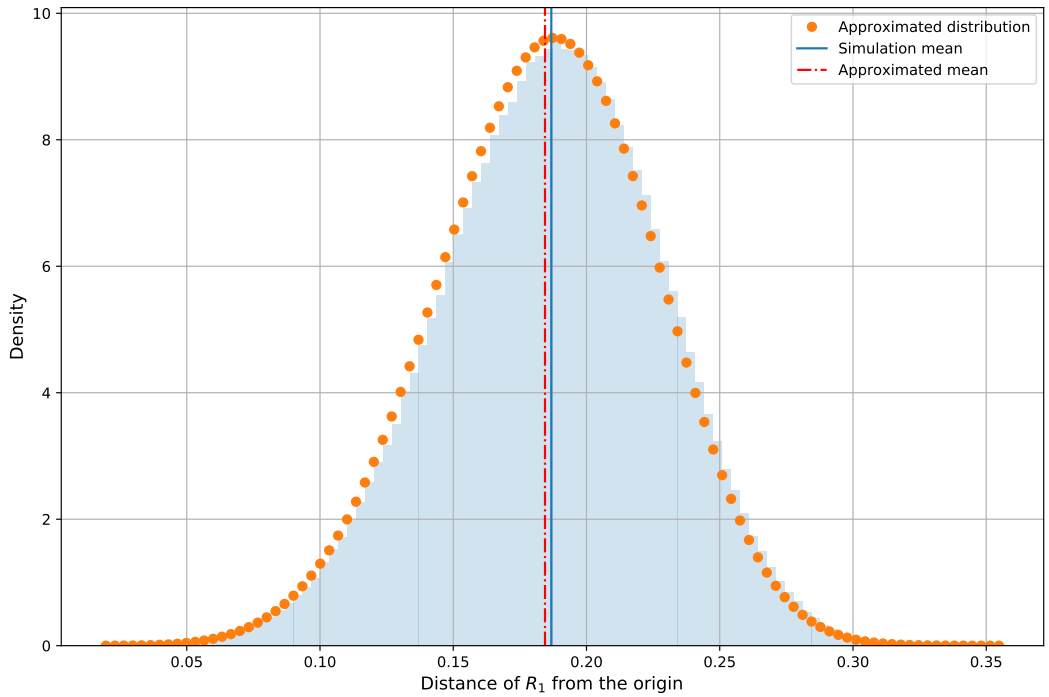

Figure 4-5: The distribution of R_1 for high value $T = 1000$ when $\gamma = 4$. The histogram shows the distribution of R_1 obtained through numerical simulations. In this case equation (4.2.5), referred to as 'Approximated distribution', matches the distribution obtained from numerical simulations. The mean R_1 obtained from equation (4.2.6) moves to the right, closer to the mean obtained through numerical simulations.

for 'Asymptotic heuristic with scaling' passes through zero, however Figure 4-7 shows that this will not always be the case for different values of γ. Although, for values of observed signal below 400 the 'Asymptotic heuristic with scaling' is more accurate than the 'Fading approximation' we see that as the value of signal increases the fading approximation becomes the more accurate method. As a result, we conclude that when $\gamma = 4$ the fading approximation is the more accurate and reliable method.

In Figure 4-7 we compare the fading approximation with the best performing of the scaling heuristics, the 'Asymptotic heuristic with scaling', when $\gamma = 3, 4$ and 6. This figure shows that the 'Asymptotic heuristic with scaling' will not always pass through zero. In fact we see that its performance is very dependent upon the value of γ and this lack of consistency means that it is not a reliable heuristic. The 'Fading approximation' shows consistency for signal ≥ 500 where the error is around $1\% - 2\%$ of the actual distance R_1. Therefore, from the numerical simulations we conclude that the fading approximation is the best method for approximating R_1 when Rayleigh fading is in effect. The 'Asymptotic heuristic

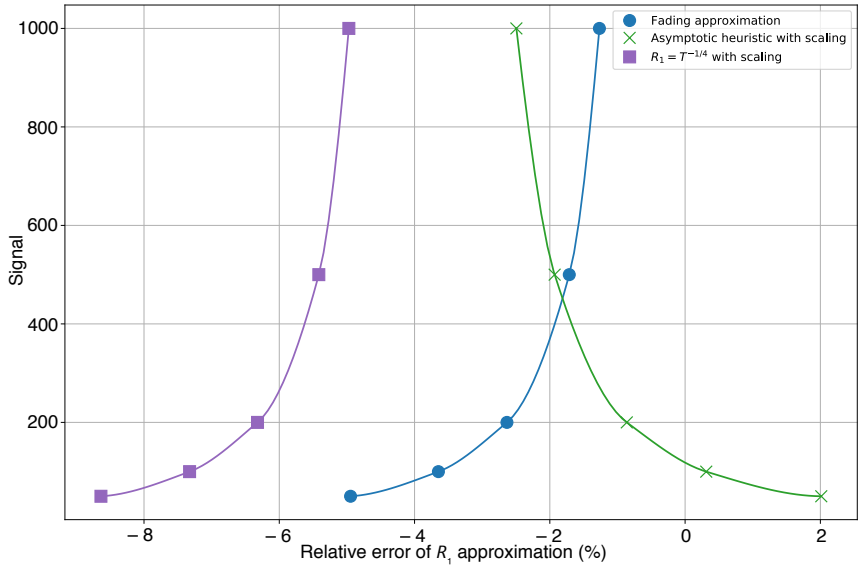

Figure 4-6: Comparison of the accuracy of the 'Fading approximation' (4.2.6) against 'Asymptotic heuristic with scaling' (4.2.3) and '$R_1 = T^{-1/4}$ with scaling' (4.2.2). We note that the 'Fading approximation' is the most accurate of the three methods, followed by the 'Asymptotic heuristic with scaling' which passed through 0. As signal increases the percentage error of the 'Fading approximation' decreases. $\gamma = 4$ in all cases.

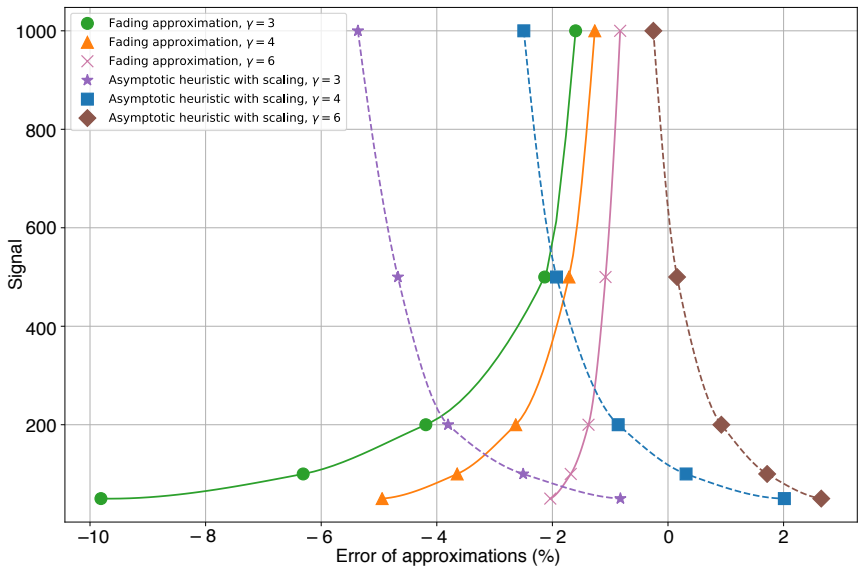

Figure 4-7: Comparison of the fading approximation (4.2.6) against the asymptotic heuristic with scaling when $\gamma = 3, 4, 6$. The accuracy of the asymptotic heuristic with scaling (4.2.3), for large signal observations, varies with γ but the fading approximation is much more consistent. It can be seen that the accuracy of the fading approximation increases as γ increases.

with scaling' had comparable accuracy in the case $\gamma = 6$ but was outperformed in all other cases.

When it is known whether Rayleigh fading is in effect, we can choose to use either the fading approximation or the asymptotic heuristic accordingly. The accuracy of the two methods, when used accordingly, are compared in Figure 4-8. In Figure 4-8 the asymptotic approximation has the smallest errors, though both methods perform well. The plots show that for an observed signal, when pathloss and the presence of Rayleigh fading is known, we can accurately estimate the distance to the nearest transmitter using the appropriate heuristic.

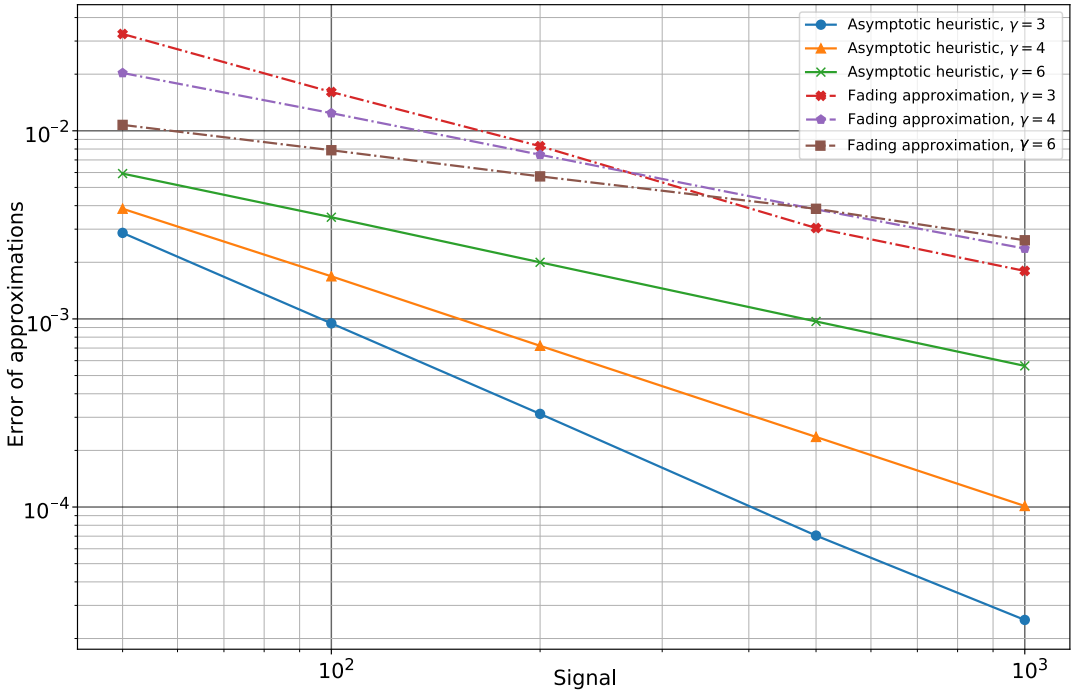

Figure 4-8: Approximation errors as a function of signal strength. For pathloss exponent $\gamma = 3, 4$ and 6, this figure compares the relative performance of the non-fading asymptotic heuristic (4.1.32) with that of the fading approximation (4.2.6). The asymptotic heuristic (4.1.32) was used with signal S where no fading was in effect. However, the fading approximation (4.2.6) was used with signal T where Rayleigh fading was applied. The plot has a log-log scale and for both methods shows how accuracy varies with signal and pathloss.

4.3 Short Summary

In this chapter we have proposed two heuristics for accurately estimating the distance to the nearest neighbour transmitter. We began by proposing an asymptotic heuristic which, with an estimation of pathloss γ and an observation of signal $S = s$ accurately estimates the distance to the nearest transmitter. In Section 4.1 we began with the heuristic that the distance to the nearest transmitter R_1 was a function of observed signal S and pathloss, such that $R_1 = S^{-1/\gamma}$. To improve on this we approximated the error of this heuristic and proposed (4.1.32) which we refer to as the asymptotic approximation. In Section 4.1.4 the accuracy of this heuristic is demonstrated with numerical simulations, it results in an improvement in accuracy when estimating neighbour distance based on observed signal and works well for small values of observed signal S.

In Section 4.2 we present the second heuristic, which offers an improved approximation for the distance to the nearest transmitter when Rayleigh fading is in effect. We began in Subsection 4.2.1 by presenting a scaling factor that can be used to scale the effect of Nakagami-m fading. We considered the most extreme case of Nakagami-m fading which is when $m = 1$, a special case known as Rayleigh fading. In Subsection 4.2.2 we proposed a distribution of the distances to the nearest transmitter R_1 conditional on observed Rayleigh faded signal T. From this distribution we found the expected value of R_1 conditional on T, this expected value (4.2.6) is referred to as the fading approximation. In Subsection 4.2.3 we showed how the scaling factor and fading approximation perform. The simulations showed that the fading approximation is the most accurate way of estimating the distance to the nearest transmitter in the case with Rayleigh fading.

Chapter 5

Non-Uniform Power Distance Estimation

In Chapter 4 we derived two expressions, (4.1.32) and (4.2.5), that accurately estimate the distance from the origin to the nearest transmitter based on a single observation of total signal at the origin. Both expressions require only minimal knowledge of the environment, such as the pathloss exponent γ and whether fading, in particular Rayleigh fading, is present. However, both expressions were derived with the assumption that all transmitters share the same power setting. In this chapter we relax this assumption and examine cases in which transmitters do not all have equal power settings. Although changes in power levels complicate interpretations of received signal strength, it also offers new opportunities for self-organisation since changes in power levels allow the system to gather additional information about transmitter distances.

Our main research questions in this chapter are as follows. Given that transmitters do not share a common power setting, how accurately can the distance to the nearest transmitter be estimated? Further to this, can we better estimate the power setting of the nearest transmitter? In this chapter we answer these two questions, showing that both can be achieved.

This chapter is organised into four sections, one for each of the methods of estimation that we explore. Where appropriate we consider the effectiveness of the methods with and without fading effects. The first section looks at the ability of the two heuristics (4.1.32) and (4.2.5) from Chapter 4 to estimate the distance to the nearest transmitter when powers are not uniform, first without and then with fading, respectively. The second section explores the way the 'Pulse Method' patented by BT [15] can be applied for distance and power estimation. We test the accuracy of this method over a range of scenarios. The third and

fourth sections build on the 'Pulse Method' by proposing a new 'Two-Part Pulse Method' (TPPM) that allows us to gain more information. In the fourth section we employ the Method of Moments (MoM) to adapt the TPPM to be applicable when fading is present. In all sections numerical simulations are used to assess the accuracy of the methods and to support the theory.

5.1 Uniform Power Heuristics

The communications regulator Ofcom has set a maximum allowed power $p_{\max}$ that limits the power transmitters can use. Previously, in Chapter 4, we assumed that all transmitters used the full amount of power. In this chapter we consider that transmitters use only a fraction of the available power. This is informed by the results in Chapter 3 on power optimisation. Let $X_1, ..., X_k$ be a set of i.i.d random variables $X_i \sim \mathsf{Unif}[0, 1]$, that represent the proportion of available power used by a given transmitter. Then transmitter T_i has power $P_i \sim p_{\max} X_i$.

As before, we consider transmitters distributed on a disk according to a Poisson point process with intensity λ. The numerical simulations use Algorithm 1.1 to efficiently generate correctly distributed transmitter distances. We assess the accuracy of the uniform power heuristics (4.1.32) and (4.2.5) in Subsections 5.1.1 and 5.1.2, respectively. A summary of their performance is given in Subsection 5.1.3.

5.1.1 Asymptotic Heuristic for Non-uniform Powers

We recall that in Chapter 4, equation (4.1.32) gave the asymptotic heuristic for estimating the expected distance to the nearest transmitter R_1 as

$$\mathbf{E}\Big[R_1\Big|S' = s\Big] \approx s^{-1/\gamma} + \frac{2\lambda\pi}{\gamma} a(\gamma) s^{-3/\gamma},$$

where $a(\gamma)$ is as defined in (4.1.2). This asymptotic heuristic assumes that all transmitters have an equal power, $p = 1$. We now wish to assess the performance of the asymptotic heuristic when transmitters do not have a uniform power setting. Instead the transmitters have power settings as described in the introduction to this section, such that transmitter T_i has power $P_i \sim \mathsf{Unif}(0, p_{\max})$. In this scenario, given that there are k transmitters in the plane, the observed signal S at the origin O is given by

$$S = \sum_{i=1}^{k} P_i r_i^{-\gamma}. \tag{5.1.1}$$

From (5.1.1) we observe that S is scaled by P_i. We could apply (4.1.32) and ignore this scaling effect. Figures 5-1a and 5-1b show the relative error against $p_{\max}$ when this scaling is ignored. We consider a rough scaling of S, since the expectation $\mathbf{E}[P_i] = \frac{p_{\max}}{2}$, the simplest way to account for the power level P_i is to define a scaled signal value S^* by

$$S^* = \frac{2S}{p_{\max}}. \tag{5.1.2}$$

Then we can estimate, roughly, the distance to the nearest transmitter as

$$\mathbf{E}\Big[R_1 \Big| S^* = s^*, p_{\max}\Big] \approx s^{*-1/\gamma} + \frac{2\lambda\pi}{\gamma} a(\gamma) s^{*-3/\gamma}. \tag{5.1.3}$$

As before, we use simulations to assess the accuracy of the asymptotic heuristic. The methodology for these simulations is as described in Chapter 4. We generate transmitter distances using Algorithm 1.1 with the density $\lambda = \pi^{-1}$ and assign powers that are uniformly distributed $\sim \mathsf{Unif}(0, p_{\max})$. We then use the value of S achieved by equation (5.1.1) in equations (4.1.32) and (5.1.3), i.e. we use S^* as computed in (5.1.2) and estimate R_1 using (5.1.3). Figure 5-1 shows the accuracy of the asymptotic heuristic for $S = 50$ and $S = 1000$ for when S is scaled by the expected power. The average error of the estimated distance is much larger when the asymptotic heuristic is used on non-uniform powers. However scaling the observed signal offers significant improvement in this scenario.

In Figures (5-1a) and (5-1b) we observe, for $S = 50$ and $S = 1000$ respectively, how as $p_{\max}$ increases the scaling of the asymptotic heuristic significantly increases the accuracy of the estimated distance to the nearest transmitter. As expected, the accuracy is better for the larger value of S, in this case the scaled asymptotic heuristic results in a more consistent estimation with an average error of 2%. The error increased as $p_{\max}$ increased. The simulations were conducted with 50000 samples and the signal observed was within 2% of the target value.

5.1.2 Fading Distance Estimation

In Chapter 4 we found the conditional probability density function for the distance to the nearest transmitter conditioned on the observed signal T in the presence of Rayleigh fading. We then used this in equation (4.2.6) to compute the expected distance to the nearest transmitter r_1, conditioned on the observed signal T:

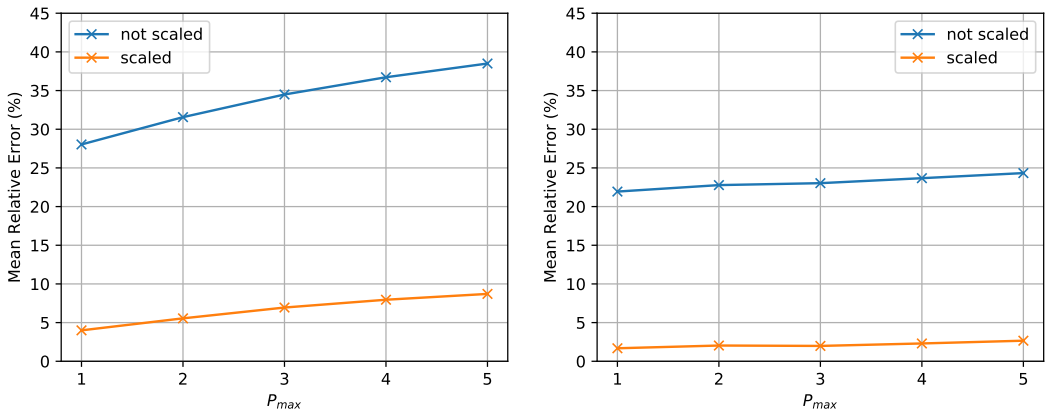

(a) $S = 50$, $\gamma = 4$ (b) $S = 1000$, $\gamma = 4$

Figure 5-1: The mean relative error of the heuristic (5.1.3) as a function of $p_{\max}$ when S is scaled by the expected power (5.1.2), is shown by the orange line labelled 'scaled'. For comparison we show when S is not scaled by the expected power and instead we used $S^* = \frac{S}{p_{\max}}$ to take into account the dependence of S on $p_{\max}$, this is shown by the blue line labelled 'not scaled'. In (a) we consider a low value $S = 50$; in (b) we consider a higher value $S = 1000$. In both cases we set $\gamma = 4$.

$$\mathbf{E}[R_1|\tilde{T}_1 = t_1] = \frac{\Gamma\left(\frac{\gamma+3}{\gamma}\right)}{t_1^{\frac{1}{\gamma}} G\left(\frac{\gamma+2}{\gamma}, \rho^\gamma t_1\right)},$$

where $G(s,x) = \int_0^x y^{s-1}e^{-y}dy$ is the lower incomplete Gamma function.

We consider the most extreme case of fading, Rayleigh fading, in which the fading variables $H_i \sim \text{Exp}(1)$. In this case we denote signal observed at the origin O as T, where

$$T = \sum_{i=1}^{k} H_i p_i r_i^{-\gamma}.$$

and as $\mathbf{E}[p_i] = \frac{p_{\max}}{2}$ we can scale the observed signal so that

$$T^* = \frac{2T}{p_{max}}. \tag{5.1.4}$$

This gives that

$$\mathbf{E}[R_1|\tilde{T}_1^* = t_1^*] = \frac{\Gamma\left(\frac{\gamma+3}{\gamma}\right)}{t_1^{*\frac{1}{\gamma}} G\left(\frac{\gamma+2}{\gamma}, \rho^\gamma t_1^*\right)}. \tag{5.1.5}$$

As before, we use simulations to assess the accuracy of this scaled heuristic.

The methodology of the numerical simulations is as described in Subsection 4.2.3. The simulations used 100 transmitters, it was found in simulations that the contribution from the furthest transmitters was negligible and that using a larger number would impact computational efficiency whilst not noticeably improving accuracy. This is further supported by the preliminary work in Chapter 4, which presents the argument that contributions from transmitters furthest away can be neglected. Two target values of T were used for assessment and comparison, they were $T = 50$ and $T = 1000$. Only simulations in which the value of T fell within 2% of one of the target values were used. Simulations were run until 100000 samples for each of the two target values of T were collected. In Figure 5-2 it is shown that scaling the observed signal increases accuracy. The unscaled distribution has the correct variance but the mean is shifted to the right. The scaling results in the variance being too small but the mean is more accurate.

5.1.3 Short Summary

The asymptotic heuristic with the rescaling (5.1.3) can provide an accurate estimation of R_1 when transmitters do not share a common power setting, paryicularly for high values of observed signal. Intuitively, the lower the proportion of power P_1 that the nearest transmitter T_1 uses, the larger the error. This is to be expected as this method is most accurate when the nearest transmitter T_1 provides the majority of the signal observed at the origin; this is less true when P_1 is small.

We see that scaling the fading heuristic provides an improvement in the accuracy of the relative error of the estimation. A limitation of both heuristics is that they only provide information regarding distance, and then only for the nearest transmitter, and do not estimate tranmitter powers. We now consider methods that can provide further information, such as the power settings of transmitters and can be used to estimate the distance for more than just the nearest transmitter.

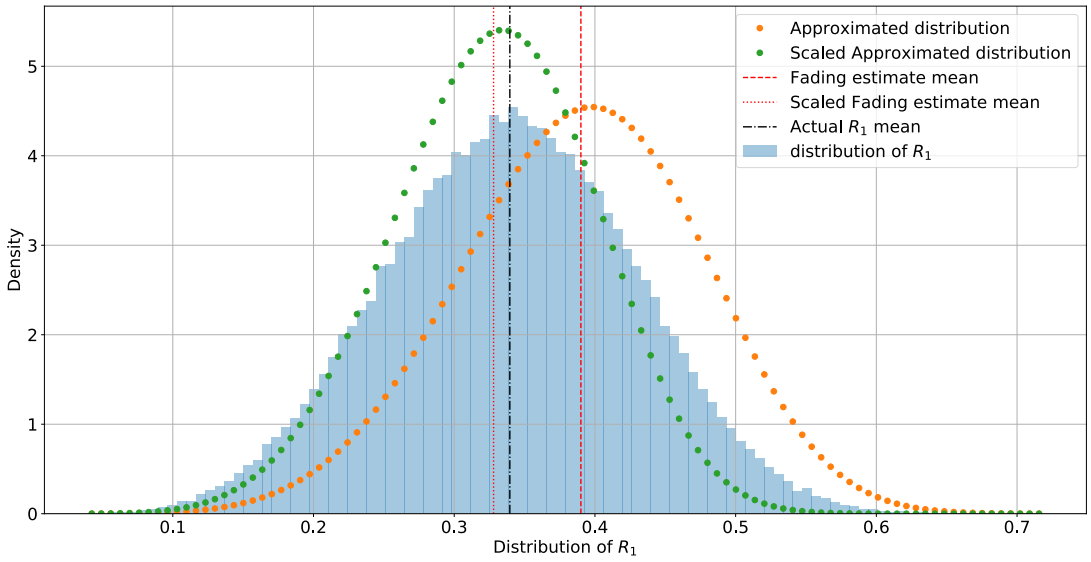

(a) When $T = 50$

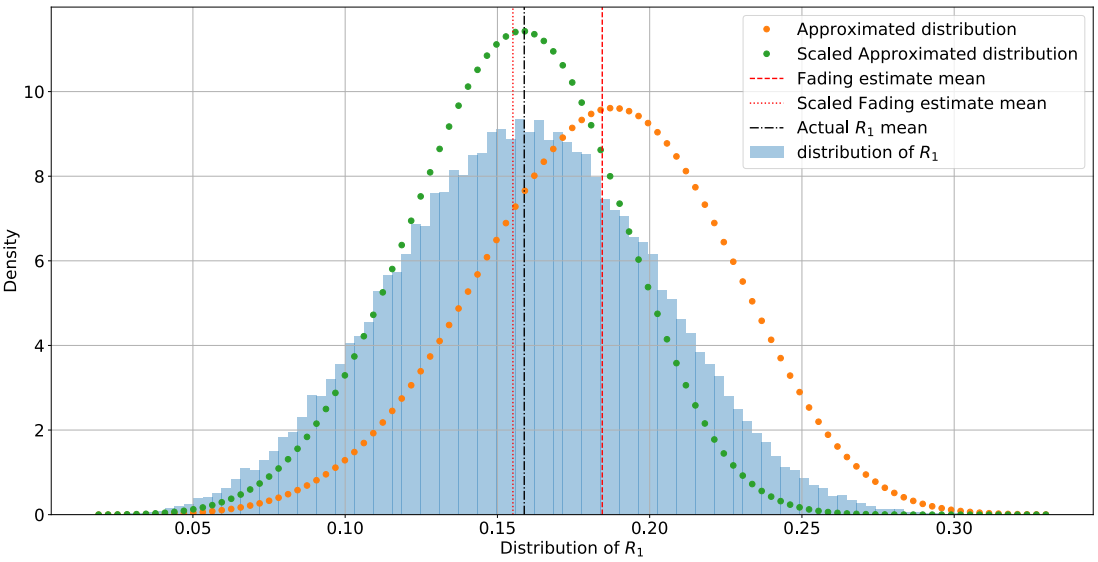

(b) When $T = 1000$

Figure 5-2: Frequency distribution of values of R_1 for which (a) $T = 50$ and (b) $T = 1000$, compared to analysis approximations of the full distribution and estimates of the expected value of R_1. In both cases $\gamma = 4$, $p_{max} = 1$ and transmitter powers are uniformly distributed between 0 and $p_{\max}$.

5.2 The Pulse Method

The 'Pulse Method' is a system procedure for a short step up and down in a transmitter's power setting that was patented by BT [15]. A transmitter briefly uses a higher power setting for a short period of time, resulting in a pulse of increased signal strength. Figure 5-3 illustrates the dynamics of power changes for an individual transmitter.

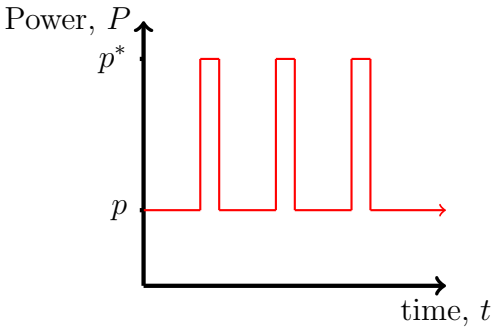

Figure 5-3: Illustration of the Pulse Method; the power setting of a transmitter briefly increases to p^* before returning to p.

The Pulse Method is described in Algorithm 5.1.

Algorithm 5.1 Pulse Procedure

Transmitter power is P
Pulse power and non pulse power are p^* and p respectively
$P = p$
$t = 0$
Pulse duration is t_{pulse}
Time between pulses is t_{start}
T is time limit
while $t \leq T$ **do**
    $t \leftarrow t + t_{\text{start}}$
    $P \leftarrow p^*$
    $t \leftarrow t + t_{\text{pulse}}$
    $P \leftarrow p$
end while

5.2.1 Distance and Power Estimation

We will show that the Pulse Method can be used to estimate both the distance and power of transmitters in a network. However, we begin by considering uniform transmit powers and show that in this scenario the method can be used

to accurately estimate all transmitter distances. This is the simplest example of how the pulse method can be used. We then consider the scenario when transmitters have non-uniform transmit powers and propose an iterative procedure for estimating power and distance.

Uniform Powers

When transmitters are on equal power settings the Pulse Method allows for transmitter distances to be found exactly. Let there be a set of N transmitters with transmit power P and pulse power P^*. Implementing the Pulse method, as described in Algorithm 5.1, we will observe N different sized increases, or pulses, in the total signal at the origin over a suitably large period of time T. A realisation of this is shown in Figure 5-4a which shows total signal at the origin varying with time.

To estimate the distances we identify increases in the observed signal at the origin. We record the positive increases in signal and remove all duplicates, this will result in N recorded signal increases. We organise these signal increases into descending order and denote each increase (or jump) as J_i with $i = 0, \ldots, N$. The distance to the ith nearest transmitter is given by

$$r_i = \left(\frac{P^* - P}{J_i} \right)^{1/\gamma}. \tag{5.2.1}$$

Figure 5-4b shows the estimated distances of transmitters using this method and the actual distances. As $\gamma = 4$ the signal contribution from the furthest transmitters will be very slight. Where two transmitters are very close together the number of significant figures held by the computer could result in two distinct pulses being treated as one. This would account for the shift of the last 50 transmitters that is seen. Only 199 distinct pulse sizes were identified, rather than 200.

Non-Uniform Powers: An Iterative Procedure

We have shown that the pulse method can be used to find transmitter distances when transmitters have uniform transmit powers. We now propose an iterative procedure that can be implemented to estimate both distance and transmit power when transmitters have non-uniform powers.

Let there be N transmitters with pulse power p^* and pathloss exponent γ. Let there be a known finite discrete set of transmit powers $\boldsymbol{P}$ and $P_1, ..., P_N$ be

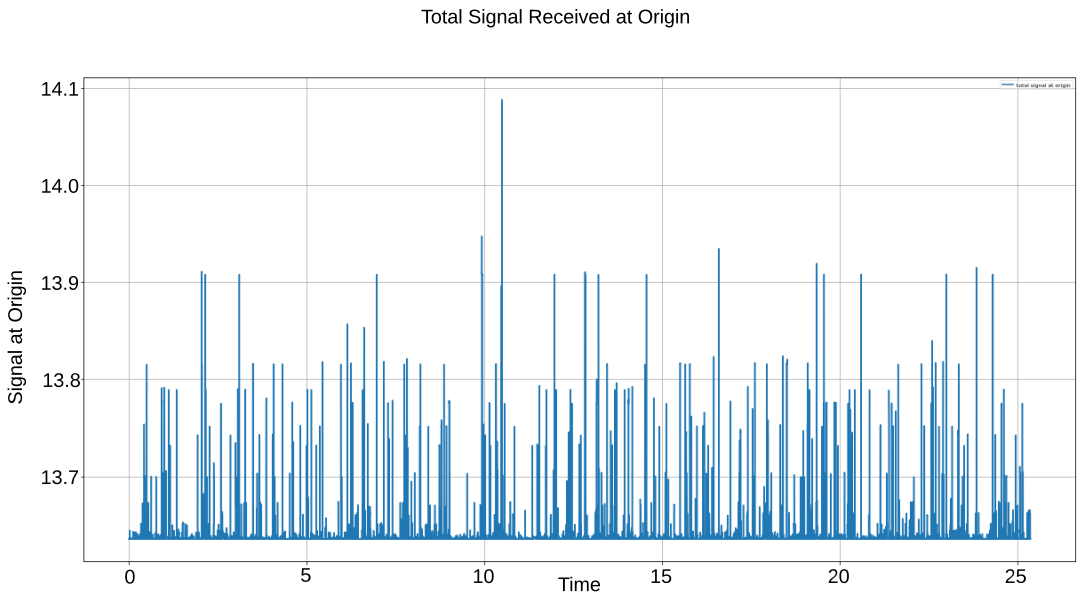

(a) Typical simulation of total signal received as a function of time when transmitters have a uniform power setting and pulse at random times.

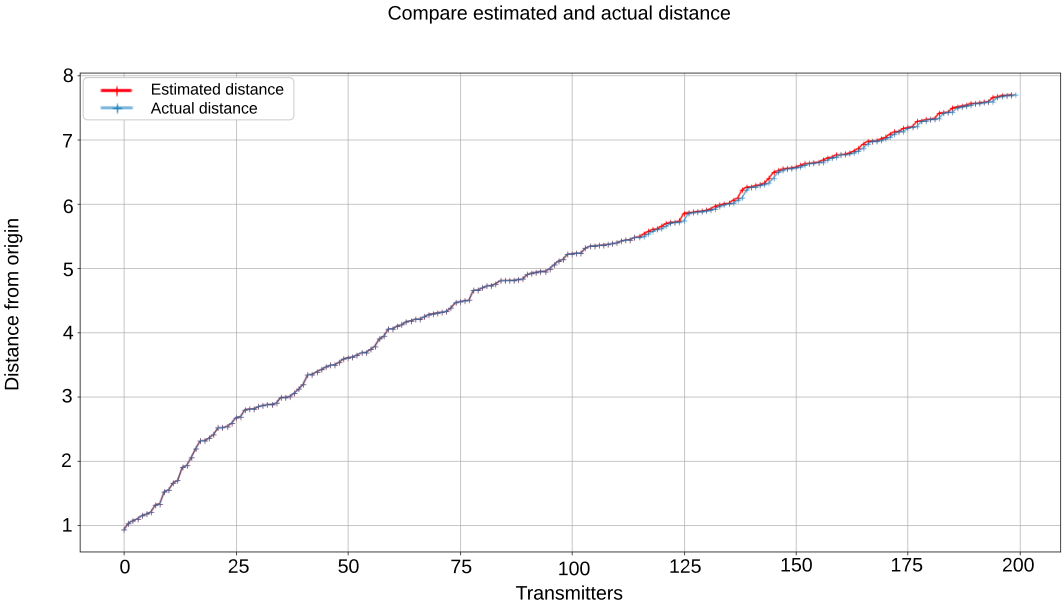

(b) A comparison of the estimated distance to each transmitter and the actual distance.

Figure 5-4: Subfigure 5-4a shows the observed signal at the origin as 200 transmitters, with uniform power setting $P = 1$, pulse at random times. Subfigure 5-4b shows the accuracy with which the Pulse Method allows the distance to all 200 transmitters to be estimated. The pathloss exponent $\gamma = 4$.

the random variables from $\boldsymbol{P}$ describing the power settings of the transmitters $T_1, \ldots, T_N$ when they are not 'pulsing'. Although $\boldsymbol{P}$ is known the values of $P_1, ..., P_N$ are not.

Implementing the pulse procedure given in Algorithm 5.1 on this set of transmitters will result in 'pulses' in the total signal at the origin such as those shown in Figure 5-5. We use these pulses, or increases in signal, to estimate the distances to near transmitters. We do this as follows: the lowest observation of signal will be when no transmitters are 'pulsed', and we can measure the signal increases when pulses occur. We assume the larger the pulse, the closer the transmitter.

Let S be the total observed signal when no pulses are occuring and S_i^* be the total signal when transmitter i is pulsed. Therefore

$$S = p_1 r_1^{-\gamma} + ... + p_i r_i^{-\gamma} + ... + p_N r_N^{-\gamma} \tag{5.2.2}$$

$$S_i^* = p_1 r_1^{-\gamma} + ... + p^* r_i^{-\gamma} + ... + p_N r_N^{-\gamma} \tag{5.2.3}$$

Our intuition is that, if we observe the system for long enough then we should observe N different size jumps in signal strength. The observed jumps are sorted into descending order so that $J_1 \leq J_2 \leq ... \leq J_N$ are the sizes of jump attributed to each transmitter, ordered from nearest to furthest.

Then to estimate the distance to the nearest transmitter we add the largest jump J_1 to the total unpulsed signal S; this gives the total signal when the nearest transmitter is pulsed, which by definition is S_1^*. We do not simply use the largest recorded signal strength as it is possible that pulses from two transmitters have overlapped in time.

Since $J_1 = (P_* - P_1) r_1^{-\gamma}$ we have $S_1^* = S + J_1$, hence

$$(S_1^*)^{-1/\gamma} = \left(p^* r_1^{-\gamma} + p^* \frac{p_2}{p^*} r_2^{-\gamma} + ... + p^* \frac{p_N}{p^*} r_N^{-\gamma} \right)^{-1/\gamma} \tag{5.2.4}$$

and so

$$\left(\frac{S_1^*}{p^*} \right)^{-1/\gamma} = r_1 \left(1 + \underbrace{\frac{p_2}{p^*}}_{<1} \underbrace{\left(\frac{r_2}{r_1} \right)^{-\gamma}}_{<1} + ... + \underbrace{\frac{p_N}{p^*}}_{<1} \underbrace{\left(\frac{r_N}{r_1} \right)^{-\gamma}}_{<1} \right)^{-1/\gamma}. \tag{5.2.5}$$

By assuming that transmitters are well spaced and that typical power levels are much less than p^*, we can make an initial estimate for the value of r_1 by taking

just the first term on the right hand side in the equation alone, which yields,

$$r_{1,\text{est}} = \left(\frac{S_1^*}{p^*}\right)^{-1/\gamma}. \tag{5.2.6}$$

This initial estimate of r_1 can then be used to estimate the power setting of transmitter 1:

$$p_{1,\text{est}} = p^* - J_1 r_{1,\text{est}}^{\gamma}. \tag{5.2.7}$$

We can then map $p_{1,\text{est}}$ to one of the known possible discrete power values, i.e. we replace $p_{1,\text{est}}$ by a known possible power level $\hat{p}_1$. We now use the newly estimated p_1 to refine our estimate for r_1,

$$\hat{r}_1 = \left(\frac{J_1}{p^* - \hat{p}_1}\right)^{-1/\gamma}. \tag{5.2.8}$$

To estimate the distances to the remaining transmitters we use the estimated power and distance settings and subtract from S their contribution,

$$S_{\text{updated}} = S - \hat{p}_1 \hat{r}_1^{-\gamma}. \tag{5.2.9}$$

We summarise this in the following algorithm.

Procedure 5.1 (Iterative Distance Estimation Algorithm)**.** *The algorithm consists of the following steps:*

(1). Observation: record total signal at the origin S for a suitable period of time t determined by the number of transmitters N and the pulse rate, until N different-sized jumps in observed signal have been detected.

(2). Sorting: Sort the signal jumps into descending size order such that $J_1 \geq J_2 \geq ... \geq J_N$. Compute the signal strength S that is received when no pulses are taking place.

(3). Initial Distance Estimation: This is the value of the largest observed pulse, which is divided by the known pulse power and put to the power of $\frac{-1}{\gamma}$ where γ is the pathloss. This is shown in equation (5.2.6)*.*

(4). Power Estimation: This is done in two parts, an initial power is estimated using the initial distance, as shown in (5.2.7)*. As powers are discrete and known this is mapped onto the closest power.*

(5). Update Distance Estimate: The power estimate is then used together with the known pulse power and observed signal increase to update the distance estimate. This is shown in equation (5.2.8)

(6). Update: remove jump J_i from $\boldsymbol{J}$ and update unpulsed signal to not include contribution from this transmitter.

(7). Iterate: return to step 3 unless $\boldsymbol{J} = \{\emptyset\}$ or $S = 0$.

We provide an example of implementing this procedure and evaluate its accuracy using numerical simulations.

5.2.2 Numerical Simulations

We show an example of how we use the Pulse procedure in Algorithm 5.1 together with the iterative pulse method given in Procedure 5.1 to estimate transmitter distances and powers. We generate 10 transmitter distances using Algorithm 1.1. We then implement the iterative pulse procedure with the set of available non-pulse powers $P = \{1, 2, 3\}$ and the pulse power $p^* = 4$. Implementing the pulse procedure produces the time series shown in Figure 5-5, in which we can identify distinct pulses.

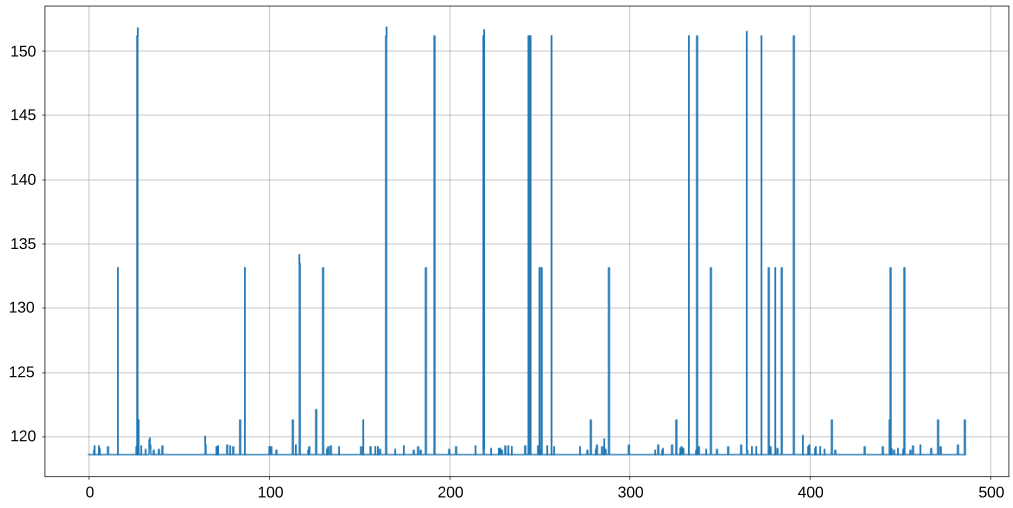

Figure 5-5: Observed signal (y-axis) at the origin as a function of time (x-axis). This is for a system of 10 transmitters with $P = \{1, 2, 3\}$ and $P^* = 4$.

We then apply the iterative pulse procedure to estimate transmitter powers and distances. The results are shown in Table 5.1. We note that for the first two

transmitters power and distance estimations are exact. For the third transmitter the power has been estimated too high which resulted with the distance estimation being too small, this error has impacted on the estimations for all further transmitters. However, the errors in the distance estimations remain small and the estimated power is never incorrect by more than one setting.

Transmitter	Actual		Estimated		Initial Estimate	
	distance	power	distance	power	distance	power
1	0.41885362	3	0.41885362	3	0.40336746	3.13988931
2	0.60948059	2	0.60948059	2	0.57883943	2.37286761
3	1.02541605	1	0.92656799	2	0.8086106	2.83994511
4	1.12023376	3	1.07159195	3	0.96111205	3.3528897
5	1.27399354	3	1.3017485	2	1.14212342	2.81484866
6	1.28692805	3	1.33218996	2	1.25886318	2.40529815
7	1.34512372	2	1.48862411	1	1.43868292	1.38277286
8	1.41029432	1	1.56121887	1	1.59111447	0.76352847
9	1.4107205	2	1.67666979	1	1.8653125	-0.5955501
10	1.44062152	1	1.69369257	1	2.14530876	-3.72221965

Table 5.1: Performance of the iterative method, Procedure 5.1, on a typical task estimating the power and distance of 10 transmitters. The initial estimates for power were rounded down if greater than 1.

Average Relative Error of the Iterative Method

The accuracy of this iterative method does largely depend on the accuracy of the estimation of the distance and power of the nearest transmitter. We now show the average relative error and its standard deviation for this method.

The iterative method does not always manage to estimate distances for larger numbers of transmitters. Therefore the sample size for higher numbered transmitters will be smaller. We expect the accuracy to decrease as the transmitter number increases and this is shown to generally be the case though the first and last transmitter do not fit this expectation. It is interesting that the standard deviation decreases in the middle of the plot before increasing again.

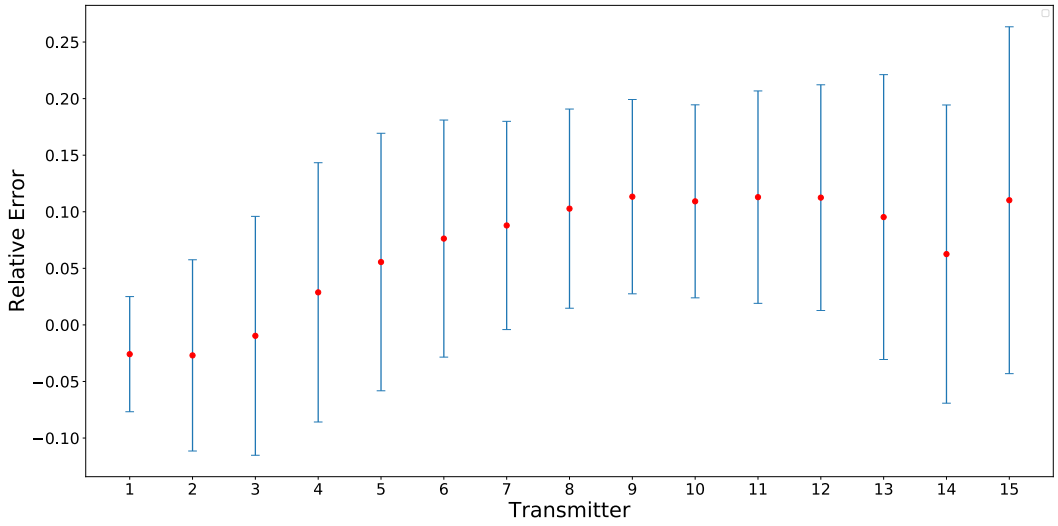

Figure 5-6: The mean and standard deviation of the relative error of the distance estimation when Procedure 5.1 is used. The red dots show the mean relative error of the distance estimation for each transmitter, ordered by distance where transmitter 1 is closest to the origin. The blue error bars show one standard deviation above and one standard deviation below each mean. The sample for this plot was 1000 instances of estimating the distances for 15 transmitters.

5.3 Two-Part Pulse Method (TPPM) Without Fading

The TPPM is an adaptation of the pulse method in which rather than pulses we have two-part pulses that consist of two parts: a 'pre-pulse' and a 'pulse'. By having two parts to a pulse we no longer require an iterative procedure to determine the distances and powers of transmitters further than the very closest one. An advantage of the method not being iterative is that early errors do not compound and thus we can expect improved accuracy for transmitters at greater distances.

Both parts of the two-part pulse involve a transmitter setting its power to a known fixed value. We denote the pre-pulse power by p^0 and the pulse power by p^*. Each transmitter will have a power setting p with $p < p^*$ which we refer to as its regular or non-pulse power. In this thesis we set that $p^0 < p$ but this is not required for the method to work, p^0 simply needs to be known. Figure 5-7 illustrates the changes in a transmitter's power setting occuring over time as a result of two-part pulses. The blue line in this figure is the change in power that will be known due to p^* and p^0 being fixed and known. It is knowing the change in power that allows distances to be estimated based on observations of

total signal at the origin.

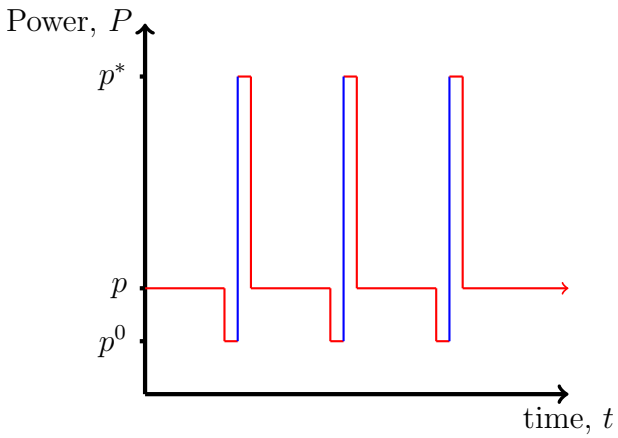

Figure 5-7: Illustration of the Two Part Pulse Method. During a two-part pulse, for a transmitter with power p, the power setting first drops to power p^0 and then increases to p^* before returning to p. This cycle is repeated at randomly-spaced time intervals. The increase in power which causes the pulse is shown in blue. It is not necessary that $p^0 < p$.

Total Signal at the Origin

Figure 5-7 shows the changes in power occuring over time for a single transmitter as a result of two-part pulses. We now consider the effect on the total signal at the origin S over time as a system of N transmitters change their power settings as a result of two-part pulses. Figure 5-8 shows the total signal at the origin changing with time as transmitters pulse and two-part pulse in Subfigures 5-8a and 5-8b respectively.

Let there be N transmitters $T_1, ..., T_N$, with the corresponding non-pulse powers $p_1, ..., p_N$ and distances from the origin $r_1, ..., r_N$. Let S denote the total signal observed at the origin when all transmitters are on their non-pulse powers and let S_k^0 and S_k^* denote observed total signal when transmitter T_k has power p^0 and p^* respectively. Then we can give the signal at the origin in terms of sum of the contribution from each of the transmitters in the system,

$$S = p_1 r_1^{-\gamma} + ... + p_k r_k^{-\gamma} + ... + p_N r_N^{-\gamma} \tag{5.3.1}$$

$$S_k^0 = p_1 r_1^{-\gamma} + ... + p^0 r_k^{-\gamma} + ... + p_N r_N^{-\gamma} \tag{5.3.2}$$

$$S_k^* = p_1 r_1^{-\gamma} + ... + p^* r_k^{-\gamma} + ... + p_N r_N^{-\gamma} \tag{5.3.3}$$

The size of S_k^* will be relative to r_k the distance of transmitter T_k. The largest

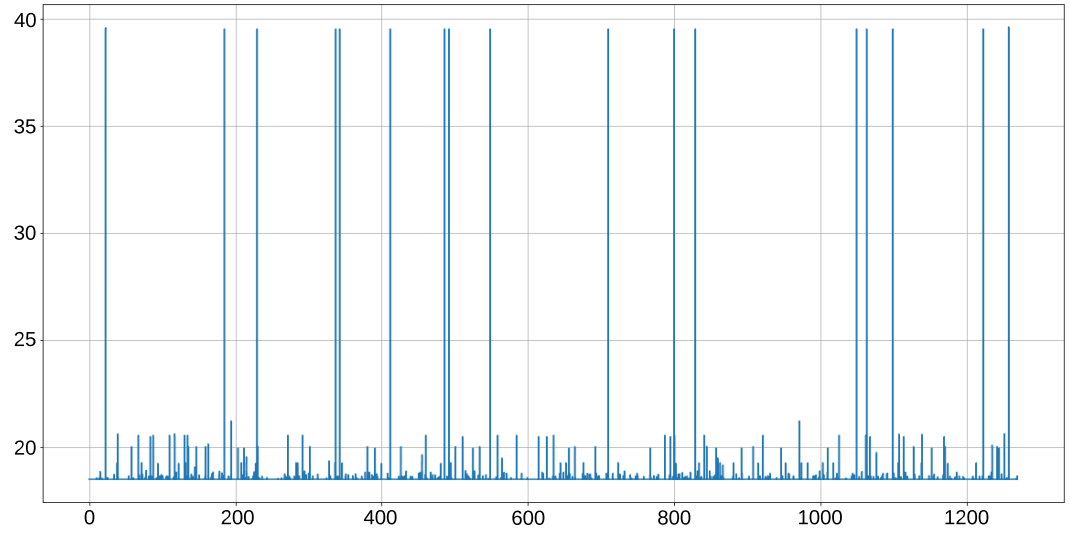

(a) The total signal at the origin varying as pulses occur.

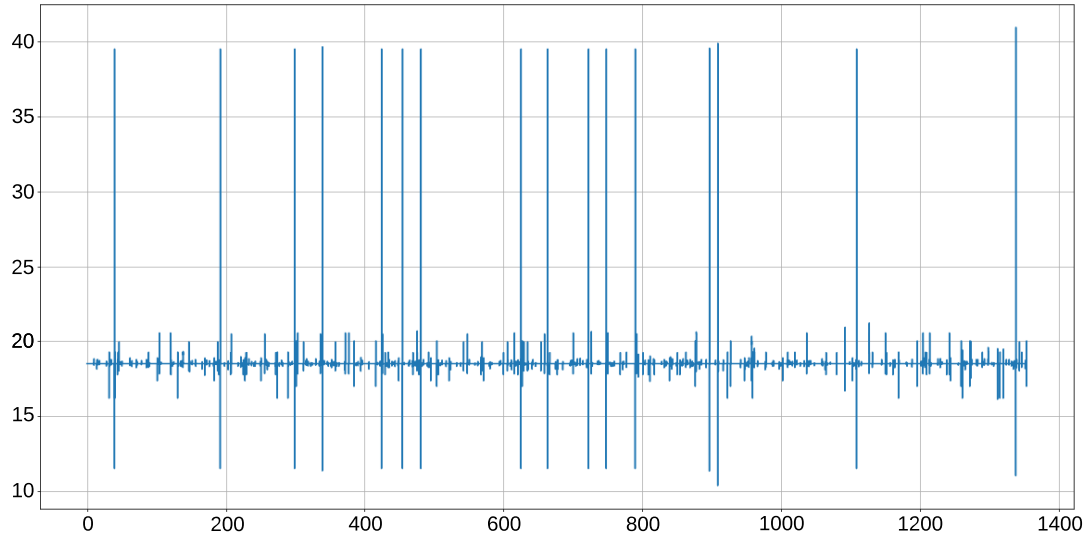

(b) The total signal at the origin varying as two-part pulses occur.

Figure 5-8: The total signal at the origin S (y-axis) as a function of time (x-axis) as a set of 30 transmitters pulse 450 times. The pulse power $p^* = 4$, the pre-pulse power $p^0 = 0$ and the regular powers are selected uniformly at random from the set of powers $P = \{1, 2, 3\}$.

pulse will be due to the closest transmitter, the kth largest pulse from the kth nearest transmitter. We note that we do not include an expression for the total signal at the origin when more than one transmitter is pulsing at a given time. The two pulse identification procedures given in Subsection 5.3.1 would not record such an event as a pulse. Further to this we set that pulses have a known fixed duration but random time intervals between pulses. This means that for a given set of transmitters pulses from particular transmitters should not overlap consistently.

Power and Distance Estimation

In equations (5.3.1) to (5.3.3) we gave the signal at the origin as the sum of the contribution from each transmitter in the system. We find that by subtracting equation (5.3.2) from (5.3.3) and rearranging we can find the distance of the transmitter pulsing as

$$r_k = \left(\frac{S_k^* - S_k^0}{p^* - p^0} \right)^{-1/\gamma}. \tag{5.3.4}$$

We previously stated that the size of increase in the total signal at the origin will correspond to the distance of the transmitter pulsing. As a result it is possible to find the distance to each of the k transmitters in the system independently of finding any others. To find the distance r_k and power p_k to the kth nearest transmitter, we simply identify the kth largest pulse. Once we have found the distance r_k using equation (5.3.4) then there are two expressions that give the power p_k of the kth nearest transmitter. We use equation (5.3.1) together with either (5.3.2) or (5.3.3), to find respectively that

$$\begin{aligned} p_k &= p^* - r_k^\gamma (S_k^* - S) \\ p_k &= p^0 + r_k^\gamma (S - S_k^0). \end{aligned} \tag{5.3.5}$$

The distance and power estimations found using the TPPM are exact. This is shown in Figure 5-9, where we also show the performance of the Pulse Method described in Section 5.2 where the iterative procedure given in Procedure 5.1 is used to estimate transmitter powers and distances.

The Two-Part Pulse Method

The procedure that we follow to implement the TPPM is given in Procedure 5.2. Step (4) of Procedure 5.2 is to identify the pulses in total signal at the origin. In Subsection 5.3.1 we propose two algorithms to identify pulses.

Procedure 5.2 (Two-Part Pulse Method)**.** *This can be described in the following steps:*

(1). Assign regular powers $p_1, \ldots, p_N$ to N transmitters.

(2). Each transmitter acts independently, after a time interval which will be random it will begin a two-part pulse, going first to power p^0 then to p^* for a fixed period of time before returning to its non-pulse power.

(3). Event based system, changes in powers count as events. Record time and Signal at origin of each event.

(4). Identify pulses.

(5). Use observed pulses to estimate transmitter distances, as in equation (5.3.4)*.*

(6). Use transmitter distances to estimate transmitter powers, as in equation (5.3.5)*.*

Consider a set of transmitters ordered by their distance to the origin. The kth largest increase $S_k^* - S_k^0$ will result from the kth nearest transmitter to the origin T_k. This allows us to order the transmitters by the size of the signal increase resulting from the change from p^0 to p^*. We note that the size of the signal increase $S_k^* - S$ resulting from the change of power from p to p^*, seen in the pulse method, cannot be relied upon to identify a transmitter's relative distance from the origin. For example, consider two transmitters close together T_{k-1} and T_k with signal contributions $p_{k-1}r_{k-1}^{-\gamma}$ and $p_k r_k^{-\gamma}$ respectively. Where $p_{k-1} > p_k$ it is possible that $\left(p^* r_k^{-\gamma} - p_k r_k^{-\gamma}\right) > \left(p^* r_{k-1}^{-\gamma} - p_{k-1} r_{k-1}^{-\gamma}\right)$ which would result in the swapping of T_{k-1} with T_k. Using $S_k^* - S$ to order transmitters can lead to incorrect assignment and hence incorrect ordering. Therefore the guaranteed correct assignment of pulses to transmitters in the TPPM is an additional advantage it offers over the Pulse Method.

5.3.1 Identifying Pulses

How do we identify when a pulse has taken place? When there is no fading present we can identify a pulse beginning and ending by noticing a change in the observed total signal at the origin. If it is the case that the durations of pulses are known then we can identify pulses by observing a change in total signal lasting for that time. We present two methods for identifying pulses, the first method identifies pulses by signal change, and the second that identifies pulses by their duration.

Pulse Identification by Signal Change

We begin with a simple method of identifying pulses. We assume that observations have a very short duration but happen with a frequency such that they will observe both the pre-pulse and pulse for any transmitter. For a given time series to identify pulses, when we discard sequential identical observations of signal S, we make three sequential observations S_1, S_2, S_3 and a pulse is identified as $S_3 - S_2$ for all cases where $S_2 < S_1 < S_3$. This is described in Algorithm 5.2.

Algorithm 5.2 Pulse Identification by Signal change

Observations are of an event based system.
We have N observations $O_1, \ldots, O_N$.
Each observation records the time t and the signal at the origin S, such that $O_i = (t_i, S_i)$.
A pulse is denoted by $\tilde{S}$.
for $i \leq N - 2$ **do**
  if $S_{i+2} > S_i$ **and** $S_i > S_{i+1}$ **then**
    $\tilde{S} \leftarrow S_{i+2} - S_{i+1}$
  end if
end for

Pulse Identification by Duration

We now describe a procedure, for an event based system, for identifying when a pulse has occured by noting the duration of time the signal change lasted for. The procedure is given in Algorithm 5.3 and unlike Algorithm 5.2 it can identify pulses that result in a decrease rather than increase in observed signal. However, it will not identify pulses that overlap with others. Also we only observe the system when an event takes place. This could be thought of as only recording the observed signal if it differs from the previous observation.

5.3.2 Numerical Simulations

We use Algorithm 5.2 to identify pulses through observed signal change. We use numerical simulations to show the relative error (%) of distance estimations provided for all transmitters in the system.

We generate 30 transmitters locations using Algorithm 1.1 with $\lambda = \pi^{-1}$. In addition to the pulse power $p^* = 4$ and pre-pulse power $p^0 = 0$ there are three power settings $P = \{1, 2, 3\}$ one of which will be assigned uniformly at random to each transmitter at the beginning of the simulation and will remain unchanged

Algorithm 5.3 Pulse Identification by Duration

Let d_{pre}, d_{pulse} be the length of time a transmitter has power p^0 and p^* respectively.
Let t_i, S_i be the time and total signal at the origin respectively of the ith observation of the system.
Let the number of observations be N.
Pulses $\tilde{S}$ are identified as follows:
for $i \leq N-2$ **do**
  if $t_{i+2} - t_i = d_{\text{pre}} + d_{\text{pulse}}$ **then**
    $\tilde{S} \leftarrow S_{i+1} - S_i$
  end if
end for

as the non-pulse power throughout. We will observe the system for 450 pulses. Pulses occur according to a Poisson process with density $\lambda = \frac{1}{3}$, such that the expected time between pulses is 3 time units. Each pre-pulse will last for 0.15 time units and each pulse will last for 0.3 time units. As usual, we set the pathloss exponent to be $\gamma = 4$.

For the set of transmitters used to generate the time series shown in 5-8 we compare the power and distance estimations from both methods against the actual values in Figure 5-9. They show that the TPPM finds powers and distances exactly. Subfigure 5-9a Shows how the iterative procedure of the pulse method is only able to estimate the powers of the nearest nine transmitters. Subfigure 5-9b shows the power estimation for each transmitter differs from the actual value. The iterative method 'estimate' is only able to correctly estimate the powers of the nearest three transmitters

Pathloss Exponent Uncertainty

We consider the effect of uncertainty in the pathloss exponent. To show the effect of not knowing the exact value used in numerical simulations we use a different value in the TPPM to estimate transmitter distances. Table 5.2 shows the sensitivity of the TPPM to the value of the pathloss exponent. We see that for the nearest transmitter (transmitter 1) the error in the distance estimation is approximately equal to the error in the pathloss exponent. For the second nearest transmitter this error approximately halves and it further decreases for the third nearest transmitter. For the fourth transmitter onwards the error gradually increases. As it is the distances to the nearest transmitters which are most important the fact that the error in distance estimation is approximately bounded by the error in the pathloss exponent shows that this method is robust.

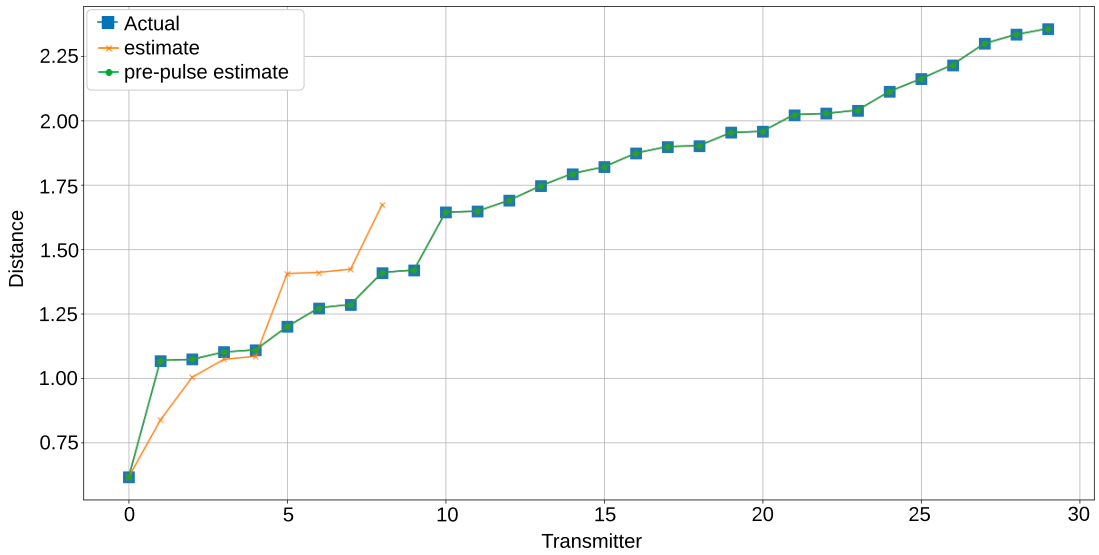

(a) The estimated and actual transmitter distances.

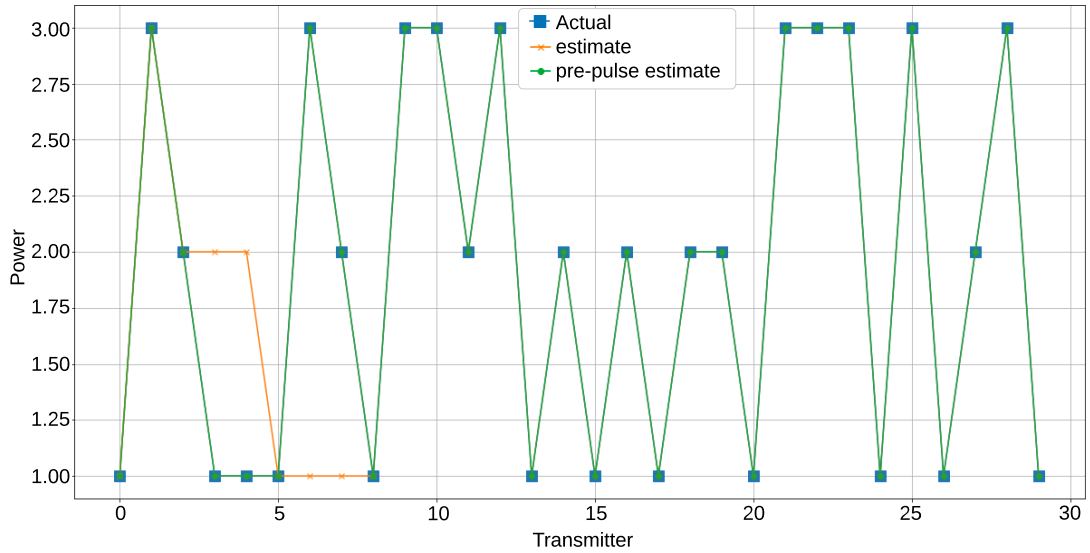

(b) The estimated and actual transmitter powers.

Figure 5-9: A comparison of the TPPM and the pulse method coupled with the iterative procedure. The legend 'Actual' refers to the known power or distance of a transmitter. The legend 'estimate' is the estimated transmitter power or distance found using the pulse method together with the iterative procedure. The legend 'pre-pulse estimate' is the transmitter distance or power found using the TPPM.

Transmitter	Pathloss exponent (Relative error)				
	2.2 (-0.45)	3 (-0.25)	3.2 (-0.2)	3.6 (-0.1)	3.8 (-0.05)
1	-0.5088	-0.2516	-0.1796	-0.0774	-0.0425
2	-0.2475	-0.1195	-0.0871	-0.0328	-0.016
3	-0.0575	-0.0416	-0.0344	-0.0039	-0.0035
4	0.0972	0.0103	0.0003	0.0108	0.0042
5	0.1836	0.0467	0.033	0.0243	0.0112
6	0.2682	0.0863	0.0597	0.0346	0.0159
7	0.3655	0.1237	0.0834	0.043	0.0201
8	0.4531	0.1499	0.1031	0.0494	0.0232
9	0.5270	0.1739	0.1215	0.0576	0.0265
10	0.5888	0.1942	0.1406	0.0650	0.0294

Table 5.2: The average relative error of the TPPM distance estimation when an incorrect pathloss exponent value is used, the actual value is $\gamma = 4$. We use a percentage of the pathloss exponent used in the numerical simulations in the TPPM, as indicated above the columns.

5.4 Two-Part Pulse Method with Fading

When fading is in effect we use the Method of Moments together with the TPPM to estimate the distances of the nearest transmitters. When fading is in effect it is more complicated to use the pre-pulse method to estimate the distance of the nearest transmitter. For at every observation a new fading variable will be scaling the contribution from each of the transmitters. This results in it being more challenging both to identify and correctly attribute the pulses in the time series. As previously we use an event based system, we only observe when an event takes place. This provides an advantage in identifying pulses which we relate to the potential ability of transmitters to indicate that they are pulsing in a real world system.

The total signal F observed when no transmitters are pulsing is given by the sum of the contribution from each transmitter individually multiplied by a random fading variable H_i. Therefore, where there are N transmitters we have that

$$F = \sum_{i=1}^{N} H_i p_i r_i^{-\gamma}.$$

When transmitter i performs a two-part pulse it temporarily uses power settings p^0 and then p^* before returning to p_i. The observed signal for the two parts of

the pulse is

$$F_i^0 = H_1' p_1 r_1^{-\gamma} + ... + H_i' p^0 r_i^{-\gamma} + ... H_N' p_N r_N^{-\gamma}$$
$$F_i^* = H_1 p_1 r_1^{-\gamma} + ... + H_i p^* r_i^{-\gamma} + ... H_N p_N r_N^{-\gamma}$$

A pulse from transmitter i is denoted by $\tilde{F}_i$ and is given by

$$\begin{aligned} \tilde{F}_i &= F_i^* - F_i^0 \\ &= (H_1 - H_1')p_1 r_1^{-\gamma} + ... + (H_i p^* - H_i' p^0) r_i^{-\gamma} + ... + (H_N - H_N') p_N r_N^{-\gamma} \end{aligned} \tag{5.4.1}$$

As fading is rapidly changing, at every observation the fading variables will have changed. The duration of the pulses is fixed and therefore it is possible to identify when a pulse is taking place and whether it is a pre-pulse or not by recording the duration of the pulse. In Subsection 5.3.1 we proposed two algorithms for identifying pulses. We note that Algorithm 5.2 could miss pulses, particularly those from transmitters that are further away. This is because the contribution from those transmitters is much smaller, even when on high pulse power, than the contributions from transmitters that are close. Therefore an increase in the fading variables for a closer transmitter could mask a decrease in power setting for a far transmitter. This would result in a pulse not being detected. However, Algorithm 5.3 would not miss these pulses. Therefore with fading effects we identify pulses by their duration.

5.4.1 Pulse Sample Reduction

The description of the Method of Moments in Subsection 1.4.3 details that for a system of N transmitters, estimating the distance of each would require computing N moments of a sample of pulses. However, solving such a system of equations may not be possible and, even when it is, higher moments may not be reliable. If a relationship between parameters and sample values can be assumed, then selectively reducing the sample reduces the number of parameters correspondingly.

We assume that the closer a transmitter is, the more extreme the observed pulse (when $p^0 \neq 0$ observed pulses can be negative). If the pulse rates are known, then for a given observation period we know the expected number of pulses per transmitter. We denote the expected number of pulses per transmitter by n. The n most extreme pulses will be assumed to be from the closest transmitter (making n from negative and positive pulse sets according to their relative sizes), the most extreme $2n$ pulses will be assumed to be from the two closest transmitters and so on.

From [13] we understand that for BT the ability to estimate the distance to the nearest one or two transmitters is adequate. Therefore we reduce our pulse sample to include only pulses assumed to be from the nearest one or two transmitters and then compute the first and/or second moment.

Distance to Two Nearest Transmitters

We observe total signal F for a system of N transmitters using the TPPM. We observe a number K of pulses $\tilde{F}$ and, where all transmitters share the same pulse rate, the expected number of pulses per transmitter is given by $n = \frac{K}{N}$. Where both positive and negative pulse values are recorded, the expected number of positive and negative pulses per transmitter can be found and denoted by n^+ and n^- respectively such that $n = n^+ + n^-$. The $2n$ most extreme ($2n^+$ positive and $2n^-$ negative) pulses are assumed to have come from the nearest two transmitters. We take these as our subsample that we will use to estimate the distances r_1 and r_2 to the two closest transmitters. We do this by computing the first μ_1 and second μ_2 moment of our subsample as follows:

The first moment:

$$\begin{aligned}
\mu_1 &= \mathbf{E}\left[\tilde{F}\right] \\
&\approx \frac{\sum_{i=1}^{2n}\left(F_i^* - F_i^0\right)}{2n} \\
&\approx \frac{1}{2n}\left[\sum_{i=1}^{n}\left(p^* H_i r_1^{-\gamma} - p^0 H_i' r_1^{-\gamma}\right) + \sum_{i=1}^{n}\left(p^* H_i r_2^{-\gamma} - p^0 H_i' r_2^{-\gamma}\right)\right] \\
&= (r_1^{-\gamma} + r_2^{-\gamma})\frac{1}{2}\left(p^*\mathbf{E}\left[H_i\right] - p^0\mathbf{E}\left[H_i'\right]\right).
\end{aligned} \tag{5.4.2}$$

The second moment:

$$\begin{aligned}
\mu_2 &= \mathbf{E}\left[\tilde{F}^2\right] \\
&\approx \frac{\sum_{i=1}^{2n}\left(F_i^* - F_i^0\right)^2}{2n} \\
&\approx \frac{1}{2n}\left[\sum_{i=1}^{n}\left(p^* H_i r_1^{-\gamma} - p^0 H_i' r_1^{-\gamma}\right)^2 + \sum_{i=1}^{n}\left(p^* H_i r_2^{-\gamma} - p^0 H_i' r_2^{-\gamma}\right)^2\right] \\
&= (r_1^{-2\gamma} + r_2^{-2\gamma})\frac{1}{2}\left(p^{*^2}\mathbf{E}\left[H_i^2\right] + p^{0^2}\mathbf{E}\left[H_i'^2\right] - 2p^* p^0\mathbf{E}\left[H_i H_i'\right]\right).
\end{aligned} \tag{5.4.3}$$

Therefore we have that

$$r_1^{-\gamma} + r_2^{-\gamma} \approx \frac{2\mu_1}{p^*\mathbf{E}[H_i] - p^0\mathbf{E}[H_i']} \tag{5.4.4}$$

and

$$r_1^{-2\gamma} + r_2^{-2\gamma} \approx \frac{2\mu_2}{p^{*2}\mathbf{E}\left[H_i^2\right] + p^{0^2}\mathbf{E}\left[H_i'^2\right] - 2p^*p^0\mathbf{E}\left[H_iH_i'\right]}. \tag{5.4.5}$$

From these two equations we can find the expected distance to r_1 and r_2. We set that $v_1 = r_1^{-\gamma} + r_2^{-\gamma}$ and $v_2 = r_1^{-2\gamma} + r_2^{-2\gamma}$ with the values of v_1 and v_2 found from equations (5.4.4) and (5.4.5) respectively. Then

$$\begin{aligned} r_1 &= \left(\frac{v_1 + \sqrt{2v_2 - v_1^2}}{2}\right)^{-1/\gamma} \\ \text{and} \quad r_2 &= \left(\frac{v_1 - \sqrt{2v_2 - v_1^2}}{2}\right)^{-1/\gamma}. \end{aligned} \tag{5.4.6}$$

Distance to Nearest Transmitter

As described above, we assume that the n most extreme pulses are caused by the closest transmitter. The more extreme the pulse the more likely this assumption is to be correct. Therefore by further reducing our sample of n pulses to exclude potentially incorrectly attributed pulses, we expect to improve the distance estimation accuracy. Let G be the fraction of the n pulses of the nearest transmitter kept for this further reduced sample, the most extreme are the ones kept. As n is the expected number of pulses from each transmitter and $0 < j \leq n$, with $j \in \mathbb{Z}$ then

$$G = \frac{j}{n} \tag{5.4.7}$$

By keeping only the most extreme j pulses we are in effect conditioning on the expected value of the fading variables and therefore the pulses. To find the conditional expected value of a pulse, we must find the probability density function (PDF) and cumulative distribution function (CDF) of the pulses. The CDF will allow us to find x such that:

$$\mathbf{P}(p^*H - p^0H' > x) = G. \tag{5.4.8}$$

This will allow us to use the PDF to find the expected value of a pulse conditional on it being in the most extreme G of pulses,

$$\mathbf{E}[p^*H - p^0H' | p^*H - p^0H' > x] \tag{5.4.9}$$

Then, for the j most extreme pulses $\tilde{F}$, we have that

$$r_1 \approx \left(\frac{\frac{1}{j}\sum_{i=1}^{j} \tilde{F}_i}{\mathbf{E}\left[\tilde{F}|\tilde{F} > x\right]} \right)^{\frac{-1}{\gamma}},$$

$$r_1 \approx \left(\frac{\frac{1}{j}\sum_{i=1}^{j} \tilde{F}_i}{\mathbf{E}[p^* H - p^0 H'|p^* H - p^0 H' > x]} \right)^{\frac{-1}{\gamma}}. \tag{5.4.10}$$

5.4.2 Rayleigh Fading

Rayleigh fading is the most extreme of the fading effects and therefore the most challenging. We ask the following question, is it possible to accurately estimate the distance and power of transmitters when Rayleigh fading is in effect? In Section 5.3 we saw that the TPPM accurately estimates the distances to neighbouring transmitters when they are on different power settings. We wish to understand how effective this method is when Rayleigh fading is in effect.

Rayleigh fading is fast varying, therefore at every observation time the fading variable affecting the contribution from each transmitter will be new. As the effect of fading will not be consistent across the pre-pulse and the pulse it will be challenging to identify the pulses themselves. A Rayleigh fading variable is applied to the signal from each transmitter at each observation. We use the two part pulse method and observe a large number of pulses.

Distance to Two Nearest Transmitters

When Rayleigh fading is in effect we know that the fading variables $H \sim \mathsf{Exp}(1)$ and so $\mathbf{E}[H_i] = \mathbf{E}[H_i'] = 1$, $\mathbf{E}[H_i^2] = \mathbf{E}[H_i'^2] = 2$ and that $\mathbf{E}[H_i H_i'] = 1$. Putting these values into equations (5.4.4) and (5.4.5) we recover that

$$\begin{aligned} v_1 &= r_1^{-\gamma} + r_2^{-\gamma} \approx \frac{2\mu_1}{p^* - p^0} \\ v_2 &= r_1^{-2\gamma} + r_2^{-2\gamma} \approx \frac{\mu_2}{p^{*2} + p^{0^2} - p^* p^0} \end{aligned} \tag{5.4.11}$$

and substituting these values of v_1 and v_2 into equation (5.4.6) we find estimates for r_1 and r_2.

The accuracy of this method can be seen in Figure 5-10. We notice that there

are three distinct spikes in the likelihood of certain errors. These correspond to the three power settings $P = 1, 2, 3$. In Figure 5-13 we use transmit powers $P \sim \mathsf{Unif}(1, 3)$ and note that we do not see these spikes. Additionally in Figure 5-11, which used the same set of pulses as those used for estimating r_1 in Figure 5-13 we see the distribution of the relative error of the r_2 estimate. The relative error of the r_2 is larger than for r_1.

In Figure 5-12 we show that the relative error of the estimation of r_1 is impacted by r_2. When r_1 and r_2 are close then we underestimate the distance r_1.

Distance to Nearest Transmitter

As stated, we reduce the sample with the aim of excluding values not from the closest transmitter. We reduce the sample by keeping only the most extreme fraction $G = \frac{j}{n} = \frac{1}{a}$ where the expected number of pulses per transmitter is n. In the case of Rayleigh fading we know that $H \sim \mathsf{Exp}(1)$ and therefore $\mathbf{P}(H > x) = e^{-x}$.

Let $\tilde{F}_1, \ldots, \tilde{F}_j$ be the j most extreme observed pulses, then

$$\mu_1 = \frac{1}{j} \sum_{i=1}^{j} \tilde{F}_i \tag{5.4.12}$$

and

$$r_1 \approx \left(\frac{a\mu_1}{(1 + \log(a))(p^* - p^0)} \right)^{-1/\gamma} \tag{5.4.13}$$

We set that $G = \frac{1}{a}$ and then look at the distribution of the relative error as we increase $a = 1, 2, ...10$. When we use the duration method of identifying pulses given in Algorithm 5.3 we find that the relative errors for each a are as follows in Table 5.3:

For Table 5.3 we generated 10 transmitters with discrete power settings $P = 1, 2, 3$ and with $p^* = 4$ and $p^0 = 0$. The relative error given is the average relative error over 100 simulations. For each simulation a set of transmitters were created the Rayleigh fading TPPM and the system was observed until 10000 pulses had taken place. Pulses were identified using the duration algorithm. For each of the 100 sets of pulses the error in the estimate of r_1 was computed. The table gives the mean and standard deviation of the relative error. We note that as the fraction decreases so does the expected error in the estimate of r_1. This supports our intuitive expectation that more stringent sampling improves accuracy.

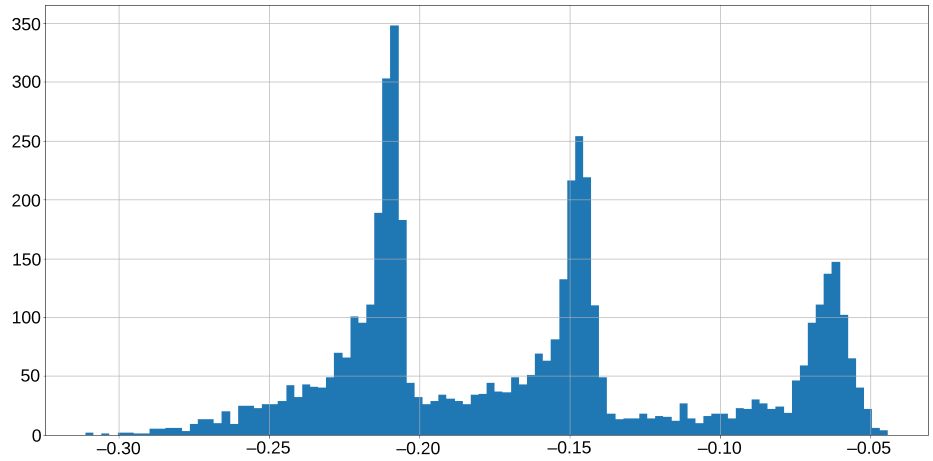

(a) Three discrete power settings $P = \{1, 2, 3\}$

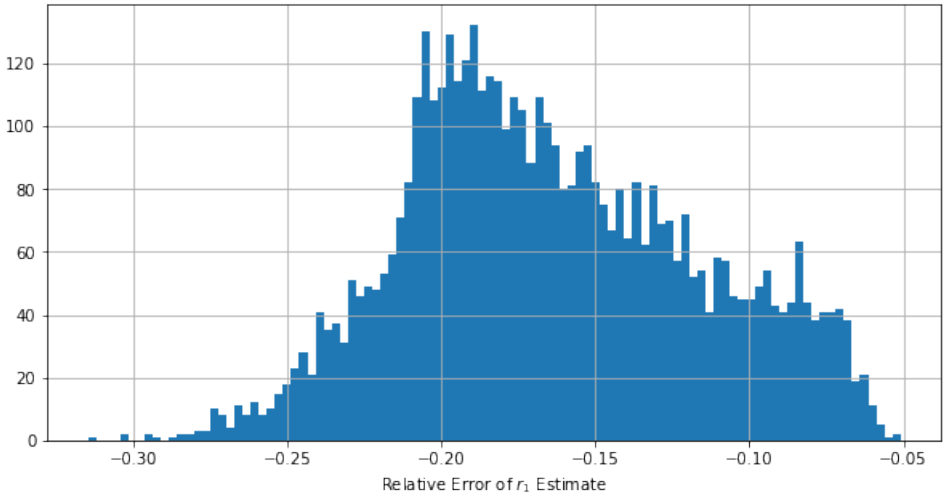

(b) Continuous transmit powers $P \sim \mathsf{Unif}(1, 3)$.

Figure 5-10: Histogram showing the frequency (y-axis) of the relative error (x-axis) of the TPPM. We generated 10 transmitters with distances generated with Algorithm 1.1 with $\lambda = \pi^{-1}$. In Subfigure 5-10a there are 3 transmit powers $P = \{1, 2, 3\}$, in Subfigure 5-10b transmit powers are continuous. For both figures the pre-pulse power was 0 and the pulse power was 4. To collect the data for these plots observed signal at the origin was recorded until 10000 pulses had taken place and repeated this was repeated 5000 times. The relative error = (actual dist - estimated dist)/(actual dist).

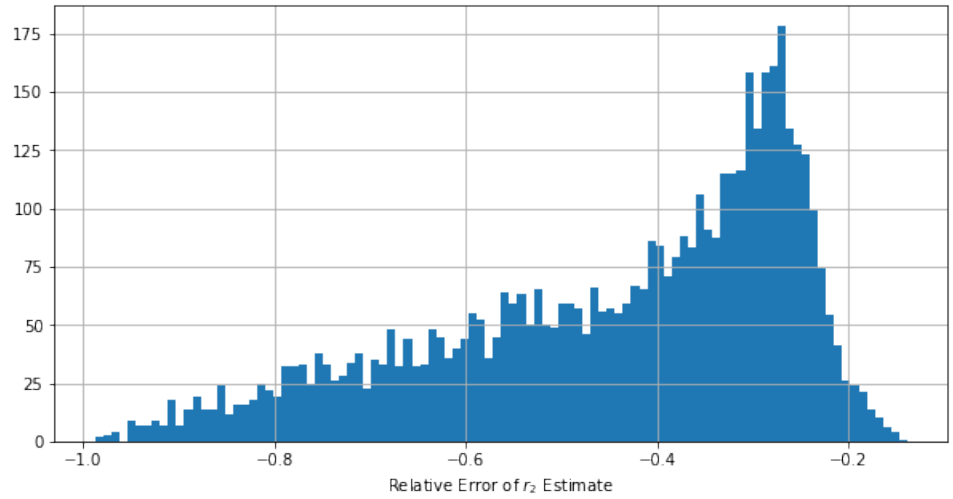

Figure 5-11: The distribution of the relative error of the r_2 estimation. 10 transmitters pulsing a combined 10000 times was repeated 5000 times to obtain the relative error. Transmit powers were continuously distributed $\sim \mathsf{Unif}(1, 3)$.

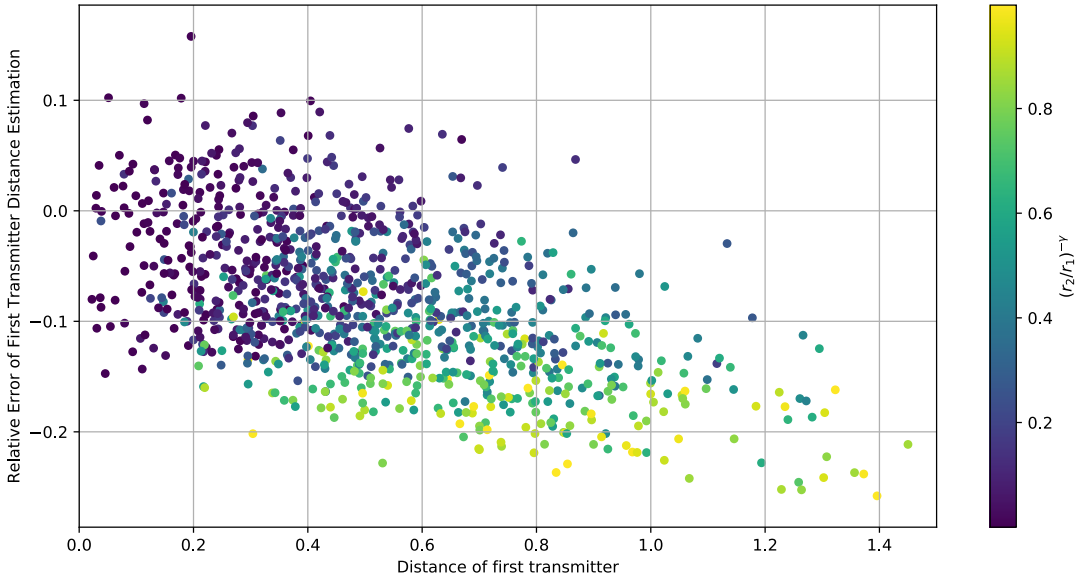

Figure 5-12: The relative error of the distance estimation for the nearest transmitter when Rayleigh fading is in effect, using the Method of Moments. We show how this relates to both the actual distance of the nearest transmitter r_1 and the second nearest transmitter r_2 relative to r_1.

a	Relative Error	
	mean	standard deviation
1	-0.11621187	0.05751156
2	-0.05813994	0.05140302
3	-0.03991012	0.04648342
4	-0.03103664	0.04291901
5	-0.02551089	0.04026556
6	-0.02104074	0.03820865
7	-0.01791739	0.03657861
8	-0.01686244	0.03528335
9	-0.01497062	0.0341989
10	-0.0137509	0.03329065

Table 5.3: Accuracy of the Method of Moments for Rayleigh fading as fraction of pulse samples decreases. 1000 pulses were recorded and 1000 iterations were done for each fraction size. No parameters were changed other than the size of a.

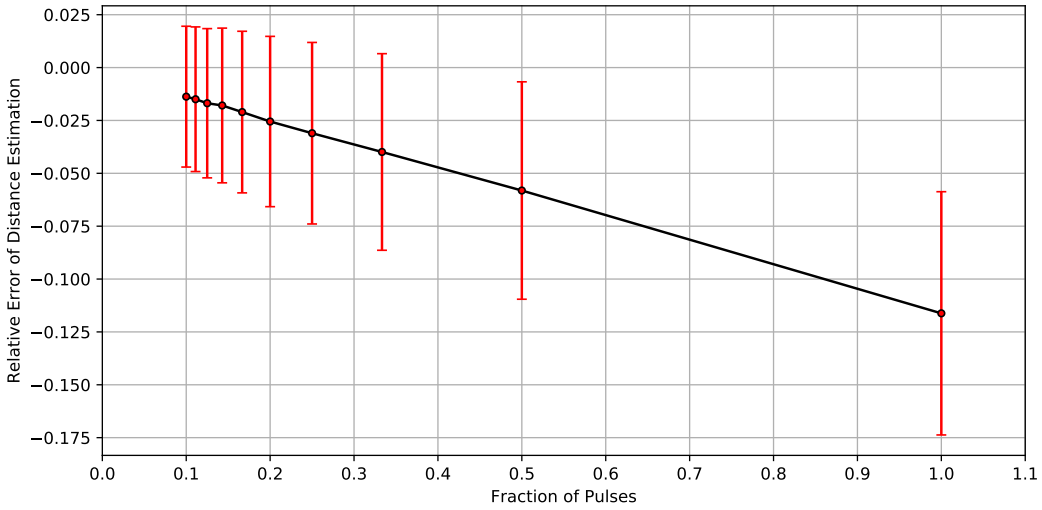

Figure 5-13: The relative error of the distance estimation as a function of the fraction of pulses used. We show the mean and standard deviation for 10 transmitters with a low power of 1 and a high power of 3, with the powers continuously uniformly distributed between these. The pulse power and pre-pulse power were 4 and 0 respectively. The pathloss exponent $\gamma = 4$. We used 500 samples of 10000 pulses and averaged the relative error of the distance estimation over these. We see that as the fraction decreases the average relative error decreases.

5.4.3 Nakagami-m Fading

When Nakagami-m fading is in effect we do not use the TPPM to estimate the transmit power of the nearest transmitter but show that by approximating the $\mathsf{Gamma}(m, \frac{1}{m})$ distribution by a normal distribution we can fairly accurately estimate the distance to the nearest transmitter.

Distance to Two Nearest Transmitters

With Nakagami-m fading, the fading variables $h \sim \mathsf{Gamma}(m, \frac{1}{m})$. From equations (5.4.4) and (5.4.5), we know that we need to find $\mathbf{E}[H_i] = \mathbf{E}[H_i']$, $\mathbf{E}[H_i^2] = \mathbf{E}[H_i'^2]$ and $\mathbf{E}[H_i H_i']$.

For $X, Y \sim \mathsf{Gamma}(m, \frac{1}{m})$, where X, Y are independent: $\mathbf{E}[X] = 1$, $\mathbf{E}[X^2] = \frac{m+1}{m}$ and $\mathbf{E}[XY] = \mathbf{E}[X]\mathbf{E}[Y] = 1$.

Therefore if we set that $X = H_i$ and $Y = H_i'$ then we find

$$\begin{aligned} v_1 &= r_1^{-\gamma} + r_2^{-\gamma} \approx \frac{2\mu_1}{p^* - p^0} \\ v_2 &= r_1^{-2\gamma} + r_2^{-2\gamma} \approx \frac{2\mu_2}{\frac{m+1}{m}(p^{*^2} + p^{0^2}) - 2p^* p^0} \end{aligned} \tag{5.4.14}$$

Equation (5.4.6) can then be used to estimate the distance to the nearest two transmitters.

Accuracy

We use numerical simulations to assess the accuracy of the estimations or r_1 and r_2. In Figure 5-14 we see that the relative error of the estimation of r_2 decreases as m increases. The relative error is negative as we estimate the second transmitter as being closer than it is. This is likely due to incorrectly attributing pulses to the second transmitter. The relative error of the estimated r_1 is within 2% of the actual distance for all values of m tested. It is estimated as being closer than it is only for the case $m = 2$. In the following subsubsection we assess whether using a reduced sample of pulses attributed to T_1 improves the accuracy. Before that we examine the relationship between the relative distance and power of T_1 and T_2 and the accuracy of the r_1 estimation. We do this for the case where $m = 20$.

We now consider the impact of the distance of the second nearest transmitter on the accuracy of the distance estimation of the first. Subfigure 5-15a shows how the relative error of the distance estimation for the nearest transmitter is

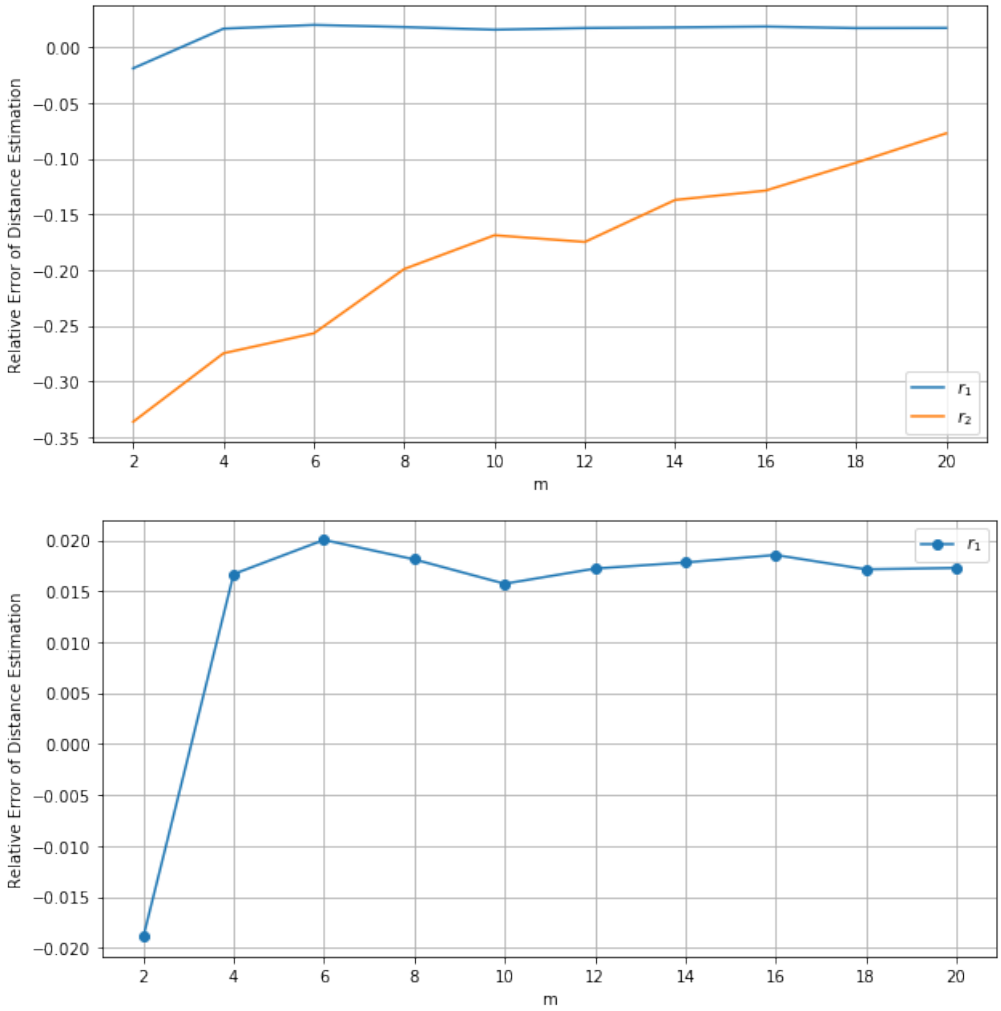

(a) The relative error of the r_1 estimate.

Figure 5-14: The error in our estimates for r_1 and r_2. Ten transmitters pulsed 500 times. From the initial sample of 500 pulses the most extreme 100 were attributed to being from the two closest transmitters and the method of moments applied to estimate distances. For each value of m the relative error averaged from 500 instances is given. For r_2 where an imaginary value was found these estimations were excluded from the averaging. Subfigure 5-14a shows the relative of r_1. Transmit powers were continuously uniformly distributed between 1 and 3, $p^* = 4$ and $p^0 = 0$.

affected by the distance of the nearest transmitter and the relative distance of the second transmitter. Subfigure 5-15b shows the relative distances of the closest two transmitters has a strong impact on the accuracy of the distance estimation of the first. Considering their relative power settings does not play a large part. Therefore relative distance seems most impactful regarding accuracy of estimation. We observe that where r_1 and r_2 are very similar the relative error of the r_1 estimation is negative. Where the relative distances are not similar it is positive. As m increases we anticipate that the accuracy of our estimates will improve as a result of the Normal approximation of the Gamma distribution being better.

Distance to Nearest Transmitter

To estimate the distance to the nearest transmitter when Nakagami-m fading is in effect using the TPPM and MoM we reduce our sample of pulses such that it only includes pulses believed to be from the nearest transmitter. We show that further reducing this sample improves accuracy. As fading is present we use Algorithm 5.3 to identify pulses as we have shown it is more accurate in this case than Algorithm 5.2.

From the description of estimating the distance to the nearest transmitter given in Subsection 5.4.1 we understand that we must find the PDF and CDF of the observed pulses to allow us to find the expected value of the pulses conditional on them being the most extreme fraction.

We begin by finding the PDF of the difference of two Gamma distributed random variables. Nakagami-m fading means that $H \sim \mathsf{Gamma}(m, \frac{1}{m})$, and with scaling $pH \sim \mathsf{Gamma}(m, \frac{p}{m})$. Therefore we know that $H, H' \sim \mathsf{Gamma}\left(m, \frac{1}{m}\right)$, and that $p^*H \sim \mathsf{Gamma}\left(m, \frac{p^*}{m}\right)$ and $p^0H' \sim \mathsf{Gamma}\left(m, \frac{p^0}{m}\right)$. Setting $X = p^*H$ and $Y = p^0H'$ allows us to represent $p^*H - p^0H'$ as $Z = X - Y$. Hence the probability density function of Z is given by the convolution of X and $-Y$,

$$f_Z(z) = f_X * f_{-Y}(z) = \begin{cases} \int_0^\infty f_X(z+y) f_Y(y) dy. & \text{for } z \geq 0; \\ \int_0^\infty f_Y(x-z) f_X(x) dx & \text{for } z \leq 0. \end{cases} \tag{5.4.15}$$

This gives that

$$f_Z(z) = \begin{cases} \frac{m^{2m}}{\Gamma(m)^2 (p^* p^0)^m} e^{\frac{-mz}{p^*}} \int_0^\infty (z+y)^{m-1} y^{m-1} e^{-my\left(\frac{1}{p^0} + \frac{1}{p^*}\right)} dy & \text{for } z \geq 0; \\ \frac{m^{2m}}{\Gamma(m)^2 (p^* p^0)^m} e^{\frac{mz}{p^0}} \int_0^\infty (x-z)^{m-1} x^{m-1} e^{-mx\left(\frac{1}{p^0} + \frac{1}{p^*}\right)} dx & \text{for } z \leq 0. \end{cases} \tag{5.4.16}$$

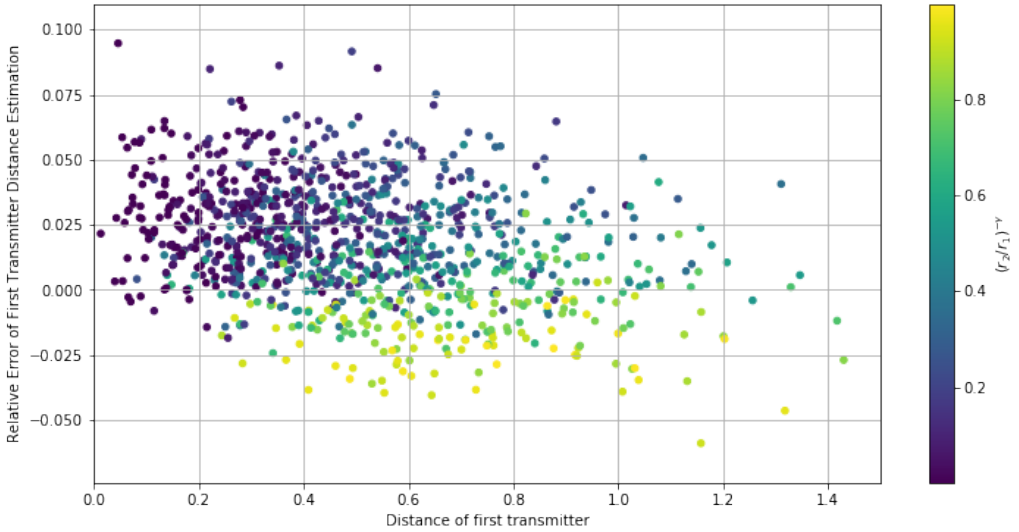

(a) The relative error of the distance estimation for the nearest transmitter when Nakagami-m fading is in effect, using the Method of Moments. We show how this relates to both the actual distance of the nearest transmitter r_1 and the second nearest transmitter r_2 relative to r_1.

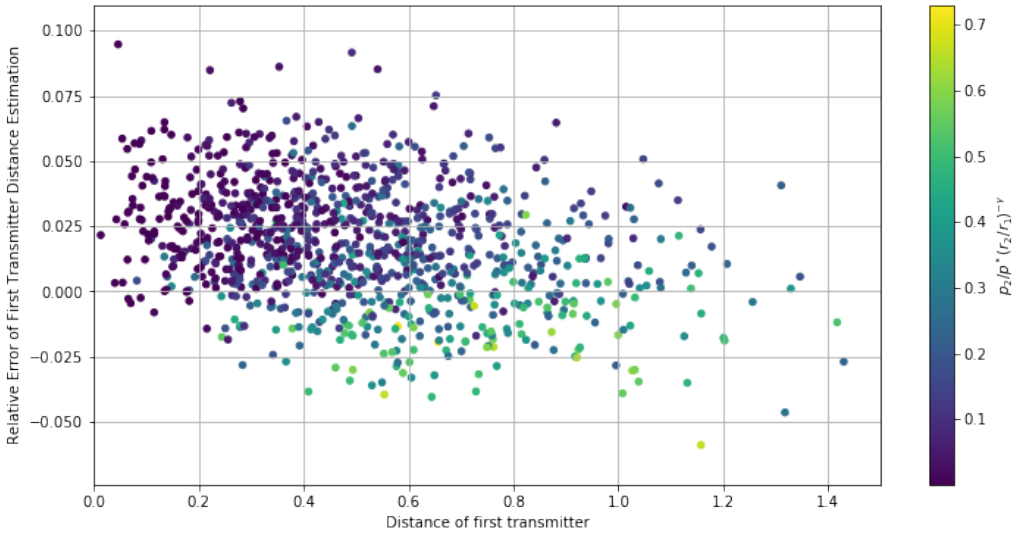

(b) The relative error of the distance estimation for the nearest transmitter when Rayleigh fading is in effect, using the Method of Moments. We show how this relates to both the actual distance of the nearest transmitter r_1 and the second nearest transmitters power p_2 and distance r_2 relative to the nearest transmitters power p_1 and distance r_1.

Figure 5-15: Nakagami-m fading with $m = 20$, 500 pulses observed, 10 transmitters, 1000 repeats. Yellow indicates distances (in 5-15a) or signal contribution (in 5-15b) of the two nearest transmitters are very close, dark blue represents a large difference.

and applying Theorem 2.1 of [51] we find that this can be expressed as

$$f_Z(z) = \begin{cases} \frac{m^m}{\Gamma(m)(p^*+p^0)^m} z^{m-1} e^{\frac{-z}{2}\left(\frac{m}{p^*}-\frac{m}{p^0}\right)} W_{0,\frac{1}{2}-m}\left(z\left(\frac{m}{p^*}+\frac{m}{p^0}\right)\right) & \text{for } z \geq 0; \\ \frac{m^m}{\Gamma(m)(p^*+p^0)^m} (-z)^{m-1} e^{\frac{z}{2}\left(\frac{m}{p^0}-\frac{m}{p^*}\right)} W_{0,\frac{1}{2}-m}\left(-z\left(\frac{m}{p^*}+\frac{m}{p^0}\right)\right) & \text{for } z \leq 0. \end{cases}, \tag{5.4.17}$$

where W denotes a Whittaker function. The Whittaker W function is related to the confluent hypergeometric function by

$$W_{k,m}(z) = e^{-z/2} z^{m+1/2} U(m-k+\frac{1}{2}, 1+2m, z).$$

The confluent hypergeometric function $U(a,b,z)$ was introducted by Francesco Tricomi in 1947 [76] and is defined as

$$U(a,b,z) = \frac{\Gamma(1-b)}{\Gamma(a+1-b)} M(a,b,z) + \frac{\Gamma(b-1)}{\Gamma(a)} z^{1-b} M(a+1-b, 2-b, z).$$

This expression is undefined for integer b but can be extended to any integer b by continuity. The generalized hypergeometric series M is known as Kummer's function and was introduced by Kummer in 1837 [45] and is given by

$$M(a,b,z) = \sum_{n=0}^{\infty} \frac{a^{(n)} z^n}{b^{(n)} n!} = {}_1F_1(a;b;z)$$

where $a^{(n)}$ is the rising factorial with $a^{(0)} = 1$ and $a^{(n)} = a(a+1)(a+2)...(a+n-1)$.

Alternatively equation (5.4.17) can be expressed as

$$f_Z(z) = \frac{\sqrt{\pi} m^{2m} \csc(\pi m) \left(-\frac{z}{\left(\frac{1}{p^0}+\frac{1}{p^*}\right)m}\right)^{m-\frac{1}{2}} e^{\frac{mz}{2}\left(\frac{1}{p^0}-\frac{1}{p^*}\right)} K_{m-\frac{1}{2}}\left(-\frac{mz}{2}\left(\frac{1}{p^0}+\frac{1}{p^*}\right)\right)}{(p^* p^0)^m \Gamma(1-m)\Gamma(m)^2} \tag{5.4.18}$$

where $K_\alpha(x)$ is the modified Bessel function of the second kind given by

$$K_\alpha(x) = \frac{\pi}{2} \frac{I_{-\alpha}(x) - I_\alpha(x)}{\sin \alpha\pi}$$

with the right of this equation being replaced by its limiting value if α is an integer or zero [3] and where $I_\alpha(x) = \sum_{n=0}^{\infty} \frac{1}{n!\Gamma(n+\alpha+1)} \left(\frac{x}{2}\right)^{2n+\alpha}$.

To employ the MoM with reduced sampling to estimate the distance r_1 we require the cumulative distribution function $F_Z(x) = \int_{-\infty}^{x} f_Z(z)dz$. This allows us to find x such that $F_Z(x) = 1 - G$ and compute $\mathbf{E}[Z|Z > x]$. We have found two forms for the probability density function (PDF) of the difference of two

Gamma distributed variables, given in (5.4.17) and (5.4.18). However, neither of these expressions allow a general form for the cumulative distribution function to be found. Therefore we consider separately the case $p^0 = 0$ and the case when $p^0 \geq 0$.

When $p^0 = 0$ we can use the Gamma distribution directly, and use its CDF to find x and then $\mathbf{E}[p^*H|p^*H > x]$, the results of this are shown in Table 5.4 and Figure 5-16.

We have that $p^*H \sim \mathsf{Gamma}(m, \frac{p^*}{m})$ and therefore from this we find that

$$\boldsymbol{P}(p^*H > x) = \frac{\Gamma\left(m, \frac{mx}{p^*}\right)}{\Gamma(m)} \tag{5.4.19}$$

and therefore

$$\begin{aligned}
\boldsymbol{E}[p^*H|p*H > x] &= \frac{\Gamma(m)}{\Gamma\left(m, \frac{mx}{p^*}\right)} \int_x^\infty \frac{1}{\Gamma(m)\left(\frac{p^*}{m}\right)^m} (p^*H)^m e^{-\frac{p^*H}{\left(\frac{p^*}{m}\right)}} dp^*H \\
&= \frac{1}{\Gamma\left(m, \frac{mx}{p^*}\right)} \int_x^\infty \left(\frac{p^*H}{\left(\frac{p^*}{m}\right)}\right)^m e^{-\frac{p^*H}{\left(\frac{p^*}{m}\right)}} dp^*H \\
&= \left(\frac{p^*}{m}\right) \frac{\Gamma\left(m+1, \frac{mx}{p^*}\right)}{\Gamma\left(m, \frac{mx}{p^*}\right)}.
\end{aligned} \tag{5.4.20}$$

We use this in numerical simulations to test its accuracy. The exact fraction of pulses used was taken to be G for each sample, when these were averaged they gave the fractions given in the fraction column of Table 5.4.

When $p^0 \geq 0$, as stated, we cannot obtain a general form of the CDF of Z. However, when $p^0 > 0$ we can compute the CDF for specific values of m. We give examples of the cases when $m = 2$ and $m = 5$. Alternatively we can obtain a general form using the Normal approximation to the Gamma distribution. The Normal approximation to the Gamma distribution increases in accuracy as m increases, as the Gamma distribution becomes more symmetric.

Relative Error of Method of Moments					
	m				
Fraction	2	5	10	15	20
1	-0.093675	-0.038167	-0.018317	-0.013364	-0.009127
1/2	-0.047365	-0.017117	-0.009101	-0.008032	-0.006103
1/3	-0.035342	-0.013662	-0.008062	-0.007539	-0.005936
1/4	-0.029479	-0.012123	-0.007625	-0.007358	-0.005903
1/5	-0.025917	-0.011223	-0.007367	-0.007263	-0.005898
1/6	-0.023477	-0.010616	-0.007192	-0.007195	-0.005903
1/7	-0.021681	-0.010172	-0.007062	-0.007145	-0.005913
1/8	-0.020297	-0.009830	-0.006963	-0.007100	-0.005920
1/9	-0.019193	-0.009557	-0.006881	-0.007060	-0.005922
1/10	-0.018283	-0.009322	-0.006811	-0.007023	-0.005925

Table 5.4: The relative error of the distance estimate when Nakagami-m fading is in effect and fractions of pulses are used in the Method of Moments. We used 10 transmitters with powers continuously uniformly distributed between 1 and 3. The pulse power was 4 and the pre-pulse power was 0. We took 1000 samples of 20000 pulses.

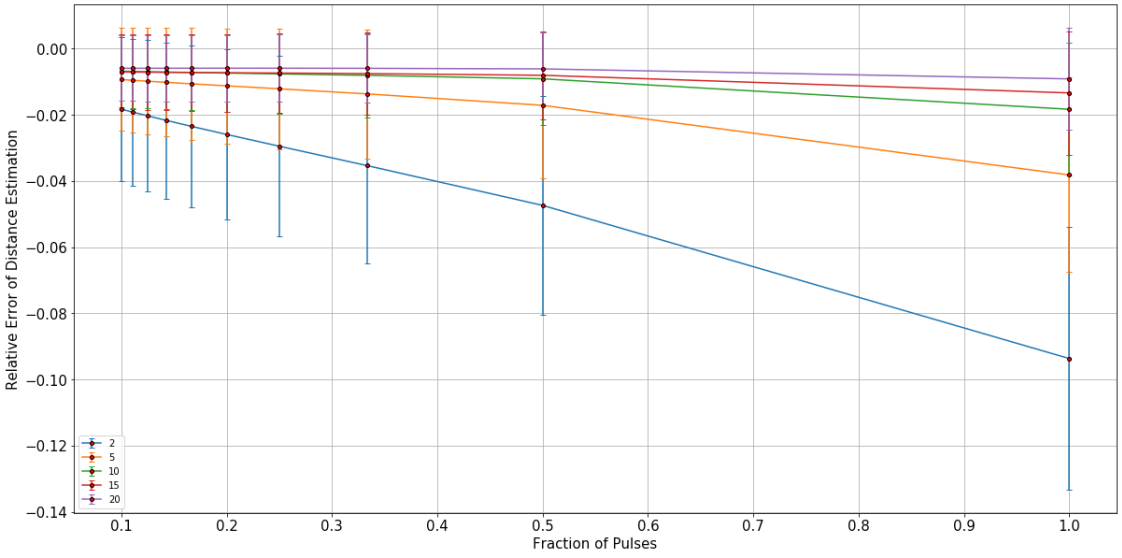

Figure 5-16: Relative error of the distance estimation when Nakagami-m fading is in effect as a function of the fraction of pulses used in the Method of Moments, for five values of m. We observe how reducing the sample size affects the relative error of the distance estimation. We observe 1000 samples of 20000 pulses.

Here we give the cases when $m = 2$ and $m = 5$:

$$\begin{aligned}
\boldsymbol{P}(Z \leq x) &= \frac{e^{\frac{2x}{p^0}} p^0 (p^0(3p^* + p^0) - 2x(p^* + p^0))}{(p^* + p^0)^3} \quad \text{for } m = 2, \text{ and} \\
\boldsymbol{P}(Z \leq x) &= \frac{p^0 e^{\frac{5x}{p^0}} \left(300 {p^0}^2 x^2 (p^* + p^0)^2 \left(21 {p^*}^2 + 7p^* p^0 + {p^0}^2\right)\right)}{24(p^* + p^0)^9} \\
&\quad - \frac{p^0 e^{\frac{5x}{p^0}} \left(120 {p^0}^3 x (p^* + p^0) \left(56 {p^*}^3 + 28 {p^*}^2 p^0 + 8p^* {p^0}^2 + {p^0}^3\right)\right)}{24(p^* + p^0)^9} \\
&\quad + \frac{p^0 e^{\frac{5x}{p^0}} \left(24 {p^0}^4 \left(126 {p^*}^4 + 84 {p^*}^3 p^0 + 36 {p^*}^2 {p^0}^2 + 9p^* {p^0}^3 + {p^0}^4\right)\right)}{24(p^* + p^0)^9} \\
&\quad + \frac{p^0 e^{\frac{5x}{p^0}} \left(625x^4 (p^* + p^0)^4 - 500 p^0 x^3 (p^* + p^0)^3 (6p^* + p^0)\right)}{24(p^* + p^0)^9} \quad \text{for } m = 5.
\end{aligned} \tag{5.4.21}$$

In both cases $m = 2$ and $m = 5$ it is clear that when $p^0 = 0$ the CDF is indeterminate and cannot be solved to find z such that $F_Z(z) = \mathbf{P}[Z \leq z] = 1 - G$. When $p^0 > 0$ we can find the expected values and assess the accuracy as we decrease the fraction. For larger m the expression of the CDF gets more complex. The normal approximation provides a general form.

When $m = 2$ then, with $P(Z > x) = G$ and the Lambert W function defined as $W(xe^x) = x$,

$$x = \frac{p^0 \left(3p^* + p^0 + (p^* + p^0) W\left(\frac{e^{\frac{-3p^* + p^0}{p^* + p^0}} (G-1)(p^* + p^0)^2}{{p^0}^2}\right)\right)}{2(p^* + p^0)}. \tag{5.4.22}$$

Therefore

$$\boldsymbol{E}[Z | Z > x] = \frac{1}{G} \int_x^\infty z f_Z(z) dz. \tag{5.4.23}$$

In the case when $m = 5$ we cannot find x.

For general $m > 0$ we use the normal approximation of the gamma distribution. We can approximate the distribution $\mathsf{Gamma}(k, \theta)$ as $\mathcal{N}(k\theta, k\theta^2)$. This approximation allows us to take that $H, H' \sim \mathcal{N}(1, \frac{1}{m})$. As shown in [57], where there is a linear function of two independent random variables Y, X such that $Y = aX + b$ then $f_Y(y) = \frac{1}{|a|} f_X\left(\frac{y-b}{a}\right)$. Therefore

$$p^* H \sim \mathcal{N}\left(p^*, \frac{{p^*}^2}{m}\right) \quad \text{and} \quad p^0 H' \sim \mathcal{N}\left(p^0, \frac{{p^0}^2}{m}\right). \tag{5.4.24}$$

As before, we represent $p^*H - p^0H'$ as $Z = X - Y$, by setting $X = p^*H$ and $Y = p^0H'$. We find the probability density function of Z using results on the characteristic functions of random variables in [29]. Let $\varphi_X(t) = \mathbb{E}\left[e^{itX}\right]$, $\varphi_Y(t) = \mathbb{E}\left[e^{itY}\right]$ be the characteristic functions of the two independent random variables X and Y, respectively. The characteristic function of their sum is $\varphi_{X+Y}(t) = \varphi_X(t)\varphi_Y(t)$. For arbitrary real numbers a and b then $\varphi_{aY+b}(t) = e^{itb}\varphi_Y(at)$ and so $\varphi_{-Y}(t) = \varphi_Y(-t)$. The characteristic function of the random variable $X \sim \mathcal{N}(\mu_X, \sigma_X^2)$ is $\varphi_X(t) = \exp(it\mu_X - \sigma_X^2 t^2/2)$. It follows that the characteristic function of the difference of independent normal random variables X and Y is

$$\varphi_{X-Y}(t) = \varphi_X(t)\varphi_Y(-t) = \exp\left(it(\mu_X - \mu_Y) - (\sigma_X^2 + \sigma_Y^2)t^2/2\right). \tag{5.4.25}$$

So for $Z = X - Y$ with $X \sim \mathcal{N}(\mu_X, \sigma_X^2)$, and $Y \sim \mathcal{N}(\mu_Y, \sigma_Y^2)$ then $Z \sim \mathcal{N}(\mu_X - \mu_Y, \sigma_X^2 + \sigma_Y^2)$. Therefore

$$Z \sim \mathcal{N}\left(p^* - p^0, \frac{p^{*2} + p^{0^2}}{m}\right). \tag{5.4.26}$$

From this we wish to identify x where $\mathbf{P}(Z > x) = G$.

$$\mathbf{P}(Z \leq x) = 1 - G = \Phi(\tilde{z}) \quad \text{where } x = \mu_Z + \sigma_Z\tilde{z} \tag{5.4.27}$$

and $\Phi(\tilde{z}) = \frac{1}{\sqrt{2\pi}}\int_{-\infty}^{\tilde{z}} e^{-\frac{t^2}{2}}dt$. Therefore as $\tilde{z} = \Phi^{-1}(1 - G)$,

$$x = p^* - p^0 + \sqrt{\left(\frac{p^{*2} + p^{0^2}}{m}\right)}\Phi^{-1}(1 - G). \tag{5.4.28}$$

As we can obtain for a given value of G the corresponding value of x, we can estimate the distance r using (5.4.10). The error function $\mathrm{Erf}(x) = \frac{2}{\sqrt{\pi}}\int_0^x e^{-t^2}dt$. Further to that we define $\mathrm{Erf}(x_0, x_1) = \mathrm{Erf}(x_1) - \mathrm{Erf}(x_0) = \frac{2}{\sqrt{\pi}}\int_{x_0}^{x_1} e^{-t^2}dt$. Then for $Z \sim \mathcal{N}(\mu_Z, \sigma_Z^2)$,

$$f_Z(z) = \frac{1}{\sqrt{2\pi\sigma_Z^2}}e^{-\frac{(z-\mu_Z)^2}{2\sigma_Z^2}} \tag{5.4.29}$$

and

$$\begin{aligned}\mathbf{E}[Z|Z > z] &= \frac{1}{\mathbf{P}(Z > x)}\int_x^\infty z f_Z(z)dz \\ &= \frac{1}{G}\int_x^\infty z f_Z(z)dz.\end{aligned} \tag{5.4.30}$$

Therefore for our case where $Z \sim \mathcal{N}\left(p^* - p^0, \frac{p^{*2}+p^{0^2}}{m}\right)$ we find that, for x as defined in equation (5.4.28),

$$\mathbf{E}[Z|Z > x] = p^* - p^0 + \frac{\sqrt{\frac{(p^{*2}+p^{0^2})}{2m\pi}}\left(e^{\frac{-\left(\Phi^{-1}(1-G)\right)^2}{2}}\right)}{G} \tag{5.4.31}$$

The accuracy, shown in terms of the averaged relative error of the distance estimation as G and m varies is shown in Table 5.5.

Relative Error of Method of Moments: Normal Approximation					
	m				
Fraction	2	5	10	15	20
1	-0.093184	-0.038772	-0.018379	-0.010820	-0.009113
1/2	-0.040895	-0.015085	-0.008589	-0.005996	-0.006113
1/3	-0.038183	-0.015969	-0.010148	-0.007417	-0.007301
1/4	-0.039079	-0.017683	-0.011656	-0.008644	-0.008311
1/5	-0.040731	-0.019300	-0.012912	-0.009635	-0.009155
1/6	-0.042528	-0.020837	-0.014047	-0.010484	-0.009884
1/7	-0.044112	-0.022057	-0.014939	-0.011159	-0.010439
1/8	-0.045711	-0.023263	-0.015898	-0.011813	-0.011003
1/9	-0.046891	-0.024132	-0.016525	-0.012240	-0.011348
1/10	-0.047951	-0.024930	-0.017050	-0.012594	-0.011638

Table 5.5: The relative error of the distance estimate when Nakagami-m fading is in effect and a fraction of pulses is used in the Method of Moments. The Normal approximation of the Gamma distribution is used. The 10 transmitters had powers continuously uniformly distributed between 1 and 3. The pulse power was 4 and the pre-pulse power was 0. We took 1000 samples of 20000 pulses.

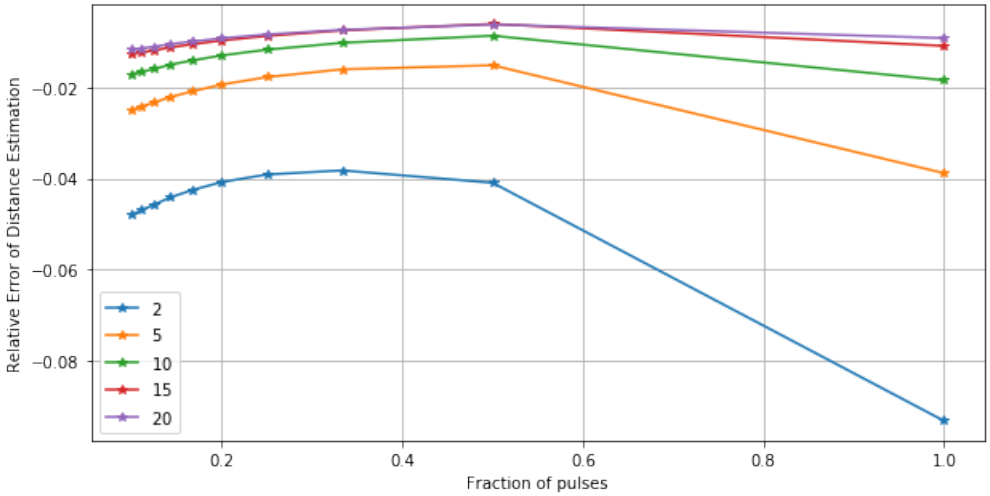

Figure 5-17: Relative error of the distance estimation for the fraction of pulses used in the Method of Moments when taking the Normal approximation to the Gamma distribution is taken. Nakagami-m fading is in effect and the error is shown for five values of m, we observe how reducing the sample size affects the relative error of the distance estimation. We observe 1000 samples of 20000 pulses.

5.5 Short Summary

We began this chapter by assessing the accuracy of the uniform-transmit-power heuristics, that we developed in Chapter 4, when transmit powers are not uniform. Following this, in Section 5.2 we introduced BT's patented Pulse Method [15]. We developed Procedure 5.1, to be used in conjunction with the Pulse Method, to predict transmitter distances and powers. We showed that these estimates are close to the actual values, particularly for the closest transmitters.

In Section 5.3 we developed a new method, the Two-Part Pulse Method (TPPM), for estimating transmitter powers and distances. When fading is not in effect, we showed that the TPPM finds transmitter powers and distances exactly. In Figure 5-8 we compared the performance of the Pulse Method to the TPPM. In Section 5.4 we used the TPPM when fading was in effect to estimate the distance of the nearest one or two transmitters. We used the Method of Moments to sample pulses from the time series of observed signal. Numerical simulations were used to demonstrate the error of these estimates.

Chapter 6

Discussion and Conclusion

This thesis has explored the mathematics of SON and what can be achieved when performing distributed optimisation with incomplete information. We have presented novel methods for enabling this optimisation that outperform existing techniques. In this chapter we discuss the new methods we have developed and their significance. We summarise what has been shown, state conclusions and propose further work. This chapter is organised into four sections with each section corresponding to a previous chapter. We begin by discussing Chapter 2.

6.1 Three Competing Self-Organisation Objectives

In Chapter 2 we studied the dynamics of a wireless communication network as it aimed to satisfy three competing self-organisation objectives. We simplified the network by not incorporating its spatial configuration or effects, such that any two transmitters in the network could be considered neighbours. We allowed that a transmitter could be in one of three states determined its power setting, these were off O, low L and high H.

To assess the dynamics of this network we began by formulating the problem as a Markov jump process in Subsection 2.1.1. Then in Subsection 2.1.2 we gave two routes (Theorem 2.1 and Kurtz's method) that allowed us to represent the evolution as an SDE. The drift term of this SDE gave the nonlinear ODEs that comprised the usual mean-field description of the dynamics in the limit in which N the number of transmitters (i.e., the system size) becomes infinite.

Following the reduction of this system of ODEs from three to two dimensions (since the total number N is constant) we show that there exists a unique interior

equilibrium point, and that is stable. We then analysed the behaviour of the system whilst approaching, and once it reached equilibrium, in Section 2.3. We used two methods to provide numerical simulations. The first was to plot solutions to the ODEs, giving a continuous representation of the dynamics in Figure 2-4 and the vector field in Figure 2-3. The second was to simulate the dynamics for a fixed, finite, number of transmitters using the Gillespie stochastic simulation algorithm (GSSA) described in Algorithm 2.1.

Figure 2-5 confirms that the GSSA followed the trajectories of the ODEs for large N, with oscillations around the equilibrium state. To analyse the oscillations about equilibrium we computed the power spectral density, both theoretically and numerically. To compute the PSD theoretically we used Theorem 1.5; numerically we took the fast Fourier transform of our time series of observations from the GSSA. We showed that power peaked at low frequencies, this is shown for the theoretical derivation in Figures 2-6 and 2-7. In these figures we observe that the peak is small and can be hard to detect.

Simulating an infinite continuous system is not possible, however when using the GSSA to enable numerical computation of the PSD the finite discretisation resulted in discrepancies between the theoretical and numerical results for higher frequencies. Increasing the system size, reducing the time step and increasing the total simulation time all help to reduce the error between the theoretical and numerical results. However, all these measures increase the computational demands of the simulation. Therefore we showed in Figures 2-8 to 2-10 the alignment of the theoretical and numerical results focussing mainly on lower frequencies. This enabled us to identify the peak in the PSD of x_H, as seen in Figure 2-8a.

In conclusion, we have developed a framework for analysing the stability of the system when it approaches, and when it is very near to, equilibrium. The analysis of this chapter was constrained by considering only pairwise interactions between transmitters. Future work could build on this by including interactions between three or more transmitters, as well as including analysis of the dynamics resulting from implementing the power control policies developed elsewhere in this thesis and used together with the new distance estimation methods.

6.2 Self-Optimising Power Configurations

In Chapter 3 we showed that, with the exception of the case in which there are only two transmitters and no noise, uniform transmit powers are usually not op-

timal for SINR. However, non-uniform powers, that are set without consideration of the network structure, do not typically perform better than uniform power settings. Given this, our aim in this chapter was to propose a power control policy that adjusted transmit powers based on network observations.

We proposed a new power control algorithm which we termed 'Switch-Off Cluster' (SOC) which appeared to outperform BT's benchmark policy 'Smart'. We showed this by comparing the CDF curves of SINR when the two policies were applied on the same transmitter network. The SOC algorithm requires a few complete iterations (every transmitter in the network updating once) to reach its optimal configuration, whereas the Smart policy only requires a single complete iteration to reach its optimal configuration. However, as seen in Figure 3-6, even after a single complete iteration SOC significantly outperforms Smart. Additionally, as shown in Figure 3-9, the improvement from an additional one or two complete iterations following the first is minimal. Therefore an advantage of SOC over Smart is that after a single complete iteration it achieves improved SINR.

A potential disadvantage in implementing SOC for distributed power control is that it requires knowledge of the distances and powers of all transmitters within a minimum distance. We addressed this requirement in Chapters 4 and 5 where we developed heuristics for estimating these distances and powers. However, we found that accurate estimation of power and distance for multiple transmitters was only achievable with non-uniform powers in the absence of fading. Therefore in Section 3.3 we moved to using reinforcement learning methods to propose policies that did not require such network knowledge but performed similarly. It should be noted that, although distributed implementation of SOC may be limited by network knowledge requirements, it is a robust benchmark for power control policy performance.

We found Q-learning to be impractical for learning a distributed power control policy due to its limitations with the sizes of action and state spaces. Therefore we instead implemented deep Q-learning. In a departure from the usual approach taken in the literature we trained the neural network on a small set of transmitters to learn a policy and then implemented this policy on an independent and much larger network of 500 transmitters. A limitation in the application of deep Q-learning for finding an optimal power control policy is that the algorithm requires a finite and discrete action space. This immediately limits, with the selected actions, the transmit powers that can be used in discovering such a policy and it may be that the discretisation excludes an optimal policy.

In an extensive, though not exhaustive, search of the literature we found limited applications of reinforcement learning for power control optimisation where the action space was continuous. We therefore turned our attention to a variant of the 'asynchronous advantage actor critic' (A3C) algorithm proposed in [55], known as advantage actor critic (A2C). The A2C algorithm allows a continuous set of transmit powers to be used when learning an optimal policy. We found that with a continuous action space, policy performance depended on the state space that we used used, whereas with deep Q-learning (a discrete action space) it had not. With a continuous action space, additional information could be acted upon, leading to improved policy performance. This supports the importance of using a continuous action space when learning an optimal policy.

This chapter has therefore shown that the reinforcement learning methods of deep Q-learning and Advantage Actor Critic (A2C) can be used to develop effective transmit power policies. With minimal training, on an appropriate model, both methods can produce a power control policy that can be applied offline and that does not require knowledge of transmitter distances only SINR at paired receivers. The performance of the policy learnt with A2C closely matched that of SOC. We believe that with further work it could learn policies that outperform our best proposed algorithm. Further work in this direction should include improving the reward structure and better training for these methods, as we now discuss.

The reward function that we used prioritises increasing the value of the 20^{th} percentile of observed SINR, with less importance placed on the 50^{th} and 70^{th} percentile and no other values taken into consideration. We designed the function in this way to ensure that increasing the lower values of SINR was prioritised over increasing higher values. This is in line with the real-world network priorities of BT. The performance of the policies was assessed by comparing the CDF curves generated by an adaptation of the sampling algorithm in [16]. Further work could explore considering more SINR measurements and adjusting the weightings given to different percentiles. Additionally, another objective could be addressed in the reward function, such as coverage, by introducing a reward based on observed signal rather than SINR.

We trained our policy on a set of transmitters a tenth of the size of the network that the policy was to be deployed on. We trained on multiple sets of transmitters as there is some dependence on the training set sharing similarities with the larger set that it is eventually implemented on for a policy to perform well. Further considerations include diversifying the training further by using

more and larger training sets; also longer training on each set could be tried. Each of the training sets began with uniform powers, we could bootstrap our training by applying SOC (or any optimisation policy) before beginning training. Additionally, allowing the policy to be updated once it has been deployed, so that a transmitter can update an individual policy for itself, could be considered. Reinforcement learning methods have the advantage of adaptability: as long as a suitable training set and reward function is provided an optimal policy can be learnt. Additionally, adaptations to the reward function allow for different objectives to be achieved without altering the neural network architecture or learning design.

In conclusion, for optimising SINR we have contributed a new benchmarking algorithm SOC that significantly improves on the one we received from BT. We have also developed a problem formulation for use with reinforcement learning methods. Through this we learnt power control policies that only required observations of the SINR of paired devices in order to optimise transmit powers on large networks of transmitters. Further to this we were able to use continuous transmit powers in our learning algorithms, which contributes to the literature on distributed power control policies.

6.3 Uniform Power Distance Estimation

From Chapter 3 we learnt that knowledge of the distance to its nearest neighbour allows a transmitter to optimise the SIR of paired receivers whilst protecting the SIR of receivers paired to neighbours. Therefore the ability of transmitters to estimate, based solely on observations, the distance to the nearest transmitter is of significant help in enabling distributed self-optimisation as described in Chapter 1. Given this, in Chapter 4 we theoretically derived two heuristics that offer improved accuracy over those commonly used in the literature.

First, in the absence of fading we considered a simple heuristic that assumes the nearest transmitter contributes all observed signal. We found the expected error of this heuristic conditioned on the observed signal and there being a fixed number of neighbours within a given distance. We then found the expected error of the heuristic conditioned only on the observed signal. We proposed an asymptotic heuristic that adjusts the simple heuristic by the expected error. Comparisons with numerical simulations showed that particularly for small values of observed signal the asymptotic heuristic we proposed offers significantly improved accuracy.

The second heuristic we proposed is for use when received signal power is effected by Rayleigh fading. We began by considering the scaling factor proposed in [38] and combined this with the asymptotic heuristic we proposed; however, this did not achieve suitable accuracy. We then pursued an alternative approach and derived the approximate probability distribution of the distance to the nearest neighbour conditioned on the observed signal. From this probability distribution the expected distance was found and is given as equation (4.2.6). Numerical simulations show that the approximated distribution closely matches the numerical distribution with accuracy improving as the value of total observed signal increases.

In conclusion, in this chapter we proposed improvements to heuristics that can be used by a transmitter to estimate the distance to its nearest neighbour, based only on observed signal. This ability allows a transmitter to configure its power settings accordingly to optimise network performance in a truly distributed way. Our new heuristics offer significant improvement, yet remain tractable and fast to compute.

The improved heuristics are given explicitly in terms of observed signal and pathloss and numerical simulations support the theoretically derived results. There are limitations in that they assume transmitters are Poisson distributed and that all transmitters are on uniform powers. However, our general approach of working in the limit of large total signal strength S is likely to be an approach that applies when these other modelling constraints are relaxed. The robustness of working asymptotically for large S allows for generally applicable better heuristics to be derived.

Future work would include a more careful investigation of the error terms, i.e., the next-order terms in the large S expansion and their dependence on the number of transmitters k. Also, we could consider employing these heuristics together with the strategies and behavioural policies developed in the earlier chapters.

6.4 Non-Uniform Power Distance Estimation

We began Chapter 5 by considering the application of the uniform-power distance estimation heuristics (4.1.32) and (4.2.5) in networks where transmit powers are not uniform. We showed that scaling the observed signal by the expected power of transmitters gives a heuristic with accuracy dependent on the maximum power as well as the observed signal. Figure 5-1 showed that for low values of signal,

such as $S = 50$, the error was more sensitive to the maximum power than for higher values of observed signal such as $S = 1000$, for which the scaled heuristic has a small average relative error. In the case of Rayleigh fading the distribution of the distance to the nearest transmitter can still be approximated as shown in Figure 5-2. Therefore in Section 5.1 we can conclude that, with a simple scaling of the observed signal, the heuristics for distance estimation presented in Chapter 4 can offer accurate estimations of the distance to the nearest transmitter when powers are not uniform.

In Section 5.2 we introduced the pulse method, which BT have patented [**?**]. We showed that this method allows the distance to all transmitters in the network to be found exactly, if they share a uniform power. In the case when the transmitters have non-uniform powers, given that the powers are discrete and known, we propose Procedure 5.1 to estimate both distances and powers of transmitters. The accuracy of the estimations obtained using Procedure 5.1 were shown to be relative to the distance of the nearest transmitter. Due to the iterative nature a lack of initial accuracy carries through to the estimations for all further transmitters. Figure 5-6 shows that the average relative error of the distance estimation generally increasing as the number of iterations increases. For a more robust method of distance and power estimation we proposed the 'Two-Part Pulse Method' (TPPM).

In Section 5.3 we presented the use of the TPPM when no fading is present. We introduced the idea of a pulse involving two distinct powers in Procedure 5.2. We also presented two methods for identifying the two-part pulses. We found that the TPPM allowed for both powers and distances to be found exactly. In Figure 5-8 we compared the accuracy of pulse method to the TPPM. In Section 5.4 we showed that, when fading was present, we used the TPPM together with the method of moments, described in Chapter 1, and showed that this accurately estimated transmitter distances. We identified pulses using Procedure 5.3 and then reduced the sample of pulses to include only pulses that were assumed to be from the nearest one or two transmitters. Therefore the TPPM allows for the distance of the nearest one or two transmitters to be estimated. It does not require that the power settings be discrete or known, with the exception of the two pulse powers.

Future work would look at estimating the distances to further transmitters as well as using these power and distance estimators together with a self-optimising power configuration strategy and assessing how well it performs. Additionally we could examine the behaviour of the relative error, shown in Figure 5-14a for

values of $2 \leq m \leq 3$ where it changes from being negative to positive.

To conclude, this thesis contributes to the field through novel methods for power estimation, distance estimation and self-optimising power control strategies. More generally, it provides insight into optimal strategies for controlling interference in SON, and sets out new directions in which mathematical modelling can contribute to the management of wireless communications networks.

Appendices

Appendix A

Power Spectral Density

In this appendix we give the proofs to two theorems used for computing the power spectral density.

A.1 Wiener-Khinchin Theorem

Here we provide the proof of Theorem 1.4, the Wiener-Khinchin theorem. The Wiener-Khinchin theorem relates the power spectral density of a stochastic process to the Fourier transform of its autocorrelation function. We begin by recalling the definition of power spectral density.

From [60] we understand that the truncated Fourier transform $\hat{x}_T(\omega)$ of a continuous-time signal $x(t)$ is where signal is integrated over the finite time interval $[0, T]$ such that

$$\hat{x}_T(\omega) = \int_0^T x(t)e^{-i\omega t}dt. \tag{A.1.1}$$

We now give the definition of power spectral density.

Definition A.1 (Power Spectral Density)**.** *The power spectral density (PSD), denoted by $\mathcal{P}(\omega)$, describes the distribution of power with angular frequency ω. It is defined as*

$$\mathcal{P}(\omega) = \lim_{T\to\infty} \frac{1}{2\pi T} \left|\hat{x}_T(\omega)\right|^2. \tag{A.1.2}$$

We recall the definition of an autocorrelation function.

Definition A.2 (Autocorrelation Function)**.** *Let $x(t)$ be a stationary stochastic process, then we define the autocorrelation $G(\tau)$ of the process as:*

$$G(\tau) = \lim_{T\to\infty} \frac{1}{T} \int_0^T x(t)x(t+\tau)dt \tag{A.1.3}$$

We now prove the Wiener-Kinchin theorem as in [88].

Theorem A.1 (Wiener-Khinchin Theorem)**.** *The Power Spectral Density of the stochastic process $x(t)$ is the Fourier Transform of its autocorrelation function*

$$\mathcal{P}(\omega) = \frac{1}{2\pi}\int_{-\infty}^{\infty} \mathrm{e}^{-i\omega\tau} G(\tau) d\tau \tag{A.1.4}$$

where the autocorrelation function $G(\tau)$ of $x(t)$ is as defined in (A.2)*.*

Proof. We begin by proving that the autocorrelation function $G(\tau)$ is an even function such that $G(\tau) = G(-\tau)$. Let us define $t' = t - \tau$, then

$$\begin{aligned} G(-\tau) =& \lim_{T\to\infty} \frac{1}{T}\int_0^T x(t)x(t-\tau)dt \\ =& \lim_{T\to\infty} \frac{1}{T}\int_{-\tau}^{T-\tau} x(t'+\tau)x(t')dt' \\ =& \lim_{T\to\infty} \frac{1}{T}\left[\int_{-\tau}^{0} x(t'+\tau)x(t')dt' + \int_0^T x(t'+\tau)x(t')dt' \right. \\ & \left. - \int_{T-\tau}^{T} x(t'+\tau)x(t')dt'\right] \\ =& G(\tau). \end{aligned} \tag{A.1.5}$$

The last equality holds in the limit $T \to \infty$.

From Definition A.1, where $\overline{\hat{x}(\omega)}$ denotes the complex conjugate of $\hat{x}(\omega)$, we can write the power spectral density as

$$\mathcal{P}(\omega) = \lim_{T\to\infty} \frac{1}{2\pi T}\hat{x}_T(\omega)\overline{\hat{x}_T(\omega)}. \tag{A.1.6}$$

In this thesis as $x(t)$ is a real-valued process $\overline{x(t)} = x(t)$. We change the integration domain from (t, t') to (t', τ), this is shown in Figure A-1. By doing so we can write

$$\mathcal{P}(\omega) = \lim_{T\to\infty} \frac{1}{2\pi T}\int_0^T x(t)e^{-i\omega t}dt \int_0^T x(t')e^{i\omega t'}dt'. \tag{A.1.7}$$

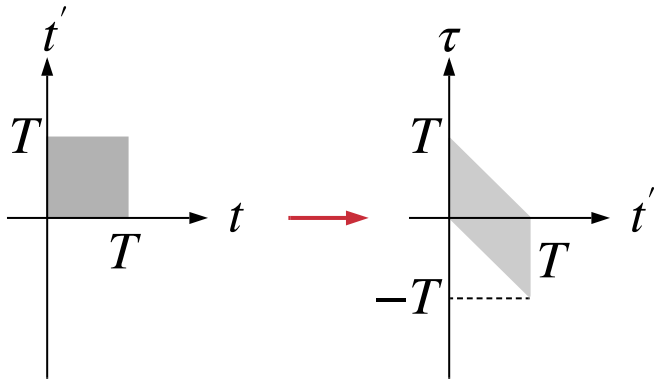

Figure A-1: The transformation of the integration domain.

as

$$\begin{aligned}
\mathcal{P}(\omega) &= \lim_{T\to\infty}\frac{1}{2\pi T}\int_0^T e^{-i\omega\tau}\int_0^{T-\tau} x(t')x(t'+\tau)dt'd\tau \\
&\quad + \lim_{T\to\infty}\frac{1}{2\pi T}\int_{-T}^0 e^{-i\omega\tau}\int_{-\tau}^{T} x(t')x(t'+\tau)dt'd\tau \\
&= \lim_{T\to\infty}\frac{1}{2\pi T}\int_0^T e^{-i\omega\tau}\int_0^{T-\tau} x(t')x(t'+\tau)dt'd\tau \\
&\quad + \lim_{T\to\infty}\frac{1}{2\pi T}\int_{-T}^0 e^{-i\omega\tau}\int_0^{T+\tau} x(t'+\tau)x(t')dt'd\tau \\
&= \lim_{T\to\infty}\frac{1}{2\pi T}\int_0^T (e^{-i\omega\tau}+e^{i\omega\tau})\int_0^{T-\tau} x(t')x(t'+\tau)dt'd\tau \\
&= \lim_{T\to\infty}\left[\frac{1}{\pi}\int_0^T \cos(\omega\tau)\frac{1}{T}\int_0^{T-\tau} x(t)x(t+\tau)dtd\tau\right]
\end{aligned} \tag{A.1.8}$$

and taking the limit $T\to\infty$, (A.1.8) is

$$\mathcal{P}(\omega) = \frac{1}{\pi}\int_0^\infty \cos(\omega\tau)G(\tau)d\tau. \tag{A.1.9}$$

As we have shown in Equation (A.1.5) that the autocorrelation is an even function, we can obtain that

$$\int_{-\infty}^{\infty} \sin(\omega\tau)G(\tau)d\tau = 0 \tag{A.1.10}$$

and

$$\int_{-\infty}^{0} \cos(\omega\tau)G(\tau)d\tau = \int_0^\infty \cos(\omega\tau)G(\tau)d\tau. \tag{A.1.11}$$

Therefore from equations (A.1.9), (A.1.10) and (A.1.11) we achieve that

$$\mathcal{P}(\omega) = \frac{1}{2\pi}\int_{-\infty}^{\infty} e^{-i\omega\tau}G(\tau)d\tau. \tag{A.1.12}$$

□

A.2 Power Spectrum Matrix

We now provide the proof of Theorem 1.5, we follow [31] (Section 4.5.6). First we restate the definition of a Multivariate Ornstein-Uhlenbeck process and the theorem itself.

Definition A.3 (Multivariate Ornstein-Uhlenbeck Process)**.** *We define this process by the linear stochastic differential equation*

$$d\boldsymbol{x}(t) = \boldsymbol{C}\boldsymbol{x}(t)dt + \boldsymbol{D}d\boldsymbol{W}(t), \tag{A.2.1}$$

where $\boldsymbol{C}$ *and* $\boldsymbol{D}$ *are constant matrices and the solution to* (A.2.1) *is*

$$\boldsymbol{x}(t) = e^{\boldsymbol{C}t}\boldsymbol{x}(0) + \int_0^t e^{\boldsymbol{C}(t-t')}\boldsymbol{D}d\boldsymbol{W}(t'). \tag{A.2.2}$$

Theorem A.2 (Spectrum Matrix in Stationary State)**.** *The spectrum matrix* $\mathcal{P}(\omega)$ *of a multivariate Ornstein-Uhlenbeck process as defined above is given by*

$$\boldsymbol{\mathcal{P}}(\omega) = \frac{1}{2\pi}(\mathbf{C} - i\omega\mathbf{I})^{-1}\mathbf{D}\mathbf{D}^T(\mathbf{C} - i\omega\mathbf{I})^{-\dagger} \tag{A.2.3}$$

with $-\dagger$ *denoting the inverse conjugate transpose.*

Proof. A Multivariate Ornstein-Uhlenbeck process is a stationary stochastic process $\boldsymbol{x}(t)$. A stochastic process $\boldsymbol{x}(t)$ is stationary if the correlation function

$$\langle \boldsymbol{x}(s), \boldsymbol{x}(t)\rangle = \langle \boldsymbol{x}(s)\boldsymbol{x}(t)\rangle - \langle \boldsymbol{x}(s)\rangle\langle \boldsymbol{x}(t)\rangle \tag{A.2.4}$$

does not change when shifted in time and depends only upon $|t-s|$. It follows that the mean $\langle \boldsymbol{x}(t)\rangle$ and variance will be constant. From Definition A.3 we see that the mean

$$\langle \boldsymbol{x}(t)\rangle = \exp(\boldsymbol{C}t)\langle \boldsymbol{x}(0)\rangle, \tag{A.2.5}$$

and the correlation function

$$\begin{aligned}\langle \boldsymbol{x}(t), \boldsymbol{x}^{\mathrm{T}}(s)\rangle \equiv & \langle [\boldsymbol{x}(t) - \langle \boldsymbol{x}(t)\rangle][\boldsymbol{x}(s) - \langle \boldsymbol{x}(s)\rangle]^{\mathrm{T}}\rangle, \\ = & \exp(\mathbf{C}t)\langle \boldsymbol{x}(0), \boldsymbol{x}^{\mathrm{T}}(0)\rangle \exp(\mathbf{C}s) \\ & + \int_0^{\min(t,s)} \exp[\mathbf{C}(t-t')]\mathbf{D}\mathbf{D}^{\mathrm{T}} \exp[\mathbf{C}^{\mathrm{T}}(s-t')]dt.\end{aligned} \tag{A.2.6}$$

If the eigenvalues of $\mathbf{C}$ have only negative real parts then there exists a stationary solution

$$\boldsymbol{x}_s(t) = \int_{-\infty}^{t} \exp[\mathbf{C}(t-t')]\mathbf{D}d\boldsymbol{W}(t'). \tag{A.2.7}$$

The stationary mean $\langle \boldsymbol{x}_s(t)\rangle = 0$ and the correlation function

$$\langle \boldsymbol{x}_s^T(t), \boldsymbol{x}_s(t)\rangle = \int_{-\infty}^{\min(t,s)} \exp[\mathbf{C}(t-t')]\mathbf{D}\mathbf{D}^{\mathrm{T}} \exp[\mathbf{C}^{\mathrm{T}}(s-t')]dt. \tag{A.2.8}$$

Let us define the stationary covariance matrix $\boldsymbol{\sigma}$ by

$$\boldsymbol{\sigma} = \langle \boldsymbol{x}_s^T(t), \boldsymbol{x}_s(t)\rangle. \tag{A.2.9}$$

We then compute that

$$\begin{aligned}\mathbf{C}\boldsymbol{\sigma} + \boldsymbol{\sigma}\mathbf{C}^{\mathrm{T}} = & \int_{-\infty}^{t} \mathbf{C} \exp[\mathbf{C}(t-t')]\mathbf{D}\mathbf{D}^{\mathrm{T}} \exp[\mathbf{C}^{\mathrm{T}}(t-t')]dt' \\ & + \int_{-\infty}^{t} \exp[\mathbf{C}(t-t')]\mathbf{D}\mathbf{D}^{\mathrm{T}} \exp[\mathbf{C}^{\mathrm{T}}(t-t')]\mathbf{C}^{\mathrm{T}}dt', \\ = & \int_{-\infty}^{t} \frac{d}{dt'}\{\exp[\mathbf{C}(t-t')]\mathbf{D}\mathbf{D}^{\mathrm{T}} \exp[\mathbf{C}^{\mathrm{T}}(t-t')]\}dt'.\end{aligned} \tag{A.2.10}$$

Computing the integral, we find that the lower limit vanishes by the assumed negativity of the eigenvalues of $\mathbf{C}$ and hence only the upper limit remains giving,

$$\mathbf{C}\boldsymbol{\sigma} + \boldsymbol{\sigma}\mathbf{C}^{\mathrm{T}} = \mathbf{D}\mathbf{D}^{\mathrm{T}}. \tag{A.2.11}$$

This is an important relation we will use later. We recall the correlation function $\langle \boldsymbol{x}_s^T(t), \boldsymbol{x}_s(t)\rangle$ given in (A.2.8) and note that if $t > s$,

$$\begin{aligned}\langle \boldsymbol{x}_s^T(t), \boldsymbol{x}_s(t)\rangle = & \exp[\mathbf{C}(t-s)] \int_{-\infty}^{s} \exp[\mathbf{C}(t-t')]\mathbf{D}\mathbf{D}^{\mathrm{T}} \exp[\mathbf{C}^{\mathrm{T}}(s-t')]dt \\ = & \exp[\mathbf{C}(t-s)]\boldsymbol{\sigma}.\end{aligned} \tag{A.2.12}$$

and similarly if $t < s$ then

$$\langle \boldsymbol{x}_s^T(t), \boldsymbol{x}_s(t) \rangle = \boldsymbol{\sigma}[\mathbf{C}^{\mathrm{T}}(s-t)]. \tag{A.2.13}$$

As expected of a stationary solution the correlation function depends only on $s-t$. By defining

$$G_s(t-s) = \langle \boldsymbol{x}_s(t), \boldsymbol{x}_s^{\mathrm{T}}(t) \rangle \tag{A.2.14}$$

we see (remembering $\boldsymbol{\sigma} = \boldsymbol{\sigma}^{\mathrm{T}}$) that

$$G_s(t-s) = [G_s(s-t)]^{\mathrm{T}} \tag{A.2.15}$$

In Section A.1 we stated and proved the Wiener-Khinchin Theorem which gives that the power spectral density

$$\mathcal{P}(\omega) = \frac{1}{2\pi} \int_{-\infty}^{\infty} \mathrm{e}^{-i\omega\tau} G(\tau) d\tau. \tag{A.2.16}$$

We now have that

$$\begin{aligned} \mathcal{P}(\omega) &= \frac{1}{2\pi} \int_{-\infty}^{\infty} \mathrm{e}^{-i\omega\tau} G(\tau) d\tau, \\ &= \frac{1}{2\pi} \{ \int_0^{\infty} \mathrm{e}^{-(i\omega - \mathbf{C})\tau} \boldsymbol{\sigma} d\tau + \int_{-\infty}^{0} \boldsymbol{\sigma} \mathrm{e}^{-(i\omega + \mathbf{C}^{\mathrm{T}})\tau} d\tau \}, \\ &= \frac{1}{2\pi} [(\mathbf{C} - i\omega)^{-1} \boldsymbol{\sigma} + \boldsymbol{\sigma} (-\mathbf{C}^{\mathrm{T}} - i\omega)^{-1}]. \end{aligned} \tag{A.2.17}$$

Hence,

$$(\mathbf{C} - i\omega)\mathcal{P}(\omega)(\mathbf{C}^{\mathrm{T}} + i\omega) = \frac{1}{2\pi}(\boldsymbol{\sigma}\mathbf{C}^{\mathrm{T}} + \mathbf{C}\boldsymbol{\sigma}), \tag{A.2.18}$$

and recalling from (A.2.11) that $\mathbf{C}\boldsymbol{\sigma} + \boldsymbol{\sigma}\mathbf{C}^{\mathrm{T}} = \mathbf{D}\mathbf{D}^{\mathrm{T}}$ we get that

$$\boldsymbol{\mathcal{P}}(\omega) = \frac{1}{2\pi}(\mathbf{C} - i\omega\mathbf{I})^{-1}\mathbf{D}\mathbf{D}^{\mathrm{T}}(\mathbf{C} - i\omega\mathbf{I})^{-\dagger}.$$

□

Appendix B

Inter-Transmitter Distances

B.1 Exponentially Distributed Interarrival Times

Definition B.1 (Poisson process)**.** *A Poisson process with intensity λ is a process $N = \{N(t) : t \geq 0\}$ taking values in the state space $S = \{0, 1, 2, \ldots\}$ such that:*

(a) $N(0) = 0$; *if* $s < t$ *then* $N(s) \leq N(t)$,

(b) $\mathbf{P}\left[N(t+h) = n + m | N(t) = n\right] = \begin{cases} \lambda h + o(h) & \text{if } m = 1, \\ o(h) & \text{if } m > 1, \\ 1 - \lambda h + o(h) & \text{if } m = 0. \end{cases}$

(c) if $s < t$, the number $N(t) - N(s)$ of arrivals in the interval $(s, t]$ is independent of the times of arrivals during $[0, s]$.

Where $N(t)$ is Poisson distributed with parameter λt such that

$$\mathbf{P}[N(t) = j)] = \frac{(\lambda t)^j}{j!} e^{-\lambda t}, \quad j \in \mathbb{Z}^+$$

it follows that $\mathbf{E}[N(t)] = \lambda t$. Let the time of the nth arrival T_n be given by $T_n = \inf\{t : N(t) = n\}$. The *interarrival times* are given by $X_n = T_n - T_{n-1}$.

Theorem B.1 (Interarrival times exponentially distributed)**.** *The random variables $X_1, X_2, \ldots$ representing the interarrival times are independent and are exponentially distributed with mean λ^{-1}.*

Proof. By Definition B.1 where,

$$\boldsymbol{P}[X_1 > t] = \boldsymbol{P}[N(t) = 0] = \frac{e^{-\lambda t}(\lambda t)^0}{0!} = e^{-\lambda t},$$

then

$$\begin{aligned} \boldsymbol{P}[X_2 > t | X_1 = s] &= \boldsymbol{P}[X_2 > s + t | X_1 = s] \\ &= \boldsymbol{P}[X_2 > s + t] \\ &= e^{-\lambda t}. \end{aligned} \tag{B.1.1}$$

This can be continued for all X_i and therefore we have shown that $\forall i \; X_i \sim \mathsf{Exp}(\frac{1}{\lambda})$. Therefore interarrival times are exponentially distributed. □

B.2 Mapping Theorem

We begin by defining a measurable space and a measure, we define these as in [7] starting with the definition of an algebra. For all definitions below let Ω be a set.

Definition B.2 (An Algebra)**.** *A collection $\mathcal{A}_0$ of subsets of Ω is called an algebra on Ω if:*

(i) $\Omega \in \mathcal{A}_0$,

(ii) $A \in \mathcal{A}_0 \Rightarrow A^c = \Omega \backslash A \in \mathcal{A}_0$

(iii) $A, B \in \mathcal{A}_0 \Rightarrow A \cup B \in \mathcal{A}_0$.

We now define a σ-algebra.

Definition B.3 (σ-algebra)**.** *An algebra $\mathcal{A}$ of subsets of Ω is called a σ-algebra on Ω if for any sequence $A_n \in \mathcal{A}$, ($n \in \mathbb{N}$) we have*

$$\bigcup_{n=1}^{\infty} A_n \in \mathcal{A}.$$

Now that we have defined a σ-algebra we can define a measurable space.

Definition B.4 (Measurable Space)**.** *A pair $(\Omega, \mathcal{A})$ is called a measurable space where $\mathcal{A}$ is a σ-algebra on the set Ω.*

Now that we have defined a measurable space we can define a measure on that space. We begin by defining what it is for a map to be countable additive and then use this to define a measure.

Definition B.5 (Countably Additive)**.** *Let Ω be a set, $\mathcal{A}$ an algebra on Ω and T a non-negative set function $T : \mathcal{A} \to [0, \infty]$ such that $T(\emptyset) = 0$. T is called:*

(i) additive, if $A, B \in \mathcal{A}$, $A \cap B = \emptyset \Rightarrow T(A \cup B) = T(A) + T(B)$

(ii) countably additive, if whenever $(A_n)_{n\in\mathbb{N}}$ is a sequence of disjoint sets in $\mathcal{A}$ with $\bigcup A_n \in \mathcal{A}$ then

$$T\left(\bigcup_{n=0}^{\infty} A_n\right) = \sum_{n=1}^{\infty} T(A_n).$$

Definition B.6 (A Measure)**.** *Let $(\Omega, \mathcal{A})$ be a measurable space. A countably additive map*

$$T : \mathcal{A} \to [0, \infty]$$

is called a measure on $(\Omega, \mathcal{A})$.

We now recall the definition of a Poisson point process and then state and prove the mapping theorem. Let $(X, \mathcal{X})$ be a measurable space. A measure ν on X is said to be s-finite if ν is a countable sum of finite measures.

Definition B.7 (Poisson point process)**.** *Let λ be an s-finite measure on X. A Poisson process with intensity measure λ is a point process η on X with the two following properties:*

(i) For every $B \in \mathcal{X}$ the distribution of $\eta(B)$ is Poisson with parameter $\lambda(B)$, such that $\mathbf{P}[\eta(B) = k] = \mathsf{Poisson}(\lambda(B); k)$ $\forall k \in \mathbb{N}^+$.

(ii) For every $m \in \mathbb{N}$ and all pairwise disjoint sets $B_1, \ldots, B_m \in \mathcal{X}$ the random variables $\eta(B_1), \ldots, \eta(B_m)$ are independent.

Theorem B.2 (Mapping Theorem)**.** *Consider two measurable spaces $(X, \mathcal{X})$ and $(Y, \mathcal{Y})$. Let η be a point process on X with intensity measure λ and let $T : X \to Y$ be measurable. Then $T(\eta)$ is a point process with intensity measure $T(\lambda)$. If η is a Poisson process, then $T(\eta)$ is a Poisson process too.*

Proof. We first note that $T(\mu) \in \mathbb{N}$ for any $\mu \in \mathbb{N}$. Indeed, if $\mu = \sum_{j=1}^{\infty} \mu_j$ then $T(\mu) = \sum_{j=1}^{\infty} T(\mu_j)$. Moreover, if the μ_j are $\mathbb{N}^+$ valued, so are the $T(\mu_j)$. For any $C \in \mathcal{Y}$, $T(\eta)(C)$ is a random variable and with intensity measure $T(\lambda)$ and therefore its expectation is

$$\mathbf{E}[T(\eta)(C)] = \mathbf{E}[\eta(T^{-1}C)] = \lambda(T^{-1}C) = T(\lambda)(C).$$

If η is a Poisson process, then from Definition B.7: $T(\eta)$ is completely independent by property (ii) and $T(\eta)(C)$ has a Poisson distribution with parameter $T(\lambda)(C)$ by property (i). □

Bibliography

[1] Smoke signals: The original status update. TIME.com, 2013. https://newsfeed.time.com/2013/03/13/smoke-signals-the-original-status-update/ [Accessed: 31 May 2019 14:03].

[2] M. Abadi, A. Agarwal, P. Barham, E. Brevdo, Z. Chen, C. Citro, G. S. Corrado, A. Davis, J. Dean, M. Devin, S. Ghemawat, I. Goodfellow, A. Harp, G. Irving, M. Isard, Y. Jia, R. Jozefowicz, L. Kaiser, M. Kudlur, J. Levenberg, D. Mané, R. Monga, S. Moore, D. Murray, C. Olah, M. Schuster, J. Shlens, B. Steiner, I. Sutskever, K. Talwar, P. Tucker, V. Vanhoucke, V. Vasudevan, F. Viégas, O. Vinyals, P. Warden, M. Wattenberg, M. Wicke, Y. Yu, and X. Zheng. TensorFlow: Large-Scale Machine Learning on Heterogeneous Systems. https://www.tensorflow.org/, 2015.

[3] M. Abramowitz and I. A. Stegun. *Handbook of Mathematical Functions with Formulas, Graphs, and Mathematical Tables*. Tenth printing, with corrections edition, December 1972.

[4] S. Al-Ahmadi and H. Yanikomeroglu. On the approximation of the generalized- distribution by a gamma distribution for modeling composite fading channels. *IEEE Transactions on Wireless Communications*, 9(2):706–713, 2010.

[5] J. Andrews, R. Ganti, M. Haenggi, N. Jindal, and S. Weber. A primer on spatial modeling and analysis in wireless networks. *IEEE communications magazine*, 48(11):156–163, 2010.

[6] P. H. Baxendale and P. E. Greenwood. Sustained oscillations for density dependent Markov processes. *Journal of Mathematical Biology*, 63(3):433–457, September 2011.

[7] N. H. Bingham and R. Kiesel. *Risk-Neutral Valuation: Pricing and Hedging of Financial Derivatives*. Springer, Second edition, 2004.

[8] K. O. Bowman and L. R. Shenton. *Estimation: Method of Moments*. Wiley, New York, 1998.

[9] S. Boyd and L. Vandenberghe. *Convex Optimization*. Cambridge University Press, seventh printing with corrections edition, 2009.

[10] K. Briggs. Personal communication, in a meeting at Adastral Park, January 2016.

[11] K. Briggs. Personal communication, in a meeting at Adastral Park, February 2017.

[12] K. Briggs. Personal communication, by email, November 2017.

[13] K. Briggs. Personal communication, by email, December 2018.

[14] K. Briggs. Personal communication, in a meeting at the University of Bath, February 2019.

[15] K. Briggs and S. Webster. Cellular telecommunications network. Patent, February 2019. Patent application number 10362555.

[16] K. Briggs and F. M. Ying. How to Estimate Quantiles Easily and Reliably. *Mathematics Today*, 2018.

[17] P. Butzer and F. Jongmans. P. L. Chebyshev (1821–1894): A Guide to his Life and Work. *Journal of Approximation Theory*, 96(1):111 – 138, 1999.

[18] G. Carle, M.-O. Pahl, D. Raumer, L. Schwaighofer, U. Baumgarten, and C. Söllner, editors. *Self-Configuration in LTE Self Organizing Networks*, volume NET-2013-08-1 of *Network Architectures and Services (NET)*, Munich, Germany, Aug. 2013. Chair for Network Architectures and Services, Department of Computer Science, Technische Universität München.

[19] W. C. Cheung, T. Q. S. Quek, and M. Kountouris. Throughput Optimization, Spectrum Allocation, and Access Control in Two-Tier Femtocell Networks. *IEEE Journal on Selected Areas in Communications*, 30(3):561–574, April 2012.

[20] M. Chiang. Nonconvex Optimization for Communication Systems. *Advanced Structured Materials*, 7:3–19, 2011.

[21] F. Chollet et al. Keras. `https://keras.io`, 2015.

[22] A. R. Constable. Marconi's Transatlantic Wireless Message, 1901. *Transactions of the Newcomen Society*, 73(1):53–70, 2001.

[23] J. Dawes and M. Souza. A derivation of Holling's type I, II and III functional responses in predator-prey systems. *Journal of Theoretical Biology*, 327(1):11–22, March 2013.

[24] T. Degris, P. M. Pilarski, and R. S. Sutton. Model-free reinforcement learning with continuous action in practice. In *American Control Conference (ACC), 2012*, pages 2177–2182. IEEE, 2012.

[25] Deloitte. Telecommunications Industry Outlook: A new era of connectivity is on the horizon. Technical report, 2018. `https://www2.deloitte.com/us/en/pages/technology-media-and-telecommunications/articles/telecommunications-industry-outlook.html` [Accessed: September 2018].

[26] P. Dhariwal, C. Hesse, O. Klimov, A. Nichol, M. Plappert, A. Radford, J. Schulman, S. Sidor, Y. Wu, and P. Zhokhov. OpenAI Baselines. `https://github.com/openai/baselines`, 2017.

[27] T. Evans. *Great Wall of China: Beijing & Northern China*. Bradt Travel Guides, 2006.

[28] G. J. Foschini and Z. Miljanic. A Simple Distributed Autonomous Power Control Algorithm and its Convergence. *IEEE Transactions on Vehicular Technology*, 42(4):641–646, 1993.

[29] J. Galambos. *Advanced Probability Theory*. Probability: Pure and Applied. Taylor & Francis, second edition, 1995.

[30] A. Galindo-Serrano and L. Giupponi. Distributed Q-learning for aggregated interference control in cognitive radio networks. *IEEE Transactions on Vehicular Technology*, 59(4):1823–1834, 2010.

[31] C. W. Gardiner. *Stochastic Methods: A Handbook for the Natural and Social Sciences*. Springer, 4th edition, 2009.

[32] E. Ghadimi, F. D. Calabrese, G. Peters, and P. Soldati. A Reinforcement Learning Approach to Power Control and Rate Adaptation in Cellular Networks. In *2017 IEEE International Conference on Communications (ICC)*, Paris, 2017.

[33] D. T. Gillespie. Exact stochastic simulation of coupled chemical reactions. *The Journal of Physical Chemistry*, 81(25):2340–2361, 1977.

[34] I. Goodfellow, Y. Bengio, and A. Courville. *Deep Learning*. MIT Press, 2016. `http://www.deeplearningbook.org`.

[35] J. S. Gordon. Alexander Graham Bell. In E. Foner and J. A. Garraty, editors, *The Reader's Companion to American History.* Houghton Mifflin Company, Boston, 1991.

[36] S. A. Grandhi, J. Zander, and R. Yates. Constrained power control. *Wireless Personal Communications*, 1(4):257–270, 1994.

[37] G. Grimmett and D. Stirzaker. *Probability and Random Processes*. Oxford University Press, third edition, 2001.

[38] M. Haenggi. A Geometric Interpretation of Fading in Wireless Networks: Theory and Applications. *IEEE Transactions on Information Theory*, 54:5500–5510, 2008.

[39] M. Haenggi. *Stochastic Geometry for Wireless Networks*. Cambridge University Press, Cambridge, 2012.

[40] K. He, X. Zhang, S. Ren, and J. Sun. Delving Deep into Rectifiers: Surpassing Human-Level Performance on ImageNet Classification. In *The IEEE International Conference on Computer Vision (ICCV)*, December 2015.

[41] A. Hill, A. Raffin, M. Ernestus, A. Gleave, R. Traore, P. Dhariwal, C. Hesse, O. Klimov, A. Nichol, M. Plappert, A. Radford, J. Schulman, S. Sidor, and Y. Wu. Stable Baselines. `https://github.com/hill-a/stable-baselines`, 2018.

[42] A. A. Jarai. Conditional distribution of the distance to the nearest transmitter. Unpublished manuscript, 2018.

[43] A. Khintchine. Korrelationstheorie der stationären stochastischen Prozesse. *Mathematische Annalen*, 109(1):604–615, December 1934.

[44] D. P. Kingma and J. L. Ba. Adam: A method for stochastic gradient descent. In *ICLR: International Conference on Learning Representations*, 2015.

[45] E. E. Kummer. De integralibus quibusdam definitis et seriebus infinitis. *Journal für die reine und angewandte Mathematik*, 17:228–242, 1837.

[46] T. G. Kurtz. Strong approximation theorems for density dependent Markov chains. *Stochastic Processes and their Applications*, 6(3):223 – 240, 1978.

[47] T. Lan, K. Sinkar, L. Kant, and K. Kerpez. Resource Allocation and Performance Study for LTE Networks Integrated with Femtocells. In *2010 IEEE Global Telecommunications Conference GLOBECOM 2010*, pages 1–6, December 2010.

[48] G. Last and M. Penrose. *Lectures on the Poisson Process*. Cambridge University Press, October 2017.

[49] H. S. Lichte, S. Valentin, and H. Karl. Expected interference in wireless networks with geometric path loss: A closed-form approximation. *IEEE Communications Letters*, 14(2):130–132, 2010.

[50] D. J. C. MacKay. *Information Theory, Inference, and Learning Algorithms*. Copyright Cambridge University Press, 2003.

[51] A. M. Mathai. On Noncentral Generalized Laplacianness of Quadratic Forms in Normal Variables. *Journal of Multivariate Analysis*, 45(2):239–246, 1993.

[52] V. H. McDonald. Advanced Mobile Phone Service: The cellular concept. *The Bell System Technical Journal*, 58:15–41, January 1979.

[53] A. J. McKane and T. J. Newman. Predator-Prey Cycles from Resonant Amplification of Demographic Stochasticity. *Physical Review Letters*, 94(218102):1–4, 2005.

[54] F. S. Melo. Convergence of Q-learning: A simple proof. Technical report, Institute Of Systems and Robotics, 2001.

[55] V. Mnih, M. Mirza, A. Graves, T. Lillicrap, T. Harley, D. Silver, and K. Kavukcuoglu. Asynchronous Methods for Deep Reinforcement Learning. In *Proceedings of The 33rd International Conference on Machine Learning*, New York, 2016.

[56] M. Nakagami. The m-distribution—a general formula of intensity distribution of rapid fading. In W. HOFFMAN, editor, *Statistical Methods in Radio Wave Propagation*, pages 3 – 36. Pergamon, 1960.

[57] A. Papoulis and S. U. Pillai. *Probability, Random Variables, and Stochastic Processes*. McGraw Hill, Boston, fourth edition, 2002.

[58] J. Peng and R. J. Williams. Incremental multi-step Q-learning. *Machine Learning*, 22(1-3):283–290, 1996.

[59] D. H. Ring. Mobile Telephony - Wide Area Coverage - Case 20564. Technical report, 1947.

[60] H. Risken and T. Frank. *The Fokker-Planck Equation: Methods of Solutions and Applications (Springer Series in Synergetics)*. Springer, 1996.

[61] L. Rose, S. M. Perlaza, M. Debbah, and C. J. L. Martret. Distributed power allocation with SINR constraints using trial and error learning. In *IEEE Wireless Communications and Networking Conference, WCNC*, number 1, pages 1835–1840. IEEE, 2012.

[62] H. Saad, A. Mohamed, and T. El Batt. A cooperative Q-learning approach for distributed resource allocation in multi-user femtocell networks. In *IEEE Wireless Communications and Networking Conference, WCNC*, volume 2, pages 1490–1495. IEEE, 2014.

[63] A. M. Saxe, J. L. McClelland, and S. Ganguli. Exact solutions to the nonlinear dynamics of learning in deep linear neural networks. In *International Conference on Learning Representations (ICLR) 2014*, 2014.

[64] T. Shaffner. *The Telegraph Manual: A Complete History and Description of the Semaphoric, Electric and Magnetic Telegraphs of Europe, Asia, Africa, and America, Ancient and Modern*. Pudney & Russell, 1859.

[65] M. Simsek, A. Czylwik, A. Galindo-Serrano, and L. Giupponi. Improved decentralized Q-learning algorithm for interference reduction in LTE-femtocells. In *2011 Wireless Advanced*, pages 138–143, London, June 2011. IEEE.

[66] C. Skarakis. Convex Optimisation theory and practice. Dissertation submitted for the MSc in mathematics with modern applications, University of York, 2008.

[67] SNS Telecom & IT. Network complexity, 5G rollouts will drive SON (Self-Organizing Network) spending to $5.5 Billion. Press statement, 2018. `http://www.snstelecom.com/network-complexity-5g-rollouts-will-drive-son-self-organizing-network-spending-to-5-5-billion-says-sns-telecom-it` [Accessed: September 2018].

[68] E. S. Sousa and J. A. Silvester. Optimum Transmission Ranges in a Direct-Sequence Spread-Spectrum Multihop Packet Radio Network. *IEEE Journal on Selected Areas in Communications*, 8(5):762–771, 1990.

[69] C. H. Sterling. *Military Communications: From Ancient Times to the 21st Century*. ABC-CLIO, 2007.

[70] R. L. Streit. *The Poisson Point Process*, pages 11–55. Springer US, Boston, MA, 2010.

[71] R. S. Sutton and A. G. Barto. *Reinforcement learning: An Introduction.* Adaptive computation and machine learning series. The MIT Press, second edition, 2018.

[72] A. Tall, R. Combes, Z. Altman, and E. Altman. Distributed coordination of self-organizing mechanisms in communication networks. *IEEE Transactions on Control of Network Systems*, 1(4):328–337, 2014.

[73] G. I. Taylor. Diffusion by Continuous Movements. *Proceedings of the London Mathematical Society*, s2-20(1):196–212, 1922.

[74] P. Tchebycheff. Sur deux théorèmes relatifs aux probabilités. *Acta Mathematica*, 14, 1890.

[75] T. Tieleman and G. Hinton. Lecture 6.5-rmsprop: Divide the gradient by a running average of its recent magnitude. *COURSERA: Neural Networks for Machine Learning*, (4):26–31, 2012.

[76] F. Tricomi. Sulle funzioni ipergeometriche confluenti. *Annali di Matematica Pura ed Applicata*, 26(1):141–175, December 1947.

[77] UK Parliament. Telecommunications Sector Report. pages 1–22, 2017. `https://www.parliament.uk/documents/commons-committees/Exiting-the-European-Union/17-19/Sectoral%20Analyses/37-Telecommunications-Report.pdf` [Accessed: September 2018].

[78] N. G. van Kampen. *Stochastic Processes in Physics and Chemistry.* North-Holland personal library. Elsevier, Amsterdam; London, third edition, 2007.

[79] F. Vaz, P. Sebastião, L. Gonçalves, and A. Correia. Femtocell deployment in LTE-A networks: A sustainability, economical and capacity analysis. *IEEE International Symposium on Personal, Indoor and Mobile Radio Communications, PIMRC*, pages 3423–3427, 2013.

[80] C. J. C. H. Watkins. *Learning from Delayed Rewards*. PhD thesis, University of Cambridge, 1989.

[81] C. J. C. H. Watkins and P. Dayan. Q-learning. *Machine Learning*, 8(3):279–292, May 1992.

[82] J. C. Watkins. *An Introduction to the Science of Statistics: From Theory to Implementation*, preliminary edition. `https://www.math.arizona.edu/~jwatkins/statbook.pdf` [Accessed: 17 May 2019 13:35].

[83] S. Webster. Distributed heuristics for optimizing femtocell performance. MSc thesis, University of Bath, 2015.

[84] N. Wiener. Generalized harmonic analysis. *Acta Math.*, 55:117–258, 1930.

[85] R. J. Williams. Simple statistical gradient-following algorithms for connectionist reinforcement learning. *Machine Learning*, 8(3):229–256, 1992.

[86] R. J. Williams and J. Peng. Function optimization using connectionist reinforcement learning algorithms. *Connection Science*, 3(3):241–268, 1991.

[87] M. Z. Win, P. C. Pinto, and L. A. Shepp. A mathematical theory of network interference and its applications. *Proceedings of the IEEE*, 97(2):205–230, 2009.

[88] Q. Yang. *Oscillations in stochastic multi-species interactions*. PhD thesis, University of Bath, 2018.

[89] J. Zander. Distributed Cochannel Interference Control in Cellular Radio Systems. *IEEE Transactions on Vehicular Technology*, 41(3):305–311, 1992.